Elucidation of Glycoside Hydrolase Mechanisms by Measuring Kinetic Isotope Effects Using Direct NMR Method

by

Natalia Sannikova

M. Sc., Moscow Technological University, 2011

B. Sc., Moscow Technological University, 2009

Thesis Submitted in Partial Fulfillment of the
Requirements for the Degree of
Doctor of Philosophy

in the
Department of Chemistry
Faculty of Science

SIMON FRASER UNIVERSITY

Fall 2018

Approval

Name:	**Natalia Sannikova**
Degree:	**Doctor of Philosophy (Chemistry)**
Title:	**Elucidation of Glycoside Hydrolase Mechanisms by Measuring Kinetic Isotope Effects Using Direct NMR Method**
Examining Committee:	**Chair: Erika Plettner** Professor
	Andrew J. Bennet Senior Supervisor Professor
	Robert A. Britton Supervisor Professor
	Daniel B. Leznoff Supervisor Professor
	David J. Vocadlo Internal Examiner Professor
	Paul J. Berti External Examiner Professor Department of Chemistry and Chemical Biology McMaster University
Date Defended/Approved:	December 12, 2018

Abstract

Enzymes that catalyze the removal of carbohydrate units from biological molecules are called glycoside hydrolases (GH). These enzymes have been categorized into more than 150 different families. This thesis presents an analysis of the mechanistic aspects of three glycoside hydrolases elucidated by measuring kinetic isotope effects (KIEs) by a direct nuclear magnetic resonance (NMR) spectroscopic method.

A review of scope and limitations of the NMR method for competitive heavy atom (^{13}C, ^{18}O, ^{15}N) and secondary deuterium KIEs measurement in biological systems is provided. A method for continuous monitoring of isotopically enriched materials is described in detail including the current state of instrumentation and computer programs for data acquisition and analysis.

In order to refine the mechanistic understanding of the glycoside hydrolase family 4 (GH4) α-galactosidase from *Citrobacter freundii* (MelA), leaving group effects were measured with various metal cations and competitive deuterium KIEs were measured with singly and doubly deuterated activated substrates, 2-fluorophenyl and 4-fluorophenyl α-D-galactopyranosides, in the presence of Sr^{2+}, Y^{3+}, and Mn^{2+}. The observations are consistent with hydride transfer at C-3 to the on-board NAD^+, deprotonation at C-2, and a non-chemical step contributing to the virtual TS for *V*/*K*.

The α-D-glucopyranosyl fluoride (α-GlcF) hydrolysis catalyzed by GH15 inverting α-glucoamylases from *A. niger* and *Rhizopus sp.* has been studied by use of multiple competitive kinetic isotope effect measurements. The experimental KIEs are consistent with the enzymatic reaction occurring via an S_N1-type mechanism, in which the transition state has significant pyranosylium-ion like character and is late with respect to C−F bond cleavage.

α-D-Glucopyranosyl fluoride is hydrolyzed by the family 55 inverting exo-1,3-β-glucanase from *Trichoderma virens* via the Hehre resynthesis–hydrolysis mechanism. The transition state for the Hehre resynthesis-hydrolysis mechanism for the GH55 catalyzed hydrolysis of α-GlcF has been studied by the use of multiple kinetic isotope effect measurements. The transition state for the Hehre resynthesis-hydrolysis reaction is late with respect to both C–F bond cleavage and proton transfer.

Keywords: glycoside hydrolase; kinetic isotope effect; transition state; nuclear magnetic resonance

To my husband. I would not have made it without you.

Acknowledgements

First, I would like to thank my supervisor, Professor Andrew Bennet, for the chance to pursue a PhD degree in his research group. I am especially grateful for providing me with an excellent learning environment and numerous opportunities to present my research projects at the national and international conferences.

I would like to thank my supervisory committee members, Professors Robert Britton and Daniel Leznoff, for their support, insightful suggestions and constructive criticism during my committee meetings. I would also like to thank my examining committee, Professors David Vocadlo and Paul Berti for reading my thesis and providing valuable feedback and knowledgeable questions.

I would especially like to thank Dr. Andrew Lewis for his help and assistance with NMR experiments, this thesis would not have been possible without his help. It was a great pleasure to collaborate with Dr. Lewis. I have gained a wealth of knowledge about NMR spectroscopy thanks to his patient training.

I also want to extend my sincere thanks to the Bennet group members whom I have had a pleasure to work with. I would like to begin by thanking my past labmates: Dr. Fahimeh Shidmoossavee, Dr. Lydia Cheng, Kobi Khazaei, Vivi Cerda, Matt Courtemanche, Emilie Phillips, Chloe Gerak, Michael Tran, Dr. Sankar Mohan, Dr. Cinzia Colombo, Yumeela Ganga-Sah, Chris Adamson and Sairvan Fernandez for being friendly, helpful and fun both in and outside the lab. I've had a chance to work with the best undergraduate students one can wish for, Chloe and Sairvan, both intelligent, passionate and hard working. I am wishing them the best of luck in all their future endeavors. I truly appreciate their help and friendship, especially Chloe's, who's basically accepted me into her family and is the one person making Canada second home for me. Next, I want to thank Dr. Saeideh Shamsi and Dr. Dustin King for helping naïve organic chemist stay afloat in the deep and dangerous waters of protein expression and purification. I am grateful to have been able to share all the ups and downs of the research and grad student life with my present labmates, Oleg Sannikov, Matt Deen, Marco Farren-Dai, Femi Akintola, Dr. John Pal Adabala, Dr. Sandeep Bhosale, Dr. Sachin Kandalkar and Dr. Weiwu Ren. I appreciate all the scientific discussions, silly jokes, hiking adventures, skiing trips and coffee breaks we have shared.

The skilled technical assistance of Colin Zhang (NMR technician), Hongwen Chen (Mass Spectrometer Technician) and Nathalie Fournier (Graduate Secretary) is highly appreciated.

I would like to thank my closest friends Olga and Natasha for their help and support despite the oceans and time zones between us.

Finally, this journey would not have been possible without the support and love of my family. I am tremendously indebted to my mom, grandmother and grandfather for their care, encouragement and patience. My earnest thanks to my husband Oleg for his love, inspiration, support and trust. I could not have accomplished what I have now without him.

Table of Contents

Approval ii
Abstract iii
Dedication iv
Acknowledgements v
Table of Contents vii
List of Tables xi
List of Figures xii
List of Schemes xiv
List of Abbreviations xv

Chapter 1. General Introduction 1
1.1. Glycoside Hydrolases 1
1.1.1. Classification 2
1.1.2. Mechanisms of Classical Glycoside Hydrolases 3
Inverting Glycoside Hydrolases 3
Retaining Glycoside Hydrolases 3
1.1.3. Mechanism of the NAD^+ - Dependent GH4 α-Galactosidase 5
1.2. Kinetic Isotope Effects (KIEs) 6
1.2.1. Classification and Origins of KIEs 6
1.2.2. Kinetics of Enzymatic Reactions 10
1.2.3. Measurement of KIEs for Enzymatic Reactions 12
1.2.4. Commitment to Catalysis 15
1.3. Glycosyl Fluorides 16
1.3.1. Substrates for Glycoside Hydrolases 16
1.3.2. Substituted Glycosyl Fluorides as Mechanistic Probes for Glycoside Hydrolases 18
1.3.3. Donors in Enzymatic Glycosylation Reactions 19
1.4. Thesis Overview 22
1.5. References 24

Chapter 2. Measurement of Kinetic Isotope Effects by Continuously Monitoring Isotopologues Ratios Using NMR Spectroscopy 32
2.1. Abstract 32
2.2. Introduction 33
2.3. Procedure 34
2.3.1. Choice of NMR-Active Probe Nucleus 35
^{1}H NMR Spectral Data Acquisition 35
^{13}C NMR Spectral Data Acquisition 37
^{19}F NMR Spectral Data Acquisition 40
2.3.2. Choosing Whether to Monitor Isotopologue Ratios in the Substrate or the Product 41
2.3.3. Sample Preparation 42
2.3.4. Acquisition of NMR Spectra 43

2.4. Data Processing 45
2.4.1. 1D NMR Data 45
2.4.2. 2D NMR Data 47
HSQC Experiments 48
HETCOR Experiments 49
2D Data Processing and Fitting 50
2.5. Data Analysis 52
2.6. Summary and Conclusion 53
2.7. References 54

Chapter 3. Both Chemical and Non-Chemical Steps Limit the Catalytic Efficiency of Family 4 Glycoside Hydrolases 58
3.1. Abstract 59
3.2. Introduction 59
3.3. Experimental Procedures 61
3.3.1. Materials 61
3.3.2. Synthesis of Aryl α-D-Galactopyranosides 62
3.3.3. Synthesis of Aryl α-D-Galactopyranoside Isotopologues 63
3.3.4. Protein Expression and Purification 65
3.3.5. Kinetic Investigation of Metal Ions 65
3.3.6. Relative Reaction Rate Measurements 66
3.3.7. KIE Calculations 67
3.3.8. Thermostability Analysis of MelA 67
3.3.9. Protein Homology Modeling for MelA 68
3.4. Results and Discussion 68
3.4.1. Substrate Specificity of MelA 68
3.4.2. Relative Rate Constants for MelA-Catalyzed Hydrolyses 70
3.4.3. Proton and Hydride Transfer Kinetic Isotope Effects Vary with Leaving Group and Activating Metal Cation 71
3.4.4. Kinetic Isotope Effects on Isotope Effects Using Doubly Deuterated Aryl α-D-Galactopyranosides 73
3.4.5. Kinetic Complexity of GH4 Enzymes 75
3.5. Conclusions 76
3.6. Associated Content 76
3.7. Abbreviations 77
3.8. References 78
3.9. Supporting Information 81
3.9.1. Materials and Methods 82
3.9.2. Equations used to calculate KIEs 82
3.9.3. Abbreviations 82

Appendix 101

Chapter 4. Kinetic Isotope Effects and the Transition State Structure for the Hydrolysis of α-d-Glucopyranosyl Fluoride by Inverting Glucoamylases ... 102

4.1. Abstract 102
4.2. Introduction 102
4.3. Experimental Procedures 103
4.3.1. Materials 103
4.3.2. KIE Measurements 105
4.4. Results 106
4.5. Discussion 108
4.5.1. ^{13}C KIE 109
4.5.2. ^{18}O KIE 110
4.5.3. Secondary Deuterium KIEs 110
α-Secondary Deuterium KIE (α-SDKIE) 110
β-Secondary Deuterium KIE (β-SDKIE) 110
γ-Secondary Deuterium KIE (γ-SDKIE) 111
4.6. Conclusions 111
4.7. References 112
4.8. Supporting Information 114

Chapter 5. A Kinetic Isotope Effect Study on the Hydrolysis of α-D-Glucopyranosyl Fluoride by an Inverting exo-1,3-β-D-Glucanase: Transition State Evaluation for the Hehre Resynthesis-Hydrolysis Mechanism 127
5.1. Abstract 127
5.2. Introduction 127
5.3. Experimental Procedures 131
5.3.1. Materials 131
5.3.2. KIE Measurements 132
5.3.3. Enzyme Kinetics in the Absence of Inert Acceptor 133
5.3.4. Protein Homology Modeling for *T. virens* exo-1,3-β-D-glucanase 133
5.4. Results and Discussion 133
5.4.1. Suggested Kinetic Pathway for the Transformation of α-D-Glucopyranosyl Fluoride by the GH55 exo-1,3-β-D-glucanase from *T. virens* 134
5.4.2. ^{13}C KIE 140
5.4.3. ^{18}O KIE 140
5.4.4. Secondary Deuterium KIEs 141
α-Secondary Deuterium KIE (α-SDKIE) 141
β-Secondary Deuterium KIE (β-SDKIE) 141
γ-Secondary Deuterium KIE (γ-SDKIE) 142
5.4.5. Homology Model Analysis 142
5.5. Conclusions 145
5.6. References 146
5.7. Supporting Information 151

Chapter 6. Future Work 154
6.1. Both Chemical and Non-Chemical Steps Limit the Catalytic Efficiency of Family 4 Glycoside Hydrolases 154

6.2. Kinetic Isotope Effects and Transition State Structure for the Hydrolysis of α-D-Glucopyranosyl Fluoride by Inverting Glucoamylases 155
6.3. A Kinetic Isotope Effect Study on the Hydrolysis of α-D-Glucopyranosyl Fluoride by an Inverting exo-1,3-β-D-Glucanase: Transition State Evaluation for the Hehre Resynthesis-Hydrolysis Mechanism 155

List of Tables

Table 1.1. α-SDKIEs on S_N1 and S_N2 reactions 9

Table 1.2. Select KIEs on hydrolysis of α-D-glucopyranosyl fluoride 9

Table 1.3. Select KIEs on hydrolyses of α- and β-D-glucosyl compounds 10

Table 2.1. Physical Properties of Potentially Useful Probe Nuclei for the Measurement of Biological KIEs by NMR Spectroscopy 36

Table 2.2. Typical Signal-to-Noise Specifications for Various 5 mm NMR Probes* at Different Field Strengths 40

Table 3.1. Ratio of V/K values for the GH4-catalyzed hydrolysis of unlabeled aryl α-D-galactopyranoside in presence of different metals.[a] 70

Table 3.2. Measured $^{2\text{-D}}(V/K)_{3\text{-H}}$ effects for the GH4-catalyzed hydrolysis of aryl α-D-(2-^{2}H)galactopyranosides with various metal activators at pH 8.0 and 25 °C.[a] 72

Table 3.3. Measured $^{3\text{-D}}(V/K)_{2\text{-H}}$ effects for the GH4-catalyzed hydrolysis of aryl α-D-(3-^{2}H)galactopyranosides with various metal activators at pH 8.0 and 25 °C.[a] 72

Table 3.4. Measured $^{3\text{-D}}(V/K)_{2\text{-D}}$ effects for the GH4-catalyzed hydrolysis of aryl α-D-(2,3-$^2H_2$)galactopyranosides relative to aryl α-D-(2-^{2}H)galactopyranosides with various metal activators at pH 8.0 and 25 °C.[a] 74

Table 3.5. Measured $^{2\text{-D}}(V/K)_{3\text{-D}}$ effects for the GH4-catalyzed hydrolysis of aryl α-D-(2,3-$^2H_2$)galactopyranosides relative to aryl α-D-(3-^{2}H)galactopyranosides with various metal activators at pH 8.0 and 25 °C.[a] 74

Table 4.1. Experimental *V/K* KIEs on hydrolysis of α-D-glucopyranosyl fluorides by glucoamylases[a] 108

Table 5.1. Hydrolysis of α-D-glycopyranosyl fluoride by *T. virens* GH55 in 100 mM sodium succinate, pH 6.02 at 40 °C. 136

Table 5.2. Experimental *V/K* KIEs on the GH55-catalyzed hydrolysis of α-D-glucopyranosyl fluorides at pH 6.05 and 40 °C[a] 139

List of Figures

Figure 1.1. General mechanism of an inverting α-glycoside hydrolase. 3

Figure 1.2. General mechanism of a retaining α-glycoside hydrolase 4

Figure 1.3. Proposed mechanism for the NAD^+-dependent GH4 α-galactosidase. 5

Figure 1.4. Zero-point energy differences and corresponding activation energy differences for the heavy and light isotopologues. 7

Figure 1.5. Mechanism of hydrolysis of α-xylosyl fluoride by an inverting α-xylosidase. 17

Figure 1.6. Hehre resynthesis-hydrolysis mechanism for the processing of the glycosyl fluoride of the 'wrong' anomeric configuration. 18

Figure 1.7. Chemical structures of several substituted glycosyl fluorides. 19

Figure 2.1. Part of the ^1H NMR spectrum of α-D-[1-$^{13}C_{0;1}$]glucopyranosyl fluoride in D_2O showing the resonances for the anomeric protons. 37

Figure 2.2. Proton-decoupled ^{13}C NMR spectrum of the C-2 resonance in 4-nitrophenyl α-D-[2-$^{13}C_{1;1}$,2-$^{18}O_{0;1}$]mannopyranoside in basic aqueous solution (NaOH = 0.1 *M*, *I* = 0.4) 38

Figure 2.3. Proton-decoupled ^{19}F NMR spectrum of α-D-[2-$^2H_{0;1}$,1-$^2H_{0;1}$]galactopyranosyl fluoride in D_2O 41

Figure 2.4. 2D ^{13}C–$^1H\{^1H,^2H\}$ HETCOR spectrum acquired for a mixture of six isotopologues with ^{13}C probe nucleus: (A) observed spectrum and (B) fit of spectrum using 3D peak deconvolution (TopSpin) 51

Figure 2.5. (A) 20 sequential rows extracted from a peak in a 2D ^1H–$^{13}C\{^2H,^{13}C\}$ HSQC spectrum and their sum. (B) Fit of sum spectrum using peak deconvolution (Mathematica): *black* = real spectrum, *red* = sum of fitted peaks, *blue* = difference (expt–fit), and *green* = baseline 52

Figure 2.6. Stacked plot of proton-decoupled ^{19}F NMR spectra of α-D-[1-$^{13}C_{0;1}$]glucopyranosyl fluoride as the fraction of reaction of α-D-glucopyranosyl fluoride 53

Figure 3.1. Compounds and Their Associated Isotopologues Used for the Measurement of Kinetic Isotope Effects on GH4-Catalyzed Hydrolyses. 61

Figure 3.2. (A) Overlay of the crystal structure of AglA α-glucosidase A from *T. maritima* (blue) and homology model of MelA α-galactosidase (beige). (B) Overlay of active site structure of AglA α-glucosidase A (blue), which includes the bound substrate maltose, the modeled active site for MelA α-galactosidase (beige), and the modeled Mn^{2+} cation (purple). Predicted key interactions with cofactors (NAD^+ and Mn^{2+}) and substrate are shown for MelA α-galactosidase; no general acid is positioned in close proximity to the leaving group. 69

Figure 3.3. Effect of leaving group ability on relative V/K rate constants for MelA-catalyzed hydrolysis of aryl α-D-galactopyranoside at 25 °C and pH 8.00. 71

Figure 4.1. α-D-Glucopyranosyl fluoride isotopologues. 106

Figure 4.2. A. Overlaid proton and ^{13}C decoupled ^{19}F NMR spectra containing a mixture of 1a – 1f in the presence of *Rhizopus sp.* glucoamylase at

fraction of reactions F_1 = 0.00 (red) and 0.82 (blue) that have normalized peak heights for the probe isotopologue (1a; black arrow). Note the relative increase in peak heights for the 1c–1f isotopologues during reaction (normal KIEs), and decrease for 1b (inverse KIE). B. Close-up of A. showing relative peak intensities change for 1b, 1c, 1e and 1f. 107

Figure 4.3. Plots of the change in integrated peak intensity ratios (R) versus fraction of reaction for the light isotopologue (F_1) for the measurement of competitive KIE values: (A) data from an experimental measurement of $k(1\text{-}^{12}C)/k(1\text{-}^{13}C)$ using 1a and 1c; (B) data from an experimental measurement of $k(5\text{-}^{16}O)/k(5\text{-}^{18}O)$ using 1a and 1b. 108

Figure 5.1. Mechanisms of classical glycoside hydrolases. 128

Figure 5.2. Generally accepted mechanism for the Hehre resynthesis-hydrolysis of the glucosyl fluoride of the 'wrong' anomeric configuration. 129

Figure 5.3. Mechanism of glycosylation with a glycosynthase. 130

Figure 5.4. Fluoride ion release rate from α-GlcF by *T. virens* GH55 exo-1,3-β-D-glucanase 136

Figure 5.5. α-D-Glucopyranosyl fluoride isotopologues 137

Figure 5.6. Overlaid proton-decoupled ^{19}F NMR spectra containing a mixture of 1a, 1d and 1e in the presence of GH55 enzyme. 138

Figure 5.7. Plots of the change in integrated peak intensity ratios (R) versus fraction of reaction for the light isotopologue (F_1) for the measurement of competitive KIE values. 139

Figure 5.8. Overlay of the structures of SacteLam55A[38], CtLam55 and the homology model for *T. virens* exo-1,3-beta-D-glucanase. 144

Figure 6.1. Conformationally constrained GH inhibitors 154

List of Schemes

Scheme 1.1. General mechanism for an enzyme-catalyzed reaction. 11

Scheme 1.2. *N. meningitidis* α-galactosyltransferase (lgtC-19) catalyzed formation of oligosaccharide (A) or UDP-Gal (B).....21

Scheme 3.1. Proposed Mechanism for GH4 Enzyme-Catalyzed Glycosidic Bond Cleavage* 60

Scheme 3.2. Current proposal for the mechanism of glycosidic bond cleavage for GH4 enzymes in which a conformational change is required for aglycone departure that does not require a general acid catalyst*.....75

Scheme 5.1. Kinetic scheme for the transformation of of α-D-glucopyranosyl fluoride by the GH55 exo-1,3-β-D-glucanase from *T. virens*.....134

List of Abbreviations

Ala	Alanine
Asp	Aspartic acid
BSA	Bovine serum albumin
CAZy	Carbohydrate Active enZymes
COSY	Homonuclear correlation spectroscopy
DFT	Density functional theory
DTT	Dithiothreitol
EC	Enzyme commission
EtOAc	Ethyl acetate
FID	Free induction decay
GalO2F	2-fluorophenyl α-D-galactopyranoside
GalO3,5diF	3,5-difluorophenyl α-D-galactopyranoside
GalO3F	3-fluorophenyl α-D-galactopyranoside
GalO4F	4-fluorophenyl α-D-galactopyranoside
GH	Glycoside hydrolase
Gln	Glutamine
Glu	Glutamic acid
GT	Glycosyl transferase
HEPES	4-(2-hydroxyethyl)-1-piperazineethanesulfonic acid
HETCOR	Heteronuclear correlation spectroscopy
HFIP	Hexafluoro-2-propanol
HSQC	Heteronuclear single-quantum correlation spectroscopy
IPTG	Isopropyl 1-thio-β-D-galactopyranoside
KIE	Kinetic isotope effect
LSD	Lysosomal storage disease
NAD	β-Nicotinamide adenine dinucleotide
NMR	Nuclear magnetic resonance spectroscopy
NOE	Nuclear Overhauser effect
PDB	Protein data bank
Phe	Phenylalanine
QM/MM	Quantum mechanics/molecular mechanics

SDKIE	Secondary deuterium kinetic isotope effect
Ser	Serine
SNR	Signal to noise ratio
TCEP	Tris(2-carboxyethyl)phosphine
Thr	Threonine
TLC	Thin layer chromatography
TMS	Tetramethylsilane
Trp	Tryptophan
TS	Transition state
TSA	Transition state analogue
Tyr	Tyrosine
UDP	Uridine diphosphate
UV/Vis	Ultraviolet/visible
ZPE	Zero point energy
α-GlcF	α-D-Glucopyranosyl fluoride

Chapter 1.

General Introduction

1.1. Glycoside Hydrolases

Glycoside hydrolases (GHs, also referred to as glycosidases) are a large group of enzymes that catalyze the hydrolysis of glycosidic bonds in complex carbohydrates. Glycosidic bond is a bond between the hemiacetal or hemiketal anomeric carbon of a sugar and a non-acyl group –OR, –SR, –SeR, $–NR^1R^2$, $–CR^1R^2R^3$.[1,2] GHs are ubiquitous in nature and play various critical biological roles that include: i) degradation of biomass such as cellulose, chitin and starch, ii) defense against bacterial infections, iii) pathogenesis of various diseases, and iv) cell-cell recognition events.

Glycoside hydrolases are found in all domains of life. In eukaryotes glycoside hydrolases are found within many cellular compartments including the endoplasmic reticulum, the Golgi apparatus, lysosomes and in cytoplasm. Deficiency in specific lysosomal glycoside hydrolases can lead to a range of lysosomal storage diseases (LSD) that result in numerous symptoms, which can include developmental problems, movement disorders, seizures, dementia, deafness, and a reduced life expectancy.[3] Also, viral glycoside hydrolases, such as influenza virus type A neuraminidase, are often involved in infection. In this case, the neuraminidase is required to complete the release of viral progeny, which completes the influenza virus replication cycle, and as a result promote the spread of the virus from infected host cells to uninfected surrounding cells.[3] This enzyme also cleaves sialic acid residues from viral glycoproteins, preventing viral particle agglutination. Another glycoside hydrolase, lysozyme, forms part of the innate immune system as it acts as an antimicrobial agent. Its function is to cleave the glycosidic bonds in murein, a major component of the cell wall of Gram-positive bacteria. Understanding the mechanism of action of these glycoside hydrolases, which are implicated in numerous genetic disorders, viral and bacterial infections, is an active area of research.

1.1.1. Classification

As glycoside hydrolases are a very large collection of enzymes several different systems have been used to classify these biological catalysts, and these approaches include: Enzyme Commission numbering, endo/exo, mechanism of action, and protein sequence alignment.

The Enzyme Commission (EC) system is a numerical classification scheme for enzymes, which is based on the chemical reactions that they catalyze. Glycoside hydrolases that catalyze the hydrolysis of *O*- or *S*-glycosides are classified as EC 3.2.1.X. Of note, different enzymes that catalyze the same reaction, for instance hydrolysis of α-galactopyranosides, will have the same EC number (3.2.1.22). However, if an enzyme catalyzes reactions that belong to more than one class, such an enzyme should have more than one EC number. There are also examples of enzymes that cleave the same type of glycosidic linkage but have different EC numbers. For instance, maltase, sucrase and isomaltase all cleave α-glucosides; their corresponding EC numbers are 3.2.1.20 (maltase, hydrolyses terminal non-reducing 1,4-α-D-glucosides), 3.2.1.48 (surcase, hydrolyses sucrose and maltose by an α-D-glucosidase-type action), and 3.2.1.10 (isomaltase, cleaves 1,6-α-D-glucosidic linkages). Glycoside hydrolases can also be classified as exo- or endo-acting. Exo- and endo- refer to where substrate cleavage occurs, which can be at the termini of a chain (exo-, typically, the non-reducing end) or somewhere in the middle of a chain (endo).[4] In addition, the anomeric stereochemical outcome of the hydrolysis catalyzed by GHs can be either inversion or retention of configuration. Based on this classification most GHs fall into two groups, which correspond to the two most common mechanisms outlined by Koshland.[5] However, other hydrolytic mechanisms are also employed by a subset of these biological catalysts.[6] Protein sequence-based classification is used to sort GHs into families based on their amino acid sequence similarity.[7] Currently, there are more than 150 GH families, and this classification system can be found on the CAZy (Carbohydrate Active enZymes) database website (http://www.cazy.org/Glycoside-Hydrolases.html). GH families can be further clustered into larger groups called Clans.[8] GH families that constitute a clan typically bear similar tertiary structures, catalytic residues, and mechanism of action.

1.1.2. Mechanisms of Classical Glycoside Hydrolases

Inverting and retaining glycoside hydrolases effect substrate hydrolysis with either net inversion or retention of the stereochemistry at the anomeric centre. The canonical mechanisms for the majority of these enzymes were put forward as hypothetical in a classical paper by Koshland.[5]

Inverting Glycoside Hydrolases

Most inverting GHs operate via a one step single-displacement mechanism that traverses a pyranosylium-ion like transition state (TS) (Fig. 1.1).[5,9] A process that involves general acid catalyzed aglycone departure (by one of the active site carboxylate residues) that occurs either prior to (S_N1) or simultaneously with (S_N2) nucleophilic attack by a water molecule, which is facilitated by general base catalysis from the second carboxylate residue. The initial product of hydrolysis possess an inverted anomeric centre configuration.

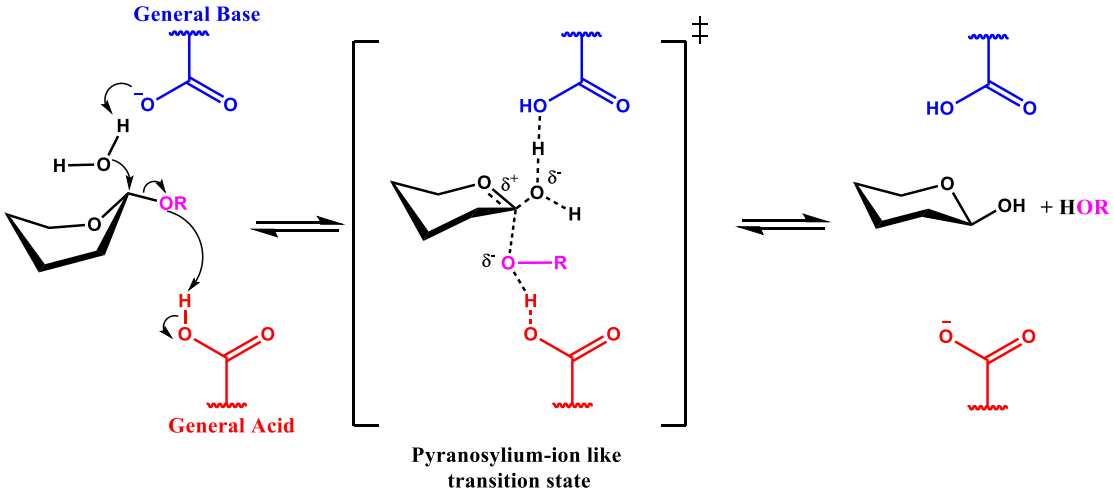

Figure 1.1. General mechanism of an inverting α-glycoside hydrolase.

Retaining Glycoside Hydrolases

Among the glycoside hydrolase families that operate via retention of configuration there are three main mechanisms: a) nucleophilic catalysis via formation of a glycosyl-enzyme intermediate; b) substrate neighbouring group assisted catalysis[9,10] and c) NAD^+-dependent oxidation/reduction mechanism.[11–13]

In the case of classical retaining glycoside hydrolases, catalysis occurs via a two step, double-displacement, mechanism that involves formation of a covalent glycosyl-enzyme intermediate (Fig. 1.2). Each step goes through a pyranosylium-ion like transition state. Typically this mechanism involves two glutamate and/or aspartate residues with one acting as a general acid/base while the other is a nucleophile during the catalytic cycle. In the first chemical step, glycosylation, the aglycone departs, a process that occurs with general-acid catalysis, either prior to (S_N1) or simultaneously with (S_N2) nucleophilic attack at the anomeric centre. The second chemical step, deglycosylation, involves hydrolysis of the glycosyl-enzyme intermediate by a water molecule attack, which occurs with catalysis by the deprotonated acid acting as a general base.

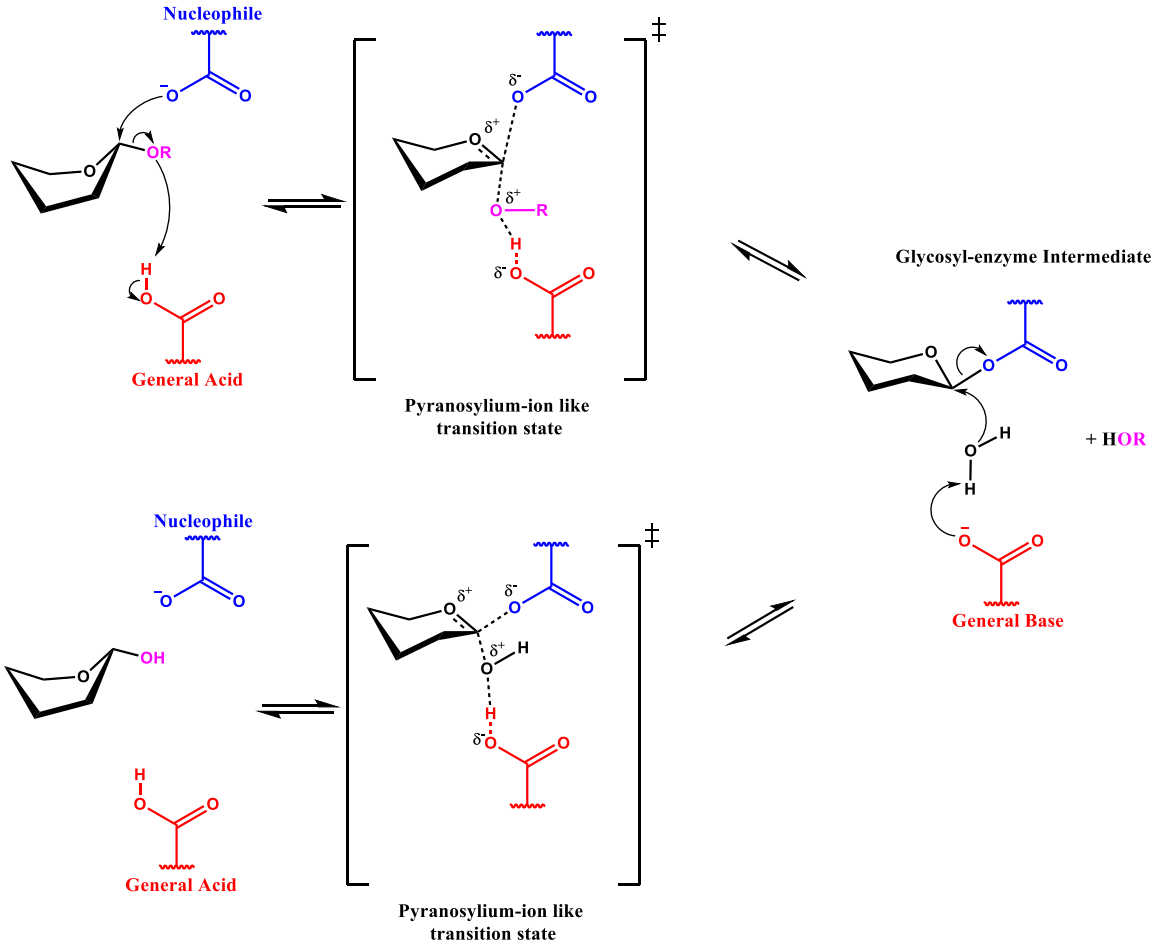

Figure 1.2. General mechanism of a retaining α-glycoside hydrolase.

1.1.3. Mechanism of the NAD$^+$ - Dependent GH4 α-Galactosidase

Families 4 and 109 glycoside hydrolases (GH4 and GH109) use a mechanism that requires a bound NAD$^+$ co-factor; and in addition GH4 requires a divalent metal cation. The mechanism for catalysis proceeds via anionic transition states with elimination and redox steps rather than the classical nucleophilic substitution mechanisms that proceed through pyranosylium-ion like transition states. As shown below for a GH4 α-galactosidase, this mechanism involves initial oxidation of the substrate's C3-hydroxyl group by the enzyme-bound NAD$^+$ cofactor to give a C3-ketone. As a result, the acidity of the C2 proton is increased and this enables a base-catalyzed elimination reaction to give an α,β-unsaturated ketone intermediate, which completes the first half of the catalytic cycle. Subsequently, a Michael addition of water to the anomeric centre, protonation at C2, and a final reduction of the ketone at C3 generates the carbohydrate product with retained anomeric stereochemistry. This mechanism was elucidated through a combination of experimental studies using NMR spectroscopy, isotope scrambling, kinetic isotope effects, linear free energy relationships, X-ray crystallography and UV/Vis spectrophotometry.[11,14,15]

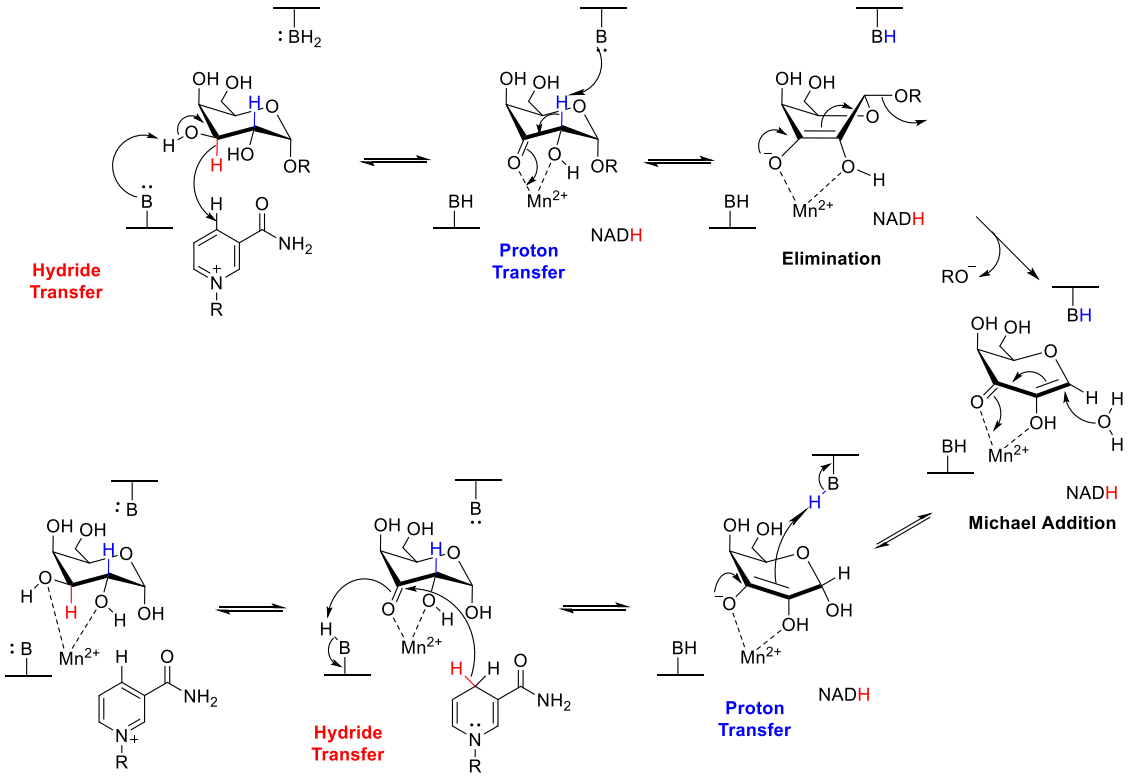

Figure 1.3. Proposed mechanism for the NAD$^+$-dependent GH4 α-galactosidase.

1.2. Kinetic Isotope Effects (KIEs)

A kinetic isotope effect (KIE) results from a change in the reaction rate constant when a light isotope within the molecule is substituted by a heavier one. Such KIEs are often measured at the centre(s) of bond cleavage and/or formation or at sites adjacent to the reaction centre.

Kinetic isotope effects (KIEs) have been used extensively by physical organic chemists as a mechanistic tool to probe reaction transition states.[16] That is, KIEs can provide valuable details about how the various chemical transformations (bond making and breaking), hybridization changes, and electronic effects are expressed at the reaction TS(s). Detailed KIE analyses allow researchers to determine features of the reaction TS that include: i) geometry; ii) extent of bond cleavage and formation; iii) charge development; and iv) whether a reaction is concerted or step-wise.[16,17]

1.2.1. Classification and Origins of KIEs

Kinetic isotope effects are expressed as a ratio of the rate constant for the light isotopologue to that for the heavy isotopologue. Measured KIE values that are greater than one are traditionally labelled as "normal" effects, whereas, values that are less than one are termed as "inverse" effects.

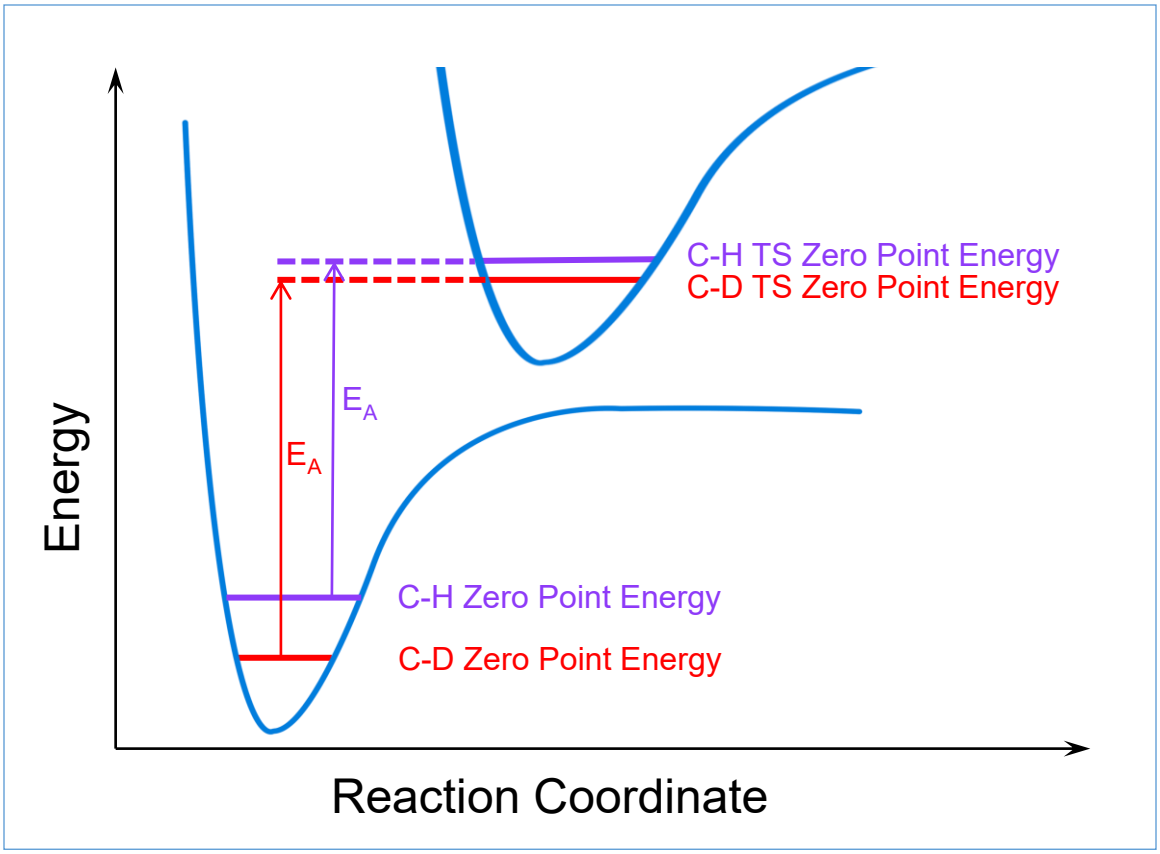

Figure 1.4. Zero-point energy differences and corresponding activation energy differences for the heavy and light isotopologues.

For organic reactions that occur at near ambient temperatures, in which a bond to the isotope is broken (e.g, proton transfers), the major factors that result in an observable KIE are isotopologue zero-point energy (ZPE) differences between the reactants and transition states (Fig. 1.4) and reaction coordinate contribution. In other cases, for example secondary deuterium KIEs (SDKIEs), ZPE differences is a main contributor to KIE. A heavier isotopologue has a lower ZPE, e.g., using the simple harmonic approximation (Hooke's Law) it is clear that a C-D bond has a lower vibrational frequency than a C-H bond because of a higher reduced mass m_r and that the bond force constant (κ) is not changed on addition of a neutron(s) to a nucleus (eq. 1.1).[18]

$$\boldsymbol{\nu} = \frac{1}{2\pi}\sqrt{\frac{\kappa}{m_r}} \quad where\ \boldsymbol{m_r} = \frac{m_1 m_2}{m_1 + m_2}\ ; \qquad (1.1)$$

$\boldsymbol{\nu}$ is a vibrational frequency of the bond;
$\boldsymbol{m}_1$ and $\boldsymbol{m}_2$ are atomic masses of the isotopologues;
$\boldsymbol{\kappa}$ stands for the bond force constant.

The ZPE can be calculated from the bond vibrational frequency according to equation 1.2. At the transition state, for C–H/D bond cleavage, the ZPE differences between the two isotopologues diminish and the lower ground state ZPE for C–D bond results in a higher activation energy for bond cleavage in comparison to a C–H bond thus giving rise to a normal KIE.

$$E = \frac{1}{2}h\nu \qquad (1.2)$$

If the position of isotopic substitution undergoes bond cleavage or formation at the reaction TS then this effect is classified as a primary KIE. Larger primary KIEs are observed when the relative isotopic mass change is significant (i.e. deuterium or tritium substitution). In cases for heavier atom substitutions (i.e., ^{13}C, ^{18}O), primary KIEs are much smaller. A maximal value of 6.9 is predicted for a primary k_H/k_D, based on the assumption that the ZPE difference between the stretching vibrations of C–H and C–D bonds fully disappears at the reaction transition state. However, much larger primary hydrogen KIEs of 5 – >100 have been observed for organic reactions and enzyme catalyzed processes.[19–21] These unusually large hydrogen KIEs can not be explained by differences in ZPEs but are a result of quantum mechanical tunneling, which occurs when the isotope "tunnels" through the potential energy barrier.[18]

When the site of isotopic substitution is not undergoing bonding changes at the TS the effects are categorized as secondary KIEs. Secondary kinetic isotope effects are generally much smaller than primary effects. Secondary deuterium KIEs (SDKIEs) can be classified as α-, β- or remote and these designations correspond to the position of attachment being at the reaction centre (α), on the adjacent heavy atom (β), or at a more remote position.

α-SDKIEs are usually analyzed in terms of reaction centre rehybridization and in certain cases allow researchers to distinguish directly between S_N1 and S_N2 reactions.[22–24] S_N1 reactions typically exhibit large secondary kinetic isotope effects that can often be close to the theoretical maximum of about 1.22, while many S_N2 reactions typically yield kinetic isotope effects that are close to unity.[22] However, in both cases α-SDKIEs are strongly dependent on the nature of the nucleophile[25] and the leaving group[23] (Table 1.1) and can vary significantly for the same reaction mechanism. In order to reach conclusions

concerning the reaction mechanism α-SDKIEs should be carefully analyzed in conjunction with primary carbon KIEs, leaving group KIEs, nucleophile KIEs and β-SDKIEs.

Table 1.1. α-SDKIEs on S_N1 and S_N2 reactions

S_N1 Solvolysis of 3-pentyn-2-yl compounds in 70% trifluoroethanol – 30% water[23]		**S_N2 Reaction between 3,5-disubstituted pyridines and methyl iodide[25]**	
Leaving group	**α-SDKIE**	**Nucleophile**	**α-SDKIE**
Br^-	1.123	3,5-diCH_3	0.908
I^-	1.089	unsubstituted	0.850
OTs^-	1.226	3,5-diCl	0.810

In case of nucleophilic substitution reactions of glycosides and glycosyl fluorides α-SDKIEs do not provide the necessary information to allow researchers to distinguish directly between mechanisms that involve dissociative TSs or "exploded"[26] associative transition states in which both the leaving group and nucleophile are present (Table 1.2) Of note the reported α-SDKIE values are not significantly different for S_N2, S_Ni, and S_N1 mechanisms. This is a consequence of the rehybridization of the anomeric carbon, which is changing from sp^3 to sp^2, being similar at the dissociative and the exploded bimolecular TSs. Primary ^{13}C-KIE and β-SDKIE help to clarify the reaction mechanism for these glycoside substitution reactions. Primary carbon KIEs are larger for exploded S_N2 reactions ($k_{12}/k_{13} > 1.02$) but are closer to unity for dissociative processes that proceed via pyranosylium ion intermediates.[27]

Table 1.2. Select KIEs on hydrolysis of α-D-glucopyranosyl fluoride

Glycosidic C–F bond cleavage pathway	**Mechanism**	**α-SDKIE**	**β-SDKIE**	**Anomeric ^{13}C-KIE**
Loose concerted TS[28]	S_N2, Nuc = N_3^-	1.192 ± 0.006	1.046 ± 0.007	1.024 ± 0.006
Internal return[29]	S_Ni, ROH = hexafluoroisopropanol	1.185 ± 0.006	1.080 ± 0.010	1.008 ± 0.007
Acid catalyzed[30]	S_N1	1.219 ± 0.021	1.099 ± 0.024	1.014 ± 0.005
α-glucoamylase catalyzed*,[31]	S_N1	1.171	1.058	1.017

*KIE values for the ^{2}H and ^{13}C are calculated from the reported KIEs of Tanaka et al.[31] for ^{3}H and ^{14}C according to the Swain equation: $ln\left(\frac{k_H}{k_T}\right)/ln\left(\frac{k_H}{k_D}\right) \approx 1.44$ *and* $ln\left(\frac{k_{12}}{k_{14}}\right)/ln\left(\frac{k_{12}}{k_{13}}\right) \approx 1.9$.

The origin of β-SDKIE for nucleophilic substitution reactions arises from a hyperconjugative weakening of the C−H/(D) bond as positive charge develops at the

reaction centre (S_N1 reactions result in an empty p-orbital). In case of glycosides and glycosyl fluorides β-SDKIEs are indicative of positive charge development at the anomeric centre and can help identifying reaction pathway and TS geometry. The magnitude of β-SDKIEs can provide insights into TS conformations,[32,33] as hyperconjugation depends on the dihedral angle between the C−H/(D) bond and the developing p-orbital. Maximum β-SDKIE is observed when the C–H/(D) bond and the developing p-orbital are exactly aligned in the TS and β-SDKIE values close to unity corresponds a close to orthogonal alignment. Hence, β-SDKIEs are different for the glycosides of different anomeric configurations[32,33] (Table 1.3, note significant differences in β-SDKIEs for α- and β- methyl glucosides and glucosyl fluorides) as they have different pyranose ring conformations in the transition state. Careful inspection of a panel of KIEs (α-SDKIE, β-SDKIE, anomeric ^{13}C, ring ^{18}O, leaving group, where possible, and remote C-5/C-6 deuterium) is therefore needed to delineate the mechanism for nucleophilic substitution at glycosides.

Table 1.3. Select KIEs on hydrolyses of α- and β-D-glucosyl compounds

Isotope label	methyl α-D-glucoside KIE[a,33]	methyl β-D-glucoside KIE[a,33]	α-D-glucopyranosyl fluoride KIE[b,32]	β-D-glucopyranosyl fluoride KIE[c,32]
α-D	1.137 ± 0.007	1.089 ± 0.006	1.142 ± 0.008	1.086 ± 0.001
β-D	1.073 ± 0.003	1.045 ± 0.004	1.067 ± 0.008	1.030 ± 0.008
^{18}O-ring	0.996 ± 0.001	0.991 ± 0.002	0.984 ± 0.005	0.985 ± 0.005
^{13}C-anomeric	1.007 ± 0.001	1.011 ± 0.002	1.032 ± 0.003	1.017 ± 0.002

[a]Acid-catalyzed in 2.0 M $HClO_4$ at 80°C. [b]In 0.2 M sodium succinate buffer, pH 6.0, I = 1.0 M ($NaClO_4$) at 50°C. [c]In 0.3 M Bis-Tris buffer, pH 6.0, I = 1.0 M ($NaClO_4$) at 50°C.

1.2.2. Kinetics of Enzymatic Reactions

In order to discuss KIEs on enzyme-catalyzed reactions an introduction to the essential kinetic parameters and the resulting equations that describe the standard kinetic model for enzyme catalysis is required. The quintessential equation that describes the reaction rate for a single substrate enzyme was introduced in 1913 by Michaelis and Menten (Eq. 1.3).[34] In this equation v_0 is the instantaneous reaction rate, V_{max} is the maximum reaction rate, K_m, the Michaelis constant, is the substrate concentration at which $v_0 = ½V_{max}$, and [S] is the substrate concentration.

$$v_0 = \frac{V_{max}[S]}{K_m + [S]} \qquad (1.3)$$

For the purposes of further discussion we will consider the following kinetic scheme for a generic retaining glycoside hydrolase-catalyzed reaction (Scheme 1.1) and we will derive a Michaelis-Menten expression, assuming that a large excess of substrate, relative to enzyme, is used ([S]>>[E]), under steady-state conditions. That is, the concentrations of enzyme bound intermediates, [ES] and [EP], are constant.

Scheme 1.1. General mechanism for an enzyme-catalyzed reaction.

$$E + S \underset{k_{-1}}{\overset{k_1}{\rightleftharpoons}} ES \xrightarrow{k_2} EP \xrightarrow{k_3} E + P$$

Application of the steady-state approximation to [ES] and [EP] gives us

$$k_1[E][S] = (k_{-1} + k_2)[ES] \tag{1.4}$$

$$k_3[EP] = k_2[ES]. \tag{1.5}$$

Applying the mass conservation law for the enzyme

$$[E]_0 = [E] + [ES] + [EP]$$

and combining eq. 1.4 and eq. 1.5 so as to eliminate [EP] and solve for [ES]:

$$k_1\left([E]_0 - [ES] - \frac{k_2}{k_3}[ES]\right)[S] = (k_{-1} + k_2)[ES]$$

$$[ES] = \frac{k_1 k_3 [E]_0[S]}{k_1(k_2 + k_3)[S] + k_3(k_{-1} + k_2)}\,. \tag{1.6}$$

Dividing the numerator and the denominator of eq. 1.6 by $k_1(k_2 + k_3)$ we get:

$$[ES] = \frac{\frac{k_3}{k_2 + k_3}[E]_0[S]}{\frac{k_3(k_{-1} + k_2)}{k_1(k_2 + k_3)} + [S]}.$$

Since the rate law for kinetic scheme 1.1 is

$$v = \frac{d[P]}{dt} = k_3[EP] = k_2[ES],$$

We now have

$$v = \frac{\frac{k_2 k_3}{k_2 + k_3}[E]_0[S]}{\frac{k_3(k_{-1} + k_2)}{k_1(k_2 + k_3)} + [S]} \tag{1.7}$$

Or, in the Michaelis-Menten form

$$v = \frac{V[S]}{K + [S]} \; where \; V = \frac{k_2 k_3 [E]_0}{k_2 + k_3} \; and \; K = \frac{k_3(k_{-1} + k_2)}{k_1(k_2 + k_3)} . \tag{1.8}$$

We also define the expression for *V/K* for later use:

$$\frac{V}{K} = \frac{k_1 k_2 [E]_0}{k_{-1} + k_2} . \tag{1.9}$$

1.2.3. Measurement of KIEs for Enzymatic Reactions

For enzyme-catalyzed reactions, KIEs can be measured on the turnover number or maximal rate (*V*) and on the enzymatic efficiency (*V/K*).[35] In general, KIEs on enzyme-catalyzed reactions are measured using two different approaches: (i) separate rate constant measurements for each isotopologue, and (ii) competitive determination of rate constant ratios.[16]

Separate measurements of rate constants allows the determination of KIEs on both *V* and *V/K*. However, separate measurements are susceptible to higher systematic errors than are competitive measurements. By considering the mechanistic scheme 1.1 for an isotopically substituted substrate S', we can derive a set of equations that are similar to eq. 1.8 and eq. 1.9, which were derived for the unlabelled substrate.

$$v' = \frac{V'[S']}{K' + [S']} \; where \; V' = \frac{k_2' k_3' [E]_0}{k_2' + k_3'} \; and \; K' = \frac{k_3'(k_{-1}' + k_2')}{k_1'(k_2' + k_3')} \tag{1.10}$$

$$\frac{V'}{K'} = \frac{k_1' k_2' [E]_0}{k_{-1}' + k_2'} \tag{1.11}$$

V and *K* can be obtained separately for each isotopologue by determining *v* as a function of [S] or [S'], which makes it possible to evaluate both *V*/*V*', that is, the KIE on the turnover number, and (*V*/*K*)/(*V*'/*K*'), the KIE on enzymatic efficiency.

In contrast, evaluation of KIEs by competitive methods only allows the determination of isotope effects on *V*/*K*, irrespective of the substrate concentration.[16] In order to illustrate this, we need to elaborate the kinetic scheme as in the competitive experiment as both S and S' are simultaneously present in the reaction mixture. Consequently, each behaves as a competitive inhibitor for the other isotopologue: specifically, active sites on the enzyme occupied by S are unavailable for S' and vice versa. Under such conditions steady-state expressions for [ES] and [ES'] can be written as:

$$k_1([E]_0 - [ES] - [ES'] - [EP] - [EP'])[S] = (k_{-1} + k_2)[ES] \qquad (1.12)$$

$$k_1'([E]_0 - [ES] - [ES'] - [EP] - [EP'])[S'] = (k'_{-1} + k_2')[ES']. \qquad (1.13)$$

Since we are interested in measuring rate constant ratio for the unlabelled isotopologue S to that of heavy isotopologue S', and the ratio *v*/*v*' is given by equation 1.14

$$\frac{v}{v'} = \frac{k_2[ES]}{k_2'[ES']}, \qquad (1.14)$$

we can solve equations 1.12 and 1.13 for [ES] and [ES'], respectively, and obtain the [ES]/[ES'] ratio, which leads to:

$$\frac{v}{v'} = \frac{\frac{k_1 k_2}{k_{-1} + k_2}[S]}{\frac{k_1' k_2'}{k'_{-1} + k_2'}[S']}.$$

If $k = v/[S]\ and\ k' = v'/[S']$, then:

$$\frac{k}{k'} = \frac{\frac{k_1 k_2}{k_{-1} + k_2}}{\frac{k_1' k_2'}{k'_{-1} + k_2'}}. \qquad (1.15)$$

Comparing this expression (Eq. 1.15) with equations 1.9 and 1.11 shows that:

$$\frac{k}{k'} = \frac{V/K}{V'/K'}.$$

Therefore, in cases of competitive experiments the separate evaluation of KIEs on *V* and *K* is not possible.

Measurement of KIEs using separate rate constant determinations requires the use of highly enriched isotopologues.[16,36] Whereas, competitive techniques are much more versatile and can be performed using radiolabelled tracers,[37–39] natural abundance (stable isotopes) materials,[40,41] or highly enriched samples.[16,42] In general, competitive techniques minimize systematic errors, which can be caused by concentration and temperature differences when separate reactions are monitored, and as a result competitive KIE measurements are intrinsically more accurate and precise.[17]

Competitive techniques for KIE measurements include the use of radiochemical scintillation counting,[16] whole molecule mass-spectrometry,[16,43] nuclear magnetic resonance spectroscopy (NMR)[40–42] and polarimetry.[44,45] However, none of these methods can be applied universally as each technique possesses intrinsic limitations. For example, radiochemical methods require the chemical synthesis of radioactive substrates, which limits measurements to readily available radioisotopes, and the ability to purify the radiolabelled starting materials from the products prior to scintillation counting. Polarimetry is not compatible with systems that are highly absorbing and it is inherently insensitive.

NMR spectroscopy has been used to measure deuterium KIEs in organic and biological reactions since 1980s.[46,47] Over the past two decades advances in NMR instrumentation and data acquistion procedures have evolved so as to allow the measurement of secondary deuterium and heavy atom isotope effects using natural abundance starting materials[41,48] and to facilitate the continuous monitoring of highly enriched materials.[42] A more detailed discussion of the latter NMR technique is provided in the Chapter 2 of this thesis, which comprises the manuscript “Measurement of Kinetic Isotope Effects by Continuously Monitoring Isotopologue Ratios Using NMR Spectroscopy” published in the book series *Methods in Enzymology* (**2017**, *596*, 547-571).

1.2.4. Commitment to Catalysis

In theory, the experimental measurement of enzymatic KIEs can be modulated by multiple kinetically significant events, such as binding and release of substrates and/or products, conformational changes associated with ligand binding or release, change of protonation states of enzymatic residues and the substrate(s), and multiple chemical conversions within the reactive complex. Thus, experimental measurements always yield an observed KIE (KIE_{obs}), whereas, the research goal is to measure the intrinsic KIE (KIE_{int}). KIE_{int} is the isotope effect on the actual bond cleavage/formation step and thus it does not contain contributions from non-chemical kinetic steps. As a result, the KIE_{int} reflects the situation where only chemical steps are kinetically significant (rate-limiting or irreversible), which is important for TS analysis in terms of delineating the chemical mechanism of enzymatic catalysis.

'Commitment to catalysis'[49] is the term used to describe the partitioning of enzyme-bound species that occur in the enzymatic mechanism. In the kinetic scheme 1.1 the chemical step is the conversion of ES to EP described by the rate constant k_2. The forward commitment (C_f) in this case can be defined as the ratio of the isotopically sensitive rate constant in the forward direction to the net rate constant for the breakdown of the reactive ES complex into E and S (equation 1.16):

$$C_f = \frac{k_2}{k_{-1}} \qquad (1.16)$$

Some enzymes are so efficient that nearly every molecule of substrate that binds is converted into products.[50] For such cases, substrate binding is the first irreversible step for these reactions. This means that the measured competitive isotope effects will only reflect binding isotope effects. Intrinsic KIEs can be calculated from observed KIEs knowing the values of commitment factors. The closer is C_f to 0, the closer is KIE_{obs} to KIE_{int}. Experimental conditions can often be modified to achieve this; for example, one can use worse substrates, mutant enzymes or non-optimal reaction conditions (pH and temperature).[51–53]

If an enzymatic reaction has several rate-limiting steps commitment factors are low for these corresponding steps.[54] Each partially rate-limiting step has its microscopic

transition state, and the observed TS is the weighted average of these microscopic transition states. In such case the observed TS is called a virtual transition state.[55]

1.3. Glycosyl Fluorides

Glycosyl fluorides are an important class of carbohydrate derivatives that are widely used to study acid-, base-, water- and enzyme-catalyzed reaction mechanisms.[26,28,29,31,32,56–59] Specifically, these materials can be used as mechanistic probes for glycoside hydrolases and other carbohydrate processing enzymes, and as reagents for enzymatic glycosylations. Glycosyl fluorides are readily accessible synthetically, have sufficient lifetimes in aqueous media for use as enzyme substrates, and they can be conveniently detected by ^{19}F-NMR spectroscopy. Thus, allowing ^{19}F-NMR spectroscopic monitoring of enzymatic reactions in aqueous solutions.

1.3.1. Substrates for Glycoside Hydrolases

Glycosyl fluorides are useful substrates for the glycoside hydrolases as most of these enzymes can process the anomer that corresponds to the substrate.[60] Typically, glycosyl fluorides are excellent substrates and show high k_{cat}/K_m values. This is beneficial when working with small amounts of enzyme and for the determination of K_i values for tight-binding inhibitors. Glycosyl fluorides are also commonly used for the determination of the stereochemical outcome of the GH-catalyzed hydrolysis due to their high k_{cat}/K_m values and that they are substrates for GHs operating via classical nucleophilic substitution mechanisms (Fig. 1.5).[61,62]

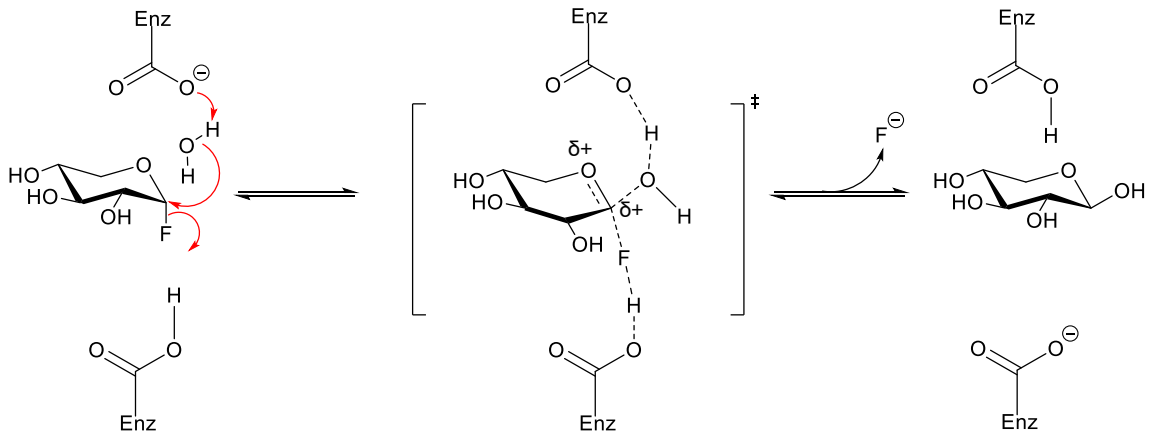

Figure 1.5. Mechanism of hydrolysis of α-xylosyl fluoride by an inverting α-xylosidase.

Hydrolytic cleavage of the C–F bond can be monitored by various methods including: the measurement of hydrogen fluoride production using a pH stat,[63] a coupled assay for the detection of either glucose or galactose released, through the use of glucose or galactose oxidase,[64] a fluoride ion-specific electrode,[58] a fluoride specific dye that allows for the direct spectrometric observation of fluoride release,[65–67] and ^{19}F-NMR spectroscopy.[28,29] The detection of fluoride with an ion-selective electrode has distinct advantages over other methods mentioned above due to its generality, simplicity and accuracy.

Many inverting glycoside hydrolases and one retaining have been shown to be able to process the glycosyl fluoride of the 'wrong' anomeric configuration.[59,68–70] This was first demonstrated in 1979 by Hehre and co-workers for β-amylase. They have shown that this inverting α-glucan hydrolase could catalyze the hydrolysis of β-maltosyl fluoride.[68] The hydrolysis proceeds via an initial transglycosylation and formation of a coupled product with inversion of the anomeric configuration (fig. 1.6). The resulting transglycosylation product has the preferred anomeric stereochemistry for the enzyme and is hydrolyzed with inversion of stereoconfiguration, resulting in the net retention of stereochemistry relative to the initial glycosyl fluoride. This mechanism is supported by the observation that the rate of hydrolysis shows a dependence on the square of the substrate concentration and that the rate increases upon addition of alternative acceptor molecules. The mechanism is commonly referred to as the Hehre resynthesis–hydrolysis mechanism.

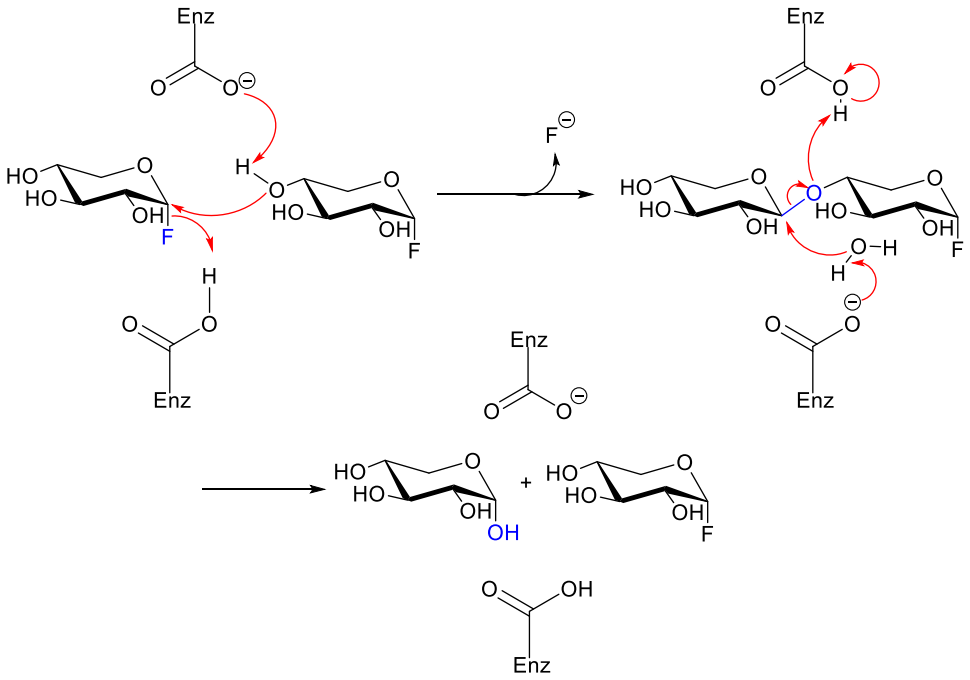

Figure 1.6. Hehre resynthesis-hydrolysis mechanism for the processing of the glycosyl fluoride of the 'wrong' anomeric configuration.

1.3.2. Substituted Glycosyl Fluorides as Mechanistic Probes for Glycoside Hydrolases

Substituted glycosyl fluorides have been successfully used to study the mechanisms of action for retaining glycoside hydrolases. The introduction of the strongly electronegative fluorine atom at C2 or C5 destabilizes pyranosylium-ion like transition states, an effect that slows both the glycosylation and deglycosylation steps and thus increases the lifetime of the glycosyl-enzyme intermediate.

The first class of substituted glycosyl fluorides that were developed to trap glycosyl-enzyme intermediates, and as a result were called mechanism-based inactivators of retaining β-glycosidases, were the aryl 2-deoxy-2-fluoro-β-D-glycosides and 2-deoxy-2-fluoro-β-D-glycosyl fluorides (fig. 1.7, compounds **1** & **2**). Introduction of the strongly electron withdrawing fluorine at the C-2 position together with the good leaving group, typically, fluorine (fig. 1.7, compound **1**) or an electron-deficient aryl group, such as 2,4-dinitrophenolate[71,72] allow structural characterization of the glycosyl-enzyme intermediate.[73–75] As noted above, introduction of a fluorine destabilizes positively charged transition states by reducing the rates of glycosylation and deglycosylation. At the same

time, introduction of a good leaving group renders the glycosyl-enzyme intermediate kinetically accessible, while its hydrolysis is very slow. The inhibition of β-glucosidase and β-mannosidase by 2-deoxy-2-fluoro-β-glucopyranosyl and mannopyranosyl fluorides has been demonstrated *in vivo*.[76] These compounds have been shown to cross the blood/brain barrier and to inactivate the corresponding glycosidase. Radiolabelled 2,6-dideoxy-2-fluoro-6-[^{18}F]-fluoro-β-D-glucopyranosyl fluoride (fig. 1.7, compound **5**) has been suggested as a potential PET-imaging probe for glucocerebrosidase.[77]

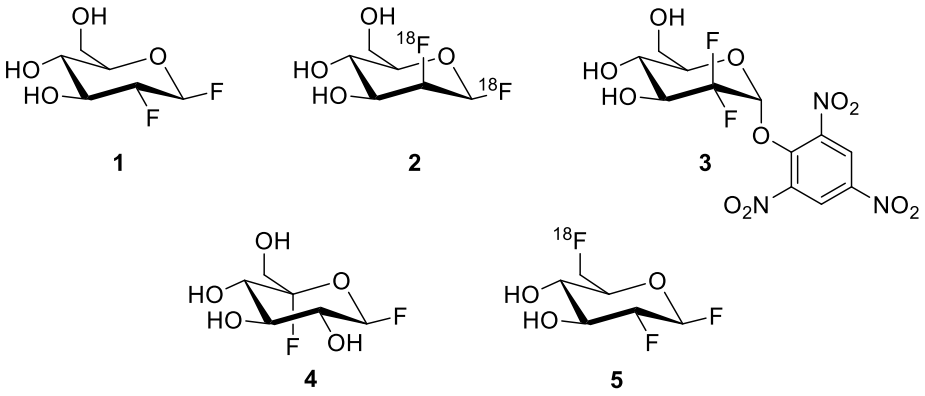

Figure 1.7. Chemical structures of several substituted glycosyl fluorides.

The second class of substituted glycosyl fluorides, e.g., 2-deoxy-2,2-difluoro-α-D-glucosides (fig. 1.7, compound **3**), developed by Withers and co-workers, are inactivators of various α-glycosidases.[78] Interestingly, the lifetime of β-glycosyl-enzyme intermediates that are formed during α-glycosidase-catalyzed reactions are short and require a second fluorine atom at C-2 to retard hydrolysis sufficiently to allow intermediate accumulation and this necessitates the use of an highly activated 2,4,6-trinitrophenoate leaving group.

A third class of substituted glycosyl fluorides are the 5-fluoro-glycosyl fluorides (fig. 1.7, compound **4**). These compounds have been demonstrated to trap effectively intermediates for both α- and β-glycosidases.[10,75,79] This class of substituted glycosyl fluorides also has the advantage of preserving all the hydroxyl groups on the carbohydrate ring, which is not possible for C2-fluorination.

1.3.3. Donors in Enzymatic Glycosylation Reactions

The synthesis of oligosaccharides, including the carbohydrate portions of various glycoproteins, is of great interest.[80–82] Chemoenzymatic approaches can provide

substantial quantities of complex oligosaccharides, in a timely fashion, and allow the simplification of protective group strategies that are necessarily complex for conventional chemical synthesis involving saccharide donors and acceptors. Glycosyl fluorides have been shown to serve as glycosyl donors in enzymatic glycosylation reactions catalyzed by glycosidases[83–85], glycosynthases[86] and glycosyltransferases.[87]

Retaining glycosidases have been successfully used in transglycosylation reactions.[88] That is, the reaction of the obligate glycosyl-enzyme intermediate (fig. 1.2) with an acceptor alcohol, rather than water, results in the formation of a new glycosidic bond (transglycosylation). Glycosyl transfer is effected by running the reaction at high concentrations, using a large excess of the acceptor, lowering the effective water concentration, and by using activated donor substrates. Glycosyl fluorides are suitable donors for transglycosylation reaction with glycosidases due to their high k_{cat}/K_m values that facilitate the accumulation of the transglycosylation product. Additionally, in cases of glycosyl fluoride donors the major by-product of glycosylation is fluoride ion, which is easy to separate from the oligosaccharide product.

Glycosynthases are mutant glycoside hydrolases that have an unreactive alanine[86,89] or serine[90] residue incorporated in place of the nucleophilic carboxyl residue. These enzymes catalyze transglycosylation without the normally associated hydrolysis of the product,[86] That is, these mutant enzymes utilize the Hehre resynthesis mechanism (fig. 1.6), which leads to accumulation of the oligosaccharide product often in high yields. Glycosynthases are particularly useful for transglycosylations with acceptors, which can function as inhibitors of the wild-type enzymes.[86]

α-Galactopyranosyl fluoride has been shown to act as a substrate for the α-galactosyltransferase from *Neisseria meningitidis*.[87] In the presence of uridine 5'-diphosphate (UDP), α-galactopyranosyl fluoride can function as a replacement for the natural substrate, uridine-5'-diphospho-α-D-galactose. When a suitable acceptor sugar is present the corresponding oligosaccharide is formed (Scheme 1.2 A). In absence of the acceptor, uridine-5'-diphospho-α-D-galactose is produced from UDP and α-galactopyranosyl fluoride. The proposed mechanism is shown in Scheme 1.2 B,[87] although a S_Ni reaction, via a bound pyranosylium ion intermediate is also a possibility.[91,92] This finding can potentially help solve problems associated with the large-scale synthesis of activated sugar nucleotide donors.

Scheme 1.2. ***N. meningitidis*** **α-galactosyltransferase (lgtC-19) catalyzed formation of oligosaccharide (A) or UDP-Gal (B).**

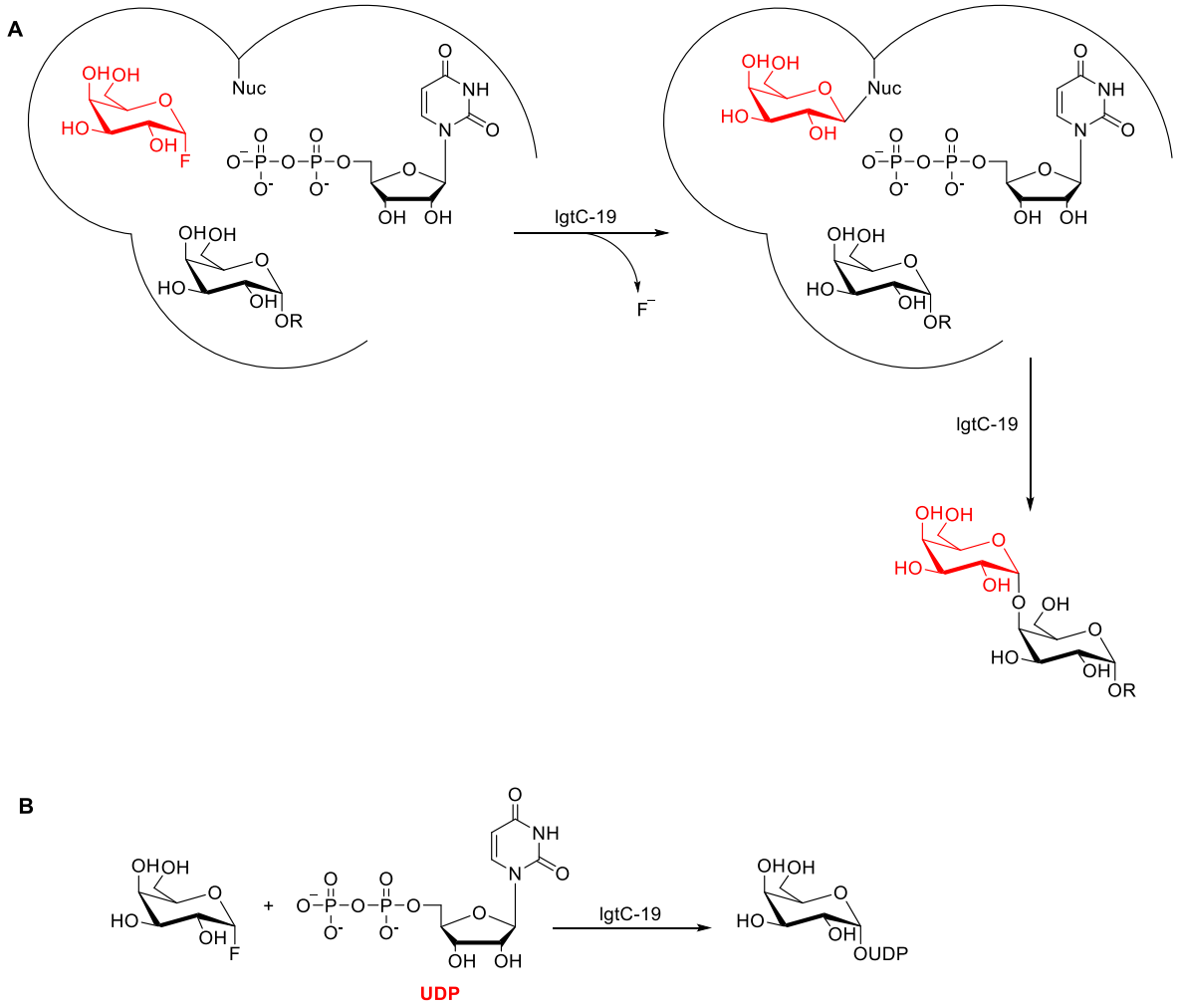

1.4. Thesis Overview

The research discussed in this thesis includes an analysis of the mechanistic aspects of several glycoside hydrolases elucidated by measuring kinetic isotope effects by a direct NMR spectroscopic method as well as a review of the scope and limitations of the NMR method for competitive KIEs measurement in biological systems.

A general introduction of the catalytic mechanisms of glycoside hydrolases has been discussed in Chapter 1. The same chapter includes an overview of the KIEs as a mechanistic tool to study reaction transition states, and glycosyl fluorides as mechanistic probes for glycoside hydrolases.

Chapter 2 presents a published manuscript in the book series *Methods in Enzymology* (N. Sannikova, A. R. Lewis and A. J. Bennet, Measurement of Kinetic Isotope Effects by Continuously Monitoring Isotopologues Ratios Using NMR Spectroscopy, *Methods in Enzymology*, **2017**, *596*, 547-571). Nuclear magnetic spectroscopic (NMR) methods are discussed for the measurement of heavy atom (^{13}C, ^{18}O, ^{15}N) and secondary deuterium kinetic isotope effects by the continuous monitoring of isotopically enriched materials including experimental design, data acquisition and analysis.

Chapter 3 comprises the published manuscript in *Biochemistry* (N. Sannikova, C. A. N. Gerak, F. S. Shidmoossavee, D. T. King, S. Shamsi Kazem Abadi, A. R. Lewis and A. J. Bennet, *Biochemistry***, 2018**, *57* (24), 3378-3386). In this study we used a ^{19}F NMR spectroscopy protocol with a remote labelling strategy to measure multiple competitive KIEs on singly and doubly deuterated substrates using a variety of metal cation activators, which allowed refinement of mechanism for *C. freundii* MelA α-galactosidase-catalyzed hydrolysis. Additionally, the synthesis of the panel of unlabelled and deuterated fluoroaryl α-D-galactopyranosides is described, combined with the kinetic assays used to measure the detailed KIEs for each isotopologue.

Chapter 4 focuses on a mechanistic investigation of two GH15 inverting α-glucoamylases from *A. niger* and *Rhizopus sp.* We have obtained complete set of competitive KIEs for both enzymes, including 5-^{18}O KIE and γ-secondary deuterium (5-^{2}H) KIE using a direct ^{19}F NMR spectroscopic method. The experimental KIEs will be used as constraints for theoretical modelling of the TS for *A. niger* α-glucoamylase using

modern computational chemistry methods (QM/MM and DFT). The synthesis of the panel of isotopically labelled α-D-glucopyranosyl fluorides is outlined.

Chapter 5 focuses on the mechanistic evaluation of the Hehre resynthesis-hydrolysis mechanism, common for GHs able to process corresponding glycosyl fluoride of the 'wrong' anomeric configuration. We have shown that GH55 inverting exo-1,3-β-D-glucanase from *T. virens* can hydrolyse α-D-glucopyranosyl fluoride via Hehre mechanism and measured multiple competitive KIEs for this reaction. This allowed to characterize the TS for Hehre resynthesis-hydrolysis mechanism.

Chapter 6 describes the proposed future work related to this thesis on the basis of our present results and interpretations.

1.5. References

1. Bourne, Y. & Henrissat, B. Glycoside hydrolases and glycosyltransferases: families and functional modules. *Curr. Opin. Struct. Biol.* **11,** 593–600 (2001).

2. McNaught, A. D. & Wilkinson, A. *International Union of Pure and Applied Chemistry. Compendium of Chemical Terminology: IUPAC Recommendations. IUPAC Compendium of Chemical Terminology* (1997). doi:10.1351/goldbook.I03352

3. Ajit Varki, Richard D Cummings, Jeffrey D Esko, Hudson H Freeze, Pamela Stanley, Carolyn R Bertozzi, Gerald W Hart, and M. E. E. *et al. Essentials of Glycobiology, 2nd edition*. *Essentials of Glycobiology. Cold Spring Harbor (NY): Cold Spring Harbor Laboratory Print* (2009). doi:10.1016/S0962-8924(00)01855-9

4. Davies, G. & Henrissat, B. Structures and mechanisms of glycosyl hydrolases. *Structure* **3,** 853–859 (1995).

5. Koshland, D. E. Stereochemistry and the Mechanism of Enzymatic Reactions. *Biol. Rev.* **28,** 416–436 (1953).

6. Jongkees, S. A. K. & Withers, S. G. Unusual enzymatic glycoside cleavage mechanisms. *Acc. Chem. Res.* **47,** 226–235 (2014).

7. Henrissat, B. A classification of glycosyl hydrolases based on amino acid sequence similarities. *Biochem. J* **280,** 309–316 (1991).

8. Davies, G. J. & Sinnott, M. L. Sorting the diverse: The sequence-based classifications of carbohydrate-active enzymes. *Biochem. (Lond).* **30,** 26–32 (2008).

9. Vocadlo, D. J. & Davies, G. J. Mechanistic insights into glycosidase chemistry. *Curr. Opin. Chem. Biol.* **12,** 539–555 (2008).

10. Zechel, D. L. & Withers, S. G. Glycosidase mechanisms: Anatomy of a finely tuned catalyst. *Acc. Chem. Res.* **33,** 11–18 (2000).

11. Yip, V. L. Y. *et al.* An unusual mechanism of glycoside hydrolysis involving redox and elimination steps by a family 4 β-glycosidase from Thermotoga maritima. *J. Am. Chem. Soc.* **126,** 8354–8355 (2004).

12. Yip, V. L. Y. & Withers, S. G. Mechanistic analysis of the unusual redox-elimination sequence employed by Thermotoga maritima BglT: A 6-phospho-β-glucosidase from glycoside hydrolase family 4. *Biochemistry* **45,** 571–580 (2006).

13. Yip, V. L. Y., Thompson, J. & Withers, S. G. Mechanism of GlvA from Bacillus subtilis: a detailed kinetic analysis of a 6-phospho-alpha-glucosidase from glycoside hydrolase family 4. *Biochemistry* **46,** 9840–52 (2007).

14. Rajan, S. S. *et al.* Novel catalytic mechanism of glycoside hydrolysis based on the structure of an NAD+/Mn2+-dependent phospho-α-glucosidase from Bacillus subtilis. *Structure* **12,** 1619–1629 (2004).

15. Chakladar, S., Cheng, L., Choi, M., Liu, J. & Bennet, A. J. Mechanistic evaluation of MelA a-galactosidase from Citrobacter freundii: A family 4 glycosyl hydrolase in which oxidation is rate-limiting. *Biochemistry* **50,** 4298–4308 (2011).

16. Melander, L. C. S. & Saunders, W. H. *Reaction rates of isotopic molecules*. (Wiley, 1980).

17. Kohen, A. & Limbach, H.-H. *Isotope effects in chemistry and biology*. (Taylor & Francis, 2006).

18. Anslyn, E. V. & Dougherty, D. A. *Modern physical organic chemistry*. (University Science, 2006).

19. Lewis, E. S. & Funderburk, L. Rates and isotope effects in the proton transfers from 2-nitropropane to pyridine bases. *J. Am. Chem. Soc.* **89,** 2322–2327 (1967).

20. Kohen, A. & Klinman, J. P. Enzyme Catalysis: Beyond Classical Paradigms. *Acc. Chem. Res.* **31,** 397–404 (1998).

21. Truhlar, D. G. *et al.* The Incorporation of Quantum Effects in Enzyme Kinetics Modeling. *Acc. Chem. Res.* **35,** 341–349 (2002).

22. Westaway, K. C. Using kinetic isotope effects to determine the structure of the transition states of SN2 reactions. *Adv. Phys. Org. Chem.* **41,** 217–273 (2006).

23. Shiner, V. J. & Dowd, W. Dependence of solvolytic .alpha.-deuterium rate effects on the nature of the leaving group. *J. Am. Chem. Soc.* **93,** 1029–1030 (1971).

24. Westaway, K. C., Lai, Z.-G. & Westaway, K. C. Solvent effects on SN2 transition state structure. II: The effect of ion pairing on the solvent effect on transition state structure. *Can. J. Chem* **67,** 345–349 (1989).

25. Harris, J. M., Paley, M. S. & Prasthofer, T. W. Transition-State Variation in the Menshutkin Reaction. *J. Am. Chem. Soc* **103,** 5915–5916 (1981).

26. Banait, N. S. & Jencks, W. P. Reactions of Anionic Nucleophiles with α-D-Glucopyranosyl Fluoride in Aqueous Solution through a Concerted, ANDN(SN2) Mechanism. *J. Am. Chem. Soc.* **113,** 7951–7958 (1991).

27. Horenstein, N. A. Mechanisms for nucleophilic aliphatic substitution at glycosides. *Adv. Phys. Org. Chem.* **41,** 275–314 (2006).

28. Chan, J., Sannikova, N., Tang, A. & Bennet, A. J. Transition-State Structure for the Quintessential S_N2 Reaction of a Carbohydrate: Reaction of α-

Glucopyranosyl Fluoride with Azide Ion in Water. *J. Am. Chem. Soc.* **136,** 12225–12228 (2014).

29. Chan, J., Tang, A. & Bennet, A. J. A Stepwise Solvent-Promoted SNi Reaction of α-D-Glucopyranosyl Fluoride: Mechanistic Implications for Retaining Glycosyltransferases. *J. Am. Chem. Soc.* **134,** 1212–1220 (2012).

30. Chan, J., Tang, A. & Bennet, A. J. Transition-state structure for the hydronium-ion-promoted hydrolysis of α- d -glucopyranosyl fluoride. *Can. J. Chem.* **93,** 463–467 (2015).

31. Tanaka, Y., Tao, W., Blanchard, J. S. & Hehre, E. J. Transition State Structures for the Hydrolysis of a-D-Glucopyranosyl Fluoride by Retaining and Inverting Reactions of Glycosylases. *J. Biol. Chem.* **269,** 32306–32312 (1994).

32. Zhang, Y., Bommuswamy, J. & Sinnott, M. L. Kinetic Isotope Effect Study of Transition States for the Hydrolyses of a- and b-Glucopyranosyl Fluorides. *J. Am. Chem. Soc.* **116,** 7557–7563 (1994).

33. Bennet, A. J. & Sinnott, M. L. Complete Kinetic Isotope Effect Description of Transition-States for Acid-Catalyzed Hydrolyzes of Methyl alpha-Glucopyranosides and beta-Glucopyranosides. *J. Am. Chem. Soc.* **108,** 7287–7294 (1986).

34. Johnson, K. A. & Goody, R. S. The Original Michaelis Constant: Translation of the 1913 Michaelis− Menten Paper. *Biochemistry* **50,** 8264–8269 (2011).

35. Cleland, W. W. Use of isotope effects to elucidate enzyme mechanism. *Crit. Rev. Biochem. Mol. Biol.* **13,** 385–428 (1982).

36. Chan, J., Lu, A. & Bennet, A. J. Turnover Is Rate-Limited by Deglycosylation for Micromonospora viridifaciens Sialidase-Catalyzed Hydrolyses: Conformational Implications for the Michaelis Complex. *J. Am. Chem. Soc.* **133,** 2989–2997 (2011).

37. Cook, P. F. & Cleland, W. W. *Enzyme kinetics and mechanism*. (Garland Science, 2007).

38. Parkin, D. W., Leung, H. B. & Schramm, V. L. Synthesis of Nucleotides with Specific Radiolabels in Ribose: Primary 14C and secondary 3H kinetic isotope effects on acid-catalyzed glycosidic bond hydrolysis of AMP, dAMP, and inosine. *J. Biol. Chem.* **259,** 9411–9417 (1984).

39. Sen, A., Stojkovic, V. & Kohen, A. Synthesis of radiolabeled nicotinamide cofactors from labeled pyridines: Versatile probes for enzyme kinetics. *Anal. Biochem.* **430,** 123–129 (2012).

40. Lee, J. K., Bain, A. D. & Berti, P. J. Probing the Transition States of Four

Glucoside Hydrolyses with13C Kinetic Isotope Effects Measured at Natural Abundance by NMR Spectroscopy. *J. Am. Chem. Soc.* **126,** 3769–3776 (2004).

41. Singleton, D. A. & Thomas, A. A. High-Precision Simultaneous Determination of Multiple Small Kinetic Isotope Effects at Natural Abundance. *J. Am. Chem. Soc.* **117,** 9357–9358 (1995).

42. Chan, J., Lewis, A. R., Gilbert, M., Karwaski, M. & Bennet, A. J. A direct NMR method for the measurement of competitive kinetic isotope effects. *Nat. Chem. Biol.* **6,** 405–407 (2010).

43. Berti, P. J., Blanke, S. R. & Schramm, V. L. Transition state structure for the hydrolysis of NAD+ catalyzed by diphtheria toxin. *J. Am. Chem. Soc.* **119,** 12079–12088 (1997).

44. Schimerlik, M. I., Rife, J. E. & Cleland, W. W. Equilibrium Perturbation by Isotope Substitution. *Biochemistry* **14,** 5347–5354 (1975).

45. Zhang, Y., Bommuswamy, J. & Sinnott, M. L. Kinetic Isotope Effect Study of Transition States for the Hydrolyses of a- and b-Glucopyranosyl Fluorides. *J. Am. Chem. Soc.* **116,** 7557–7563 (1994).

46. Pascal, R. A., Baum, M. W., Wagner, C. K., Rodgers, L. R. & Huang, D.-S. Measurement of Deuterium Kinetic Isotope Effects in Organic and Biochemical Reactions by Natural Abundance Deuterium NMR Spectroscopy. *J. Am. Chem. Soc* **108,** 6477–6482 (1986).

47. Sawada, M., Takai, Y., Chong, C., Hanafusa, T. & Misumi, S. Determination of the Secondary a-Deuterium Kinetic Isotope Effect on a Reverse Menschutkin Reaction Using Phosphorus-31 Nuclear Magnetic Resonance Spectrometry. *Anal. Chem.* **58,** 231–233 (1986).

48. Singleton, D. A. & Szymanski, M. J. Simultaneous Determination of Intermolecular and Intramolecular 13 C and 2 H Kinetic Isotope Effects at Natural Abundance. *J. Am. Chem. Soc.* **121,** 9455–9456 (1999).

49. Northrop, D. B. Steady-state analysis of kinetic isotope effects in enzymic reactions. *Biochemistry* **14,** 2644–2651 (1975).

50. Blacklow, S. C., Raines, R. T., Lim, W. A., Zamore, P. D. & Knowles, J. R. Triosephosphate isomerase catalysis is diffusion controlled. *Biochemistry* **27,** 1158–1165 (1988).

51. Schramm, V. L. & Grubmeyer, C. Phosphoribosyltransferase Mechanisms and Roles in Nucleic Acid Metabolism. *Prog. Nucleic Acid Res. Mol. Biol.* **78,** 261–304 (2004).

52. Loveridge, E. J., Behiry, E. M., Guo, J. & Allemann, R. K. Evidence that a

'dynamic knockout' in Escherichia coli dihydrofolate reductase does not affect the chemical step of catalysis. *Nat. Chem.* **4,** 292–297 (2012).

53. Kohen, A., Cannio, R., Bartolucci, S. & Klinman, J. P. Enzyme dynamics and hydrogen tunnelling in a thermophilic alcohol dehydrogenase. *Nature* **399,** 496–499 (1999).

54. Ruszczycky, M. W. & Anderson, V. E. Interpretation of V/K isotope effects for enzymatic reactions exhibiting multiple isotopically sensitive steps. *J. Theor. Biol.* **243,** 328–342 (2006).

55. Gandour, R. D. & Schowen, R. L. *Transition states of biochemical processes*. (Plenum Press, 1978).

56. Sinnott, M. L. & Jencks, W. P. Solvolysis of D-Glucopyranosyl Derivatives in Mixtures of Ethanol and 2,2,2-Trifluoroethanoll. *J. Am. Chem. Soc.* **102,** 2026–2032 (1980).

57. Banait, N. S. & Jencks, W. P. General-acid and general-base catalysis of the cleavage of .alpha.-D-glucopyranosyl fluoride. *J. Am. Chem. Soc.* **113,** 7958–7963 (1991).

58. Konstantinidis, A. & Sinnott, M. L. The interaction of 1-fluoro-D-glucopyranosyl fluoride with glucosidases. *Biochem. J.* **279 (Pt 2),** 587–93 (1991).

59. Matsui, H., Tanaka, Y., Brewer, C. F., Blanchard, J. S. & Hehre, E. J. Hydrolysis of α- and β-d-glucosyl fluoride by individual glucosidases: new evidence for separately controlled "plastic" and "conserved" phases in glycosylase catalysis. *Carbohydr. Res.* **250,** 45–56 (1993).

60. Williams, S. J. & Withers, S. G. Glycosyl fluorides in enzymatic reactions. *Carbohydr. Res.* **327,** 27–46 (2000).

61. Knowles, J. K. C., Lentovaara, P., Murray, M. & Sinnott, M. L. Stereochemical Course of the Action of the Cellobioside Hydrolases I and II of Trichoderma reesei. *J. Chem. Soc. Chem. Commun.* 1401–1402 (1988). doi:10.1039/C39880001401

62. Copa-Patiño, J. L. *et al.* Polarimetry and 13C n.m.r. show that the hydrolyses of beta-D-glucopyranosyl fluoride by beta(1-->3)-glucanases from Phanerochaete chrysosporium and Sporotrichum dimorphosporum have opposite stereochemistries. *Biochem. J.* **293,** 591–594 (1993).

63. Hofstein, B. V. Fluoro-D-galactosides as substrates and inducers of the β-galactosidase of Escherichia coli. *Biochim. Biophys. Acta* **48,** 159–163 (1961).

64. Barnett, J. E., Jarvis, W. T. & Munday, K. A. The hydrolysis of glycosyl fluorides by glycosidases. *Biochem. J.* **105,** 669–72 (1967).

65. Barnett, J. E., Jarvis, W. T. & Munday, K. A. Enzymic hydrolysis of the carbon-fluorine bond of alpha-D-glucosyl fluoride by rat intestinal mucosa. Localization of intestinal maltase. *Biochem. J.* **103,** 699–704 (1967).

66. Hehre, E. J., Genghof, D. S. & Okada, G. The α-amylases as glycosylases, with wider catalytic capacities than envisioned or explained by their representation as hydrolases. *Arch. Biochem. Biophys.* **142,** 382–393 (1971).

67. Street, I. P., Kempton, J. B. & Withers, S. G. Inactivation of a b-Glucosidase through the Accumulation of a Stable 2-Deoxy-2-fluoro-a-D-glucopyranosyl-Enzyme Intermediate: A Detailed Investigation. *Biochemistry* **31,** 9970–9978 (1992).

68. Hehre, E. J., Brewer, C. F. & Genghof, D. S. Scope and Mechanism of Carbohydrase Action: Hydrolytic and Nonhydrolytic Actions of b-Amylase on a- and b-Maltosyl Fluoride. *J. Biol. Chem.* **254,** 5942–5950 (1979).

69. Hehre, E. J., Sawai, T., Brewer, C. F., Nakano, M. & Kanda, T. Trehalase: Stereocomplementary Hydrolytic and Glucosyl Transfer Reactions with a- and b-D-Glucosyl Fluoride. *Biochemistry* **21,** 3090–3097 (1982).

70. Hehre, E. J., Matsui, H. & Brewer, C. F. Hydrolysis of β-d-glucopyranosyl fluoride to α-d-glucose catalyzed by Aspergillus niger α-d-glucosidase. *Carbohydr. Res.* **198,** 123–132 (1990).

71. Withers, S. G., Rupitz, K. & Street, I. P. 2-Deoxy-2-fluoro-D-glycosyl Fluorides: A New Class of Specific Mechanism-Based Glycosidase Inhibitors. *J. Biol. Chem.* **263,** 7929–7932 (1988).

72. Withers, S. G., Street, I. P., Bird, P. & Dolphin, D. H. 2-Deoxy-2-fluoroglucosides: A Novel Class of Mechanism-Based Glucosidase Inhibitors. *J. Am. Chem. Soc.* **109,** 7530–7531 (1987).

73. White, A., Tull, D., Johns, K., Withers, S. G. & Rose, D. R. Crystallographic observation of a covalent catalytic intermediate in a β-glycosidase. *Nat. Struct. Biol.* **3,** 149–154 (1996).

74. Notenboom, V. *et al.* Insights into transition state stabilization of the β-1,4-glycosidase Cex by covalent intermediate accumulation in active site mutants. *Nat. Struct. Biol.* **5,** 812–818 (1998).

75. Uitdehaag, J. C. M. *et al.* X-ray structures along the reaction pathway of cyclodextrin glycosyltransferase elucidate catalysis in the α-amylase family. *Nat. Struct. Biol.* **6,** 432–436 (1999).

76. McCarter, J. D., Adam, M. J., Hartman, N. G. & Withers, S. G. In vivo inhibition of beta-glucosidase and beta-mannosidase activity in rats by 2-deoxy-2-fluoro-beta-glycosyl fluorides and recovery of activity in vivo and in vitro. *Biochem. J.* **301 (Pt 2),** 343–8 (1994).

77. Wong, A. W., Adam, M. J. & Withers, S. G. Synthesis of 2,6-dideoxy-2-fluoro-6-[18F]-fluoro-β-D-glucopyranosyl fluoride (2,6FGF) as a potential imaging probe for glucocerebrosidase. *J. Label. Compd. Radiopharm.* **44,** 385–394 (2001).

78. Braun, C., Brayer, G. D. & Withers, S. G. Mechanism-based Inhibition of Yeast a-Glucosidase and Human Pancreatic a-Amylase by a New Class of Inhibitors 2-Deoxy-2,2-difluoro-a-glycosides. *J. Biol. Chem.* **270,** 26778–26781 (1995).

79. Zechel, D. L. & Withers, S. G. in *Comprehensive Natural Products Chemistry* 279–314 (Elsevier, 1999). doi:10.1016/B978-0-08-091283-7.00118-1

80. Dwek, R. A. Glycobiology: Toward Understanding the Function of Sugars. *Chem. Rev.* **96,** 683–720 (1996).

81. Ge, M. *et al.* Vancomycin Derivatives That Inhibit Peptidoglycan Biosynthesis Without Binding d-Ala-d-Ala. *Science (80-.).* **284,** 507–511 (1999).

82. Hudlicky, T. Design Constraints in Practical Syntheses of Complex Molecules: Current Status, Case Studies with Carbohydrates and Alkaloids, and Future Perspectives. *Chem. Rev.* **96,** 3–30 (1996).

83. Svensson, S. C. T. & Thiem, J. Purification of α-l-fucosidase by C-glycosylic affinity chromatography, and the enzymic synthesis of α-l-fucosyl disaccharides. *Carbohydr. Res.* **200,** 391–402 (1990).

84. Yoshimura, Y., Kitahata, S. & Okada, S. Effects of Temperature on 6-0-a-Maltosyl Cyclodextrin Production from a-Maltosylfluoride and Cyclodextrins. *Agric. Biol. Chem* **52,** 1655–1659 (1988).

85. Armand, S., Drouillard, S., Schü, M., Henrissat, B. & Driguez, H. A Bifunctionalized Fluorogenic Tetrasaccharide as a Substrate to Study Cellulases*. *J. Biol. Chem.* **272,** 2709–2713 (1997).

86. Mackenzie, L. F., Wang, Q., Antony, R., Warren, J. & Withers, S. G. Glycosynthases: Mutant Glycosidases for Oligosaccharide Synthesis. *J. Am. Chem. Soc.* **120,** 5583–5584 (1998).

87. Lougheed, B., Ly, H. D., Wakarchuk, W. W. & Withers, S. G. Glycosyl fluorides can function as substrates for nucleotide phosphosugar-dependent glycosyltransferases. *J. Biol. Chem.* **274,** 37717–37722 (1999).

88. Crout, D. H. G. & Vic, G. Glycosidases and glycosyl transferases in glycoside and oligosaccharide synthesis. *Curr. Opin. Chem. Biol.* **2,** 98–111 (1998).

89. Johnson, P. E., Brun, E., Mackenzie, L. F., Withers, S. G. & Mcintosh, L. P. The Cellulose-binding Domains from Cellulomonas fimi b b b-1,4-Glucanase CenC Bind Nitroxide Spin-labeled Cellooligosaccharides in Multiple Orientations. *J. Mol. Biol.* **287,** 609–625 (1999).

90. Mayer, C., Zechel, D. L., Reid, S. P., Warren, R. A. J. & Withers, S. G. The E358S mutant of Agrobacterium sp. β-glucosidase is a greatly improved glycosynthase. *FEBS Lett.* **466,** 40–44 (2000).

91. Chan, J., Tang, A. & Bennet, A. J. A stepwise solvent-promoted S Ni reaction of α-d- glucopyranosyl fluoride: Mechanistic implications for retaining glycosyltransferases. *J. Am. Chem. Soc.* **134,** 1212–1220 (2012).

92. Lee, S. S. *et al.* Mechanistic evidence for a front-side, SNi-type reaction in a retaining glycosyltransferase. *Nat. Chem. Biol.* **7,** 631–638 (2011).

Chapter 2.
Measurement of Kinetic Isotope Effects by Continuously Monitoring Isotopologues Ratios Using NMR Spectroscopy

This Chapter comprises the manuscript **"Measurement of Kinetic Isotope Effects by Continuously Monitoring Isotopologues Ratios Using NMR Spectroscopy"**, which was published in the book series *Methods in Enzymology* (**2017**, *596*, 547-571).

Natalia Sannikova, Andrew R. Lewis, Andrew J. Bennet[1]

[1]Simon Fraser University, Burnaby, BC, Canada

The following manuscript is a verbatim copy of the original chapter published in *Methods in Enzymology*, **2017**, *596*, 547-571 and is formatted as per thesis rules and regulations of Simon Fraser University. Permission to reproduce the published material was obtained from Elsevier, and from co-author Dr. Andrew R. Lewis. The manuscript was prepared by myself and Dr. Andrew R. Lewis in collaboration with my thesis supervisor.

2.1. Abstract

Nuclear magnetic spectroscopic (NMR) methods are discussed for the measurement of heavy atom (^{13}C, ^{18}O, ^{15}N) and secondary deuterium kinetic isotope effects. The discussion focuses primarily on the NMR methods that enable the measurement of quantitative spectra and not on methods to make labeled substrates. Two main techniques are considered: single-point determinations on natural abundance material and the continuous monitoring of isotopically enriched materials. The second method is described in more detail, and we include a discussion of the current state of instrumentation and computer programs for data acquisition and analysis.

2.2. Introduction

Kinetic isotope effects (KIEs) have been used for many decades by physical organic chemists, as an integral component of their mechanistic toolbox, to probe reaction transition states.[1] In general, for many reactions the rate-limiting step involves chemical bond making and breaking, a fact that makes analysis of mechanism using KIE data relatively straightforward.[2–4] In contrast, for enzyme-catalyzed reactions it is rarer for a chemical bond-breaking (or bond-making) step to be the only kinetically significant (rate-limiting) step during the catalytic cycle.[5] In addition, for enzymatic reactions two types of KIEs can be measured, those on the turnover number (V) and on the enzymatic efficiency (V/K).[6] As a result, the number of researchers using KIEs to study enzymatic reactions initially lagged behind that for nonenzymatic reactions. These earlier limitations have been circumvented largely with the development of both the theory for enzyme reactions with multiple significant transition states[7] and the experimental techniques for determining intrinsic KIEs on individual chemical steps during catalysis.[8–10]

In essence, two different approaches are used for the measurement of KIEs on enzyme-catalyzed reactions: (i) separate rate constant determinations for each isotopologue and (ii) a competitive determination of the rate ratios.[11] Of note, competitive techniques can be employed using either radiolabeled tracer[9,12,13] or natural abundance (stable isotopes) isotopologues,[14–17] as well as highly enriched samples.[11,18] On the other hand, for separate determinations of rate constants, highly enriched isotopologues are required.[11,19]

Competitive techniques, in general, yield more accurate and precise KIE measurements because systematic errors, which can be caused by concentration and temperature differences when separate reactions are monitored, are minimized.[3] Of note, competitive KIE experiments on enzymatic reactions only report on the KIE for the second-order rate constant (V/K), irrespective of the substrate concentration.[11]

The use of nuclear magnetic resonance spectroscopy (NMR) to measure deuterium KIEs in organic and biological reactions was reported twice in 1986. Specifically, Pascal et al. used NMR to measure changes in natural abundance levels of deuterium in order to evaluate several primary deuterium KIEs[20], while Sawada and coworkers acquired phosphorus-31 NMR spectra to evaluate the secondary deuterium

KIE for the S_N2 iodide ion demethylation (CL_3; L = H or D) of a pyridinium salt by using triphenylphosphine to trap the methyl iodide product.[21] Notably, Singleton and Thomas refined the procedures of Pascal et al. markedly to yield secondary deuterium and C-13 KIEs using natural abundance starting material.[15] Singleton and coworkers further refined their methods to improve sensitivity.[22] In 2010, a modified spectroscopic method was introduced by Chan et al. in which isotopologue ratio data were acquired continuously using quantitative C-13 NMR with highly enriched singly and doubly labeled starting materials.[18]

The information provided herein aims to: (a) highlight the pros and cons for the use of NMR spectroscopy to measure competitive KIEs in biochemical systems, with single-point or continuous monitoring of isotopologue ratios, (b) outline practicable considerations for experimental design, and (c) describe strategies for the acquisition of quantitative NMR data for determining KIEs. Throughout this chapter, we will use IUPAC nomenclature for isotopically substituted and selectively labeled compounds.[23] That is, an isotopically substituted compound is one in which all molecules have the specific nuclide at the assigned position (we use this definition for >98% enrichment), whereas selective labeling conventionally arises from mixing, potentially several, isotopically substituted compounds. For example, methyl α-D-[1-$^{2}H_{0;1}$,1-$^{13}C_{1;1}$]glucopyranoside is a mixture of doubly labeled methyl α-D-(1-^{2}H,1-^{13}C)glucopyranoside and singly substituted methyl α-D-(1-^{13}C)glucopyranoside.[23]

2.3. Procedure

Several points must be evaluated when deciding how to measure KIEs using continuously monitored NMR spectroscopy. These include: (a) the specific KIE(s) to be measured, for example, primary C-13, O-18, or secondary deuterium; (b) the choice of NMR-active “probe” nucleus; (c) the sensitivity of the NMR spectrometer; (d) the rate constants for spin– lattice relaxation (T_1 values); (e) the ease of synthesis of isotopically enriched substrates; (f) the availability of labeled starting material(s); (g) the chemical shifts (and coupling constants) for the probe nucleus in the starting material and product(s); and (h) any interference from natural abundance signals in the NMR spectra. Points (a) – (d) address the ability to acquire acceptable progress curves of isotopologue ratio vs the fraction of reaction. Points (e) and (f) are relevant if complex labeling patterns are required, given that several milligrams of material are required for each triplicate KIE

measurement. Points (g) and (h) are pertinent to the ease of peak integration and isotopologue ratio determinations.

2.3.1. Choice of NMR-Active Probe Nucleus

The main factors to consider in selecting the NMR probe nucleus are spectral dispersion, sensitivity, and ease of isotopic labeling. Shown in Table 2.1 are the isotopic abundances, magnetic properties, and typical chemical shift ranges for nuclei with spin = ½ (and ^{2}H, I = 1) that can be potentially used to measure biochemical KIEs by NMR spectroscopy. The use of the highest field instrument available will provide the best sensitivity. For each experiment, 4 times as much material would be needed when using a 300 MHz vs a 750 MHz system to obtain spectra with identical signal-to-noise ratio (SNR) using similar NMR probes.

^{1}H NMR Spectral Data Acquisition

Apart from tritium, ^{1}H is the most sensitive nucleus in NMR spectroscopy; however, there are two main disadvantages inherent to KIE measurements of biological processes by proton NMR: resonances from the solvent and limited spectral dispersion. As a result, only simple organic substrates, in general, allow the use of ^{1}H NMR for the continuous monitoring of isotopologue ratios. For example, when using water as solvent the concentration of ^{1}H from the H_2O signal is 110 *M*, and this must be suppressed in order to achieve sufficient signal intensity (and SNRs) to detect the isotopologues of interest, which are present at significantly lower concentrations (usually 1–100 m*M*). In fortunate cases, signals from the proton of interest do not overlap with other signals, such as when 1-phenyl[1-$^{13}C_{0;1}$]ethene was used to measure a ^{13}C KIE for the benzylic carbon during the hydroamination of styrene with aniline.[25] Another example is the anomeric protons in monosaccharide derivatives, as these resonances generally occur separately from other ring C–H protons, as shown in the ^{1}H NMR resonances associated with the anomeric C–H for α-D-[1-$^{13}C_{0;1}$]glucopyranosyl fluoride in D_2O (Fig. 2.1).

Table 2.1. Physical Properties of Potentially Useful Probe Nuclei for the Measurement of Biological KIEs by NMR Spectroscopy

Isotope	NMR Frequency* (MHz)	Natural Abundance[24] (%)	Relative Sensitivity	Relative Sensitivity at Natural Abundance	Spin Number	Typical Chemical Shift Range (ppm)
^{1}H	100.000	99.944	1.000	1.000	½	+10 to 0
^{2}H	15.351	0.0156	9.6×10^{-3}	1.45×10^{-6}	1	+10 to 0
^{13}C	25.144	1.108	1.59×10^{-2}	1.76×10^{-4}	½	+220 to 0
^{15}N	10.133	0.366	1.04×10^{-3}	3.85×10^{-6}	½	+620 to –420
^{19}F	94.077	100	0.834	0.834	½	+550 to –250
^{31}P	40.481	100	6.64×10^{-2}	6.64×10^{-2}	½	+1400 to –500

*At a field strength of ~ 2.35 T

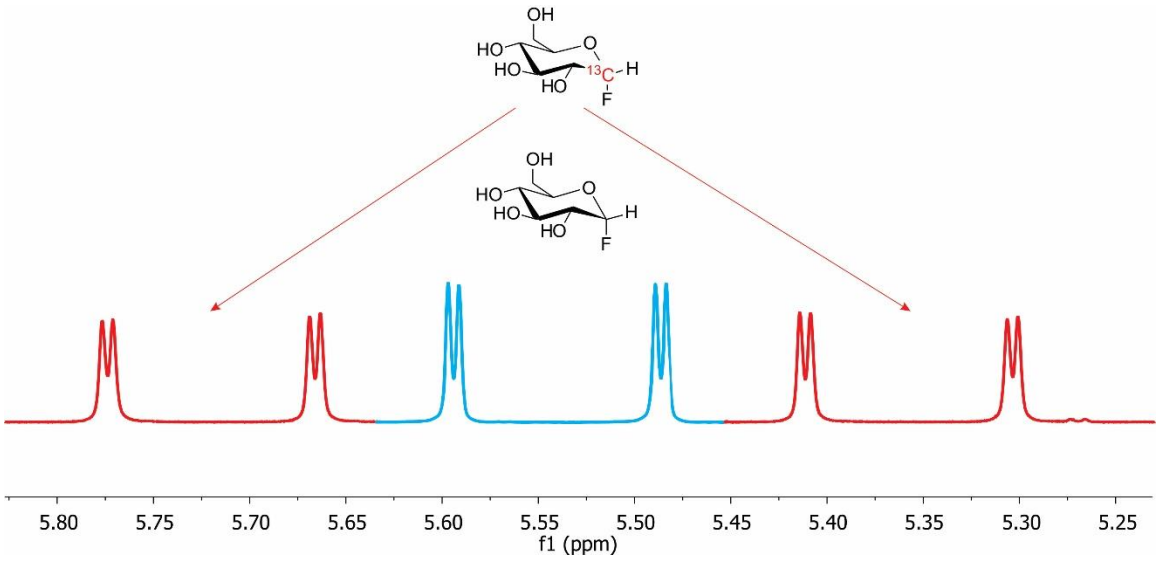

Figure 2.1. Part of the ^{1}H NMR spectrum of α-D-[1-$^{13}C_{0.1}$]glucopyranosyl fluoride in D_2O showing the resonances for the anomeric protons.

The time required to monitor reactions by NMR spectroscopy is typically of the order of a few to tens of hours. Therefore, it is essential that magnetic field drift be eliminated during the course of reaction monitoring to ensure that the resonances in the spectrum do not move. This requirement is achieved easily with modern NMR spectrometers by "locking" the field using a ^{2}H frequency lock. In aqueous systems this means having sufficient $^{2}H_2O$ (D_2O) present; however, the presence of D_2O can influence the reaction due to solvent isotope effects, so the amount of heavy water should be kept to the minimum needed for a stable lock signal. With regular NMR probes this typically requires >5% D_2O by volume, whereas for cryogenically cooled NMR probes the higher lock channel sensitivity allows one to reduce the amount of D_2O to 2–20 μL in a 500–600 μL sample.

^{13}C NMR Spectral Data Acquisition

The discontinuous method developed by Singleton and Thomas for the measurement of a full set of ^{2}H (using ^{2}H NMR) and ^{13}C KIEs, which require an explicit assumption that at least one KIE is 1.0, is useful for many reactions.[14,15,22,26] However, such procedures are limited to the evaluation of KIEs for NMR-active nuclei,[15,22] which makes it unsuitable for the measurement of ^{18}O KIEs. Natural abundance measurements have grown in popularity due to increases in NMR spectrometer sensitivity,[27]

measurement of product-specific KIEs,[28] and implementation of selective pulse sequences.[29]

The use of selectively labeled material for the measurement of ^{2}H, ^{13}C, and ^{18}O KIEs using a ^{13}C nucleus as the magnetic probe allows continuous monitoring of isotopic ratios in aqueous solution.[18] That is, the isotopologues are distinguished by coupling to the probe nucleus (if NMR active) and/or by isotopic chemical shift perturbation (for $I = 0$ nuclei such as ^{16}O and ^{18}O), as indicated in the ^{13}C NMR spectrum for 4-nitrophenyl α-D-[2-$^{13}C_{1;1}$,2-$^{18}O_{0;1}$]mannopyranoside in basic aqueous solution (NaOH = 0.1 *M*, *I* = 0.4) displayed in Fig. 2.2.

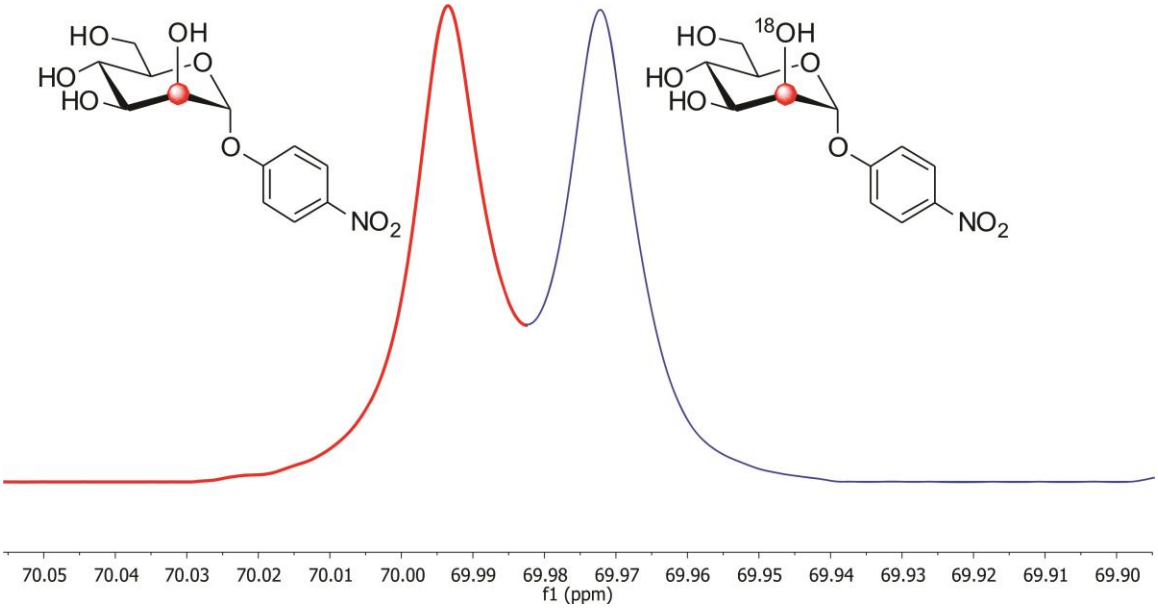

Figure 2.2. Proton-decoupled ^{13}C NMR spectrum of the C-2 resonance in 4-nitrophenyl α-D-[2-$^{13}C_{1;1}$,2-$^{18}O_{0;1}$]mannopyranoside in basic aqueous solution (NaOH = 0.1 *M*, *I* = 0.4)

Indeed, the use of a ^{13}C probe nucleus allows the routine measurement of ^{18}O KIEs in carbohydrate substitution reactions, for the leaving group,[18,30,31] the ring oxygen, which stabilizes pyranosylium ion intermediates,[18,30] and an intramolecular nucleophile.[31] A major limitation for the continuous monitoring protocols is the requirement for selectively labeled substrates; however, for biological systems, the availability of ^{13}C-labeled materials is improving markedly and as such the cost for each KIE measurement, in terms of labeled materials, is generally not prohibitive.

The use of ^{13}C as a probe nucleus can be advantageous owing to a number of factors: simpler spectra due to fewer peaks and limited coupling, appreciable chemical shift differences due to the presence of nearby labeled nuclei, and elimination of problems from strong solvent signals (none in water). However, using ^{13}C NMR also has certain disadvantages: lower sensitivity in comparison to other NMR-active nuclei (^{1}H, ^{19}F, ^{31}P, see Table 2.1), potentially complex syntheses from available starting materials, overlapping NMR peaks leading to the need for extensive spectral deconvolution, or multiplet signals due to coupling with adjacent (also isotopically enriched) ^{13}C or other nuclei that cannot be decoupled for various reasons.

When using ^{13}C (or ^{31}P or ^{19}F) as the detected nucleus, care must be exercised to ensure that any decoupling of other nuclei (normally ^{1}H, but also potentially ^{2}H, ^{19}F, and ^{13}C) does not lead to changes in native signal intensities due to enhancement by nuclear Overhauser effects (NOEs).[32] Heteronuclear enhancements can result in up to a three-fold sensitivity for ^{13}C nuclei coupled to ^{1}H. NOEs occur through space (dipolar coupling) and not through bond (scalar coupling), so they can be dissimilar for the same carbon atom in isotopologues.[32] To minimize the NOE, any decoupling (at least for one-dimensional experiments) should be inverse gated, meaning that decoupling is only applied during the acquisition of the FID, and not during the recycle delay between successive scans as is typically done for normal ^{13}C NMR spectroscopy (i.e., power-gated decoupling).

The wider availability of higher magnetic field instruments (9.4 T and greater) and commercial cryogenically cooled probe electronics (cryoprobes) provide significant sensitivity enhancements for many nuclei (including ^{13}C) that partially mitigate these limitations (Table 2.2).

Another way to overcome the limitations of a ^{13}C-based approach is to use other types of NMR experiments, for example, sensitivity-enhanced two-dimensional (2D) [^{13}C, ^{1}H]-heteronuclear single-quantum coherence spectroscopy (HSQC).[33] The combined ^{1}H excitation and detection can potentially increase sensitivity by up to 32-fold compared to 1D ^{13}C NMR. 2D [^{13}C, 1H]-HSQC requires that a proton is attached to the ^{13}C reporter nucleus. Many organic substrates meet this criterion, for either the starting material or reaction product, allowing the measurement of KIEs.

On occasions, NMR signal overlap of starting material and product can be resolved, if the product can be enzymatically modified, thus resulting in its in situ removal from the spectral region of interest.[18]

Table 2.2. Typical Signal-to-Noise Specifications for Various 5 mm NMR Probes* at Different Field Strengths

Observed Nucleus	Reference Sample	9.4 T (400 MHz)	11.7 T (500 MHz)	14.1 T (600 MHz)
^{1}H	0.1% Ethylbenzene in $CDCl_3$	300 (BBO), 600 (BBI), 1050 (P– CP)	260 (TBO), 800 (TXI)	400 (BBO), 1200 (TXI), 1580 (QNP–CP), 4500 (QCI–CP), 6000 (TCI–CP)
^{19}F	0.05% Trifluorotoluene in $CDCl_3$	275 (BBO), 850 (P– CP)	200 (TBO), 450 (TXI)	4500 (QCI – CP)
^{31}P	48.5 mM Triphenylphosphine in acetone-d_6	150 (BBO), 300 (P– CP)	140 (TBO)	220 (BBO), 640 (QNP– CP)
^{13}C	40% Dioxane in C_6D_6	190 (BBO), 475 (P– CP)	150 (TBO), 160 (TXI)	160 (TXI), 300 (BBO), 750 (TCI–CP), 1500 (QNP–CP)
^{15}N	90% Formamide in DMSO-d_6	20 (BBO), 40 (P–CP)	30 (TBO)	50 (BBO), 110 (QNP– CP)

BBI**, broadband inverse (inverse, ^{15}N – ^{31}P, ^{1}H); ***BBO, broadband observe (direct, ^{1}H, ^{15}N – ^{31}P); ***P – CP***, broadband observe nitrogen-cooled cryoprobe; ***QCI – CP***, quad carbon inverse helium-cooled cryoprobe (^{1}H, ^{19}F, ^{13}C); ***QNP – CP***, quad nucleus carbon helium-cooled cryoprobe (^{13}C or ^{31}P or ^{15}N, ^{1}H); ***TBO***, triple broadband observed (^{15}N – ^{31}P, ^{1}H); ***TCI – CP***, triple carbon inverse helium-cooled cryoprobe (^{13}C, ^{1}H); ***TXI***, triple X inverse (^{1}H, ^{13}C, ^{15}N). *Notes*: Inverse probes have ^{1}H coil closest to the sample, direct probes have ^{1}H coil farthest from the sample, observable nuclei are indicated, SNRs are for single-scan acquisition.

^{19}F NMR Spectral Data Acquisition

Fluorine-19 is another potential probe nucleus due to its high sensitivity, 100% natural abundance, and broad range of chemical shifts (Table 2.1). Moreover, isotopic substitution can produce significant chemical shift perturbations which allows for simple integration without multistep deconvolution. For example, the ^{19}F NMR resonances associated with α-D-[2-$^{2}H_{0;1}$,1-$^{2}H_{0;1}$]galactopyranosyl fluoride in H_2O are displayed in Fig. 2.3.

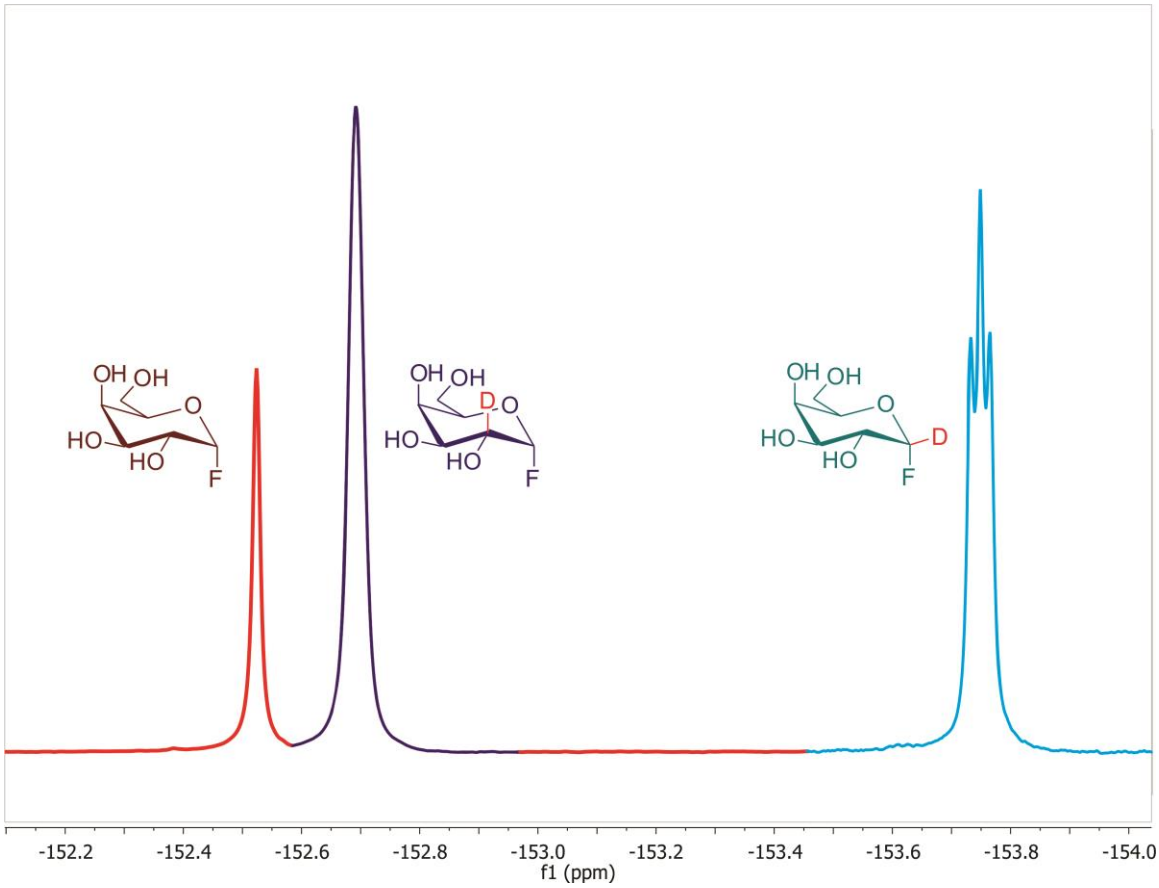

Figure 2.3. Proton-decoupled ^{19}F NMR spectrum of α-D-[2-$^{2}H_{0;1}$,1-$^{2}H_{0;1}$]galactopyranosyl fluoride in D_2O

Introduction of the fluorine into a substrate can also result in lowering the commitment to catalysis for the chemical steps within the enzyme catalytic cycle,[34] facilitating the measurement of intrinsic KIEs.[34,35] Using ^{19}F as a probe can also result in simpler and cheaper synthesis of substrates compared to the preparation of ^{13}C-labeled materials.

2.3.2. Choosing Whether to Monitor Isotopologue Ratios in the Substrate or the Product

Competitive KIE experiments can be devised in which the change in isotopologue ratio is measured as the reaction proceeds either in the remaining starting material or in the product.

During the course of a reaction that exhibits a normal KIE, which is defined as one where the light isotopologue reacts faster ($k_{light}/k_{heavy} > 1$), the starting material becomes enriched with the heavy isotopologue, while the product becomes enriched with the lighter and more reactive isotopologue.[11] Thus, KIEs can be determined based on either reactant or product analysis (or both).

In general, for reactions in which two reactants form a single product the analysis of product isotopologues is more efficient as it allows the determination of KIEs with respect to both reactants in a single set of experiments.[29] Moreover, product-specific KIEs reflect isotopic fractionation that occurs at both rate- and product-determining steps in multiproduct reactions.[28] On the other hand, the remaining starting material becomes increasingly enriched as the reaction progresses, which can be an advantage for the measurement of KIE values that are close to unity.[11]

2.3.3. Sample Preparation

A critical component for the successful measurement of KIE data is the choice of a suitable internal standard. An internal standard is required in order to determine the fraction of reaction and to normalize the peaks area ratios for all isotopologues. Also, the internal standard must be inert to the experimental conditions: ideally have a simple NMR spectrum that does not overlap with the resonances of the species of interest (singlet preferred), one of its corresponding NMR signal(s) should have a chemical shift close to the signals of interest, and its T_1 relaxation time should be comparable to those of the isotopologues being analyzed.

A deuterated solvent is generally used as a lock for the spectrometer frequency (i.e., D_2O is added to the aqueous buffer). However, NMR tubes with coaxial inserts that contain a deuterated solvent can be used instead. Importantly, normal manual or automated (gradient) ^{2}H-shimming techniques must be used with caution in this case because these methods will tend to optimize field homogeneity only for the ^{2}H-containing capillary. In addition, because this lock solvent is not in contact with the reaction mixture, in principle it can be any deuterated solvent and does not have to match the reaction solvent, but a matched solvent is usually preferred for the best magnetic field homogeneity. The sample volume should be enough that the liquid height in the NMR tube is at least three times the length of the r.f. observation coil in the probe being used. If only

limited quantities of com- pounds are available, the sample volume can be reduced by using either a smaller diameter NMR tube (e.g., 3 mm) or a Shigemi tube whose susceptibility is matched to the solvent being used.

For enzymatic reactions, the amount of enzyme added should be adjusted such that the reaction goes to 80%–90% completion in a time period that permits the acquisition of sufficient spectra (generally >20–30) with a suitable SNR, such that the time required to acquire the individual spectra is small compared to the total time of monitoring the reaction. The NMR-based measurements of KIEs described here are very versatile because the experimental parameters may be adjusted to optimize data collection depending on the (usually limited) quantities of labeled reactants available for each reaction, the sensitivity of the NMR probe used (time needed to acquire spectra with usable SNR), and the duration of the reaction (amount of enzyme added).

2.3.4. Acquisition of NMR Spectra

For NMR spectra to be useful for quantitative analysis, important parameters to be considered are the instrumentation setup and optimization, relaxation delay, digitization, and pulse sequence design, as well as use of appropriate postacquisition processing parameters and procedures for optimal peak area determinations.[36,37]

Shimming can provide a homogeneous magnetic field and result in symmetrical peak shapes that are very important, especially when peaks overlap and require spectral deconvolution. In some cases the best way to achieve symmetrical peak shape is to adjust the room temperature shims while directly observing the FID or real-time Fourier-transformed spectrum in single-scan mode. After shimming, the lock phase should be adjusted to ensure optimal performance and stability.

In cases where the reaction itself, spectrometer stability, or NMR laboratory environmental conditions (temperature and air pressure) cause changes in the shimming over the duration of the experiment, it may be necessary to automate shimming after the acquisition of each spectrum, or to make on-going automated adjustments to specific shims (to maintain the lock level). Such automated adjustments are easily implemented on most modern NMR spectrometers.

To obtain spectra with peak areas that accurately reflect the relative number of nuclei, the acquisition conditions must be set correctly.[37] The SNR of all peaks being integrated should be at least 10 (generally accepted minimum for limit of quantitation), but ideally much higher. There should also be at least 10 points defining each peak above half height, which is directly related to the acquisition time (dwell time and number of points acquired in the time domain), spectral width, and zero filling. To ensure that nuclei are fully relaxed between successive scans, the relaxation delay (i.e., the sum of acquisition time and interpulse delay) should be at least seven times the spin–lattice (T_1) relaxation time (>99.9% relaxation).[37]

Approximate T_1's can be estimated using a 1D inversion-recovery pulse sequence ($T_1 \approx 1.45 \times t_{null}$).[32] T_1 relaxation times should be measured for the specific nuclei in the compounds being used to measure the KIE (reactants or products and internal standard) at the same approximate concentration, solvent, buffer solution, pH, temperature, and field strength that will be used. This operation can be done using a standard inversion-recovery (180 - τ - 90 - AQ) or a saturation-recovery pulse sequence.[37]

The transmitter offset for the observed nucleus should be close to the peaks of interest, but not exactly on any resonance, and ideally centered between the internal reference standard and the peaks of compounds being measured. The transmitter offset for any decoupling channels should also be set to match closely the frequencies of the directly bonded nuclei for optimal performance. Modern composite pulse decoupling methods (e.g., WALTZ or GARP)[32] are preferred for their better performance and reduced radio frequency (r.f.) power.[37]

The pulse lengths for observation and decoupling channel(s) should be measured for each sample. Typically, the pulse length for a 90-degree excitation should be close to 10 μs to ensure uniform excitation over all resonances (for a 90-degree pulse of 10 μs, the excitation bandwidth is ca. 1/(4 × 0.000010) = 25,000 Hz, which is ample for the typical range of proton resonances in organic samples; 5000 – 7000 Hz at 500 MHz). It is also important to maintain a constant sample temperature throughout the experiment to avoid peak shifting and broadening. Sample temperature settings can be calibrated using, e.g., 99.98% deuterated methanol.[38] The use of buffers raises the ionic strength of aqueous solutions, and this means that r.f.-induced sample heating can occur, especially when multiple types of nuclei are being decoupled for several seconds during acquisition.

Dummy scans may be required to reach a steady state in such cases. If the desired reaction temperature is outside the recommended range for normal sample turbines, ceramic sample spinners should be used. Sample spinning (20 Hz) can be used but is usually not recommended for systems operating at 500 MHz and higher,[37] or for 2D NMR acquisitions.[39]

Note that because an internal standard is used, the peak areas can be normalized relative to the area of the reference peak(s). Thus, the reaction can be followed from any time after the addition of the enzyme (or other reagent) because the initial spectrum defines the zero point for the fraction of reaction. This means that, in general, time can be taken to achieve stable spectrometer conditions (shimming, tuning, and sample temperature). Furthermore, the number of scans can be increased for individual spectra as the reaction proceeds to allow the acquisition of spectra having similar SNR as the concentration of starting material decreases. Alternatively, additional data points or improved SNR may be obtained by coadding successive FIDs and plotting them vs the average fraction of reaction for the summed spectrum. For the best accuracy and precision of KIEs, it is recommended that spectra are acquired until the fraction of reaction reaches ~80%.

2.4. Data Processing

2.4.1. 1D NMR Data

Typically, Bruker TopSpin (Topspin User Manual, Version 3.5; Bruker BioSpin GmbH, Germany, 2016) or Mestrelab MNova (Mnova User Manual, Version 11.0; Mestrelab S.L. Spain, 2016) software is used for NMR data processing. Spectra processing parameters are set to obtain accurate integrals for precise KIE measurement, as follows:

1. Fourier transformation of FIDs is performed with two- to fourfold zero filling and appropriate apodization by applying exponential line broadening to increase the SNR. In theory, the best value for the parameter is that which approximates the peak width at half height of the peaks in Hz.[37]

2. Spectra should be properly phased and baseline corrected. This directly affects the precision and accuracy of the peak area measurements. If using automated

processing, it is recommended to check each spectrum for proper phasing and manually adjust any spectra that are misphased.

3. FIDs can be summed together, for the latter stages of the reaction as the SNR decreases, which compensates for any deterioration in sensitivity.

4. All peaks should be referenced to the chemical shift of the chosen signal of the internal standard.

5. Integration regions must be set up. In order to cover 99.0% of the area of any peak, the region must spread over a range that is at least 25 times the line width of the peak in both directions.[40] To achieve an accuracy of 0.1%, the regions must cover about 75 times the peak width in both directions.

6. If the peaks of interest are overlapping, deconvolution must be used. Integral regions should not overlap. For example, two singlets 1 Hz wide should be separated by at least 50 Hz (0.1 ppm at 500 MHz) to be integrated individually with an accuracy of at least 1%. Various algorithms can be used to achieve desired results. Mestrelab Mnova software has implemented deconvolution functionality, and a Mathematica (Mathematica, Version 11.1; Wolfram Research Inc., Champaign, IL, 2017) notebook has been used successfully to deconvolve $^{13}C[^{1}H]$ quantitative spectra.[18,31] An improved method for integration that removes the areas of small unrelated (impurity) peaks overlapped with the peak-of-interest area has been developed recently by Schoenberger et al.[41] This methodology has been implemented in the Mnova software and is called “edited sum.” Ideal liquid NMR resonances have a Lorentzian shape, but in practice this is difficult to achieve.[42] Commonly, a mixed Lorentzian–Gaussian peak shape or the newer “generalized Lorentzian” peak shape can be used to fit peaks.[41] If shimming is poor and peaks are asymmetric, then reference peak deconvolution may be applied to regain symmetrical peak shapes (albeit at some expense to the SNR levels).[43]

7. The obtained peak areas are then normalized by dividing values for the peaks of interest by that obtained for the internal standard in the same spectrum. This operation can be performed automatically in Mnova.

2.4.2. 2D NMR Data

When measuring KIEs by NMR spectroscopy, the chemical shifts of the various reactants or products are by nature often quite similar, with only small differences expected for the isotopologues. Hence, there is a high probability that at least some of the peaks will overlap to some degree in the one-dimensional NMR spectra. As the number of species that are present increases, this overlap can complicate the measurement of accurate peaks areas for the various species, even when using peak deconvolution. 2D NMR offers the possibility to simultaneously determine the relative concentrations of similar compounds in a mixture thanks to its capacity to separate overlapping resonances.

However, 2D NMR requires significantly longer acquisition times (owing to the reduced sensitivity vs 1D and the need to acquire a series of FIDs at incremented delays to create the second dimension, which can be reduced somewhat if sparse sampling methods are used), and there can be significant differences in signal response (peak volumes), which can be highly site specific.[39] The peak volumes in 2D spectra are typically not comparable between different carbon types (methyl, methine, and methylene), but in the case of KIE measurements, the reporter nuclei are all exactly the same types of carbons in all the isotopologues, so the peak volumes are directly comparable in principle as long as appropriate precautions are taken (namely, the use of inverse-gated decoupling to reduce NOE enhancements).

The use of Shigemi tubes is recommended when applying 2D NMR techniques because they can reduce the solvent volume by one-half, and thus double the concentrations of the labeled compounds if the same quantities are used. This has three direct benefits: reducing the solvent signal, maximizing the dynamic range, and providing a fourfold sensitivity gain. The latter translates to a reduction of the experiment time by a (theoretical) factor of 0.5 for an equivalent SNR, which is highly significant given the relatively long experiment times required for 2D NMR spectroscopy. Making use of ^{1}H for excitation and detection in a ^{1}H–^{13}C correlation experiment (e.g., HSQC), SNR vs direct 1D^{13}C observation can be improved by $4^{5/2}$ (i.e., 32-fold).

In the following sections, we discuss 2D experiments in terms of ^{1}H and ^{13}C, but other nuclei can also be used (e.g., ^{19}F or ^{31}P). The best 2D NMR experiments will be those that offer high sensitivity and high resolution in both dimensions. The most efficient

2D NMR techniques are those based on correlations between heteronuclei that share a chemical bond, for example, $^{1}H–^{13}C$ spin pairs. Two experiments of interest are the heteronuclear single-quantum correlation (HSQC)[44] and heteronuclear correlation (HETCOR).[45] To achieve the highest sensitivity and minimize spectral artifacts, one-bond $^{1}H–^{13}C$ scalar coupling (J) should be measured for the compounds being studied and the delays in both the HETCOR (¼J) and HSQC (¼J and ⅛J) experiments should be set appropriately.

The optimal values of the acquisition times in the direct (F2) and indirect (F1) dimensions can be estimated based on the spin–spin (T_2) relaxation times of the appropriate nuclei. For F2 the number of acquired points in the time domain of the FID multiplied by the dwell time should be ≥ 5 × T_2 of the observed nucleus. In the indirect dimension the number of increments (FIDs) multiplied by the t1 increment should be ≥ 5 × T_2 of the nondetected nucleus. Note also that power limitations for NMR probes and amplifiers should be carefully considered when setting the FID acquisition times (number of acquisition point and spectral width) and recycle delays to avoid damaging sensitive and expensive equipment. Dummy scans (typically 16 or 32) are used to achieve a steady state, but this is only done prior to acquisition of the first FID.

Recently, it has become relatively straightforward to utilize sophisticated prediction algorithms to increase the final spectral resolution or to reduce the acquisition time.[46,47] Extrapolation of the FIDs using forward linear prediction can be applied to increase (usually double at least) the effective resolution in both dimensions. Interpolation techniques based on sparely sampled data (e.g., nonuniform sampling) can be used to significantly reduce (often by >75%) the number of increments acquired in a 2D NMR experiment, which may be employed to either reduce the total experiment time or to increase the resolution in the indirect dimension.

HSQC Experiments

Based on sensitivity arguments alone, gradient HSQC would in general be considered the superior experiment, because it detects the higher sensitivity nucleus (^{1}H rather than ^{13}C), and incorporates field gradient pulses that significantly reduce the phase cycle and minimize artifacts. Because the initial polarization in an HSQC experiment typically comes from the ^{1}H nuclei (which usually have shorter T_1 relaxation times), the interscan delays can be significantly (often > 5-fold) shorter. The optimal recycle delay for

HSQC is 1.27 × T_1 (of ^{1}H) less the FID acquisition time, but usually longer delays are used to permit probe r.f. duty cycle limits to be adhered to, and to prevent r.f. heating of the sample.[47]

However, there also disadvantages for HSQC experiments: ^{1}H detection means that there can be artifacts from incompletely suppressed ^{1}H–^{12}C signals, or signals arising from the solvent used (95% H_2O for example). Although many solvent suppression techniques have been developed, the application of these usually results in distortions of the baseline and sometimes also peak shapes. There are two (INEPT) polarization transfer steps (^{1}H → ^{13}C → ^{1}H) in an HSQC experiment, which means there is potential for larger variations between different isotopologues. Furthermore, to resolve the small chemical shift differences adequately (sometimes < 0.05 ppm) expected in the ^{13}C spectral dimension, a high number of increments are needed which dramatically increases the experiment time. This latter requirement can be reduced somewhat by restricting the spectral width in the ^{13}C dimension (e.g., to 3–10 ppm) or by applying band-selective (shaped) ^{13}C r.f. pulses. Note that because the indirect dimension is not filtered by digital or analog filters, through judicious choice of the transmitter offset and spectral width in the indirect (F1) dimension, it may be possible to have the signal from the internal standard (usually several ppm away from the peaks of interest) fold-back into the observation window to reduce the required number of increments and consequently also the time required for the experiment.

One other problem with the signals in HSQC spectra is that they are not single, symmetrically shaped peaks, but are actually split in F2 dimension due to residual ^{1}H — ^{1}H couplings which are not removed and cannot be decoupled.

HETCOR Experiments

HETCOR experiments have an advantage in comparison to the corresponding HSQC experiments in that the resolution achievable in the direct dimension (less sensitive ^{13}C) is greatly increased without the need for increasing the experiment time dramatically, unlike HSQC where a large number of t1 increments (and thus very long experiments) are needed to achieve high resolution in the ^{13}C dimension. In addition, carbons with no protons attached do not show up in HSQC experiments, and there is no need to suppress the magnetization of protons bonded to ^{12}C atoms, a problem that plagues all of the ^{1}H-detected sequences.

Decoupling of ^{1}H is easier than ^{13}C (as used for HQSC) mainly due to the smaller bandwidth and thus lower r.f. power requirements. This means that the number of points in the time domain (FID) can be significantly higher in HETCOR, again offering higher resolution. This also permits the use of exponential apodization in F2 rather than QSINE so less peak distortion, which effectively suppresses residual truncation artifacts. The resulting 2D spectra will have better peak shapes and minimal baseline distortions. Also, because there is usually no strong solvent signal (and none if water is the solvent), higher receiver gains can be used which result in improved dynamic range.

The major drawback with HETCOR is the significantly lower sensitivity, but as the compounds are typically ^{13}C enriched (i.e., 99-fold enhancement), this is somewhat mitigated. Cryogenically cooled NMR probes with cooled preamplifiers for the ^{13}C channel also provide another ca. 4-fold gains in sensitivity for ^{13}C detection. We recommend using a modified HETCOR with refocusing of chemical shifts[48] so that the final echo is balanced. This also permits ^{2}H decoupling to be applied throughout the pulse sequence (including FID acquisition), but be turned off during the recycle delay so that ^{2}H field locking can be used.

2D Data Processing and Fitting

For any quantitative NMR spectra, proper postacquisition data processing is critical as the values of the KIEs being measured can be very small (ca. 1.01). The choice of apodization functions is critical because the number of data points in each dimension is significantly less than for typical 1D spectra (typically at least 32 times). It is recommended that at least twofold zero filling be applied, as well as linear prediction to increase the resolution. Once the 2D Fourier transformation has been carried out, the spectrum should also be correctly phased in both dimensions, and then baseline corrections must be carried out on both the F1 and F2 dimensions. The data should be inspected by taking slices (rows or columns) from the 2D spectrum and checking that the phasing and baseline corrections are appropriately done (this operation is especially important when automated processing procedures using default methods have been used).

The choice of apodization functions will depend on the software used and the type of spectrum being processed. They should be selected so that the (truncated) FIDs are smoothed to zero intensity at the end to avoid truncation artifacts at the base of the peaks in the resulting spectrum. The resulting peak shape should also be considered, as this can

simplify the next step of measuring the peak volume. Such artifacts severely interfere with the ability to accurately integrate the peak volumes.

If the peaks are all well resolved and there is no overlap, then the preferred method of determining the peak volumes is integration. This method typically involves defining rectangular boxes around the peaks of interest. In cases where there is overlap of peaks there now exists options in the Topspin and Mnova software for 3D deconvolution. Use of this option typically requires defining the peak maxima on the 2D spectrum. Fig. 2.4 shows an example of this approach for the HETCOR spectrum acquired on mixture of six isotopologues. The major drawback with this approach is that most commercial software implementations currently use symmetrical Lorentzian peak shapes (which are not usually a very close match to the actual peaks shapes) and unlike deconvolutions of 1D spectra, there is limited or no ability to restrain or adjust the peak-fitting parameters.

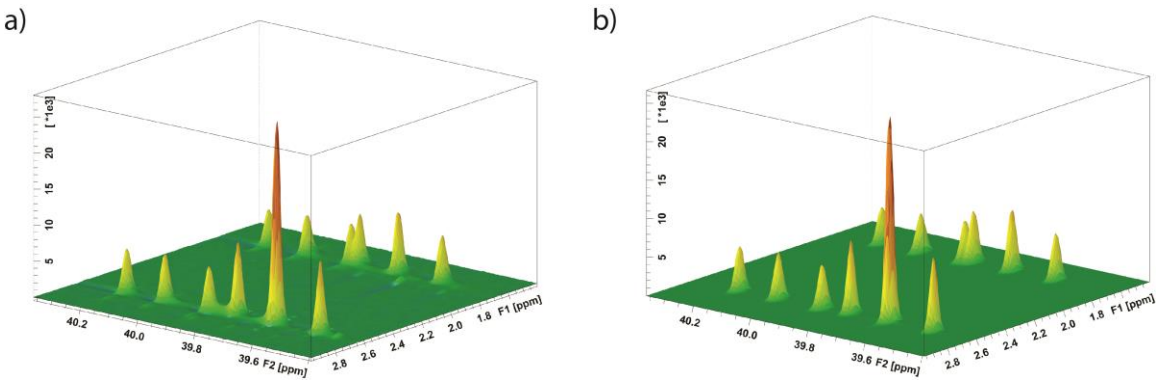

Figure 2.4. 2D ^{13}C–$^{1}H\{^{1}H,^{2}H\}$ HETCOR spectrum acquired for a mixture of six isotopologues with ^{13}C probe nucleus: (A) observed spectrum and (B) fit of spectrum using 3D peak deconvolution (TopSpin)

A third, practical approach for approximating peak volumes in 2D NMR spectra was recently described by Manning et al.[33] The principle is that a series of (10–40) consecutive slices covering the width of a given peak are extracted from the 2D spectrum. These individual 1D slices are then added to create a 1D sum spectrum for each peak. The resulting 1D sum spectra for each peak in the 2D spectrum can then be integrated (or deconvoluted if there is peak overlap) and the peak area (which approximates the peak volume) can thus be determined. Fig. 2.5 shows an example of this approach for a group of peaks extracted from a series of columns (i.e., the F1 or ^{13}C dimension) 2D HSQC spectrum. This approach works well regardless of the peak shapes and allows individual

slices to be utilized, either rows or columns from the 2D spectrum, whichever has the best peak shape in each case. Note that whatever method is used to determine peak volumes, only peaks volumes measured by the same method should be compared or used for calculations.

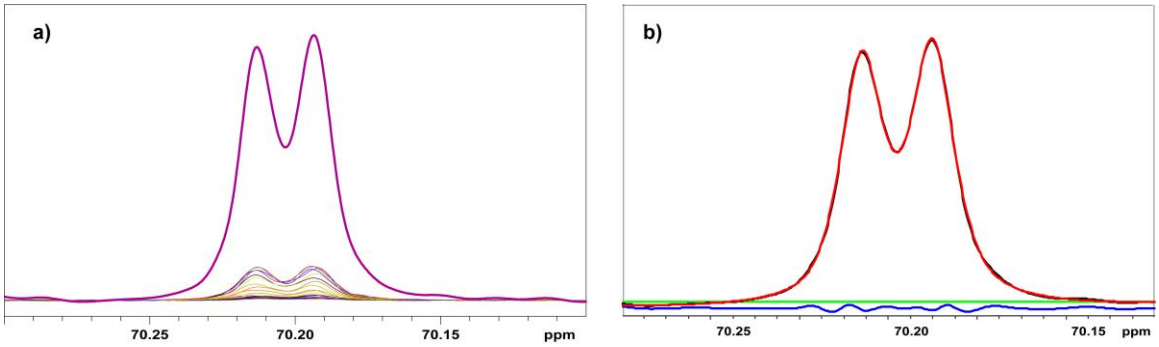

Figure 2.5. **(A) 20 sequential rows extracted from a peak in a 2D $^{1}H–^{13}C\{^{2}H,^{13}C\}$ HSQC spectrum and their sum. (B) Fit of sum spectrum using peak deconvolution (Mathematica): *black*** = real spectrum, ***red*** = sum of fitted peaks, ***blue*** = difference (expt–fit), and ***green*** = baseline

2.5. Data Analysis

The two equations (Eqs. 1 and 2) that are used to fit the experimental KIE data obtained by analyzing the isotopomer ratios in the substrate and product, respectively, are shown below and discussed in detail by Melander and Saunders.[11] Where k_1 and k_2 are the rate constants for the light and heavy isotopologues, respectively. F_1 is the fraction of reaction for the light isotopologue, R is the ratio of heavy-to-light isotopologue in remaining starting material, R_0 is the ratio at $T = 0$, and R_p is the ratio in the product.

$$\frac{k_1}{k_2} = \frac{\ln(1 - F_1)}{\ln[(1 - F_1)R/R_0]} \qquad (1)$$

and

$$\frac{k_1}{k_2} = \frac{\ln(1 - F_1)}{\ln\left[1 - \left(F_1 R_p/R_0\right)\right]} \qquad (2)$$

These authors also give a detailed error analysis for the standard equations that are used to calculate the KIE values.[11] Shown in Fig. 2.6 are typical ^{19}F NMR spectra

acquired during a reaction of α-D-[1-$^{13}C_{0;1}$]glucopyranosyl fluoride as a function of the fraction of reaction for α-D-glucopyranosyl fluoride (F_1).

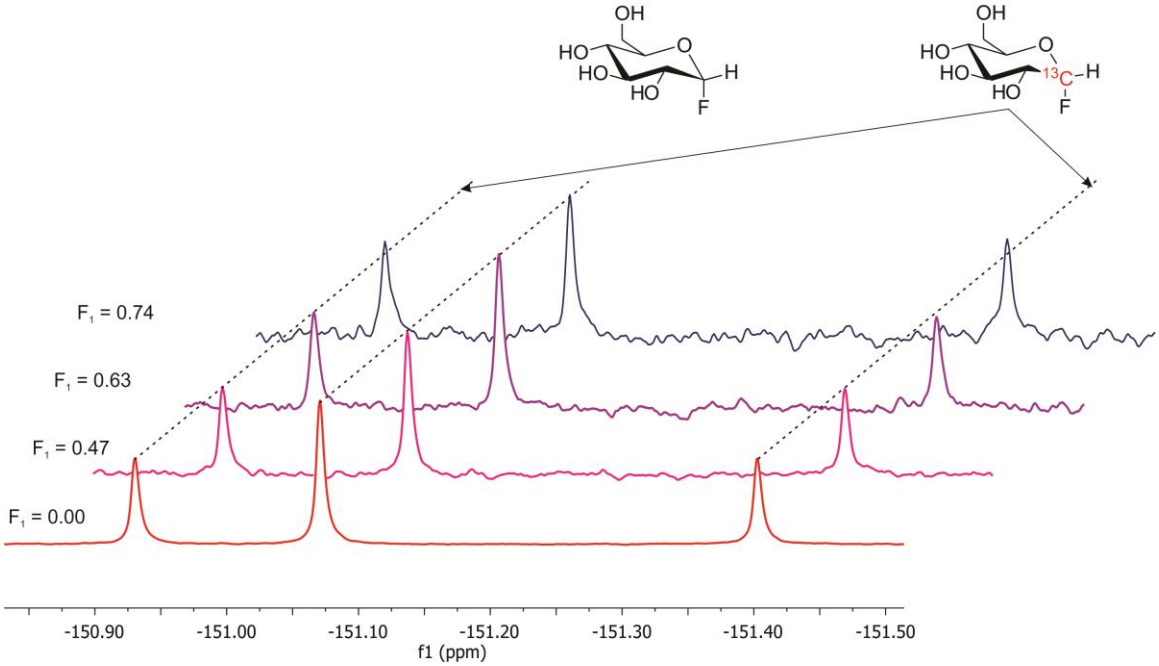

Figure 2.6. Stacked plot of proton-decoupled ^{19}F NMR spectra of α-D-[1-$^{13}C_{0;1}$]glucopyranosyl fluoride as the fraction of reaction of α-D-glucopyranosyl fluoride.
The *parallel dotted lines* are for visualization of the change in relative peak intensity as the reaction progresses.

2.6. Summary and Conclusion

For the measurement of competitive KIEs using NMR spectroscopy, it is imperative to decide what NMR-active nucleus will be used and whether to use isotopically enriched substrates. Knowledge of the SNR of available NMR probes will allow estimates of both the amount of material needed and the time frame for spectral acquisition. Isotopically enriched materials also allow the measurement of KIEs for NMR-inactive nuclei such as O-16 and O-18.

Recent advances in NMR spectrometer design and more importantly the advent of “cryoprobe” technology have greatly extended the number and types of experiments that can be performed without other specialized equipment.

2.7. References

1. L. Melander. *Isotope Effects on Reaction Rates*. (1960).

2. Berti, P. & Tanaka, K. Transition state analysis using multiple kinetic isotope effects: mechanisms of enzymatic and non- enzymatic glycoside hydrolysis and transfer. *Adv. Phys. Org. Chem.* **37,** (2002).

3. Kohen, A. & Limbach, H.-H. *Isotope effects in chemistry and biology*. (Taylor & Francis, 2006).

4. Meyer, M. P. *New Applications of Isotope Effects in the Determination of Organic Reaction Mechanisms*. *BS:APOC* **46,** (Elsevier, 2012).

5. Cleland, W. W. Enzyme Mechanisms from Isotope Effects. in *Isotope Effects in Chemistry and Biology* (eds. Kohen, A. & Limbach, H.-H.) 915–930 (Taylor & Francis, 2006).

6. Wallace Cleland, W. Use of Isotope Effects to Elucidate Enzyme Mechanism. *Crit. Rev. Biochem.* **13,** 385–428 (1982).

7. Ruszczycky, M. W. & Anderson, V. E. Interpretation of V/K isotope effects for enzymatic reactions exhibiting multiple isotopically sensitive steps. *J. Theor. Biol.* **243,** 328–342 (2006).

8. Cleland, W. W. Use of isotope effects to determine enzyme mechanisms. *J. Label. Compd. Radiopharm.* **50,** 1006–1015 (2007).

9. Cook, P. F. & Cleland, W. W. (William W. *Enzyme kinetics and mechanism*. (Garland Science, 2007).

10. Schramm, V. L. Enzymatic Transition States, Transition-State Analogs, Dynamics, Thermodynamics, and Lifetimes. *Annu. Rev. Biochem.* **80,** 703–732 (2011).

11. Melander, L. C. S. & Saunders, W. H. *Reaction rates of isotopic molecules*. (Wiley, 1980).

12. Parkin, D. W., Leung, H. B. & Schramm, V. L. Synthesis of Nucleotides with Specific Radiolabels in Ribose: Primary 14C and secondary 3H kinetic isotope effects on acid-catalyzed glycosidic bond hydrolysis of AMP, dAMP, and inosine. *J. Biol. Chem.* **259,** 9411–9417 (1984).

13. Sen, A., Stojkovic, V. & Kohen, A. Synthesis of radiolabeled nicotinamide cofactors from labeled pyridines: Versatile probes for enzyme kinetics. *Anal. Biochem.* **430,** 123–129 (2012).

14. Lee, J. K., Bain, A. D. & Berti, P. J. Probing the Transition States of Four Glucoside Hydrolyses with13C Kinetic Isotope Effects Measured at Natural Abundance by NMR Spectroscopy. *J. Am. Chem. Soc.* **126,** 3769–3776 (2004).

15. Singleton, D. A. & Thomas, A. A. High-Precision Simultaneous Determination of Multiple Small Kinetic Isotope Effects at Natural Abundance. *J. Am. Chem. Soc.* **117,** 9357–9358 (1995).

16. Adam G. Cassano, Vernon E. Anderson & Michael E. Harris. Analysis of Solvent Nucleophile Isotope Effects: Evidence for Concerted Mechanisms and Nucleophilic Activation by Metal Coordination in Nonenzymatic and Ribozyme-Catalyzed Phosphodiester Hydrolysis. *Biochemistry* **43,** 10547–10559 (2004).

17. Rosenberg, S. & Kirsch, J. F. Measurement of heavy atom kinetic isotope effects by direct mass spectrometric analysis. *Anal. Chem.* **51,** 1375–1379 (1979).

18. Chan, J., Lewis, A. R., Gilbert, M., Karwaski, M. & Bennet, A. J. A direct NMR method for the measurement of competitive kinetic isotope effects. *Nat. Chem. Biol.* **6,** 405–407 (2010).

19. Chan, J., Lu, A. & Bennet, A. J. Turnover Is Rate-Limited by Deglycosylation for Micromonospora viridifaciens Sialidase-Catalyzed Hydrolyses: Conformational Implications for the Michaelis Complex. *J. Am. Chem. Soc.* **133,** 2989–2997 (2011).

20. Pascal, R. A., Baum, M. W., Wagner, C. K., Rodgers, L. R. & Huang, D. S. Measurement of deuterium kinetic isotope effects in organic and biochemical reactions by natural abundance deuterium NMR spectroscopy. *J. Am. Chem. Soc.* **108,** 6477–6482 (1986).

21. Sawada, M., Takai, Y., Chong, C., Hanafusa, T. & Misumi, S. Determination of the Secondary a-Deuterium Kinetic Isotope Effect on a Reverse Menschutkin Reaction Using Phosphorus-31 Nuclear Magnetic Resonance Spectrometry. *Anal. Chem.* **58,** 231–233 (1986).

22. Singleton, D. A. & Szymanski, M. J. Simultaneous Determination of Intermolecular and Intramolecular 13 C and 2 H Kinetic Isotope Effects at Natural Abundance. *J. Am. Chem. Soc.* **121,** 9455–9456 (1999).

23. McNaught, A. D. & Wilkinson, A. *International Union of Pure and Applied Chemistry. Compendium of Chemical Terminology: IUPAC Recommendations*. *IUPAC Compendium of Chemical Terminology* (1997). doi:10.1351/goldbook.I03352

24. De Laeter, J. R. *et al.* Atomic weights of the elements: Review 2000 (IUPAC Technical Report). *Pure Appl. Chem.* **75,** 683–800 (2003).

25. Pabis, A., Kamiński, R., Ciepielowski, G., Jankowski, S. & Paneth, P. Measurements of Heavy-Atom Isotope Effects Using 1H NMR Spectroscopy. *J. Org. Chem.* **76,** 8033–8035 (2011).

26. Hirschi, J. S., Takeya, T., Hang, C. & Singleton, D. A. Transition-State Geometry Measurements from 13C Isotope Effects. The Experimental Transition State for the Epoxidation of Alkenes with Oxaziridines. *J. Am. Chem. Soc.* **131,** 2397–2403 (2009).

27. Huang, M. *et al.* Dissecting the mechanisms of a class of chemical glycosylation using primary 13C kinetic isotope effects. *Nat. Chem.* **4,** 663–667 (2012).

28. Xiang, S. & Meyer, M. P. A General Approach to Mechanism in Multiproduct Reactions: Product-Specific Intermolecular Kinetic Isotope Effects. *J. Am. Chem. Soc.* **136,** 5832–5835 (2014).

29. Kwan, E. E., Park, Y., Besser, H. A., Anderson, T. L. & Jacobsen, E. N. Sensitive and Accurate 13C Kinetic Isotope Effect Measurements Enabled by Polarization Transfer. *J. Am. Chem. Soc.* **139,** 43–46 (2017).

30. Chan, J., Tang, A. & Bennet, A. J. A Stepwise Solvent-Promoted SNi Reaction of α-D-Glucopyranosyl Fluoride: Mechanistic Implications for Retaining Glycosyltransferases. *J. Am. Chem. Soc.* **134,** 1212–1220 (2012).

31. Speciale, G., Farren-Dai, M., Shidmoossavee, F. S., Williams, S. J. & Bennet, A. J. C2-Oxyanion Neighboring Group Participation: Transition State Structure for the Hydroxide-Promoted Hydrolysis of 4-Nitrophenyl α- D -Mannopyranoside. *J. Am. Chem. Soc.* **138,** 14012–14019 (2016).

32. Claridge, T. D. W. *High-resolution NMR techniques in organic chemistry*. (Elsevier, 2009).

33. Manning, K. A., Sathyamoorthy, B., Eletsky, A., Szyperski, T. & Murkin, A. S. Highly Precise Measurement of Kinetic Isotope Effects Using 1H-Detected 2D [13C, 1H]-HSQC NMR Spectroscopy. *J. Am. Chem. Soc.* **134,** 20589–20592 (2012).

34. Williams, S. J. & Withers, S. G. Glycosyl fluorides in enzymatic reactions. *Carbohydr. Res.* **327,** 27–46 (2000).

35. Tanaka, Y., Tao, W., Blanchard, J. S. & Hehre, E. J. Transition State Structures for the Hydrolysis of a-D-Glucopyranosyl Fluoride by Retaining and Inverting Reactions of Glycosylases. *J. Biol. Chem.* **269,** 32306–32312 (1994).

36. Bharti, S. K. & Roy, R. Quantitative 1H NMR spectroscopy. *TrAC Trends Anal. Chem.* **35,** 5–26 (2012).

37. Guido F. Pauli & Birgit U. Jaki, Lankin, D. C. Quantitative 1H NMR: Development and Potential of a Method for Natural Products Analysis. *J. Nat. Prod.* **68,** 133–149 (2005).

38. Findeisen, M., Brand, T. & Berger, S. A1H-NMR thermometer suitable for cryoprobes. *Magn. Reson. Chem.* **45,** 175–178 (2007).

39. Giraudeau, P. Quantitative 2D liquid-state NMR. *Magn. Reson. Chem.* **52,** 259–272 (2014).

40. Griffiths, L. & Irving, A. M. Assay by nuclear magnetic resonance spectroscopy: Quantification limits. *Analyst* **123,** 1061–1068 (1998).

41. Schoenberger, T. *et al.* Improving the Performance of High-Precision qNMR Measurements by a Double Integration Procedure in Practical Cases. *Anal. Chem.* **88,** 3836–3843 (2016).

42. Metz, K. R., Lam, M. M. & Webb, A. G. Reference deconvolution: A simple and effective method for resolution enhancement in nuclear magnetic resonance spectroscopy. *Concepts Magn. Reson.* **12,** 21–42 (2000).

43. Morris, G. A., Barjat, H. & Home, T. J. Reference deconvolution methods. *Prog. Nucl. Magn. Reson. Spectrosc.* **31,** 197–257 (1997).

44. Bodenhausen, G. & Ruben, D. J. Natural abundance nitrogen-15 NMR by enhanced heteronuclear spectroscopy. *Chem. Phys. Lett.* **69,** 185–189 (1980).

45. Martin, G. E. & Zektzer, A. S. Long-range two-dimensional heteronuclear chemical shift correlation. *Magn. Reson. Chem.* **26,** 631–652 (1988).

46. Mobli, M., Maciejewski, M. W., Schuyler, A. D., Stern, A. S. & Hoch, J. C. Sparse sampling methods in multidimensional NMR. *Phys. Chem. Chem. Phys.* **14,** 10835–10843 (2012).

47. Palmer, M. R. *et al.* Sensitivity of Nonuniform Sampling NMR. *J. Phys. Chem. B* **119,** 6502–6515 (2015).

48. Bax, A. & Morris, G. A. An improved method for heteronuclear chemical shift correlation by two-dimensional NMR. *J. Magn. Reson.* **42,** 501–505 (1981).

Chapter 3.

Both Chemical and Non-Chemical Steps Limit the Catalytic Efficiency of Family 4 Glycoside Hydrolases

This Chapter comprises the manuscript **"Both Chemical and Non-Chemical Steps Limit the Catalytic Efficiency of Family 4 Glycoside Hydrolases"**, which was published in the journal *Biochemistry* (**2018**, *57* (24), 3378-3386).

Natalia Sannikova,[a] Chloe A. N. Gerak,[a] Fahimeh S. Shidmoossavee,[a] Dustin T. King,[b] Saeideh Shamsi Kazem Abadi,[b] Andrew R. Lewis,[a] and Andrew J. Bennet[a,b]

[a]Department of Chemistry, Simon Fraser University, 8888 University Drive, Burnaby, British Columbia V5A 1S6, Canada

[b]Department of Molecular Biology and Biochemistry, Simon Fraser University, 8888 University Drive, Burnaby, British Columbia V5A 1S6, Canada

The following manuscript is a verbatim copy of the original paper published in *Biochemistry* **2018**, *57* (24), 3378-3386 and is formatted as per thesis rules and regulations of Simon Fraser University. Permission to reproduce the published material was obtained from the American Chemical Society. The authors made the following contribution to this work: Chloe A.N. Gerak aided in substrate synthesis, Dr. Fahimeh S. Shidmoossavee performed the preliminary kinetic investigation of metal ion dependence, Dr. Dustin T. King performed the thermostability analysis for the MelA enzyme, Dr. Saeideh Shamsi Kazem Abadi trained the author of this thesis to express and purify MelA, and Dr. Andrew R. Lewis helped with the set up for the NMR experiments. All experimental synthetic work and KIE measurements were performed by the author of this thesis. The manuscript was prepared by myself in collaboration with my thesis supervisor.

3.1. Abstract

The glycoside hydrolase family 4 (GH4) α-galactosidase from *Citrobacter freundii* (MelA) catalyzes the hydrolysis of fluoro-substituted phenyl α-D-galactopyranosides by utilizing two cofactors, NAD^+ and a metal cation, under reducing conditions. In order to refine the mechanistic understanding of this GH4 enzyme, leaving group effects were measured with various metal cations. The derived β_{lg} value on *V*/*K* for strontium activation is indistinguishable from zero (0.05 ± 0.12). Deuterium kinetic isotope effects (KIEs) were measured for the activated substrates 2-fluorophenyl and 4-fluorophenyl α-D-galactopyranosides in the presence of Sr^{2+}, Y^{3+}, and Mn^{2+}, where the isotopic substitution was on the carbohydrate at C-2 and/or C-3. To determine the contributing factors to the virtual transition state (TS) on which the KIEs report, kinetic isotope effects on isotope effects were measured on these KIEs using doubly deuterated substrates. The measured $^{D}V/K$ KIEs for MelA-catalyzed hydrolysis of 2-fluorophenyl α-D-galactopyranoside are closer to unity than the measured effects on 4-fluorophenyl α-D-galactopyranoside, irrespective of the site of isotopic substitution and of the metal cation activator. These observations are consistent with hydride transfer at C-3 to the on-board NAD^+, deprotonation at C-2, and a non-chemical step contributing to the virtual TS for *V*/*K*.

3.2. Introduction

A central metabolic process in all kingdoms of life involves the transfer of carbohydrates from a donor sugar to an acceptor molecule. Nature has evolved several different mechanisms for biological catalysts to cleave glycosidic linkages. The main group of enzymes that cleave glycosidic bonds are the glycoside hydrolases (GHs), and these enzymes use water as the acceptor to cleave a glycoconjugate donor. GH families can be subdivided into those in which the reaction at the anomeric center occurs with an inversion of configuration and those that give a retained aldose or ketose as the first-formed product. Among the retaining glycoside hydrolase families there are three main mechanisms, and two of these involve double S_N2-like inversions occurring via the formation of either a glycosyl-enzyme intermediate or a carbohydrate fused to an oxazole ring (substrate assisted catalysis).[1,2] The third catalytic mechanism involves an oxidation of the C-3-hydroxyl group, a step that involves hydride transfer to an obligatory NAD^+ cofactor to give a ketone that undergoes C-2−H deprotonation and anomeric aglycone departure to give an enzyme bound 3-ketoglycal intermediate (Scheme 3.1).[3–5] Interestingly, the two glycoside hydrolase families (GH4 and GH109) that function via this unusual mechanism contain enzymes from only archaea and bacteria.[6] Indeed, detailed mechanistic studies on three GH4 family members, BglT, GlvA, and MelA, have shown that in addition to NAD^+ this family requires

a divalent ion (generally Mn^{2+}) in concert with reducing conditions to catalyze the hydrolysis of glycosidic linkages.[3–5,7] Also, it has been shown that GlvA, a 6-phospho-α-glucosidase from *Bacillus subtilis*, hydrolyzes both α- and β-linked substrates.[3]

Scheme 3.1. Proposed Mechanism for GH4 Enzyme-Catalyzed Glycosidic Bond Cleavage*

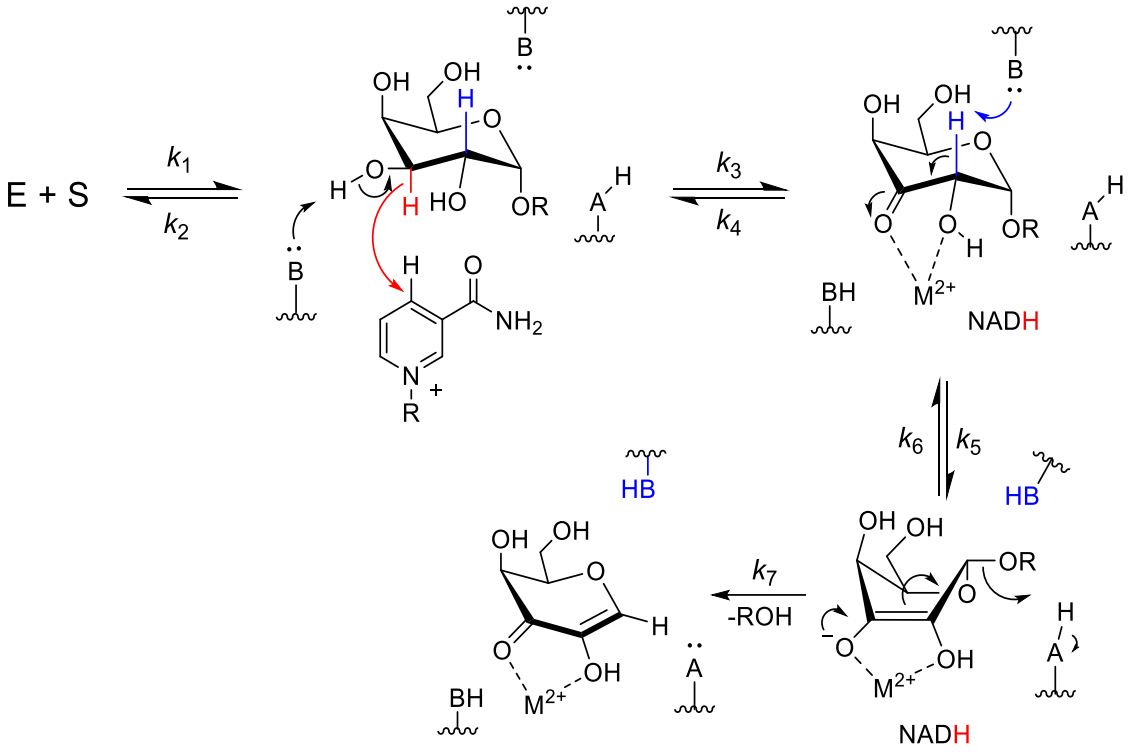

* Charges are not shown on the active site acid/base residues. Subsequent steps, which complete the catalytic cycle, are the microscopic reverse of those shown with water (R = H) as the nucleophile. The C-3 – H that undergoes a hydride transfer is shown in red, while the C-2 – H that is transferred as a proton is shown in blue.

On the basis of elegant kinetic isotope effect (KIE) studies, Yip and co-workers proposed that oxidation of C-3 (Scheme 3.1, k_3) and deprotonation of C-2 (k_5) are both kinetically significant steps, while aglycone departure (k_7) occurs rapidly.[3–5] The so-formed 3-ketoglycal intermediate subsequently acts as a Michael acceptor, and the catalytic cycle is completed by protonation at C-2 followed by ketone reduction by the on-board NADH.

Previously, Chakladar and co-workers reported that the obligate hydride and proton transfers that occur during the catalytic cycle of MelA,[8,9] a GH4 α-galactosidase from *Citrobacter freundii*, were coupled.[7] This surprising conclusion was based on the results of classic kinetic isotope effect experiments that were pioneered by Cleland and co-workers.[10–12] Specifically, for two sequential chemical steps that give rise to a virtual transition state (TS), which has no other contributing steps, the kinetic isotope effect on deprotonation should decrease for the C-3-

deuterated isotopologue (Scheme 3.1, k_3 and k_5);[7] however, Chakladar and co-workers noted no decrease in the proton transfer KIE on deuteration at C-3.[7]

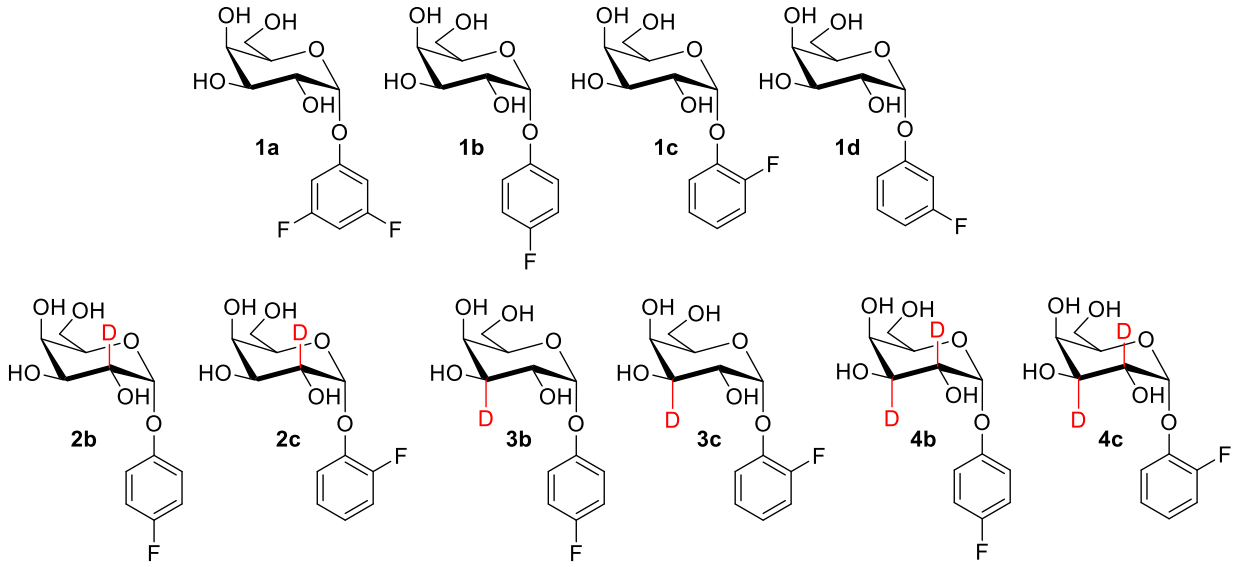

Figure 3.1. Compounds and Their Associated Isotopologues Used for the Measurement of Kinetic Isotope Effects on GH4-Catalyzed Hydrolyses.

In this report we detail the synthesis and characterization of four isotopologues of 2-fluorophenyl and 4-fluorophenyl α-D-galactopyranosides and their use with 3,5- difluorophenyl α-D-galactopyranoside to measure a series of competitive KIEs using ^{19}F NMR spectroscopy (Fig. 3.1). We measure a series of hydride and proton transfer KIEs for various metal cation activated MelA-catalyzed reactions. In addition, we report a series of kinetic isotope effects on isotope effects. Our results show that MelA is mechanistically more complex than previously assumed with at least two chemical and one non-chemical step contributing to the virtual transition state for *V*/*K*. Our findings should enable the design of inhibitors for this GH family that have potential therapeutic applications.

3.3. Experimental Procedures

3.3.1. Materials

1,2,3-Tri-*O*-acetyl-D-galactal and D-galactal were purchased from Carbosynth Ltd. 4-Fluorophenol, 2-fluorophenol, 3-fluorophenol, and 3,5-difluorophenol were purchased from Oakwood Chemicals. All other reagents were purchased from Sigma-Aldrich and used without purification. Thin-layer chromatography (TLC) was performed on aluminum-backed TLC plates

precoated with Merck silica gel 60 F_{254}. Compounds were visualized with UV light and/or staining with *p*-anisaldehyde solution or Seebach stain. Flash chromatography was performed on a Teledyne CombiFlash Rf system using RediSep Rf Gold normal-phase silica flash columns. Solvents in anhydrous reactions were dried and distilled immediately prior to use. THF was dried and distilled over sodium metal/benzophenone, and dichloromethane was dried and distilled over calcium hydride. For anhydrous reactions, all glassware was flame-dried and cooled under a nitrogen atmosphere immediately prior to use. Milli-Q water (18.2 MΩ cm) was used for all kinetic experiments. All pH values were measured using a standard pH electrode attached to a VWR pH meter. All NMR spectra were recorded on a Bruker Advance 500 or 600 MHz spectrometer. Chemical shifts are reported in parts per million downfield from TMS. Coupling constants (*J*) are reported in hertz. All NMR peak assignments are based on $^{1}H-^{1}H$ COSY and $^{1}H-^{13}C$ HSQC experiments. All fitting of kinetic data was performed using the appropriate nonlinear least-squares equation in GraphPad Prism (version 5.04).

3.3.2. Synthesis of Aryl α-D-Galactopyranosides

All aryl α-D-galactopyranosides were synthesized from 1,2,3,4,6-penta-*O*-acetyl-β-D-galactopyranose using stannic chloride in CH_2Cl_2. Typically, 1,2,3,4,6-penta-*O*-acetyl-β-D-galactopyranose (1.0 g, 2.56 mmol) and the appropriate phenol (5.12 mmol) were dissolved in anhydrous CH_2Cl_2 (30 mL), and then $SnCl_4$ (0.6 mL, 5.12 mmol) was added to the reaction mixture. The resulting mixture was stirred at room temperature under an inert atmosphere for 72 h, at which time TLC analysis showed that the reaction was complete. Following the addition of water (20 mL), the reaction mixture was neutralized by addition of saturated aqueous $NaHCO_3$ solution (15 mL). The product was extracted from the aqueous layer with CH_2Cl_2 (3 × 30 mL), and the combined organic layer was washed with water (30 mL) and brine (30 mL), dried over Na_2SO_4, and concentrated under reduced pressure to yield the crude product. This material was purified by flash chromatography using EtOAc/hexanes as the eluent to give pure α-anomer. Deprotection was accomplished under Zemplen conditions using catalytic sodium methoxide in methanol followed by neutralization with Amberlite IR120 H^+ resin. Final products were purified by recrystallization from aqueous ethanol.

3,5-Difluorophenyl α-D-galactopyranoside (1a): ^{1}H NMR (600 MHz, D_2O) δ 6.82 (qd, *J* = 7.3, 3.1 Hz, 2H, Ar H), 6.70 (tt, *J* = 9.3, 2.1 Hz, 1H, Ar H), 5.69 (d, *J* = 3.8 Hz, 1H, H-1), 4.10−4.04 (m, 2H, H-5, H-3), 4.03−3.97 (m, 2H, H-4, H-2), 3.76−3.67 (m, 2H, H-6, H-6′); ^{13}C NMR (151 MHz, D_2O) δ 163.21 (dd, *J* = 244.5, 15.9 Hz, Ar), 157.80 (t, *J* = 14.0 Hz, Ar), 100.74 (dd, *J* = 23.0, 6.4 Hz, Ar), 98.10 (t, *J* = 26.2 Hz, Ar), 97.23 (C-1), 71.96 (C-5), 69.32 (C-3), 69.02 (C-4),

67.86 (C-2), 60.94 (C-6); ^{19}F NMR (471 MHz, D_2O) δ −109.76 (t, *J* =8.8 Hz); ESI-MS for $C_{12}H_{14}O_6F_2$ *m*/*z* calcd for (M + Na^+) 315.0651, found 315.0651.

4-Fluorophenyl α-D-galactopyranoside (1b): ^{1}H NMR (600 MHz, D_2O) δ 7.18 (dd, *J* = 9.0, 4.5 Hz, 2H, Ar H), 7.13 (t, *J* = 8.8 Hz, 2H, Ar H), 5.59 (d, *J* = 3.7 Hz, 1H, H-1), 4.11 (app t, *J* = 6.1 Hz, 1H, H-5), 4.09−4.03 (m, 2H, H-4, H-3), 3.99 (dd, *J* = 9.4, 3.4 Hz, 1H, H-2), 3.72 (app d, *J* = 6.1 Hz, 2H, H-6, H-6′); 13C NMR (151 MHz, D_2O) δ 158.35 (d, *J* = 238.2 Hz, Ar), 152.24 (d, *J* = 2.2 Hz, Ar), 119.04 (d, *J* = 8.5 Hz, Ar), 116.01 (d, *J* = 23.3 Hz, Ar), 98.16 (C-1), 71.69 (C-5), 69.38 (C-3), 69.14 (C-4), 68.04 (C-2), 61.00 (C-6); ^{19}F NMR (471 MHz, D_2O) δ −121.39 (tt, *J* = 8.5, 4.4 Hz); ESI-MS for $C_{12}H_{15}O_6F$ *m*/*z* calcd for (M + Na^+) 297.0745, found 297.0748.

2-Fluorophenyl α-D-galactopyranoside (1c): ^{1}H NMR (600 MHz, D_2O) δ 7.35 (td, *J* = 8.3, 1.7 Hz, 1H, Ar H), 7.24 (ddd, *J* = 11.5, 8.0, 1.7 Hz, 1H, Ar H), 7.20 (tdd, *J* = 8.0, 1.8, 0.9 Hz, 1H, Ar H), 7.16 (ddd, *J* = 7.9, 4.6, 1.7 Hz, 1H, Ar H), 5.67 (d, *J* = 3.8 Hz, 1H, H-1), 4.20 (dd, *J* = 7.1, 5.3 Hz, 1H, H-5), 4.12 (dd, *J* = 10.3, 3.3 Hz, 1H, H-3), 4.09 (d, *J* = 3.2 Hz, 1H, H-4), 4.02 (dd, *J* = 10.3, 3.8 Hz, 1H, H-2), 3.73 (d, *J* = 1.8 Hz, 1H, H-6), 3.72 (d, *J* = 4.1 Hz, 1H, H-6′); ^{13}C NMR (151 MHz, D_2O) δ 153.56 (d, *J* = 244.2 Hz, Ar), 143.40 (d, *J* = 10.9 Hz, Ar), 124.82 (d, *J* = 3.8 Hz, Ar), 124.31 (d, *J* = 7.3 Hz, Ar), 120.07 (Ar), 116.63 (d, *J* = 18.6 Hz, Ar), 99.00 (C-1), 72.02 (C-5), 69.25 (C-3), 69.12 (C-4), 68.07 (C-2), 60.97 (C-6); ^{19}F NMR (471 MHz, D_2O) δ −133.42 (ddd, *J* = 12.2, 8.5, 4.6 Hz); ESI-MS for $C_{12}H_{15}O_6F$ *m*/*z* calcd for (M + Na^+) 297.0745, found 297.0749.

2-Fluorophenyl α-D-galactopyranoside (1d): ^{1}H NMR (600 MHz, D_2O) δ 7.37 (q, *J* = 7.9 Hz, 1H, Ar H), 6.99 (dd, *J* = 14.8, 9.9 Hz, 2H, Ar H), 6.88 (t, *J* = 8.6 Hz, 1H, Ar H), 5.68 (d, *J* = 3.8 Hz, 1H, H-1), 4.10−4.01 (m, 3H, H-3, H-4, H-5), 3.99 (dd, *J* = 10.2, 3.8 Hz, 1H, H-2), 3.71 (app d, *J* = 6.2 Hz, 2H, H-6, H- 6′); ^{13}C NMR (151 MHz, D_2O) δ 163.12 (d, *J* = 243.5 Hz, Ar), 157.30 (d, *J* = 11.1 Hz, Ar), 130.68 (d, *J* = 10.0 Hz, Ar), 112.92 (d, *J* = 2.9 Hz, Ar), 109.55 (d, *J* = 21.2 Hz, Ar), 104.77 (d, *J* = 24.9 Hz, Ar), 97.33 (C-1), 71.83 (C-5), 69.46 (C-3), 69.13 (C-4), 68.02 (C-2), 60.98 (C-6); ^{19}F NMR (471 MHz, D_2O) δ −112.00 (dt, *J* = 9.8, 7.6 Hz); ESI-MS for $C_{12}H_{15}O_6F$ *m*/*z* calcd for (M + Na^+) 297.0745, found 297.0747.

3.3.3. Synthesis of Aryl α-D-Galactopyranoside Isotopologues

Aryl α-D-(2-^{2}H)galactopyranosides were synthesized from dimeric 3,4,6-tri-*O*-acetyl-2-deoxy-2-nitroso-α-D-galactopyranosyl chloride,[13] and aryl α-D-(3-^{2}H)- and α-D-(2-^{2}H,3-^{2}H)galactopyranosides were synthesized from dimeric 3,4,6-tri-*O*-acetyl-2-deoxy-2-nitroso-α-D-(3-^{2}H)galactopyranosyl chloride according to the reported procedure[7] except that the appropriately

substituted fluorophenol was used in place of phenol. A slightly modified synthesis of 3,4,6-tri-*O*-acetyl-D-(3-^{2}H)galactal, which gives higher yields, is detailed in the Supporting Information.

2-Fluorophenyl α-D-(2-^{2}H)galactopyranoside (2b): ^{1}H NMR (600 MHz, D_2O) δ 7.20 (dd, *J* = 8.7, 4.6 Hz, 2H, Ar H), 7.15 (t, *J* = 8.6 Hz, 2H, Ar H), 5.61 (s, 1H, H-1), 4.12 (app t, *J* = 6.1 Hz, 1H, H-5), 4.09 (s, 2H, H-3, H-4), 3.74 (app d, *J* = 6.0 Hz, 2H, H-6, H-6′); ^{13}C NMR (151 MHz, D_2O) δ 118.59 (d, *J* = 8.5 Hz, Ar), 115.55 (d, *J* = 23.3 Hz, Ar), 97.67 (C-1), 71.23 (C-5), 68.87 (C-3), 68.68 (C-4), 60.54 (C-6); ^{19}F NMR (471 MHz, D_2O) δ −121.39 (tt, *J* = 8.4, 4.4 Hz); ESI-MS for $C_{12}H_{14}DO_6F$ *m*/*z* calcd for (M + Na^+) 298.0808, found 298.0811.

2-Fluorophenyl α-D-(2-^{2}H)galactopyranoside (2c): ^{1}H NMR (600 MHz, D_2O) δ 7.35 (td, *J* = 8.2, 1.4 Hz, 1H, Ar H), 7.24 (ddd, *J* = 11.4, 8.1, 1.5 Hz, 1H, Ar H), 7.20 (tt, *J* = 8.0, 0.8 Hz, 1H, Ar H), 7.15 (ddd, *J* = 7.6, 4.7, 1.7 Hz, 1H, Ar H), 5.66 (s, 1H, H-1), 4.20 (app t, *J* = 6.4 Hz, 1H, H-5), 4.12 (d, *J* = 3.3 Hz, 1H, H-3), 4.10−4.07 (m, 1H, H-4), 3.73−3.71 (m, 2H, H-6, H-6′); ^{13}C (151 MHz, D_2O) δ 153.56 (d, *J* = 244.2 Hz, Ar), 143.41 (d, *J* = 10.8 Hz, Ar), 124.82 (d, *J* = 3.7 Hz, Ar), 124.31 (d, *J* = 7.3 Hz, Ar), 120.06 (Ar), 116.63 (d, *J* = 18.6 Hz, Ar), 98.97 (C-1), 72.01 (C-5), 69.19 (C-3), 69.12 (C-4), 60.97 (C-6); ^{19}F NMR (471 MHz, D_2O) δ −133.40 (ddd, *J* = 12.4, 8.9, 4.8 Hz); ESI-MS for $C_{12}H_{14}DO_6F$ *m*/*z* calcd for (M + Na^+) 298.0808, found 298.0811.

4-Fluorophenyl α-D-(3-^{2}H)galactopyranoside (3b): ^{1}H NMR (600 MHz, D_2O) δ 7.18 (dd, *J* = 9.2, 4.5 Hz, 2H, Ar H), 7.13 (dd, *J* = 9.3, 8.4 Hz, 2H, Ar H), 5.59 (d, *J* = 3.9 Hz, 1H, H-1), 4.10 (td, *J* = 6.1, 1.2 Hz, 1H, H-5), 4.06 (d, *J* = 1.1 Hz, 1H, H-4), 3.99 (d, *J* = 3.9 Hz, 1H, H-2), 3.72 (app d, *J* = 6.2 Hz, 2H, H-6, H-6′); ^{13}C NMR (151 MHz, D_2O) δ 158.35 (d, *J* = 238.3 Hz, Ar), 152.24 (d, *J* = 2.3 Hz, Ar), 119.04 (d, *J* = 8.4 Hz, Ar), 116.01 (d, *J* = 23.3 Hz, Ar), 98.16 (C-1), 71.69 (C-5), 69.09 (C-4), 67.99 (C-2), 60.99 (C-6); ^{19}F NMR (471 MHz, D_2O) δ −121.39 (tt, *J* = 8.6, 4.4 Hz); ESI-MS for $C_{12}H_{14}DO_6F$ *m*/*z* calcd for (M + Na^+) 298.0808, found 298.0810.

2-Fluorophenyl α-D-(3-^{2}H)galactopyranoside (3c): ^{1}H NMR (600 MHz, D_2O) δ 7.37 (t, *J* = 8.3 Hz, 1H, Ar H), 7.30−7.24 (m, 1H, Ar H), 7.22 (t, *J* = 7.8 Hz, 1H, Ar H), 7.18 (dd, *J* = 6.9, 5.3 Hz, 1H, Ar H), 5.69 (d, *J* = 3.7 Hz, 1H, H-1), 4.26−4.19 (m, 1H, H-5), 4.11 (s, 1H, H-4), 4.04 (d, *J* = 3.7 Hz, 1H, H-2), 3.78−3.68 (m, 2H, H-6, H-6′); ^{13}C NMR (151 MHz, D_2O) δ 124.12 (d, *J* = 76.3 Hz, Ar), 119.60 (Ar), 116.17 (d, *J* = 18.5 Hz, Ar), 98.54 (C-1), 71.56 (C-5), 68.62 (C-4), 67.56 (C-2), 60.51 (C-6); ^{19}F NMR (471 MHz, D_2O) δ −133.42 (ddd, *J* = 12.2, 8.5, 4.6 Hz); ESI-MS for $C_{12}H_{14}DO_6F$ *m*/*z* calcd for (M + Na^+) 298.0808, found 298.0809.

4-Fluorophenyl α-D-(2,3-$^{2}H_2$)galactopyranoside (4b): ^{1}H NMR (600 MHz, D_2O) δ 7.26−7.17 (m, 2H, Ar H), 7.15 (t, *J* = 8.3 Hz, 2H, Ar H), 5.61 (s, 1H, H-1), 4.12 (app t, *J* = 6.1 Hz,

1H, H-5), 4.08 (s, 1H, H-4), 3.74 (app d, *J* = 5.8 Hz, 2H, H-6, H-6′); ^{13}C NMR (151 MHz, D_2O) δ 118.58 (d, *J* = 8.4 Hz, Ar), 115.55 (d, *J* = 23.4 Hz, Ar), 97.66 (C-1), 71.23 (C-5), 68.63 (C-4), 60.53 (C-6); ^{19}F NMR (471 MHz, D_2O) δ −121.40 (tt, *J* = 8.4, 4.4 Hz); ESI-MS for $C_{12}H_{13}D_2O_6F$ *m*/*z* calcd for (M + Na^+) 299.0870, found 299.0870.

2-Fluorophenyl α-D-(2,3-$^2H_2$)galactopyranoside (4c): ^{1}H NMR (600 MHz, D_2O) δ 7.34 (td, *J* = 8.3, 1.7 Hz, 1H, Ar H), 7.24 (ddd, *J* = 11.5, 8.1, 1.7 Hz, 1H, Ar H), 7.19 (tdd, *J* = 8.3, 1.8, 0.9 Hz, 1H, Ar H), 7.15 (ddd, *J* = 8.0, 4.7, 1.7 Hz, 1H, Ar H), 5.66 (s, 1H, H-1), 4.19 (dddd, *J* = 7.0, 5.1, 1.2, 0.6 Hz, 1H, H-5), 4.08 (dd, *J* = 1.2, 0.6 Hz, 1H, H-4), 3.72 (d, *J* = 1.9 Hz, 1H, H-6), 3.71 (d, *J* = 4.1 Hz, 1H, H-6′); ^{13}C NMR (151 MHz, D_2O) δ 153.56 (d, *J* = 244.2 Hz), 143.41 (d, *J* = 10.8 Hz), 124.82 (d, *J* = 3.8 Hz), 124.30 (d, *J* = 7.3 Hz), 120.05 (d, *J* = 1.1 Hz), 116.63 (d, *J* = 18.6 Hz), 98.99, 72.03, 69.10, 60.98; 19F NMR (471 MHz, D_2O) δ −133.41 (ddd, *J* = 12.9, 8.9, 4.7 Hz); ESI-MS for $C_{12}H_{13}D_2O_6F$ *m*/*z* calcd for (M + Na^+) 299.0870, found 298.0877.

3.3.4. Protein Expression and Purification

The previously described[6] plasmid containing the MelA gene, which encodes the α-galactosidase in a pET28a vector, was transformed into *Escherichia coli* BL21 (DE3) cells. Cultures were grown at 37 °C in TB (terrific broth) media supplemented with 30 μg/mL kanamycin to an OD_{600} of approximately 0.6 absorbance units. Protein expression was induced with 0.5 mM IPTG, and cells were cultured for a further 5 h at 25 °C. Cells were harvested by centrifugation, resuspended in binding buffer (15 mL, 250 mM phosphate, 50 mM NaCl, pH 7.5, 5 mM imidazole), and lysed using 0.5 mg/mL chicken egg white lysozyme and a protease inhibitor cocktail tablet (Pierce Protease Inhibitor Tablets, EDTA free, Thermo Scientific) followed by sonication. The GH4 α-galactosidase was purified on an ACTA FPLC system using a nickel affinity chromatography column (1 mL HisTrap HP, GE Healthcare) and a 5 to 500 mM imidazole gradient. Fractions containing pure enzyme as determined by 10% sodium dodecyl sulfate−polyacrylamide gel electrophoresis were combined. The enzyme was buffer exchanged into 100 mM HEPES, pH 8.0, 50 mM NaCl, and 6 mM DTT and stored at −80 °C in 25 μL aliquots. Protein concentration was determined by Abs280 values on a NanoDrop UV−vis spectrophotometer.

3.3.5. Kinetic Investigation of Metal Ions

Enzyme assays were performed following the reported procedure by monitoring hydrolysis of 4-nitrophenyl α-D-galactopyranoside at λ = 400 nm at pH 7.5.[7] Specifically, the reaction mixture, which contained HEPES (50 mM), MCl_2 (1.0 mM; M = Mn, Sr, or Zn), NAD^+ (0.1 mM), 2-

mercaptoethanol (10 mM), BSA (0.1%, w/v), and enzyme (2 µL of the purified batch), was incubated for 15 min at 37 °C before the addition of substrate (50 µM), and the absorbance at 400 nm was monitored for 30 min.

3.3.6. Relative Reaction Rate Measurements

In the Presence of Sr^{2+}. The ratios of *V*/*K* values for unlabeled aryl α-D-galactopyranosides were determined via ^{19}F NMR spectroscopy on a Bruker Avance III 500 MHz spectrometer.[14,15] Reactions were performed in a 5 mm NMR tube in 100 mM HEPES buffer (pH 8.0), containing 1 mM NAD^+, 10 mM $SrCl_2$, 1 mM TCEP, 50 mM NaCl, 1% w/v BSA, and 10% v/v D_2O for spectral locking. Fluorine-19 T_1 values were measured for unlabeled aryl α-D-galactopyranosides and 3-fluoro-4-nitrophenol (internal standard) using standard inversion recovery pulse sequence and were determined to be 1.157, 2.900, 1.007, 1.372, and 1.928 s for **1a**, **1b**, **1c**, **1d**, and 3-fluoro-4-nitrophenol, respectively.

In a typical experiment, a portion (540 µL) of a stock solution, which contained a mixture of aryl α-D-galactopyranosides **1a** (3.2 mg), **1b** (9.2 mg), **1c** (10.8 mg), and **1d** (4.5 mg) and internal standard 3-fluoro-4-nitrophenol (2.0 mg) in 1.9 mL of Milli-Q H_2O and 260 µL D_2O, was added to a concentrated buffer solution containing all cofactors (85 µL). The reaction was initiated by the addition of enzyme (25 µL of a stock solution containing 7.3 mg/mL). Quantitative proton-decoupled ^{19}F spectra were acquired using an inverse-gated pulse sequence (spectral width, 28409 Hz). The FID was acquired for 16 scans (acquisition time, 1.15 s) accumulated with a recycle delay of 30 s between scans (8.05 min per spectrum). Fourier transformation of the FIDs was performed with 2-fold zero filling and application of an exponential line broadening between 1.8 and 2.5 Hz. Spectra were phased manually and baseline corrected using MestReNova version 10.0.2. The ^{19}F signals corresponding to **1a** (−109.72 ppm), **1d** (−111.94 ppm), 3-fluoro-4-nitrophenol (−113.92 ppm), **1b** (−121.36 ppm), and **1c** (−133.39 ppm) were integrated. Normalization of substrate peak areas to the standard was performed automatically using the MestReNova integration algorithm. The resultant fraction of the reaction (F_1) for 1a and individual peak areas were calculated; these data were input into GraphPad Prism 5.04, and a nonlinear least-squares fit to eq. 3.1[16] was performed, where $(V/K)_X/(V/K)_{3,5diF}$ is the ratio *V*/*K* values for the GH4−catalyzed hydrolysis of **1b** (**1c** or **1d**) to **1a** and *R* and R_0 are the concentration ratios of **1b** (**1c** or **1d**) to **1a** at $F_1 = F_1$ and 0, respectively.

$$\frac{R}{R_0} = (1 - F_1)^{\left((V/K)_X/(V/K)_{3,5-diF}\right)-1} \qquad (3.1)$$

In the Presence of Y^{3+} and Mn^{2+}. Experiments were performed following the same procedure as described above for the strontium-promoted reactions except the enzyme was pre-incubated with 10 μM $Y(NO_3)_3$ or $MnCl_2$ for 15 min at 25 °C prior to addition to the NMR tube. The low metal ion concentrations used were necessary to avoid precipitate formation between Y^{3+} and TCEP and to minimize line broadening effects for NMR experiments performed with the paramagnetic Mn^{2+} ion.

Measurement of the Rate Constant Ratios for Aryl α-D-Galactopyranoside Isotopologues. Experiments for labeled aryl α-D-galactopyranoside were performed in an identical manner to those described above for the unlabeled compound panel. The resultant rate constant ratios were calculated relative to **1a**. Three series of experiments were performed for each metal ion (Sr^{2+}, Y^{3+}, and Mn^{2+}): (1) **2b**, **2c** versus **1a**; (2) **3b**, **3c** versus **1a**; and (3) **4b**, **4c** versus **1a**.

3.3.7. KIE Calculations

Isotope effects on *V*/*K* were calculated by taking a ratio of two competitive *V*/*K* values from experiments using unlabeled **1a** versus aryl α-D-galactopyranoside and **1a** versus an isotopologue of aryl α-D-galactopyranoside (eqs S1−S4 in the Supporting Information). The nomenclature for KIEs developed by Cleland is used throughout this manuscript.[17] For example, $^{3\text{-D}}(V/K)_{2\text{-H}}$ and $^{3\text{-D}}(V/K)_{2\text{-D}}$ refer specifically to KIEs measured for hydride/deuteride transfer from C-3 on the C-2−H and C-2−D isotopologues, respectively.

3.3.8. Thermostability Analysis of MelA

The stability of MelA in various buffers was measured as a function of temperature dependent protein unfolding by differential scanning fluorimetry (DSF) using the Protein Thermal Shift kit (ThermoFisher Scientific). Briefly, 4.6 μM purified MelA protein in various buffers was added to 2.5 μL of 10 × thermal shift dye to give a final volume of 25 μL in a 0.1 mL MicroAmp Fast Optical 96-Well reaction plate. Samples were sealed using MicroAmp optical adhesive film and incubated on ice for 30 min. Following pre-incubation, thermal ramping experiments were performed using a StepOnePlus Real-Time PCR system. The heating cycle included a 1 min warming step at 26 °C and a subsequent gradient between 26 and 97 °C at a constant ramp rate of 1.5 °C/min. Data were collected using the setting for ROX reporter detection (λ_{ex} = 570 nm; λ_{em} = 591 nm) installed on the instrument. The resulting RFU values were plotted as a function of

temperature using a Boltzmann sigmoidal nonlinear regression in GraphPad Prism 7.0, where the inflection point of each fitted curve was defined as the melting temperature, T_m.

3.3.9. Protein Homology Modeling for MelA

The sequence of MelA α-galactosidase from *C. freundii* (GenBank: BAB20428.1) was used for fold recognition and homology modeling. The MelA α-galactosidase sequence analysis and fold recognition were carried out using IntFOLD (http://www.reading.ac.uk/ bioinf/IntFOLD/); ligand binding site prediction was carried out using FunFOLD (http://www.reading.ac.uk/bioinf/ FunFOLD/). The structure of AglA α-glucosidase A from *Thermotoga maritima* (PDB code: 1OBB)[18] was used as a template (21% sequence identity). The structure was also predicted using Phyre2 (http://www.sbg.bio.ic.ac.uk/phyre2/ html/page.cgi?id=index) to validate the model. The MelA α-galactosidase model analysis was carried out using UCSF Chimera version 1.12. Superposition of the model and template structures showed the identity of the active sites and Mn^{2+} and NAD^+ cofactor binding sites.

3.4. Results and Discussion

3.4.1. Substrate Specificity of MelA

The Mn^{2+} activated GH4 α-galactosidase from *C. freundii* efficiently hydrolyzes aryl α-D-galactopyranoside with no effect of leaving group ability on either the first-order (k_{cat}) or the second-order (k_{cat}/K_m) enzymatic rate constants.[7] In order to utilize a ^{19}F NMR methodology[15,19,20] for the measurement of competitive rate constants, we decided to use a diamagnetic divalent metal cation to activate the enzyme rather than paramagnetic Mn^{2+}. Therefore, we tested the relative activity of MelA, in comparison to manganous ion, in the presence of Zn^{2+} and Sr^{2+} using UV−vis spectroscopy with 4-nitrophenyl α-D-galactopyranoside as the substrate. We noted no observable activity with Zn^{2+}, but Sr^{2+} (at a concentration of 1 mM) displays a relative activity of 50% compared to that of Mn^{2+} (at the same concentration, data not shown). We initially planned to use α-D-galactopyranosyl fluoride and the appropriate isotopologues as substrates for the measurement of relative rate constants by ^{19}F NMR spectroscopy:[15,19,20] a choice that was based on literature reports that glycosyl fluorides are universally good substrates for the corresponding glycosidase. For example, Williams and Withers stated in their review articles that "... there are no known examples of glycosidases that cannot process the glycosyl fluoride that corresponds to the substrate".[21] As a result, we made the corresponding fluoride for testing; however, we quickly ascertained that α-D-galactopyranosyl fluoride is an exceedingly poor substrate for MelA.

Specifically, we only observed nonenzymatic hydrolyses, with the faster reactions occurring at higher pH values (HEPES buffer, pH 8.0, all material hydrolyzed in 4−5 h; NaOAc buffer, pH 5.0, hydrolysis complete in 3 days). These observations are, to the best of our knowledge, unprecedented, with their origin being the unusual mechanism for GH4 (and GH109) enzymes. Consequently, we generated a homology model of MelA using the structure AglA α-glucosidase A from *T. maritima*, which is inactive as the critical cysteine has been oxidized, and so it contains a bound molecule of substrate.[18] The model was created using "IntFOLD",[22,23] with the manganese and NAD^+ cofactors added separately,[24,25] and is shown in Figure 3.2.

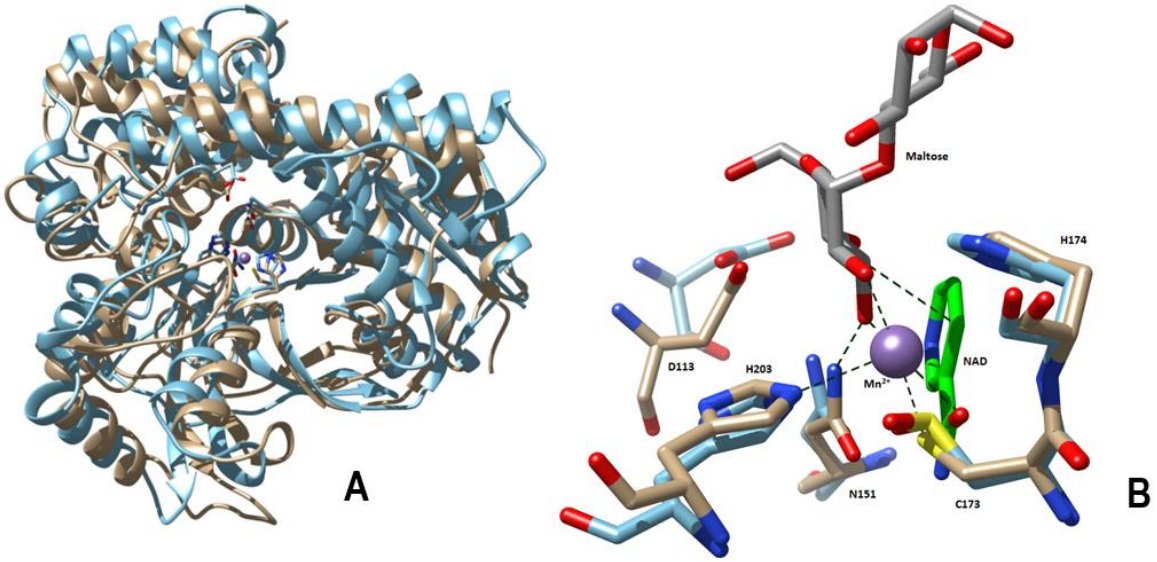

Figure 3.2. **(A)** Overlay of the crystal structure of AglA α-glucosidase A from *T. maritima* (blue) and homology model of MelA α-galactosidase (beige). **(B)** Overlay of active site structure of AglA α-glucosidase A (blue), which includes the bound substrate maltose, the modeled active site for MelA α-galactosidase (beige), and the modeled Mn^{2+} cation (purple). Predicted key interactions with cofactors (NAD^+ and Mn^{2+}) and substrate are shown for MelA α-galactosidase; no general acid is positioned in close proximity to the leaving group.

That is, the amino acid sequence analysis of MelA suggests that the protein folds, with high confidence, in a structure similar to AglA (1OBB),[18] with the IntFOLD model having a high C-score and a TM-score of 0.73. Superposition of the modeled MelA and the AglA X-ray structure exhibits an RMSD value for the Cα atoms of the theoretical model and template crystal structure of 2.69 Å.

We were unable to locate any general acid residue in MelA that would be positioned in close proximity to the corresponding position that the glucose aglycone occupies in the structure of AglA. We conclude that formation of the α,β-unsaturated ketone intermediate has a sufficient

driving force for elimination of a sugar alkoxide leaving group without the need for general acid catalysis. We suggest that the lack of general acid catalysis results in the catalytic inefficiency of MelA toward α-D-galactopyranosyl fluoride and in the observations by Yip and Withers that family GH4 enzymes possess thioglycosidase activity.[26] That is, fluoride is a very poor leaving group in the absence of catalysis,[27] as it will be poorly solvated within the enzymatic active site, whereas thiolates do not require catalysis to depart from anionic transition states.

3.4.2. Relative Rate Constants for MelA-Catalyzed Hydrolyses

To measure relative *V*/*K* values for the reactions of MelA by ^{19}F NMR spectroscopy, we used a remote labeling protocol. Specifically, the relative rates of reactions of mixtures containing fluorophenyl α-D-galactopyranosides were monitored in an NMR tube. First, we modified the experimental conditions from those reported by Chakladar and co-workers[7] by (i) lowering the reaction temperature (to 25 °C) so that multiple NMR spectra could be acquired per kinetic experiment and (ii) raising the pH slightly (8.0 instead of 7.5) so as to increase the stability of MelA (see Figure S1 for melting temperature data). Second, we verified that the use of a different divalent cation (Sr^{2+}) does not introduce a leaving group dependence on *V*/*K*, which is not evident for the Mn^{2+}-activated enzyme[7] (Table 3.1).

Table 3.1. Ratio of V/K values for the GH4-catalyzed hydrolysis of unlabeled aryl α-D-galactopyranoside in presence of different metals.[a]

Compound 1	Compound 2	Sr^{2+}	Mn^{2+}	Y^{3+}
GalO3,5diF	GalO4F	0.65 ± 0.01	0.76 ± 0.07	0.67 ± 0.01
GalO3,5diF	GalO2F	0.55 ± 0.03	0.63 ± 0.13	0.56 ± 0.02
GalO3,5diF	GalO3F	0.88 ± 0.06	ND[b]	ND[b]

[a]Ratio is for $(V/K)_{cmpd1}/(V/K)_{cmpd2}$; experimental conditions are given in the materials and methods section, values are the mean and standard deviation for four experimental determinations. [b]ND = not determined.

A Brønsted plot is shown in Figure 3.3, which exhibits a β_{lg} value of 0.05 ± 0.12 for the relative rates of hydrolysis for four fluoroaryl α-D-galactopyranosides (a typical reaction panel of acquired ^{19}F NMR spectra is shown in Figure S2). Last, we note that the least reactive aryl α-D-galactopyranoside (3,5-difluorophenyl) has the most acidic conjugate acid.

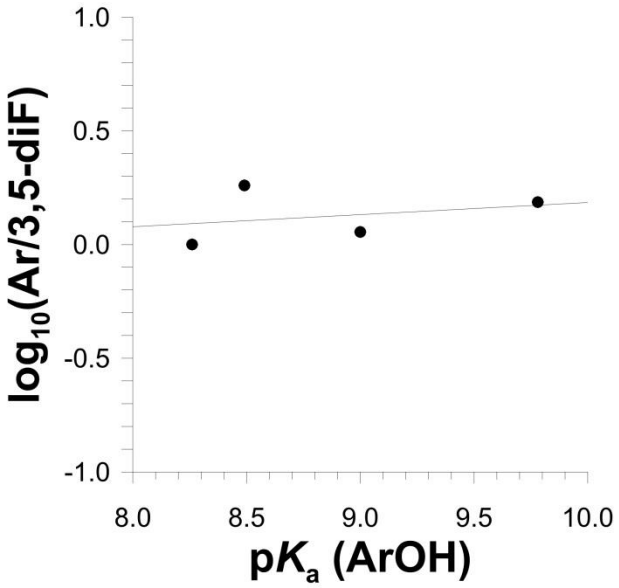

Figure 3.3. Effect of leaving group ability on relative V/K rate constants for MelA-catalyzed hydrolysis of aryl α-D-galactopyranoside at 25 °C and pH 8.00.

Leaving group ability is represented as pK_a (BH^+) as follows: 3,5-difluorophenol (8.26), 2-fluorophenol (8.49), 3-fluorophenol (9.00), and 4-fluorophenol (9.78). The solid line represents the best linear fit to the data, error bars are contained within the symbol diameter.

3.4.3. Proton and Hydride Transfer Kinetic Isotope Effects Vary with Leaving Group and Activating Metal Cation

We note that, surprisingly, the measured KIEs for both proton (C-2−H) and hydride (C-3−H) transfer depend on the identity of the leaving group despite the lack of leaving group dependence on *V*/*K* (entry 1 in Tables 3.2 and 3.3).[6] Moreover, the KIEs measured for proton transfer from C-2, for the strontium-containing enzyme, are significantly larger than the previously reported value for the manganese-activated MelA- catalyzed hydrolysis of phenyl α-D-galactopyranoside ($k_H/k_D \sim 1.7$).[7]

Table 3.2. Measured $^{2\text{-D}}(V/K)_{3\text{-H}}$ effects for the GH4-catalyzed hydrolysis of aryl α-D-(2-^{2}H)galactopyranosides with various metal activators at pH 8.0 and 25 °C.[a]

Entry	Metal	pK_a $(M^{X+})_{aq}$[b]	Aglycone	$^{2\text{-D}}(V/K)_{3\text{-H}}$	Aglycone	$^{2\text{-D}}(V/K)_{3\text{-H}}$
1	Sr^{2+}	13.18	2-fluorophenyl	2.45 ± 0.12	4-fluorophenyl	3.13 ± 0.22
2	Mn^{2+}	10.59	2-fluorophenyl	1.08 ± 0.12	4-fluorophenyl	1.43 ± 0.13
3	Y^{3+}	8.04	2-fluorophenyl	1.47 ± 0.08	4-fluorophenyl	1.89 ± 0.06

[a] Values are the mean and standard deviation for either four (strontium) or three (yttrium and manganese) experimental determinations. [b] pK_a data taken from reference 28.

Table 3.3. Measured $^{3\text{-D}}(V/K)_{2\text{-H}}$ effects for the GH4-catalyzed hydrolysis of aryl α-D-(3-^{2}H)galactopyranosides with various metal activators at pH 8.0 and 25 °C.[a]

Entry	Metal	pK_a $(M^{X+})_{aq}$[b]	Aglycone	$^{3\text{-D}}(V/K)_{2\text{-H}}$	Aglycone	$^{3\text{-D}}(V/K)_{2\text{-H}}$
1	Sr^{2+}	13.18	2-fluorophenyl	1.33 ± 0.06	4-fluorophenyl	1.73 ± 0.04
2	Mn^{2+}	10.59	2-fluorophenyl	1.02 ± 0.09	4-fluorophenyl	1.50 ± 0.13
3	Y^{3+}	8.04	2-fluorophenyl	1.24 ± 0.04	4-fluorophenyl	1.65 ± 0.06

[a] Values are the mean and standard deviation for either four (strontium) or three (yttrium and manganese) experimental determinations. [b] pK_a data taken from reference 28.

Consequently, we decided to probe the effect the activating metal has on the magnitude of these primary deuterium KIEs. In order to perform these experiments, we optimized our reaction conditions for the measurement of ^{19}F NMR spectra in the presence of Mn^{2+} and Y^{3+}. In order to avoid problems associated with the paramagnetic Mn^{2+} cation and precipitation with Y^{3+}, we used nonsaturating concentrations of the cations for the acquisition of ^{19}F NMR spectra. Of note, because we were measuring competitive rate ratios, the enzyme activity was identical in each rate comparison as the compounds were simultaneously present in the same reaction vessel, an NMR tube. Specifically, we observed that in the presence of low concentrations of Mn^{2+} (10 μM) the signals of fluoroaryl α-D-galactopyranosides in the ^{19}F NMR spectra were broadened only slightly with typical peak widths at half height for the various cations used: 1.7 Hz (Sr^{2+}), 1.9 Hz (Y^{3+}), and 2.1−2.4 Hz (Mn^{2+}). Also, at 10 μM Y^{3+} the solution was homogeneous. Again, we noticed no appreciable effect of leaving group ability, with either metal cation, on *V*/*K* among the fluoroaryl α-D-galactopyranoside substrates (Table 3.1).

We propose that the proton transfer isotope effects for strontium-activated MelA result from a less acidic C-2 proton in the ketone intermediate, an effect that is caused by activation using the least electropositive metal in the series (Scheme 3.1). Indeed, we note that the calculated $^{2\text{-D}}(V/K)_{3\text{-H}}$ values are significantly lower for the more electrophilic metal cations, effects

that are consistent with more acidic C-2 protons and earlier proton transfer TSs (entries 2 and 3 in Table 3.2). Of note, the $^{2\text{-D}}(V/K)_{3\text{-H}}$ value for MelA activated with its natural cofactor Mn^{2+}, although the pK_a for the aqua Mn^{2+} complex[28] is flanked by those of the strontium and yttrium ions, is the closest to unity (entry 2 in Table 3.2). Notably, the effects are again markedly different for the 2-fluorophenyl and 4-fluorophenyl leaving groups even though there is little difference in relative reaction rates (Table 3.1).

Three notable trends are apparent in the calculated KIE values on changing the metal cation: (i) the magnitude for $^{2\text{-D}}(V/K)_{3\text{-H}}$ decreases within each series (2-fluorophenyl and 4-fluorophenyl aglycones) $Sr^{2+} > Y^{3+} > Mn^{2+}$; (ii) for both $^{2\text{-D}}(V/K)_{3\text{-H}}$ and $^{3\text{-D}}(V/K)_{2\text{-H}}$ the measured KIEs are always of greater magnitude for the 4-fluorophenyl α-D-galactopyranoside than for the corresponding 2-fluorophenyl isomer irrespective of the metal activator; and (iii) the magnitude for the $^{3\text{-D}}(V/K)_{2\text{-H}}$ values show only a small apparent trend ($Sr^{2+} > Y^{3+} > Mn^{2+}$). We are forced to conclude that, in contrast to the conclusions reported in previous mechanistic studies, the virtual transition state for GH4-catalyzed reactions must incorporate another step, likely non-chemical, in addition to the previously assumed partially rate limiting hydride and proton transfer steps.[3,5,7,26] That is, for two substrates that react at similar rates, if one step is less kinetically significant (lower KIE) for one substrate then that substrate should exhibit a larger KIE on the other step, and given that this behavior is not observed then at least three steps must influence the overall reaction rate and the magnitude of the deuterium KIE values.

Of note, the natural Mn^{2+}-activated enzyme exhibits the smallest KIE values (entry 2 in Tables 3.2 and 3.3). Although changing the activating metal from strontium to more electrophilic cations reduces the proton transfer KIE, the effect does not follow a linear free energy relationship (LFER) with the pK_a of the metal−aqua complex.[28] Such LFERs have been reported for a series of bimetallic complexes containing a redox-active metal, where the reduction potential of the complex depends on the pK_a of the redox-inactive metal−aqua complex.[29,30]

3.4.4. Kinetic Isotope Effects on Isotope Effects Using Doubly Deuterated Aryl α-D-Galactopyranosides

In an effort to deconvolve the interdependence of the two primary deuterium KIEs we measured isotope effects on KIEs. Specifically, we measured the proton and hydride transfer KIEs on C-3 and C-2 deuterated materials, respectively (Tables 3.4 and 3.5). We note that the Sr^{2+}-activated enzyme, which exhibits the largest $^{2\text{-D}}(V/K)_{3\text{-H}}$ values (Table 3.2), results in a significant diminution in the hydride transfer KIE values (entry 1 in Tables 3.3 and 3.4). Our interpretation is

that C-2-deuteration, which raises the barrier for deprotonation, results in hydride transfer becoming kinetically nonsignificant for the Sr^{2+}-activated enzyme [$^{3\text{-D}}(V/K)_{2\text{-D}} < {}^{3\text{-D}}(V/K)_{2\text{-H}}$].

Table 3.4. Measured $^{3\text{-D}}(V/K)_{2\text{-D}}$ effects for the GH4-catalyzed hydrolysis of aryl α-D-(2,3-$^2H_2$)galactopyranosides relative to aryl α-D-(2-^{2}H)galactopyranosides with various metal activators at pH 8.0 and 25 °C.[a]

Entry	Metal	pK_a (M^{X+})$_{aq}$[b]	Aglycone	$^{3\text{-D}}(V/K)_{2\text{-D}}$	Aglycone	$^{3\text{-D}}(V/K)_{2\text{-D}}$
1	Sr^{2+}	13.18	2-fluorophenyl	0.88 ± 0.05	4-fluorophenyl	0.90 ± 0.06
2	Mn^{2+}	10.59	2-fluorophenyl	0.97 ± 0.07	4-fluorophenyl	1.46 ± 0.11
3	Y^{3+}	8.04	2-fluorophenyl	1.29 ± 0.11	4-fluorophenyl	1.42 ± 0.13

[a] Values are the mean and standard deviation for either four (strontium) or three (yttrium and manganese) experimental determinations. [b] pK_a data taken from reference 28.

Table 3.5. Measured $^{2\text{-D}}(V/K)_{3\text{-D}}$ effects for the GH4-catalyzed hydrolysis of aryl α-D-(2,3-$^2H_2$)galactopyranosides relative to aryl α-D-(3-^{2}H)galactopyranosides with various metal activators at pH 8.0 and 25 °C.[a]

Entry	Metal	pK_a (M^{X+})$_{aq}$[b]	Aglycone	$^{2\text{-D}}(V/K)_{3\text{-D}}$	Aglycone	$^{2\text{-D}}(V/K)_{3\text{-D}}$
1	Sr^{2+}	13.18	2-fluorophenyl	1.61 ± 0.08	4-fluorophenyl	1.63 ± 0.04
2	Mn^{2+}	10.59	2-fluorophenyl	0.93 ± 0.02	4-fluorophenyl	1.40 ± 0.11
3	Y^{3+}	8.04	2-fluorophenyl	1.53 ± 0.12	4-fluorophenyl	1.62 ± 0.15

[a] Values are the mean and standard deviation for either four (strontium) or three (yttrium and manganese) experimental determinations. [b] pK_a data taken from reference 28.

All other measured $^{3\text{-D}}(V/K)_{2\text{-D}}$ values are similar in magnitude to the corresponding $^{3\text{-D}}(V/K)_{2\text{-H}}$ effects (entries 2 and 3 in Tables 3.3 and 3.4), as was reported for the Mn^{2+}-activated MelA hydrolysis of phenyl α-D-galactopyranoside.[7] Again, perhaps surprisingly it is only the Sr^{2+}-activated MelA that exhibits values for $^{2\text{-D}}(V/K)_{3\text{-D}}$ that are significantly lower than those of $^{2\text{-D}}(V/K)_{3\text{-H}}$ (entry 1 in Tables 3.2 and 3.5). We conclude that the strontium-activated enzyme exhibits the expected reduction in KIE values upon deuterium substitution in the adjacent C−H bond for the simple two, kinetically significant, step model proposed previously.[3,5] In contrast, all other $^{2\text{-D}}(V/K)_{3\text{-D}}$ values are of a similar magnitude to the $^{2\text{-D}}(V/K)_{3\text{-H}}$ effects (entries 2 and 3 in Tables 3.2 and 3.5), and we are again forced to conclude that a non-isotopically sensitive step must be included in the analysis.

3.4.5. Kinetic Complexity of GH4 Enzymes

A final comment is warranted regarding the results of the current study. Clearly, the kinetic complexity of MelA is greater than previously assumed,[7] with at least three separate events contributing to the virtual TS. The requisite kinetic expressions are available for analysis of the measured KIE values for this type of system.[31] Given that the enzyme-catalyzed hydrolysis of 2-fluorophenyl α-D-galactopyranoside exhibits KIE values that are significantly closer to unity than those for the 4-fluorophenyl isomer, even though they are hydrolyzed at similar rates, we suggest that the kinetic complexity in this system is subtly perturbed by small differences in interactions between the active site and the individual fluorophenyl leaving groups. These subtle differences extend to nonfluorinated leaving groups as a comparison of the KIEs for the Mn^{2+}-enzyme (entry 2 in Tables 3.2 and 3.3), with the reported values for hydrolysis of phenyl α-D-galactopyranoside [$^{2\text{-D}}(V/K)_{3\text{-H}}$ = 1.74 and $^{3\text{-D}}(V/K)_{2\text{-H}}$ = 1.74, pH 7.5 at 37 °C][7] indicative of small changes in the virtual transition state.

In the active site of AglA α-glucosidase A,[18] Phe238 is proximal to the aglycone of the bound maltose; however, due to a poor overlap in the amino acid sequences in this region we could not locate a similarly positioned aromatic residue in the homology model of MelA. We suggest that such an interaction between an active site residue and the aryl leaving group could be the basis of a kinetically significant conformational change required for leaving group expulsion. That is, the enediolate intermediate, which has two coplanar atoms, C-2 and C-3, has four low energy boat and half chair conformations ($^{1,4}B$, $B_{1,4}$, $^{5}H_{O}$, or $^{O}H_{5}$) while the α,β-unsaturated ketone intermediate with three coplanar atoms (C-1−C-3) has two low energy envelope conformations (^{5}E or E_{5}).[32] As a result, we suggest that the mechanism for GH4 enzyme-catalyzed glycosidic bond cleavage be modified to that shown in Scheme 3.2 to accommodate the proposed kinetically significant conformational change.

Scheme 3.2. Current proposal for the mechanism of glycosidic bond cleavage for GH4 enzymes in which a conformational change is required for aglycone departure that does not require a general acid catalyst*

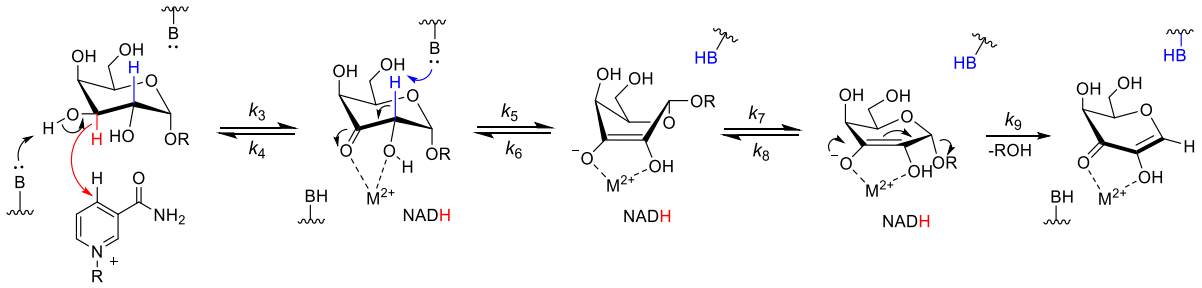

* Charges are not shown on the active site acid/base residues.

3.5. Conclusions

Fluorine-19 NMR spectroscopy was used with a remote labeling strategy to measure multiple KIEs on singly deuterated substrates. Although these involve the calculation of ratios of competitive rate measurements, the calculated KIEs are sufficiently precise to detect subtle changes in KIE magnitudes caused by substrate modification. Protocols such as this provide a reasonable alternative to incorporating an NMR active probe nucleus in close proximity to the site of bond breaking and bond forming, thus circumventing isotope incorporation issues associated with expensive labeled starting materials and/or synthetic complexity.

Further, the measurement of multiple KIEs, using a variety of metal cation activators for the *C. freundii* MelA α-galactosidase-catalyzed hydrolysis of fluoroaryl α-D-galactopyranoside has revealed the existence of a third kinetically significant step, which we propose to be a conformational change of the bound enediolate intermediate, in addition to the hydride and proton transfer steps identified previously for this glycoside hydrolase family (GH4). In addition, this new mechanistic insight into the GH4 enzyme suggests that design of conformationally rigid compounds might have a detrimental impact on the catalytic ability of these bacterial glycoside hydrolases. That is, our findings on the subtleties of GH4 catalysis will provide new avenues for the development of potential inhibitors.

3.6. Associated Content

Supporting Information. Synthesis of (3-^{2}H)galactal, equations for calculation of KIE values, relative rate constants for hydrolysis of 3,5-difluorophenyl α-D-galactopyranoside and one of 2-fluorophenyl, 3-fluorophenyl, or 4-fluorophenyl α-D-galactopyranoside and the corresponding (2-^{2}H), (3-^{2}H), and (2,3-^{2}H$_2$)-isotopologues (Tables S1−12); melting temperature graphs for MelA in various buffers, stacked plot of ^{19}F NMR spectra for a typical relative rate constant measurement, and ^{1}H and ^{13}C NMR spectra for 3,5-difluorophenyl α-D-galactopyranoside and one of 2-fluorophenyl, 3-fluorophenyl or 4-fluorophenyl α-D-galactopyranoside and the corresponding (2-^{2}H), (3-^{2}H), and (2,3-^{2}H$_2$)-isotopologues. The Supporting Information is available free of charge on the ACS Publications website at DOI: 10.1021/acs.bio- chem.8b00117.

3.7. Abbreviations

BSA, bovine serine albumin; COSY, homonuclear correlation spectroscopy; DTT, dithiothreitol; EtOAc, ethyl acetate; FID, free induction decay; GalO2F, 2-fluorophenyl α-D-galactopyranoside; GalO3F, 3-fluorophenyl α-D-galactopyranoside; GalO3,5diF, 3,5-difluorophenyl α-D-galactopyranoside; GalO4F, 4-fluorophenyl α-D-galactopyranoside; HEPES, 4-(2-hydroxyethyl)-1-piperazineethanesulfonic acid; HSQC, heteronuclear single-quantum correlation spectroscopy; IPTG, isopropyl 1-thio-β-D-galactopyranoside; KIE, kinetic isotope effect; NAD^+, β-nicotinamide adenine dinucleotide; NMR, nuclear magnetic resonance spectroscopy; TCEP, tris(2-carboxyethyl)phosphine; TLC, thin layer chromatography; TMS, tetramethylsilane.

3.8. References

1. Zechel, D. L. & Withers, S. G. Glycosidase mechanisms: Anatomy of a finely tuned catalyst. *Acc. Chem. Res.* **33,** 11–18 (2000).

2. Vocadlo, D. J. & Davies, G. J. Mechanistic insights into glycosidase chemistry. *Curr. Opin. Chem. Biol.* **12,** 539–555 (2008).

3. Yip, V. L. Y., Thompson, J. & Withers, S. G. Mechanism of GlvA from Bacillus subtilis: a detailed kinetic analysis of a 6-phospho-alpha-glucosidase from glycoside hydrolase family 4. *Biochemistry* **46,** 9840–52 (2007).

4. Yip, V. L. Y. *et al.* An unusual mechanism of glycoside hydrolysis involving redox and elimination steps by a family 4 β-glycosidase from Thermotoga maritima. *J. Am. Chem. Soc.* **126,** 8354–8355 (2004).

5. Yip, V. L. Y. & Withers, S. G. Mechanistic analysis of the unusual redox-elimination sequence employed by Thermotoga maritima BglT: A 6-phospho-β-glucosidase from glycoside hydrolase family 4. *Biochemistry* **45,** 571–580 (2006).

6. Lombard, V., Golaconda Ramulu, H., Drula, E., Coutinho, P. M. & Henrissat, B. The carbohydrate-active enzymes database (CAZy) in 2013. *Nucleic Acids Res.* **42,** D490–D495 (2014).

7. Chakladar, S., Cheng, L., Choi, M., Liu, J. & Bennet, A. J. Mechanistic evaluation of MelA a-galactosidase from citrobacter freundii: A family 4 glycosyl hydrolase in which oxidation is rate-limiting. *Biochemistry* **50,** 4298–4308 (2011).

8. Anggraeni, A. A. *et al.* Characterization of Bacillus halodurans -Galactosidase Mel4A Encoded by the mel4A Gene (BH2228). *Biosci. Biotechnol. Biochem.* **72,** 2459–2462 (2008).

9. Liljestoüm, P. L. & Liljestrom, P. Nucleotide sequence of the melA gene, Coding for α-galactosidase in Escherichia coli K-12. *Nucleic Acids Res.* **15,** 2213–2220 (1987).

10. Hermes, J. D., Roeske, C. A., O'leary, M. H. & Cleland, W. W. Use of Multiple Isotope Effects To Determine Enzyme Mechanisms and Intrinsic Isotope Effects. Malic Enzyme and Glucose-6-phosphate Dehydrogenase. *Biochemistry* **21,** 5106–5114 (1982).

11. Hermes, J. D. & Cleland, W. W. Evidence from Multiple Isotope Effect Determinations for Coupled Hydrogen Motion and Tunneling in the Reaction Catalyzed by Glucose-6-phosphate Dehydrogenase. *J. Am. Chem. Soc* **106,** 7263–7264 (1984).

12. Edens, W. A., Urbauer, J. L. & Cleland, W. W. Determination of the Chemical Mechanism of Malic Enzyme by Isotope Effects. *Biochemistry* **36,** 1141–1147 (1997).

13. R. U. Lemieux, Nagabhushan, T. L. & O'Neill, I. K. The reactions of nitrosyl chloride and dinitrogen tetroxide with acetylated glycals . Acetylated 2-deoxy-2-nitroso-c-D-hexopyranosyl chlorides and nitrates and acetylated 2-nitroglycalsl. *Can. J. Chem.* **46,** 1–6 (1968).

14. Chan, J., Lewis, A. R., Gilbert, M., Karwaski, M.-F. & Bennet, A. J. A direct NMR method for the measurement of competitive kinetic isotope effects. *Nat. Chem. Biol.* **6,** 405–407

(2010).

15. Chan, J., Sannikova, N., Tang, A. & Bennet, A. J. Transition-state structure for the quintessential S<inf>N</inf>2 reaction of a carbohydrate: Reaction of α-glucopyranosyl fluoride with azide ion in Water. *J. Am. Chem. Soc.* **136,** (2014).

16. Melander, L. C. S. & Saunders, W. H. *Reaction rates of isotopic molecules*. (Wiley, 1980).

17. Cleland, W. W. Enzyme Mechanisms from Isotope Effects. in *Isotope Effects in Chemistry and Biology* (eds. Kohen, A. & Limbach, H.-H.) 915–930 (Taylor & Francis, 2006).

18. Lodge, J. A., Maier, T., Liebl, W., Hoffmann, V. & Sträter, N. Crystal structure of Thermotoga maritima α-glucosidase AglA defines a new clan of NAD+-dependent glycosidases. *J. Biol. Chem.* **278,** 19151–19158 (2003).

19. Chan, J., Tang, A. & Bennet, A. J. A Stepwise Solvent-Promoted SNi Reaction of α-D-Glucopyranosyl Fluoride: Mechanistic Implications for Retaining Glycosyltransferases. *J. Am. Chem. Soc.* **134,** 1212–1220 (2012).

20. Chan, J., Tang, A. & Bennet, A. J. Transition-state structure for the hydronium-ion-promoted hydrolysis of α- d -glucopyranosyl fluoride. *Can. J. Chem.* **93,** 463–467 (2015).

21. Williams, S. J. & Withers, S. G. Glycosyl fluorides in enzymatic reactions. *Carbohydr. Res.* **327,** 27–46 (2000).

22. McGuffin, L. J., Atkins, J. D., Salehe, B. R., Shuid, A. N. & Roche, D. B. IntFOLD: an integrated server for modelling protein structures and functions from amino acid sequences. *Nucleic Acids Res.* **43,** W169–W173 (2015).

23. Buenavista, M. T., Roche, D. B. & McGuffin, L. J. Improvement of 3D protein models using multiple templates guided by single-template model quality assessment. *Bioinformatics* **28,** 1851–1857 (2012).

24. Roche, D. B., Buenavista, M. T. & McGuffin, L. J. FunFOLDQA: A Quality Assessment Tool for Protein-Ligand Binding Site Residue Predictions. *PLoS One* **7,** e38219 (2012).

25. Roche, D. B., Tetchner, S. J. & McGuffin, L. J. FunFOLD: an improved automated method for the prediction of ligand binding residues using 3D models of proteins. *BMC Bioinformatics* **12,** 160 (2011).

26. Yip, V. L. Y. & Withers, S. G. Family 4 Glycosidases Carry Out Efficient Hydrolysis of Thioglycosides by an α,β-Elimination Mechanism. *Angew. Chemie Int. Ed.* **45,** 6179–6182 (2006).

27. Banait, N. S. & Jencks, W. P. General-acid and general-base catalysis of the cleavage of .alpha.-D-glucopyranosyl fluoride. *J. Am. Chem. Soc.* **113,** 7958–7963 (1991).

28. Perrin, D. D. (Douglas D. & International Union of Pure and Applied Chemistry. Commission on Equilibrium Data. *Ionisation constants of inorganic acids and bases in aqueous solution*. (Pergamon Press, 1982).

29. Tsui, E. Y., Tran, R., Yano, J. & Agapie, T. Redox-inactive metals modulate the reduction potential in heterometallic manganese–oxido clusters. *Nat. Chem.* **5,** 293–299 (2013).

30. Tsui, E. Y. & Agapie, T. Reduction potentials of heterometallic manganese-oxido cubane complexes modulated by redox-inactive metals. *Proc. Natl. Acad. Sci. U. S. A.* **110,** 10084–8 (2013).

31. Ruszczycky, M. W. & Anderson, V. E. Interpretation of V/K isotope effects for enzymatic reactions exhibiting multiple isotopically sensitive steps. *J. Theor. Biol.* **243,** 328–342 (2006).

32. Schwarz, J. C. P. Rules for conformation nomenclature for five- and six-membered rings in monosaccharides and their derivatives. *J. Chem. Soc. Chem. Commun.* **0,** 505 (1973).

33. Hayashi, M., Yamada, K. & Arikita, O. Practical and catalytic synthesis of 1,5-anhydrohex-1-en-3-uloses. *Tetrahedron* **55,** 8331–8340 (1999).

3.9. Supporting Information

Both Chemical and Non-Chemical Steps Limit the Catalytic Efficiency of Family 4 Glycoside Hydrolases

Natalia Sannikova, Chloe A. N. Gerak, Fahimeh S. Shidmoossavee, Dustin T. King, Saeideh Shamsi Kazem Abadi, Andrew R. Lewis, and Andrew J. Bennet

Department of Chemistry and Department of Molecular Biology and Biochemistry, Simon Fraser University, 8888 University Drive, Burnaby, British Columbia V5A 1S6, Canada

3.9.1. Materials and Methods

3,4,6-Tri-O-acetyl-1,5-anhydro-2-deoxy-D-(3-^{2}H)lyxo-hex-1-enitol. 1,5-anhydro-2-deoxy-D-*threo*-hex-1-en-3-ulose (2.1 g, 9.25 mmol)[33] was dissolved in anhydrous THF (50 mL) and this solution was cooled to 0 °C under an inert atmosphere. Subsequent addition of a solution of $NaBD_4$ (103 mg, 2.4 mmol) in cold D_2O (1 mL) was followed by stirring the mixture at 0 °C for 1 h. At this point TLC analysis (50% EtOAc-Hexane) showed completion of the reaction. The reaction was quenched by the addition of aqueous AcOH (1%, 5 mL) and the resultant solution was diluted with water (20 mL) and extracted with CH_2Cl_2 (3 × 50 mL). The combined organic layer was washed with water (2 × 20 mL), brine (20 mL) and dried over Na_2SO_4. Removal of volatiles under reduced pressure gave a pale yellow solid which was dissolved in 30 mL of dry CH_2Cl_2 and acetylated under standard conditions, pyridine (3 mL, 37 mmol) and Ac_2O (1.8 mL, 18.5 mmol) with stirring overnight at room temperature. The reaction mixture was diluted with 70 mL of CH_2Cl_2 washed with 20% $CuSO_4$ (3 × 30 mL), water (2 × 30 mL), brine (30 mL) and dried over Na_2SO_4. Removal of the volatiles under reduced pressure gave yellow syrup and this material was purified by flash chromatography (25% EtOAc-Hexane) to give pure deuterated tri-*O*-acetylgalactal (2.1 g, 83 % yield over 2 steps).

3.9.2. Equations used to calculate KIEs

$$^{D}(V/K_{C\text{-}2})_{C\text{-}3H} = (k_{2H}/k_{3,5\text{-}DiF}) \div (k_{2D}/k_{3,5\text{-}DiF}) \quad \text{(S1)}$$

$$^{D}(V/K_{C\text{-}3})_{C\text{-}2H} = (k_{3H}/k_{3,5\text{-}DiF}) \div (k_{3D}/k_{3,5\text{-}DiF}) \quad \text{(S2)}$$

$$^{D}(V/K_{C\text{-}2})_{C\text{-}3D} = (k_{3D}/k_{3,5\text{-}DiF}) \div (k_{2,3D2}/k_{3,5\text{-}DiF}) \quad \text{(S3)}$$

$$^{D}(V/K_{C\text{-}3})_{C\text{-}2D} = (k_{2D}/k_{3,5\text{-}DiF}) \div (k_{2,3D2}/k_{3,5\text{-}DiF}) \quad \text{(S4)}$$

3.9.3. Abbreviations

GalO2F, 2-fluorophenyl α-D-galactopyranoside; GalO3F, 3-fluorophenyl α-D-galactopyranoside; GalO3,5diF, 3,5-difluorophenyl α-D-galactopyranoside; GalO4F, 4-fluorophenyl α-D-galactopyranoside; (2-^{2}H)GalO2F, 2-fluorophenyl α-D-(2-^{2}H)galactopyranoside; (2-^{2}H)GalO4F, 4-fluorophenyl α-D-(2-^{2}H)galactopyranoside; (2,3-$^2H_2$)GalO2F, 2-fluorophenyl α-D-(2,3-$^2H_2$)galactopyranoside; (2,3-$^2H_2$)GalO4F, 4-fluorophenyl α-D-(2,3-$^2H_2$)galactopyranoside; (3-^{2}H)GalO2F, 2-fluorophenyl α-D-(3-^{2}H)galactopyranoside; (3-^{2}H)GalO4F, 4-fluorophenyl α-D-(3-^{2}H)galactopyranoside.

Table S3.1: Individual measurements of ratios of *V*/*K* values for the GH4-catalyzed hydrolysis of unlabeled aryl α-D-galactopyranosides in presence of Sr^{2+}, at pH 8.0 and 25 °C, the corresponding means and standard deviations.

Compound 1	**Compound 2**	$k_{3,5diF}/k_X$	**Mean and SD**
GalO3,5diF	GalO4F	0.6447	0.65±0.01
		0.6683	
		0.6597	
		0.6382	
GalO3,5diF	GalO2F	0.5376	0.55±0.03
		0.5649	
		0.5693	
		0.5117	
GalO3,5diF	GalO3F	0.8150	0.88±0.06
		0.8555	
		0.9424	
		0.9241	

Table S3.2: Individual measurements of ratios of *V*/*K* values for the GH4-catalyzed hydrolysis of aryl α-D-(2-^{2}H)galactopyranosides in presence of Sr^{2+}, at pH 8.0 and 25 °C, the corresponding means and standard deviations.

Compound 1	**Compound 2**	$k_{3,5diF}/k_X$	**Mean and SD**
GalO3,5diF	(2-^{2}H)GalO4F	1.928 2.067 1.944 2.222	2.04±0.14
GalO3,5diF	(2-^{2}H)GalO2F	1.560 1.566 1.566 1.699	1.60±0.07

Table S3.3: Individual measurements of ratios of *V*/*K* values for the GH4-catalyzed hydrolysis of aryl α-D-(3-^{2}H)galactopyranosides in presence of Sr^{2+}, at pH 8.0 and 25 °C, the corresponding means and standard deviations.

Compound 1	**Compound 2**	$k_{3,5diF}/k_X$	**Mean and SD**
GalO3,5diF	(3-^{2}H)GalO4F	1.111 1.128 1.140 1.142	1.13±0.01
GalO3,5diF	(3-^{2}H)GalO2F	0.8688 0.8508 0.8423 0.9141	0.87±0.03

Table S3.4: Individual measurements of ratios of *V*/*K* values for the GH4-catalyzed hydrolysis of aryl α-D-(2-^{2}H,3-^{2}H)galactopyranosides in presence of Sr^{2+}, at pH 8.0 and 25 °C, the corresponding means and standard deviations.

Compound 1	**Compound 2**	$k_{3,5diF}/k_X$	**Mean and SD**
GalO3,5diF	(2,3-$^{2}H_2$)GalO4F	1.855 1.885 1.792 1.844	1.84±0.04
GalO3,5diF	(2,3-$^{2}H_2$)GalO2F	1.441 1.360 1.437 1.362	1.40±0.05

Table S3.5: Individual measurements of ratios of *V*/*K* values for the GH4-catalyzed hydrolysis of unlabelled aryl α-D-galactopyranosides in presence of Y^{3+}, at pH 8.0 and 25 °C, the corresponding means and standard deviations.

Compound 1	**Compound 2**	$k_{3,5diF}/k_X$	**Mean and SD**
GalO3,5diF	GalO4F	0.6760 0.6800 0.6589	0.67±0.01
GalO3,5diF	GalO2F	0.5357 0.5795 0.5634	0.56±0.02

Table S3.6: Individual measurements of ratios of *V*/*K* values for the GH4-catalyzed hydrolysis of aryl α-D-(2-^{2}H)galactopyranosides in presence of Y^{3+}, at pH 8.0 and 25 °C, the corresponding means and standard deviations.

Compound 1	**Compound 2**	$k_{3,5diF}/k_X$	**Mean and SD**
GalO3,5diF	(2-^{2}H)GalO4F	1.308 1.258 1.236	1.27±0.04
GalO3,5diF	(2-^{2}H)GalO2F	0.9699 1.050 0.9499	0.99±0.05

Table S3.7: Individual measurements of ratios of *V*/*K* values for the GH4-catalyzed hydrolysis of aryl α-D-(3-^{2}H)galactopyranosides in presence of Y^{3+}, at pH 8.0 and 25 °C, the corresponding means and standard deviations.

Compound 1	**Compound 2**	$k_{3,5diF}/k_X$	**Mean and SD**
GalO3,5diF	(3-^{2}H)GalO4F	1.075 1.115 1.143	1.11±0.03
GalO3,5diF	(3-^{2}H)GalO2F	0.8107 0.8613 0.8248	0.83±0.03

Table S3.8: Individual measurements of ratios of *V*/*K* values for the GH4-catalyzed hydrolysis of aryl α-D-(2-^{2}H,3-^{2}H)galactopyranosides in presence of Y^{3+}, at pH 8.0 and 25 °C, the corresponding means and standard deviations.

Compound 1	**Compound 2**	$k_{3,5diF}/k_X$	**Mean and SD**
GalO3,5diF	(2,3-$^2H_2$)GalO4F	1.629 1.923 1.839	1.80±0.15
GalO3,5diF	(2,3-$^2H_2$)GalO2F	1.171 1.341 1.308	1.27±0.09

Table S3.9: Individual measurements of ratios of *V*/*K* values for the GH4-catalyzed hydrolysis of unlabelled aryl α-D-galactopyranosides in presence of Mn^{2+}, at pH 8.0 and 25 °C, the corresponding means and standard deviations.

Compound 1	**Compound 2**	$k_{3,5diF}/k_X$	**Mean and SD**
GalO3,5diF	GalO4F	0.7166 0.8126 0.7646	0.76±0.05
GalO3,5diF	GalO2F	0.5419 0.7190 0.6305	0.63±0.09

Table S3.10: Individual measurements of ratios of *V*/*K* values for the GH4-catalyzed hydrolysis of aryl α-D-(2-^{2}H)galactopyranosides in presence of Mn^{2+}, at pH 8.0 and 25 °C, the corresponding means and standard deviations.

Compound 1	**Compound 2**	$k_{3,5diF}/k_X$	**Mean and SD**
GalO3,5diF	(2-^{2}H)GalO4F	1.111 1.081 1.097	1.10±0.02
GalO3,5diF	(2-^{2}H)GalO2F	0.7951 0.8862 0.7868	0.82±0.06

Table S3.11: Individual measurements of ratios of *V*/*K* values for the GH4-catalyzed hydrolysis of aryl α-D-(3-^{2}H)galactopyranosides in presence of Mn^{2+}, at pH 8.0 and 25 °C, the corresponding means and standard deviations.

Compound 1	**Compound 2**	$k_{3,5diF}/k_X$	**Mean and SD**
GalO3,5diF	(3-^{2}H)GalO4F	1.135 1.148 1.156	1.15±0.01
GalO3,5diF	(3-^{2}H)GalO2F	0.7931 0.7687 0.7758	0.78±0.01

Table S3.12: Individual measurements of ratios of *V*/*K* values for the GH4-catalyzed hydrolysis of aryl α-D-(2-^{2}H,3-^{2}H)galactopyranosides in presence of Mn^{2+}, at pH 8.0 and 25 °C, the corresponding means and standard deviations.

Compound 1	Compound 2	$k_{3,5diF}/k_X$	Mean and SD
GalO3,5diF	(2,3-$^2H_2$)GalO4F	1.527 1.533 1.736	1.60±0.12
GalO3,5diF	(2,3-$^2H_2$)GalO2F	1.069 1.049 1.063	1.06±0.01

Figure S3.1. GH4 melting temperature (T_m) analysis in presence of 0.5 mM TCEP.

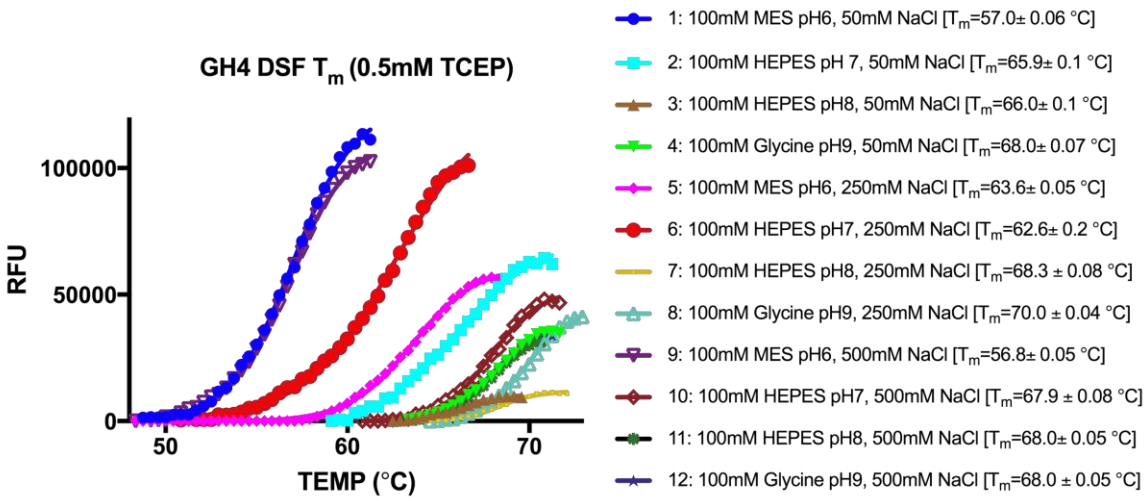

Figure S3.2. Stacked plot of proton-decoupled ^{19}F NMR spectra for the enzyme-catalyzed hydrolysis of four unlabelled fluoroaryl α-D-galactopyranosides as the fraction of reaction of 3,5-difluorophenyl α-D-galactopyranoside (**1a**) in presence of Sr^{2+} at pH 8.0 and 25 °C.[a]

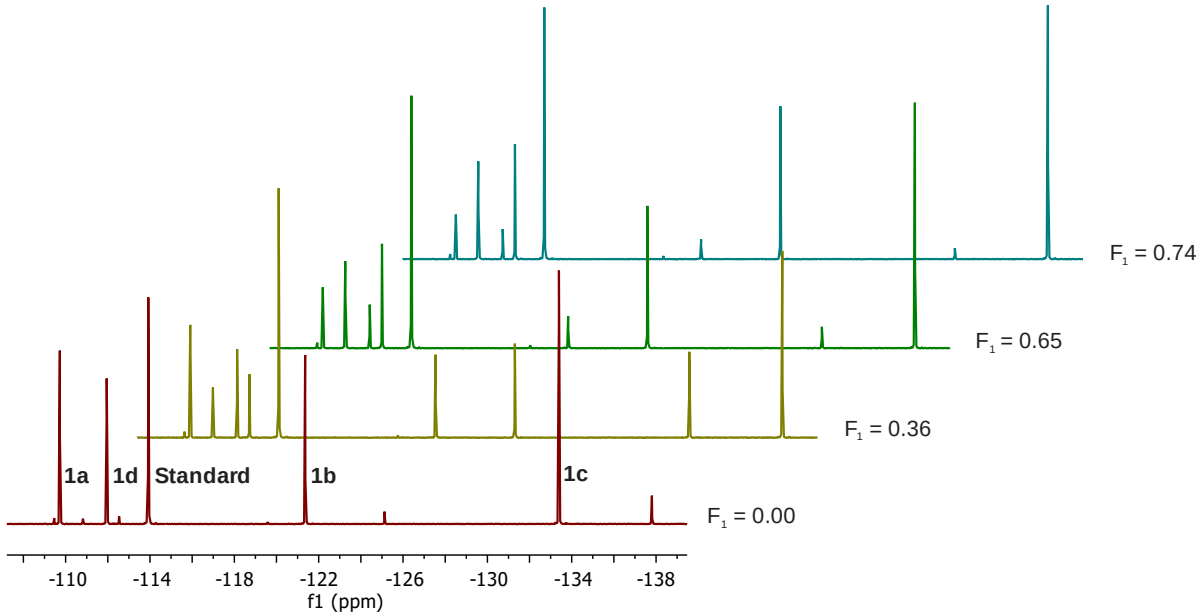

[a] The peaks appearing upfield of the aryl α-D-galactopyranoside resonances are for the corresponding phenol.

Figure S3.3: ^{1}H NMR spectrum for 3,5-difluorophenyl α-D-galactopyranoside (600 MHz, D_2O)

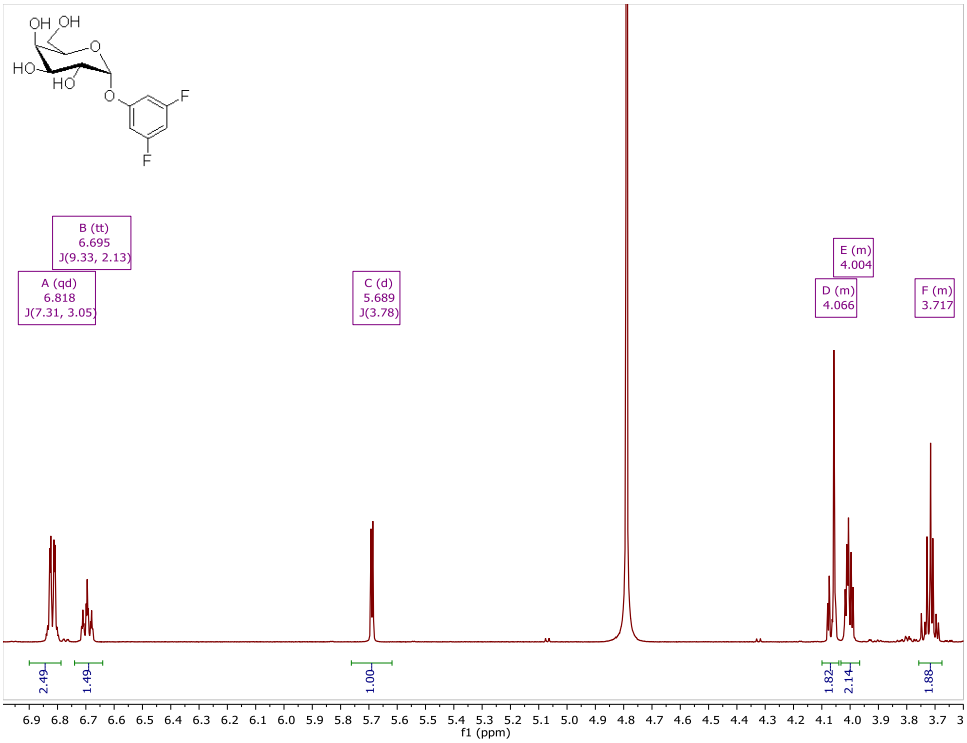

Figure S3.4: ^{13}C NMR spectrum for 3,5-difluorophenyl α-D-galactopyranoside (151 MHz, D_2O)

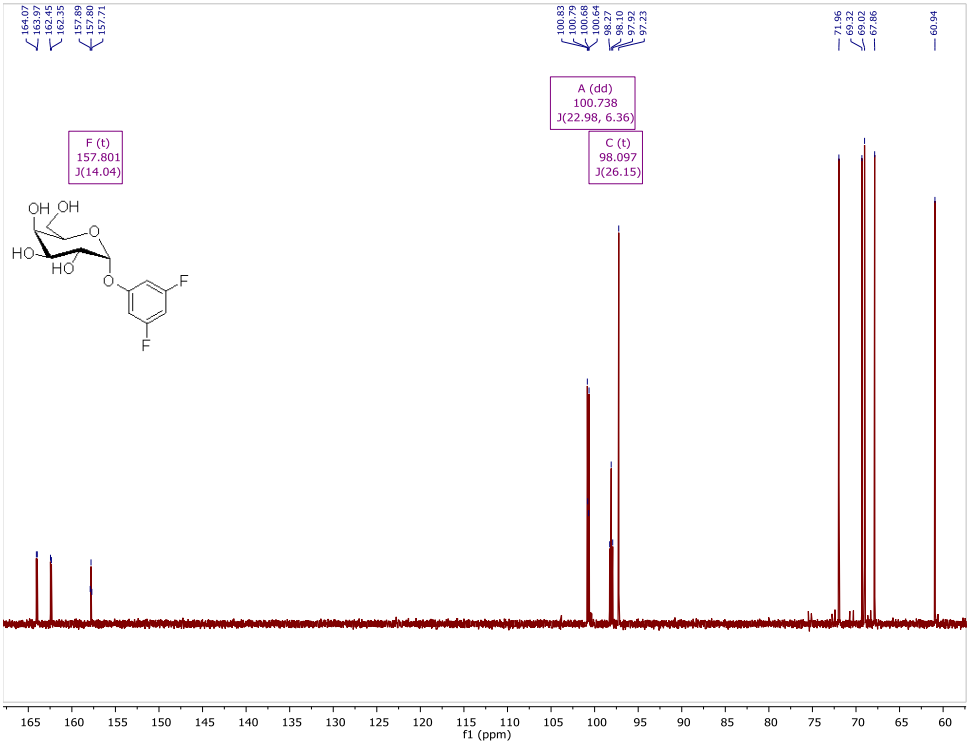

Figure S3.5: ^{1}H NMR spectrum for 4-fluorophenyl α-D-galactopyranoside (600 MHz, D_2O)

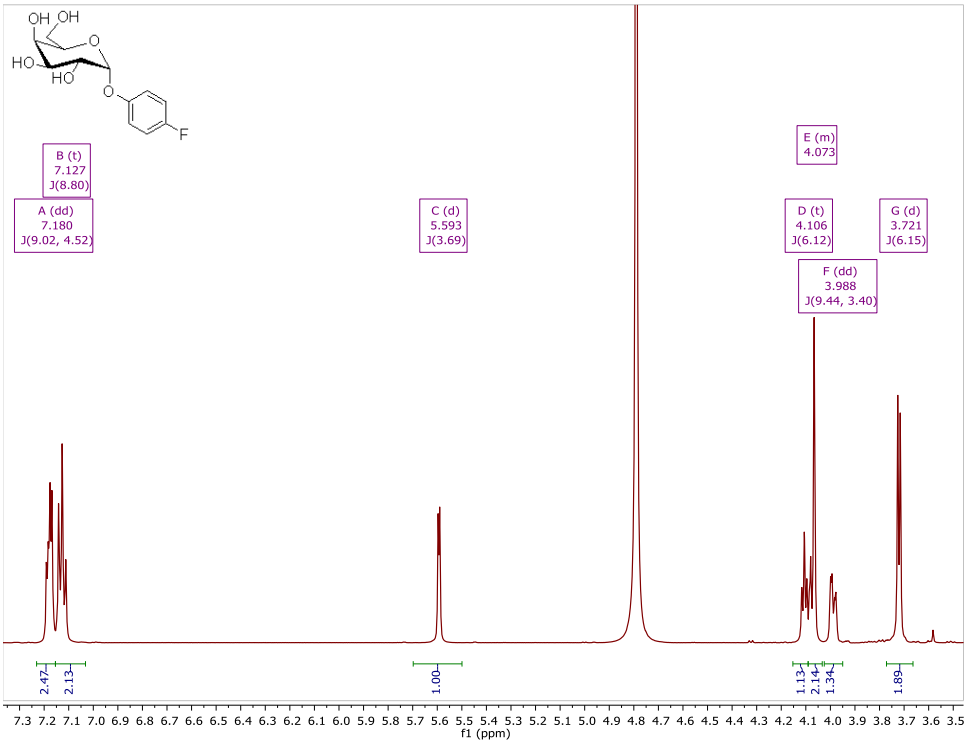

Figure S3.6: ^{13}C NMR spectrum for 4-fluorophenyl α-D-galactopyranoside (151 MHz, D_2O)

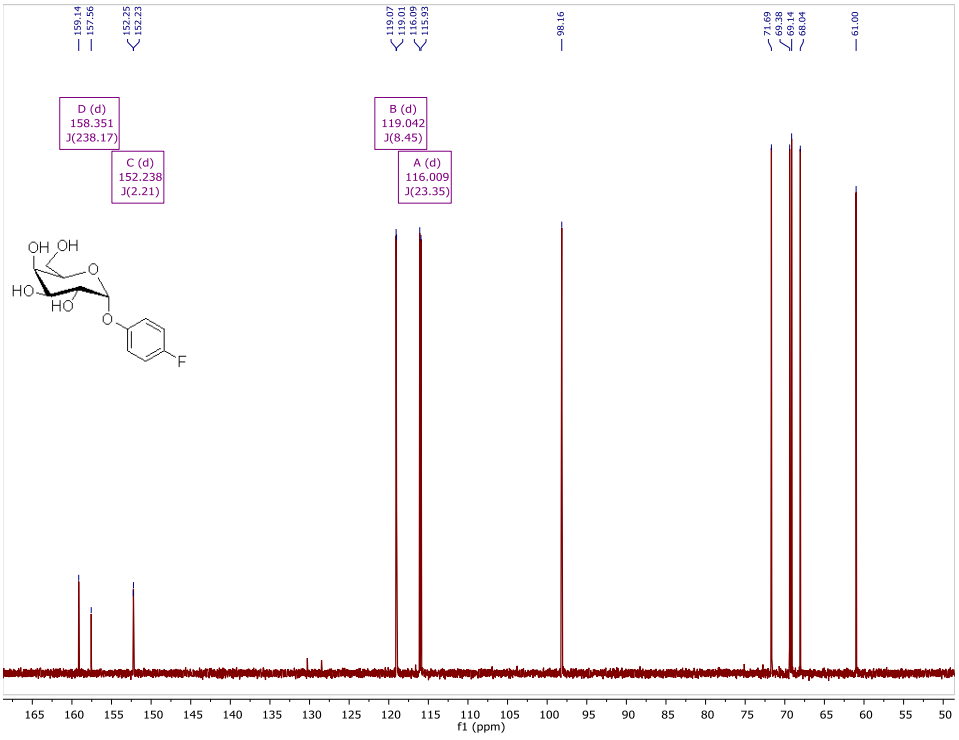

Figure S3.7: ^{1}H NMR spectrum for 2-fluorophenyl α-D-galactopyranoside (600 MHz, D_2O)

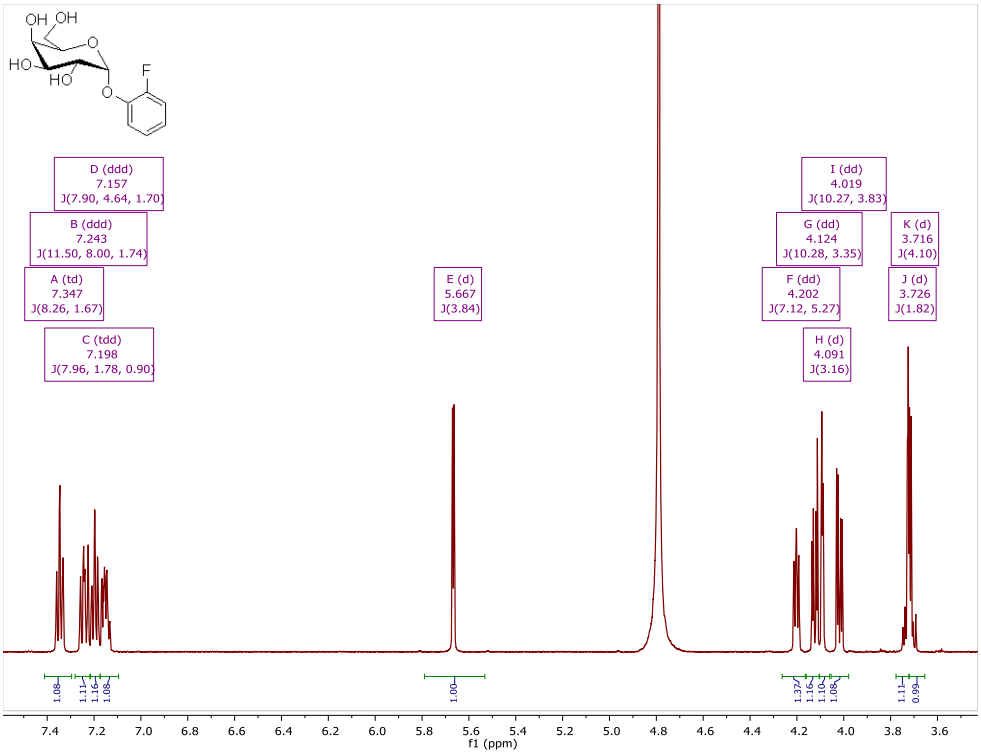

Figure S3.8: ^{13}C NMR spectrum for 2-fluorophenyl α-D-galactopyranoside (151 MHz, D_2O)

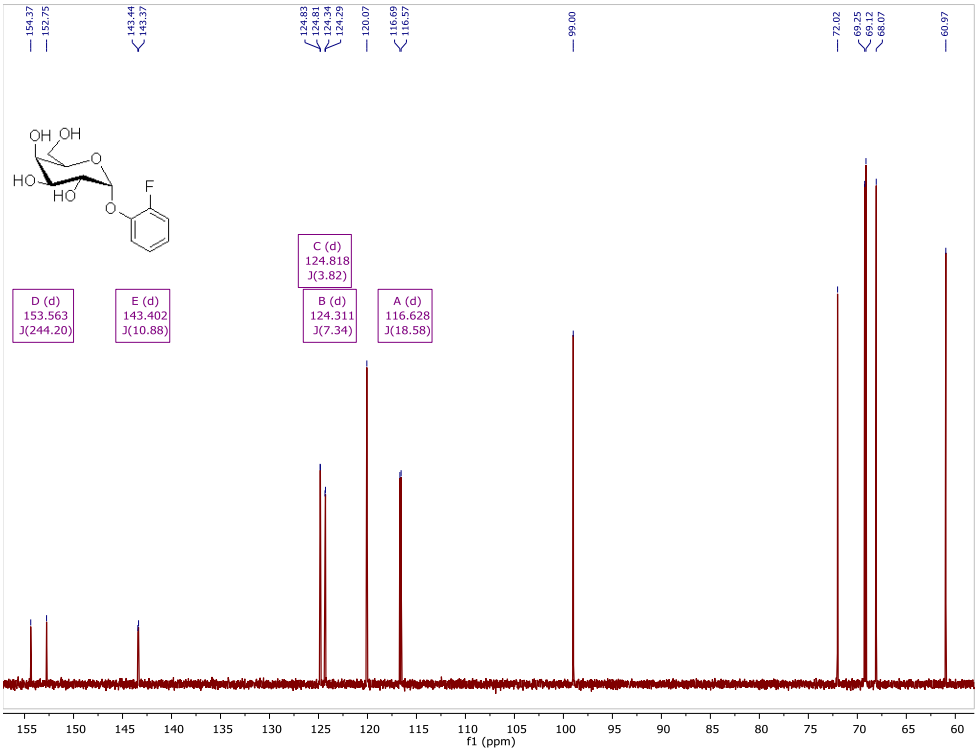

Figure S3.9: ^{1}H NMR spectrum for 3-fluorophenyl α-D-galactopyranoside (600 MHz, D_2O)

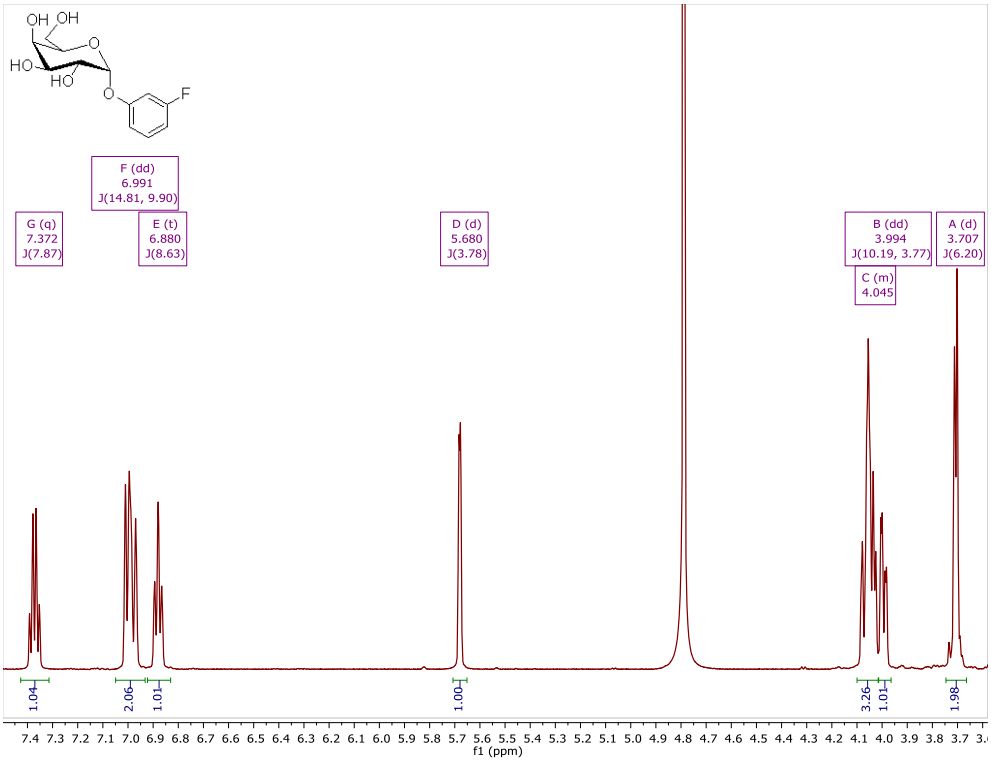

Figure S3.10: ^{13}C NMR spectrum for 3-fluorophenyl α-D-galactopyranoside (151 MHz, D_2O)

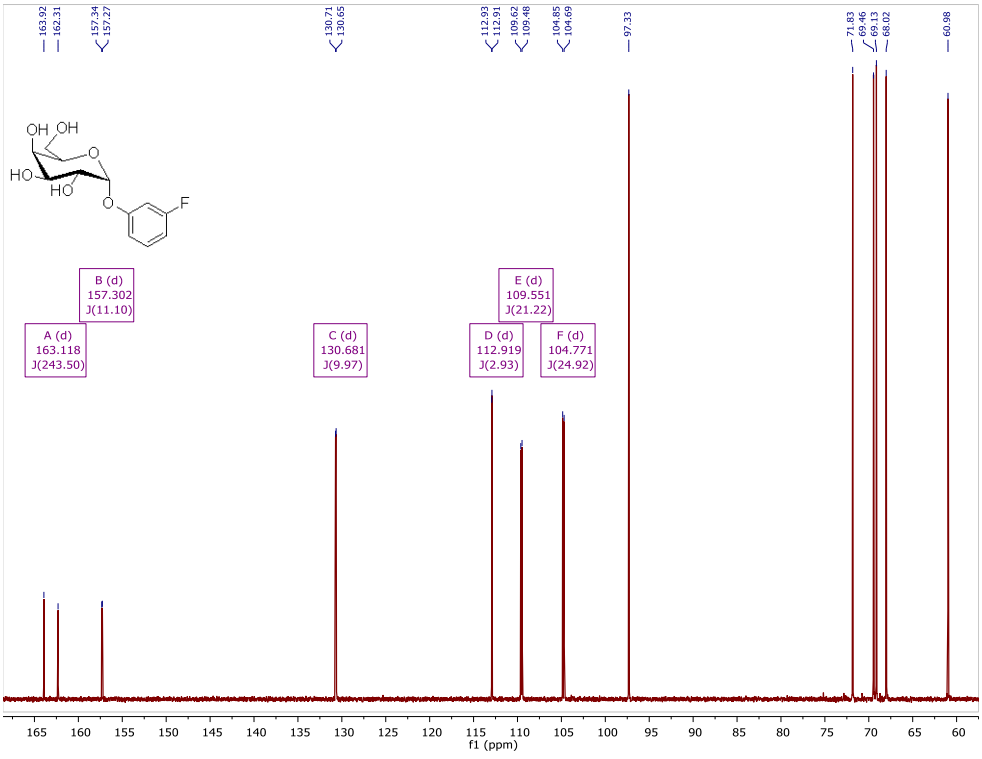

Figure S3.11: ^{1}H NMR spectrum for 4-fluorophenyl α-D-[2-^{2}H]galactopyranoside (600 MHz, D_2O)

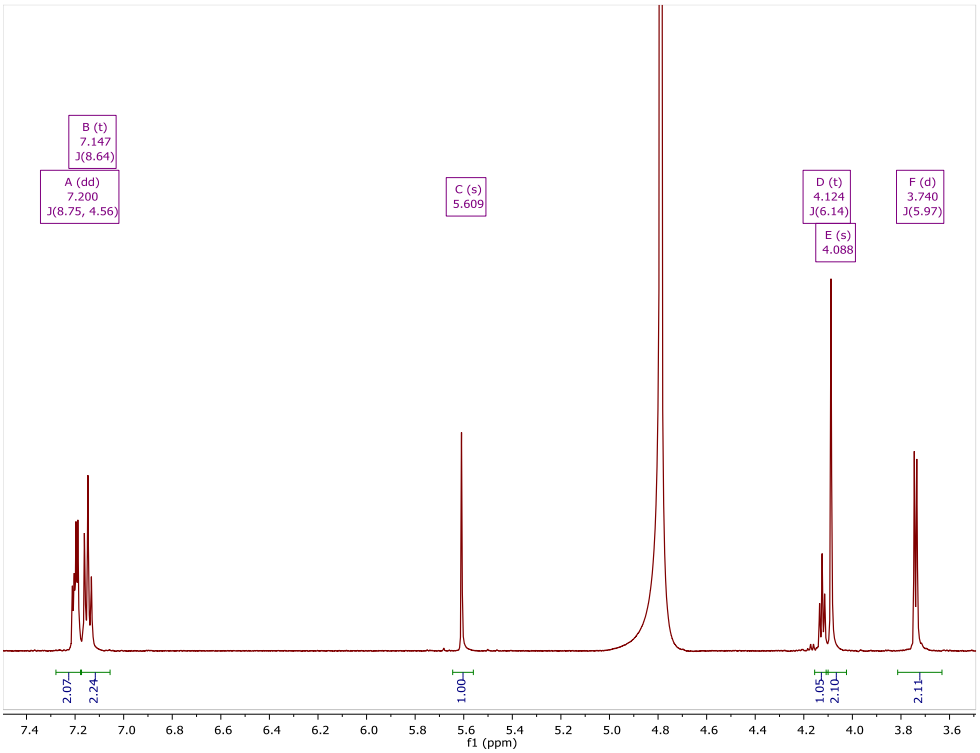

Figure S3.12: ^{13}C NMR spectrum for 4-fluorophenyl α-D-[2-^{2}H]galactopyranoside (151 MHz, D_2O)

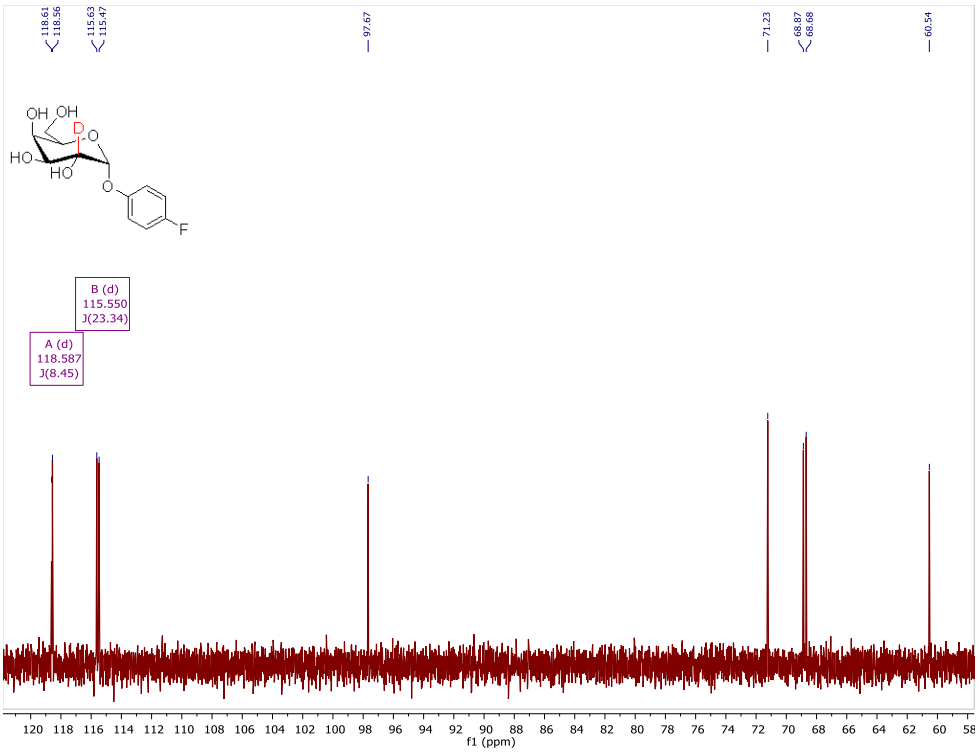

Figure S3.13: ^{1}H NMR spectrum for 2-fluorophenyl α-D-[2-^{2}H]galactopyranoside (600 MHz, D_2O)

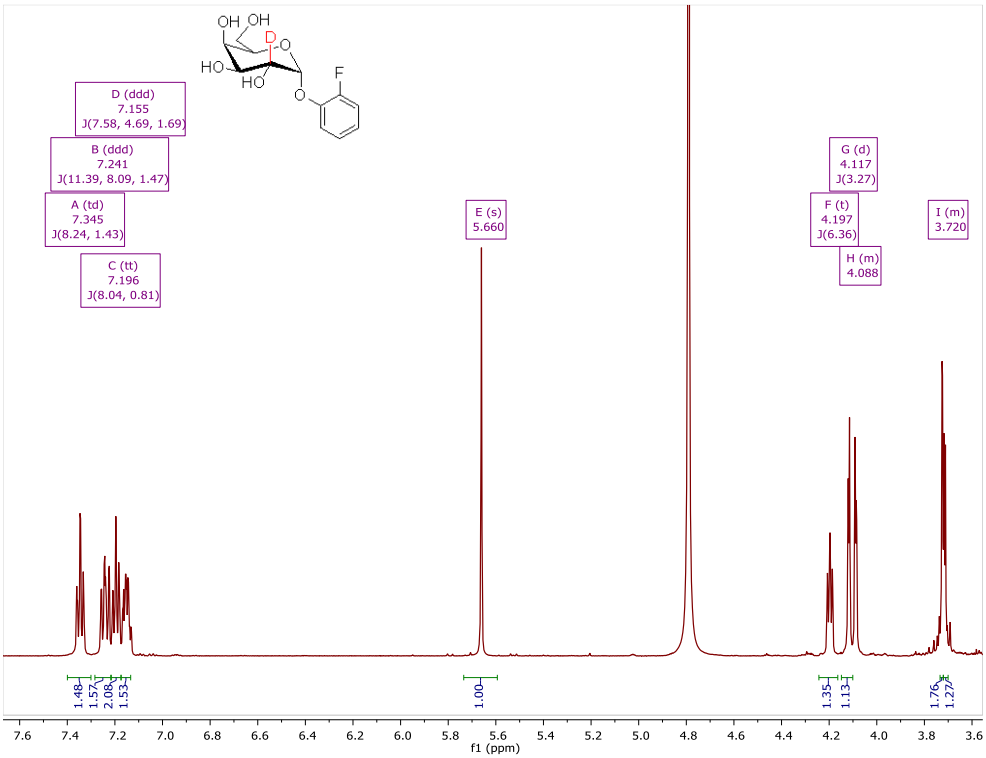

Figure S3.14: ^{13}C NMR spectrum for 2-fluorophenyl α-D-[2-^{2}H]galactopyranoside (151 MHz, D_2O)

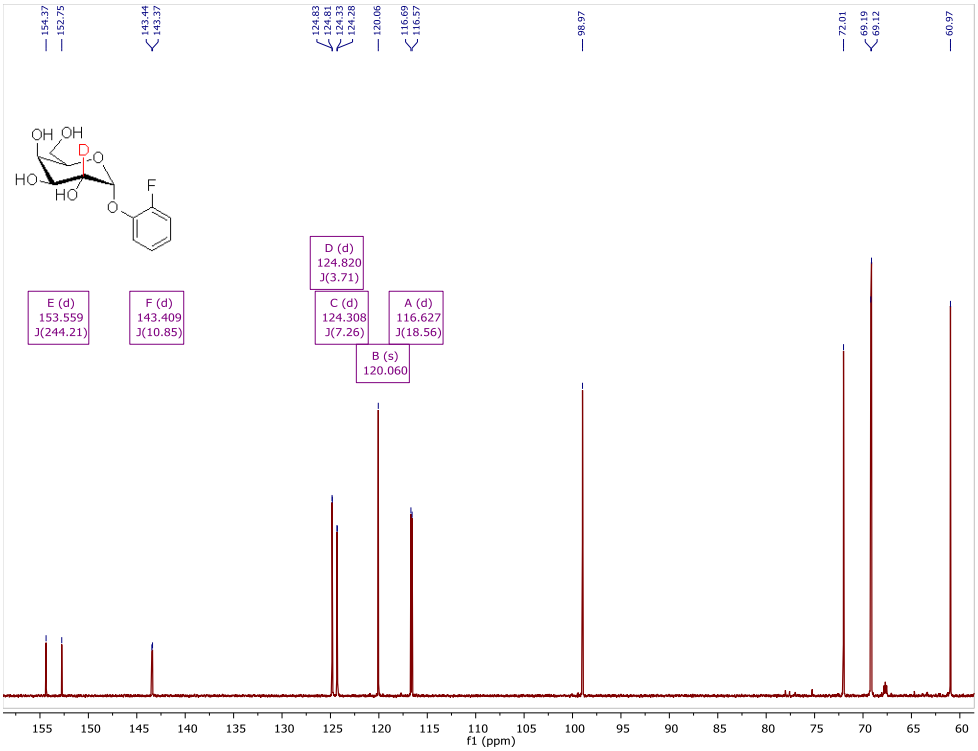

Figure S3.15: ^{1}H NMR spectrum for 4-fluorophenyl α-D-[3-^{2}H]galactopyranoside (600 MHz, D_2O)

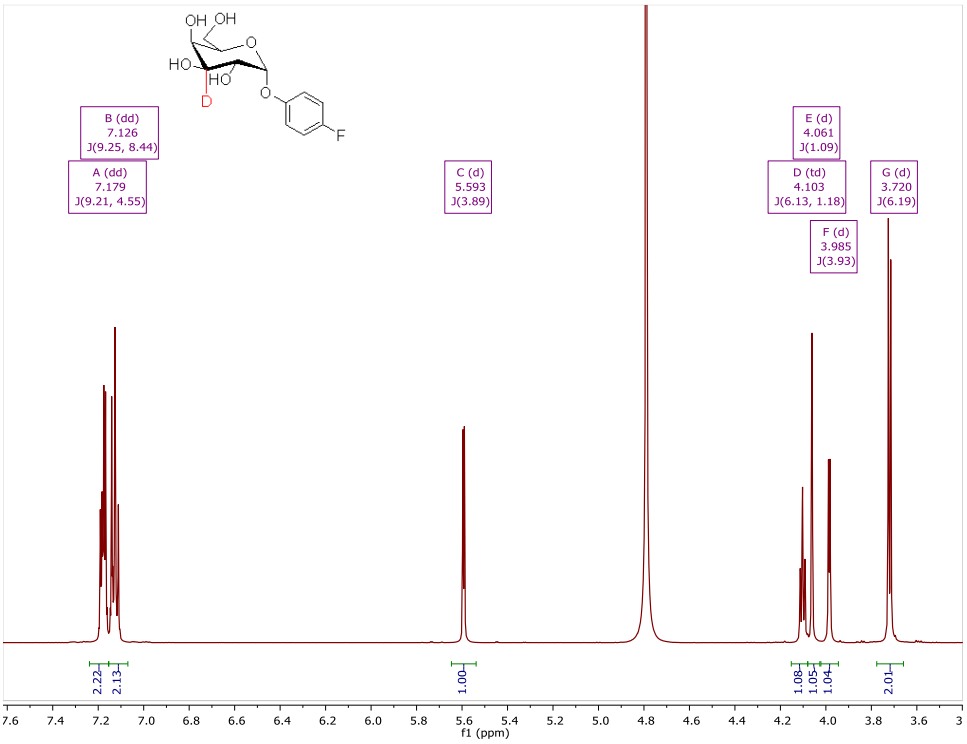

Figure S3.16: ^{13}C NMR spectrum for 4-fluorophenyl α-D-[3-^{2}H]galactopyranoside (151 MHz, D_2O)

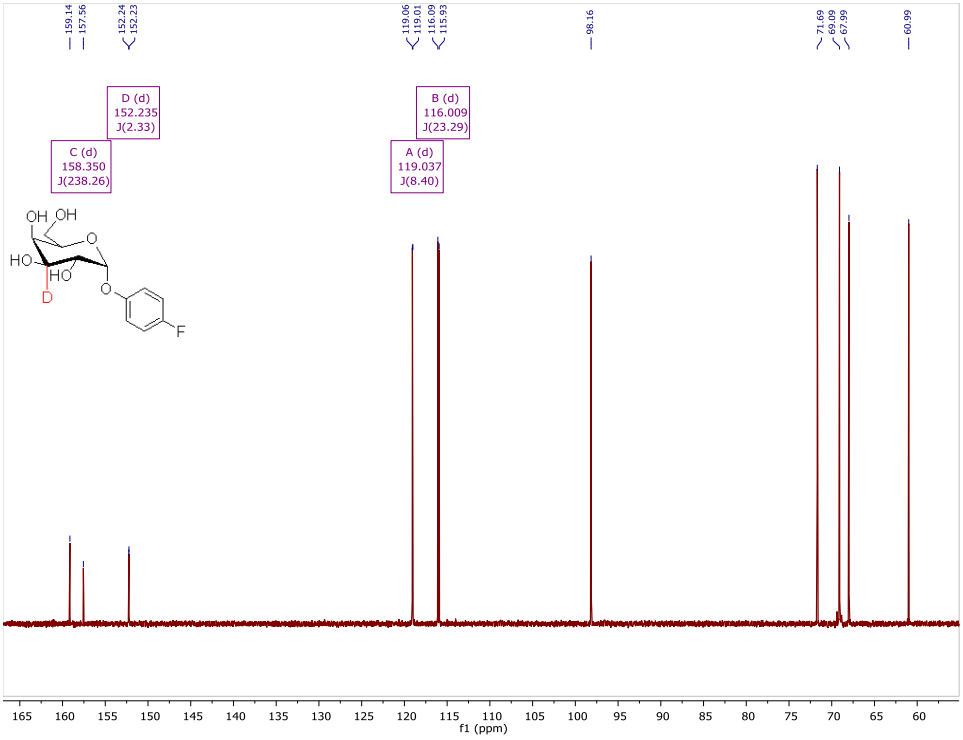

Figure S3.17: ^{1}H NMR spectrum for 2-fluorophenyl α-D-[3-^{2}H]galactopyranoside (600 MHz, D_2O)

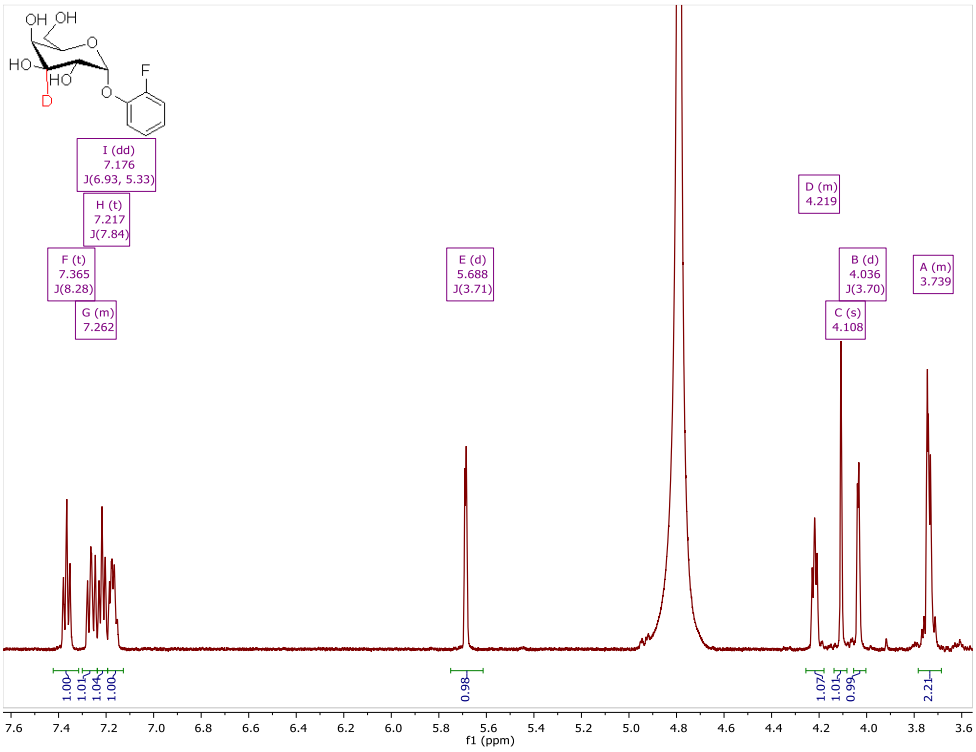

Figure S3.18: ^{13}C NMR spectrum for 2-fluorophenyl α-D-[3-^{2}H]galactopyranoside (151 MHz, D_2O)

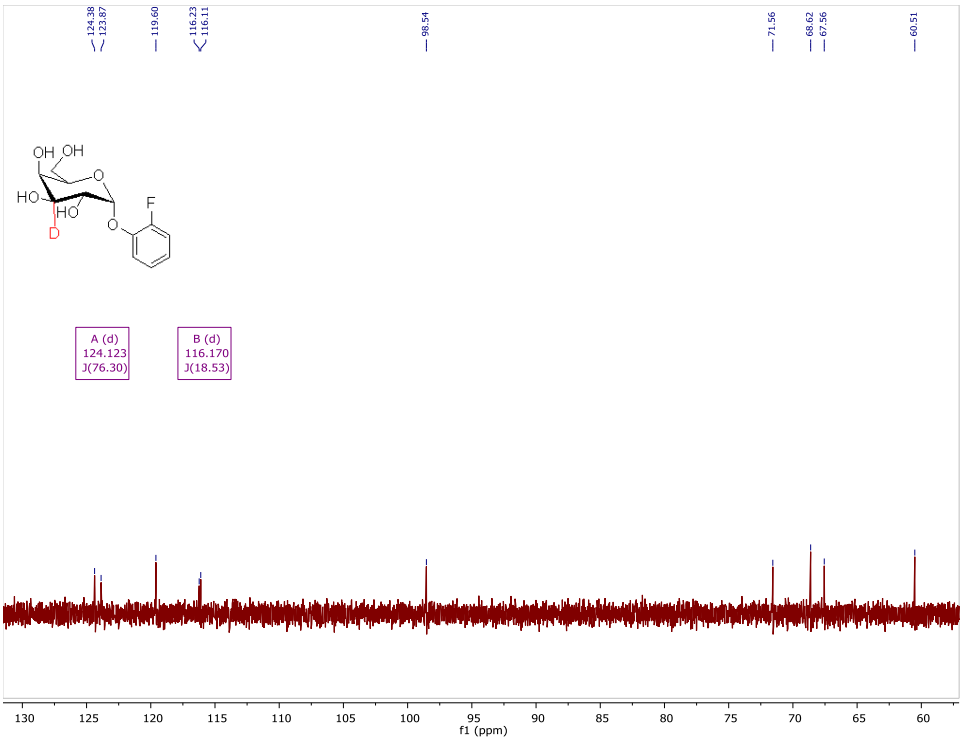

Figure S3.19: ^{1}H NMR spectrum for 4-fluorophenyl α-D-[2-^{2}H,3-^{2}H]galactopyranoside (600 MHz, D_2O)

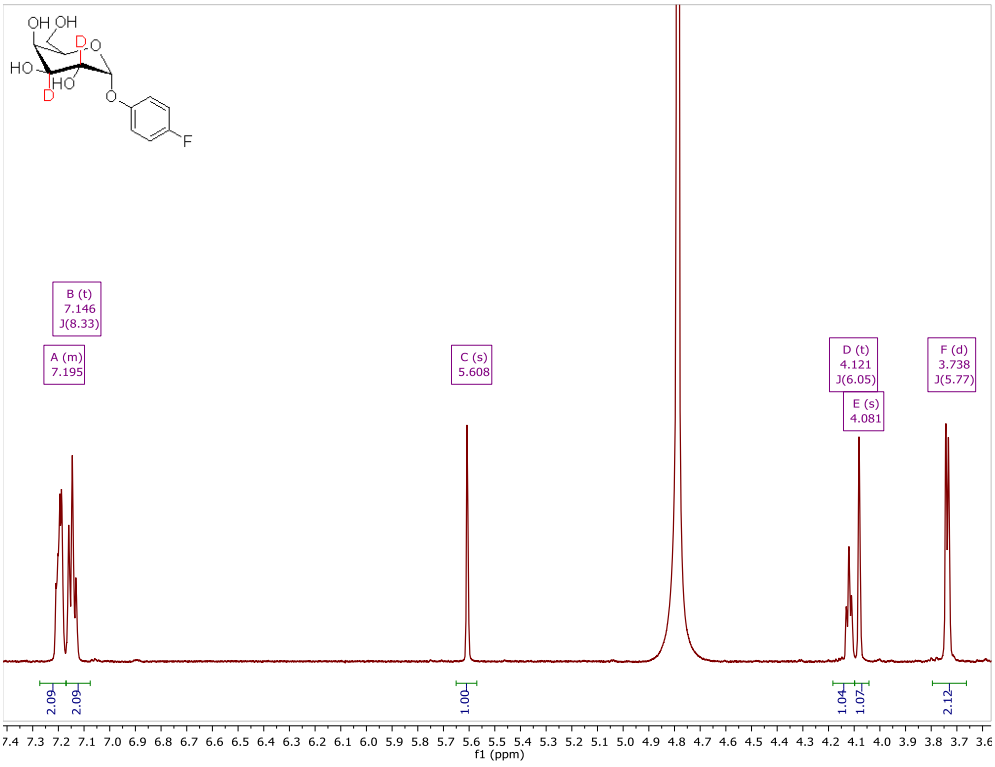

Figure S3.20: ^{13}C NMR spectrum for 4-fluorophenyl α-D-[2-^{2}H,3-^{2}H]galactopyranoside (151 MHz, D_2O)

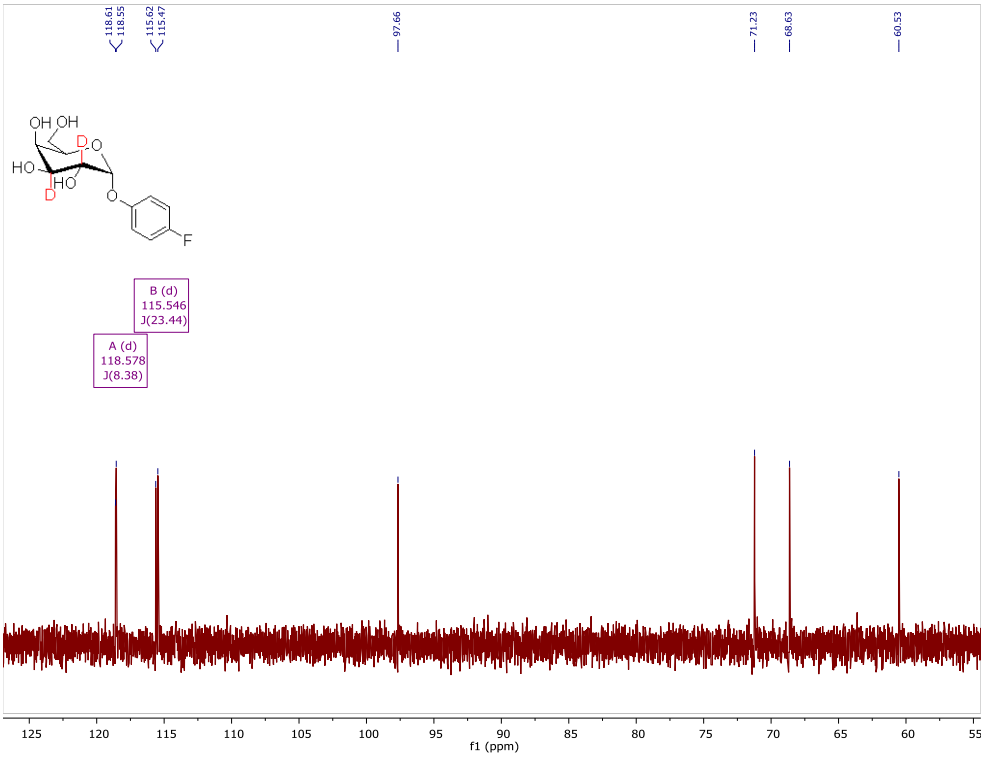

Figure S3.21: ^{1}H NMR spectrum for 2-fluorophenyl α-D-[2-^{2}H,3-^{2}H]galactopyranoside (600 MHz, D_2O)

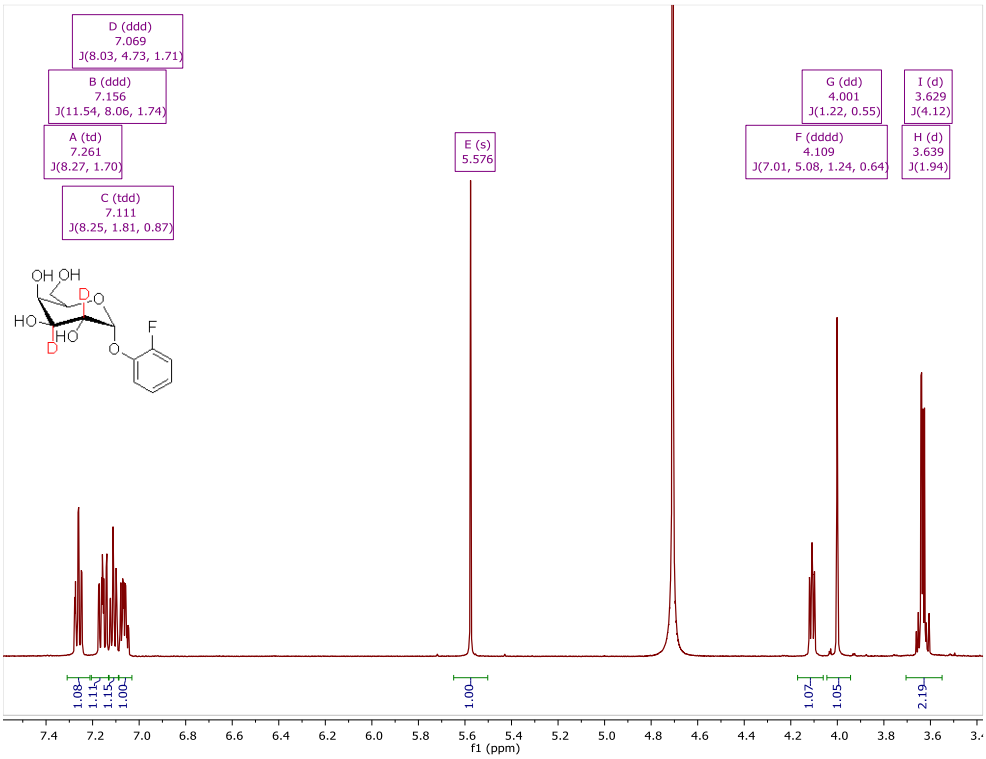

Figure S3.22: ^{13}C NMR spectrum for 2-fluorophenyl α-D-[2-^{2}H,3-^{2}H]galactopyranoside (151 MHz, D_2O)

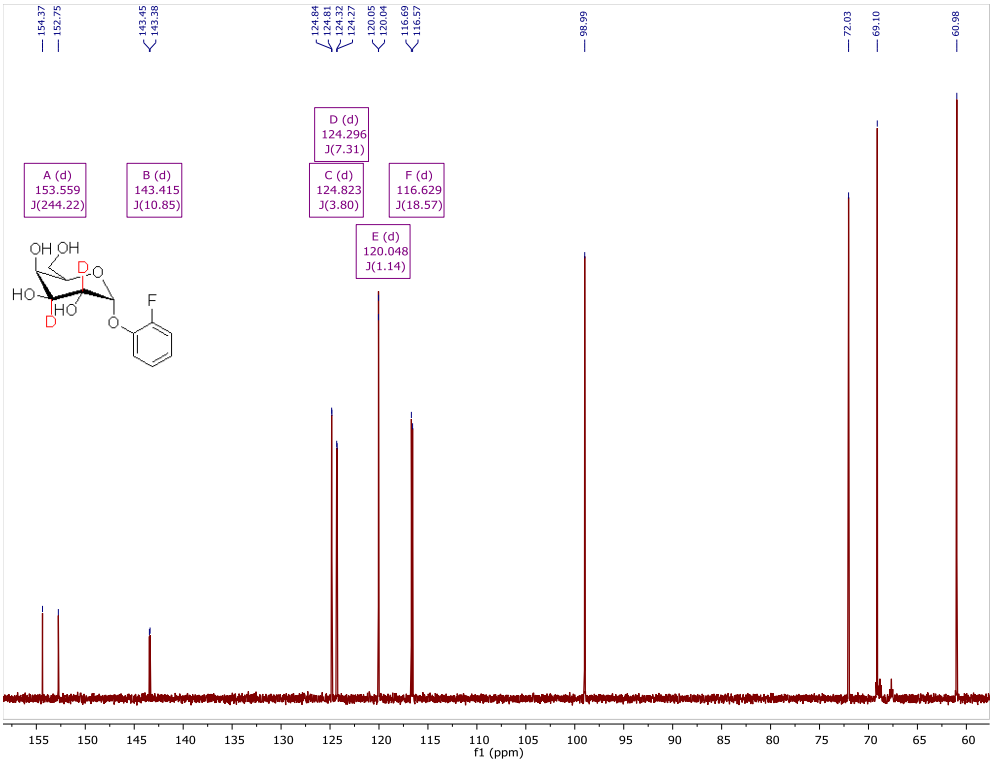

Appendix

Synthesis of Aryl α-D-Galactopyranosides

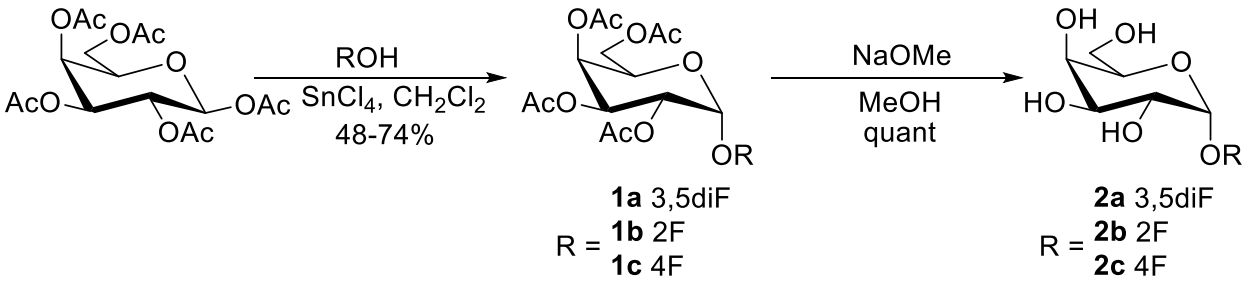

Preparation of 3,4,6-Tri-O-acetyl-1,5-anhydro-2-deoxy-D-(3-^{2}H)lyxo-hex-1-enitol

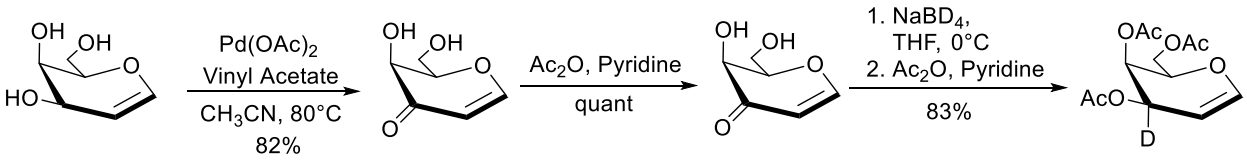

Synthesis of Aryl α-D-Galactopyranoside Isotopologues

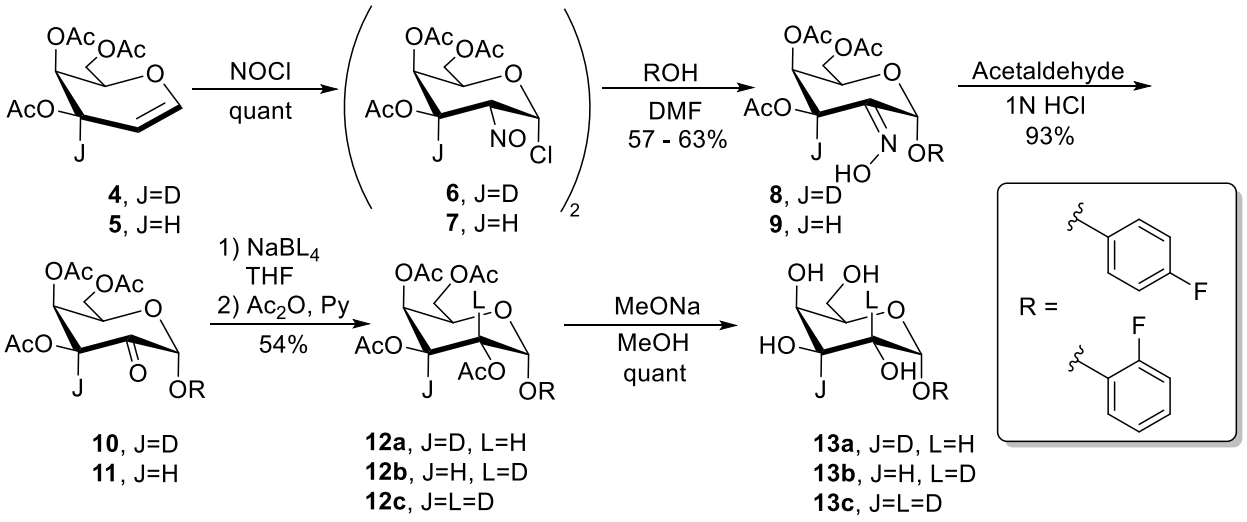

Chapter 4.

Kinetic Isotope Effects and the Transition State Structure for the Hydrolysis of α-d-Glucopyranosyl Fluoride by Inverting Glucoamylases

4.1. Abstract

Hydrolysis of α-D-glucopyranosyl fluoride catalyzed by the GH15 inverting α-glucoamylases from *A. niger* and *Rhizopus sp.* has been studied by use of multiple competitive kinetic isotope effect (KIE) measurements. The experimental KIEs are 1-^{2}H (1.137 ± 0.027), 2-^{2}H (1.039 ± 0.004), 5-^{2}H (1.004 ± 0.007), anomeric 1-^{13}C (1.012 ± 0.003), and ring 5-^{18}O (0.986 ± 0.003) for *A. niger* glucoamylase; and 1-^{2}H (1.149 ± 0.021), 2-^{2}H (1.053 ± 0.013), 5-^{2}H (1.018 ± 0.014), anomeric 1-^{13}C (1.013 ± 0.002), and ring 5-^{18}O (0.9896 ± 0.0003) for *Rhizopus sp.* glucoamylase. Both KIE panels are consistent with the enzymatic reaction occurring via an S_N1-type mechanism, in which the transition states has significant pyranosylium-ion like character and is late with respect to C−F bond cleavage.

4.2. Introduction

Glycoconjugates are ubiquitous in nature, abundant, and are characterized by the presence of glycosidic bonds that connect monosaccharides units to other carbohydrates, lipids, proteins, and numerous other molecules. Naturally, the transfer of carbohydrate units from a donor sugar to an acceptor biomolecule is one of the most fundamental biological transformations. As a consequence, the mechanisms of two enzyme families that are responsible for the addition or removal of the majority of carbohydrate residues, glycoside hydrolases (GHs) and glycosyl transferases (GTs), are being studied extensively. The transition state (TS) structures traversed by substrates during enzymatic catalysis are of particular interest for the design of transition state analogue (TSA) inhibitors, compounds with potential therapeutic applications. A common approach to TS structure determination involves measuring multiple kinetic isotope effect (KIEs), which can then be used as constraints for modern *ab initio* theoretical modelling of the TS.[1,2] This strategy gives information about the geometry, charge development, and the extent of bond cleavage and formation at the reaction TS.[3]

Glycosyl fluorides have been shown to be particularly useful for mechanistic studies of GHs. Typically, they are excellent substrates with high k_{cat}/K_m values for most glycoside

hydrolases,[4] and their reactions can be readily monitored by fluoride ion specific electrodes and ^{19}F-NMR spectroscopy (^{19}F has a spin quantum number of ½). α-Glucopyranosyl fluoride is perhaps the most studied carbohydrate based on the reported mechanisms for many different reactions.[5–11] Specifically, several distinct pathways have been noted for cleavage of the glycosidic C–F bond, with the precise mechanism depending on the reaction conditions. These pathways involve: loose, concerted, transition states (S_N2, Nuc = N_3^-),[6] internal return (S_Ni, ROH = hexafluoroisopropanol (HFIP), trifluoroethanol),[5,9] specific-base promoted (S_N2, nuc = hydroxide, ionized sugar-OH group,[8] general-base catalyzed (nuc = solvent),[10] and acid catalyzed (S_N1)[7,10] reactions. For enzyme-catalyzed hydrolysis reactions of α-D-glucopyranosyl fluoride (α-GlcF) catalyzed by *R. niveus* and *A. niger* glucoamylases and by sugar beet seed α-glucosidase the reported KIEs suggest that these reaction occur by S_N1 mechanisms rather than S_N2.[12] However, development of the direct NMR method for measuring competitive *V/K* KIEs allows for more detailed KIE investigations including the ring-^{18}O KIE measurement.[13]

This report will discuss a follow up KIE study to that reported by Tanaka et al,[12] in which they measured *V/K* KIEs, using radiolabelled techniques, and calculated possible TSs for the catalyzed hydrolysis of α-GlcF by inverting and retaining α-glucosidases. Our focus is on the GH15 inverting α-glucoamylases from *A. niger* and *Rhizopus sp.* for which we have measured 5-^{18}O KIE and γ-secondary deuterium (5-^{2}H) KIE in addition we used stable isotopes to determine ^{2}H- and ^{13}C-KIEs that correspond to those obtained previously by Tanaka et al. (^{3}H and ^{14}C). We will use our complete set of KIEs, including 5-^{18}O ring oxygen, as constraints to identify the various bond orders and charge delocalization at the enzymatic transition state for the *A. niger* α-glucoamylase by modern computational chemistry methods (QM/MM and DFT).

4.3. Experimental Procedures

4.3.1. Materials

D-(1-^{13}C)Glucose was purchased from Omicron Biochemicals, Inc. D-(1-^{2}H)Glucose, D-(2-^{2}H)glucose, D-(5-^{2}H)glucose, and D-(5-^{18}O)glucose were prepared according to known protocols.[14,15] α-D-Glucopyranosyl fluoride and its singly labelled isotopologues were prepared from the correspondingly labelled 1,2,3,4,6-penta-*O*-acetyl-D-glucopyranose in two steps according to previously reported procedure.[16] Amyloglucosidases from *A. niger* and *Rhizopus sp.* were purchased from Megazyme.

α-D-Glucopyranosyl fluoride*:* mp 121.2–122.9 °C (lit.[11] 118 – 120 °C) ; ^{1}H NMR (600 MHz, D_2O) δ 5.70 (dd, *J* = 53.5, 2.8 Hz, 1H, H-1), 3.88 (dd, *J* = 12.1, 2.1 Hz, 1H, H-6), 3.84

(ddd, *J* = 10.0, 5.0, 1.6 Hz, 1H, H-5), 3.80 (dd, *J* = 12.1, 5.0 Hz, 1H, H-6'), 3.75 (t, *J* = 9.6 Hz, 1H, H-3), 3.62 (ddd, *J* = 26.4, 9.9, 2.8 Hz, 1H, H-2), 3.52 (t, *J* = 9.7 Hz, 1H, H-4); ^{13}C NMR (151 MHz, D_2O) δ 107.32 (d, *J* = 222.9 Hz, C-1), 74.14 (d, *J* = 3.2 Hz, C-5), 72.34 (C-3), 71.01 (d, *J* = 24.9 Hz, C-2), 68.51 (C-4), 60.08 (C-6); ^{19}F NMR (565 MHz, D_2O) δ -151.20 (dd, *J* = 53.6, 26.4 Hz); ESI-MS for $C_6H_{11}O_5F$ *m/z* calcd for ($M+Na^+$) 205.0483, found 205.0484.

α-D-(1-^{2}H)Glucopyranosyl fluoride*:* mp 121.4–123.3 °C; ^{1}H NMR (600 MHz, D_2O) δ 3.88 (dd, *J* = 12.1, 2.0 Hz, 1H, H-6), 3.84 (ddd, *J* = 9.9, 5.0, 1.9 Hz, 1H, H-5), 3.80 (dd, *J* = 12.1, 5.0 Hz, 1H, H-6'), 3.75 (t, *J* = 9.6 Hz, 1H, H-3), 3.62 (dd, *J* = 26.3, 9.9 Hz, 1H, H-2), 3.52 (t, *J* = 9.6 Hz, 1H, H-4); ^{13}C NMR (151 MHz, D_2O) δ 74.11 (d, *J* = 3.3 Hz, C-5), 72.34 (C-3), 70.91 (d, *J* = 25.1 Hz, C-2), 68.51 (C-4), 60.08 (C-6); ^{19}F NMR (565 MHz, D_2O) δ -151.92 (dt, *J* = 26.4, 7.9 Hz); ESI-MS for $C_6H_{10}DO_5F$ *m/z* calcd for ($M+Na^+$) 206.0545, found 206.0552.

α-D-(2-^{2}H)Glucopyranosyl fluoride*:* mp 121.5–123.0 °C; ^{1}H NMR (600 MHz, D_2O) δ 5.70 (d, *J* = 53.5 Hz, 1H, H-1), 3.88 (dd, *J* = 12.1, 2.0 Hz, 1H, H-6), 3.84 (ddd, *J* = 10.0, 5.0, 2.0 Hz, 1H, H-5), 3.80 (dd, *J* = 12.1, 4.9 Hz, 1H, H-6'), 3.75 (d, *J* = 9.4 Hz, 1H, H-3), 3.52 (t, *J* = 9.7 Hz, 1H, H-4); ^{13}C NMR (151 MHz, D_2O) δ 107.31 (d, *J* = 222.6 Hz, C-1), 74.13 (d, *J* = 3.3 Hz, C-5), 72.29 (C-3), 68.51 (C-4), 60.08 (C-6); ^{19}F NMR (565 MHz, D_2O) δ -151.40 (dt, *J* = 53.6, 3.2 Hz); ESI-MS for $C_6H_{10}DO_5F$ *m/z* calcd for ($M+Na^+$) 206.0545, found 206.0549.

α-D-(5-^{2}H)Glucopyranosyl fluoride*:* mp 121.9–123.7 °C; ^{1}H NMR (600 MHz, D_2O) δ 5.70 (dd, *J* = 53.5, 2.8 Hz, 1H, H-1), 3.88 (d, *J* = 12.5 Hz, 1H, H-6), 3.79 (d, *J* = 12.5 Hz, 1H, H-6'), 3.75 (t, *J* = 9.6 Hz, 1H, H-3), 3.62 (ddd, *J* = 26.4, 9.9, 2.8 Hz, 1H, H-2), 3.52 (d, *J* = 9.3 Hz, 1H, H-4); ^{13}C NMR (151 MHz, D_2O) δ 107.33 (d, *J* = 222.8 Hz, C-1), 72.33 (C-3), 71.01 (d, *J* = 25.0 Hz, C-2) , 68.45 (C-4), 60.02 (C-6); ^{19}F NMR (565 MHz, D_2O) δ -151.17 (dd, *J* = 53.8, 26.6 Hz); ESI-MS for $C_6H_{10}DO_5F$ *m/z* calcd for ($M+Na^+$) 206.0545, found 206.0546.

α-D-(5-^{18}O)Glucopyranosyl fluoride*:* mp 121.7–123.4 °C; ^{1}H NMR (600 MHz, D_2O) δ 5.70 (dd, *J* = 53.5, 2.8 Hz, 1H, H-1), 3.88 (dd, *J* = 12.1, 2.1 Hz, 1H, H-6), 3.84 (ddd, *J* = 9.9, 5.0, 1.9 Hz, 1H, H-5), 3.80 (dd, *J* = 12.1, 5.0 Hz, 1H, H-6'), 3.75 (t, *J* = 9.6 Hz, 1H, H-3), 3.62 (ddd, *J* = 26.4, 9.9, 2.8 Hz, 1H, H-2), 3.52 (t, *J* = 9.6 Hz, 1H, H-4); ^{13}C NMR (151 MHz, D_2O) δ δ107.31 (d, *J* = 222.8 Hz, C-1), 74.11 (d, *J* = 3.4 Hz, C-5), 72.34 (C-3), 71.00 (d, *J* = 25.0 Hz, C-2), 68.51 (C-4), 60.08 (C-6); ^{19}F NMR (471 MHz, D_2O) δ -151.23 (dd, *J* = 53.5, 26.4 Hz); ESI-MS for $C_6H_{11}O_4{}^{18}OF$ *m/z* calcd for ($M+Na^+$) 207.0525, found 207.0528.

α-D-(1-^{13}C)Glucopyranosyl fluoride*:* mp 120.7–122.7 °C; ^{1}H NMR (600 MHz, D_2O) δ 5.70 (ddd, *J* = 183.7, 53.5, 2.8 Hz, 1H, H-1), 3.88 (dd, *J* = 12.1, 2.1 Hz, 1H, H-6), 3.86 – 3.82

(m, 1H, H-5), 3.80 (dd, *J* = 12.1, 4.9 Hz, 1H, H-6'), 3.75 (t, *J* = 9.6 Hz, 1H, H-3), 3.62 (dddd, *J* = 26.4, 9.9, 2.9, 1.3 Hz, 1H, H-2), 3.52 (t, *J* = 9.6 Hz, 1H, H-4); ^{13}C NMR (151 MHz, D_2O) δ 107.33 (d, *J* = 222.9 Hz, C-1), 74.13 (dd, *J* = 3.2, 2.4 Hz, C-5), 72.34 (C-3), 71.00 (dd, *J* = 46.1, 25.0 Hz, C-2), 68.51 (C-4), 60.08 (d, *J* = 3.5 Hz, C-6); ^{19}F NMR (565 MHz, D_2O) δ -151.30 (ddd, *J* = 222.8, 53.5, 26.4 Hz); ESI-MS for $C_5{}^{13}CH_{11}O_5F$ *m/z* calcd for ($M+Na^+$) 206.0516, found 206.0520.

4.3.2. KIE Measurements

Competitive *V/K* KIEs were measured using ^{19}F NMR spectroscopy on a Bruker AVANCE III QCI cryoprobe 600 MHz spectrometer.[13] Fluorine-19 T_1 values were measured for 3,5-difluorophenyl β-D-(1-^{2}H)galactopyranoside (internal standard), unlabelled α-D-glucopyranosyl fluoride and α-D-(1-^{13}C)glucopyranosyl fluoride at 25 °C using standard inversion recovery pulse sequence and determined to be 1.157 s, 0.760 s and 0.704 s, respectively. In a typical experiment, a mixture of two or three labelled α-GlcF isotopologues (approx. 1.0 mg of each) and 3,5-difluorophenyl β-D-(1-^{2}H)galactopyranoside (0.5 mg) was dissolved in 650 µL buffer (100 mM sodium succinate, pH 6.05, 1% w/v BSA, 50 mM NaCl, 10% v/v D_2O) and transferred into a standard 5 mm glass NMR tube. Reactions were initiated by the addition of enzyme (8–10 µL of 1 mg mL^{-1}). The magnetic field was shimmed to obtain symmetrical (as close to a Lorentzian shape as possible) peaks. A ^{1}H NMR and ^{19}F NMR spectra were then acquired before sequentially acquiring more than fifty quantitative proton-decoupled ^{19}F NMR spectra using an inverse-gated pulse sequence.[17,18] FIDs were acquired for 16 scans (acquisition time per scan of 0.6 s) with a relaxation delay of 21 s (5.75 min per spectrum).

The resultant quantitative ^{19}F spectra were deconvolved by performing the following operations: i) Fourier transformation of the FIDs was performed with two-fold zero-filling and application of an exponential line broadening between 2.0–2.5 Hz; ii) spectra were manually phased and baseline corrected using MestReNova version 10.0.2; iii) spectra were fit using standard MestReNova line fitting algorithm for a generalized Lorentzian line shape; iv) to optimize the calculated fit peak positions, peak widths at half-height, peak heights and optimal combination of Lorentzian and Gaussian (L/G) shapes for each individual peak were allowed to vary; and v) the peak areas were normalized relative to that of the internal standard. Then, for each spectrum the fraction of reaction (F_1) for the lighter isotopologue and the associated R values were calculated from the respective integrals. These data were then fit using GraphPad Prism 5.04 and a non-linear least squares regression to equation (4.1).[19]

$$R = R_0(1 - F_1)^{(1/KIE-1)} \qquad (4.1)$$

4.4. Results

Advances in NMR spectroscopy have enabled the development of a sensitive NMR spectroscopic method that allows the high precision measurement of competitive KIEs.[13] The method requires milligram quantities of light and heavy isotopologues, with each possessing an NMR-active nucleus at a probe site (in this case ^{19}F), and an adjacent site labelled with light and heavy isotopes. Application of this method for the measurement of five competitive KIEs, where the label is at C1, H1, H2, H5 and O5, on the enzyme-catalyzed hydrolysis of α-D-glucopyranosyl fluoride (α-GlcF) necessitated the synthesis of six isotopologues (Fig. 4.1, **1a–f**).

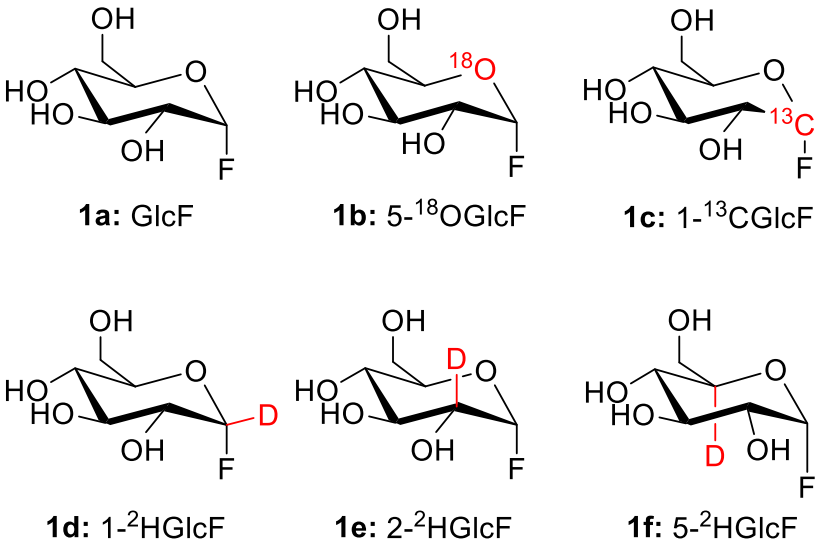

1a: GlcF **1b:** 5-^{18}OGlcF **1c:** 1-^{13}CGlcF

1d: 1-^{2}HGlcF **1e:** 2-^{2}HGlcF **1f:** 5-^{2}HGlcF

Figure 4.1. α-D-Glucopyranosyl fluoride isotopologues.

The ^{19}F atom probe nucleus was used to report on changes in isotopologue ratios for remaining starting material. Individual ^{19}F probe nucleus signals were integrated, and the relative ratio (R) for each isotopologue was calculated. The fraction of reaction (F_1) was determined by comparing the integration for the light isotopologue (**1a**) with that of the inert internal standard [3,5-difluorophenyl β-D-(1-^{2}H)galactopyranoside]. A representative overlay of NMR spectra at F_1 = 0 and at F_1 = 0.82 is shown in Figure 4.2, and typical examples of the nonlinear least-squares fit of the fraction of reaction versus R to equation 1 for the experimental KIE data are illustrated in Figure 4.3. Table 4.1 lists the mean and standard deviation values for each KIE derived from three replicate experiments.

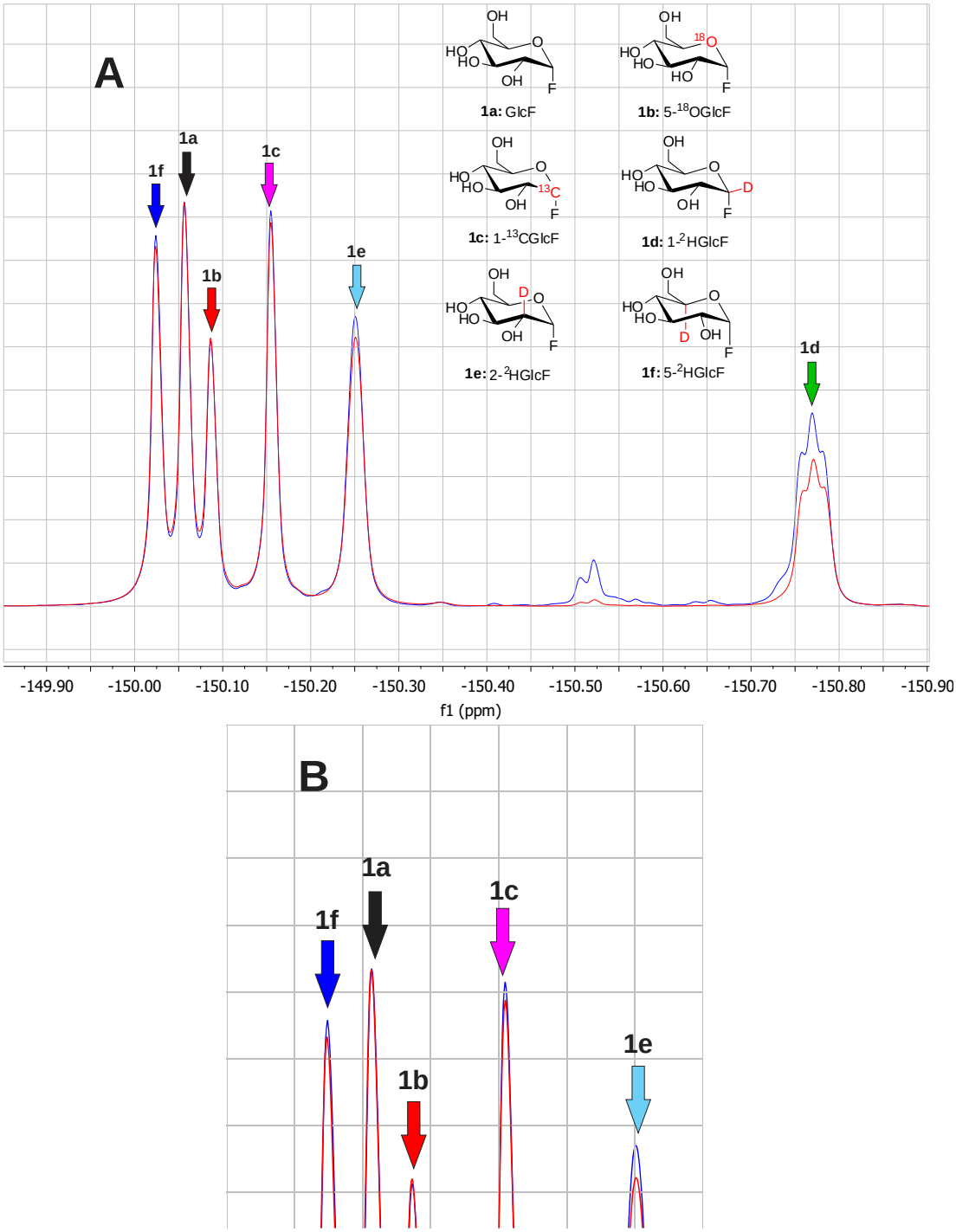

Figure 4.2. **A.** Overlaid proton and ^{13}C decoupled ^{19}F NMR spectra containing a mixture of **1a – 1f** in the presence of *Rhizopus sp.* glucoamylase at fraction of reactions F_1 = 0.00 (red) and 0.82 (blue) that have normalized peak heights for the probe isotopologue (1a; black arrow). Note the relative increase in peak heights for the **1c–1f** isotopologues during reaction (normal KIEs), and decrease for **1b** (inverse KIE). **B.** Close-up of **A.** showing relative peak intensities change for **1b**, **1c**, **1e** and **1f.**

Note: peak at -150.50 ppm is a fluorinated impurity that doesn't affect KIE measurement.

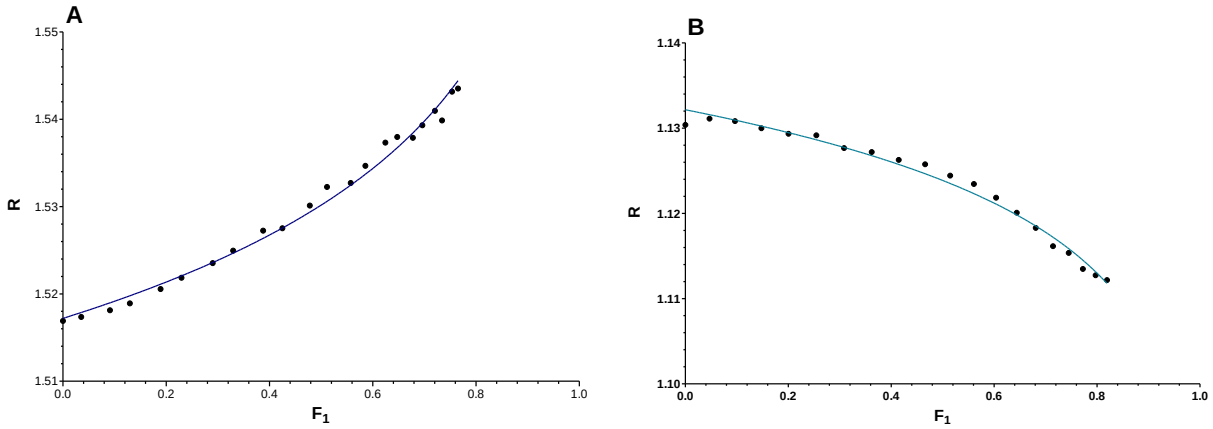

Figure 4.3. Plots of the change in integrated peak intensity ratios (R) versus fraction of reaction for the light isotopologue (F_1) for the measurement of competitive KIE values: **(A)** data from an experimental measurement of $k(1\text{-}^{12}C)/k(1\text{-}^{13}C)$ using **1a** and **1c**; **(B)** data from an experimental measurement of $k(5\text{-}^{16}O)/k(5\text{-}^{18}O)$ using **1a** and **1b.**

Table 4.1. Experimental *V/K* KIEs on hydrolysis of α-D-glucopyranosyl fluorides by glucoamylases[a]

Enzyme	Primary ^{13}C	α-Secondary ^{2}H	β-Secondary ^{2}H	Ring ^{18}O	γ-Secondary ^{2}H
Rhizopus sp.	1.013 ± 0.002	1.149 ± 0.021	1.053 ± 0.013	0.9896 ± 0.0003	1.018 ± 0.014
R. niveus[b]	1.017	1.171	1.058		
A. niger	1.012 ± 0.003	1.137 ± 0.027	1.039 ± 0.004	0.986 ± 0.003	1.004 ± 0.007

[a]Values are the mean and standard deviation for three experimental determinations. [b]Calculated from the ^{14}C and ^{3}H-KIEs reported by Tanaka et al. at pH = 4.80 and 30 °C.[12]

4.5. Discussion

V/K KIEs for α-GlcF hydrolysis catalyzed by GH15 glycoamylases from *R. niveus* and *A. niger* have been previously measured by Tanaka et al. using radiolabelled isotopologues. Experimental values measured for *R. niveus* glycoamylase at optimal conditions (pH = 4.80 and T = 30 °C) for primary ^{14}C, α-secondary ^{3}H and β-secondary ^{3}H are 1.033 ± 0.012, 1.255 ± 0.012 and 1.085 ± 0.011, respectively.[12] This equates to a primary ^{13}C KIE of ~1.017, α-SDKIE of 1.171 and β-SDKIE of 1.058 (Table 4.1) as calculated according to equations 4.2 and 4.3.[19,20]

$$\frac{\ln\left(\frac{k_{12}}{k_{14}} \times \frac{s_{12}^{\ddagger}}{s_{14}^{\ddagger}} \times \frac{s_{14}}{s_{12}}\right)}{\ln\left(\frac{k_{12}}{k_{13}} \times \frac{s_{12}^{\ddagger}}{s_{13}^{\ddagger}} \times \frac{s_{13}}{s_{12}}\right)} \approx 1.9, \qquad i.e.$$

$$\ln\left(\frac{k_{12}}{k_{13}}\right) \approx \ln\left(\frac{k_{12}}{k_{14}}\right)/1.9 \tag{4.2}$$

$$\frac{\ln\left(\frac{k_H}{k_T}\right)}{\ln\left(\frac{k_H}{k_D}\right)} = \frac{1-\sqrt{m_H/m_T}}{1-\sqrt{m_H/m_D}} = \frac{1-\sqrt{1/3}}{1-\sqrt{1/2}} \cong 1.44, \qquad i.e.$$

$$\ln\left(\frac{k_H}{k_D}\right) \approx \ln\left(\frac{k_H}{k_T}\right)/1.44 \tag{4.3}$$

We decided to use different experimental conditions (pH = 6.05 and T = 25 °C), to those used by Tanaka et al in their studies, for two reasons: 1) to ensure that C–F bond cleavage is rate-limiting and 2) tuning and matching frequencies for the ^{19}F NMR spectrometer cryoprobe is problematic at pH values lower than 5.0 and at elevated temperatures (> 28 °C). As a result, we measured slightly different KIE values for *Rhizopus sp*. glycoamylase than those previously reported (Table 1).[12] However, our KIE data is in a good agreement with the pH dependence pattern observed for the *V/K* KIEs for the *R. niveus* and *A. niger* reported by Tanaka et al.: they found *V/K* KIE values decreasing with increasing pH, maximum *V/K* KIEs being observed at the enzymatic pH optimum of 4.80.[12]

4.5.1. ^{13}C KIE

The experimentally determined anomeric ^{13}C KIEs for the hydrolysis of α-GlcF by GH15 glycoamylases from *Rhizopus sp*. and *A. niger* are 1.013 ± 0.002 and 1.012 ± 0.003, respectively. These values are in the range that is typically associated with dissociative S_N1-like TSs. That is, anomeric carbon KIEs (k_{12}/k_{13}) for the reactions of glycopyranosides in solution are typically in the range of 1.005 to 1.030. Substitution reactions that proceed via dissociative transition states exhibit anomeric ^{13}C-KIE values that are closer to unity;[5,7,15,21] for instance, the reported ^{13}C-KIEs for spontaneous hydrolysis of α-D-glucopyranosyl 4-bromoisoquinolinium bromide and the acid-catalyzed reaction of the anomeric methyl D-xylopyranosides and methyl α-D-glucopyranoside are 1.005 ± 0.002,[22] 1.006 ± 0.001,[21] and 1.007 ± 0.001,[15] respectively. For the enzyme-catalyzed

hydrolysis of glycosides typical anomeric carbon ^{13}C-KIEs are in the range of 1.018–1.032 for concerted S_N2 mechanisms,[23,24] and 1.002−1.018 for stepwise S_N1 reactions.[23] It is therefore likely that these reactions have similar TS structures and that the GH15 glycoamylases catalyzed hydrolysis of α-GlcF has a late TS with significant C−F bond cleavage.

4.5.2. ^{18}O KIE

For non-enzymatic reactions in water where cleavage of one of the two C−O acetal bonds is rate-limiting, the leaving group ^{18}O-KIE is normal ($k_{16}/k_{18} > 1$) while the ^{18}O-KIE associated with formation of the cationic ion intermediate is inverse ($k_{16}/k_{18} < 1$).[15,21,25] Using α-GlcF as a substrate does not allow measurement of leaving group KIE, while ring ^{18}O-KIEs for the hydrolysis of α-GlcF by GH15 glycoamylases from *Rhizopus sp*. and *A. niger* are inverse being 0.9896 ± 0.0003 and 0.986 ± 0.003, respectively. These values are consistent with an increased anomeric carbon to ring oxygen bond order at the respective TSs, an effect that originates from the positive charge delocalization onto the ring oxygen atom at the TS for cleavage of the C–F bond.

4.5.3. Secondary Deuterium KIEs

α-Secondary Deuterium KIE (α-SDKIE)

In general, maximal α-SDKIE values are associated with S_N1 reactions with the magnitude varying with the leaving group[26–28]. These effects are primarily associated with weakening of an out-of-plane bending vibration as the steric crowding lessens at a dissociative TS, as the reaction centre hybridization goes from sp^3 to sp^2. The measured α-SDKIEs for the hydrolysis of α-GlcF catalyzed by GH15 glycoamylases from *Rhizopus sp*. and *A. niger* are 1.149 ± 0.021 and 1.136 ± 0.027, respectively. In comparison, the reported α-SDKIE for the solvolysis of α-GlcF in HFIP is 1.185 ± 0.006,[5] while the corresponding values for its uncatalyzed hydrolysis is 1.142 ± 0.007,[11] and for its S_N2 reaction with azide is 1.192 ± 0.006.[6] Solvolysis of α-GlcF in HFIP occurs by internal return from a solvent separated ion pair (S_Ni; $D_N^{\ddagger} * A_N$ss) that is characterized by a late transition state for C–F bond cleavage,[5] while the uncatalyzed hydrolysis and substitution with azide occur via an exploded S_N2 (A_ND_N) TSs.[8,11]

β-Secondary Deuterium KIE (β-SDKIE)

The experimental β-SDKIEs, which originate from a hyperconjugative weakening of the C−H/(D) bond by electron delocalization into the developing empty p-orbital at the anomeric centre, for the hydrolysis of α-GlcF by GH15 glycoamylases from *Rhizopus sp*. and *A. niger* are 1.053 ± 0.013 and 1.039 ± 0.004, respectively. The corresponding effects for HFIP solvolysis,

uncatalyzed hydrolysis of α-GlcF, and its reaction with the azide are 1.080 ± 0.010,[5] 1.067 ± 0.008,[11] and 1.046 ± 0.007,[6] respectively. The magnitude of β-SDKIEs provides insight into possible TS conformations,[11,15] as the hyperconjugative bond weakening depends on the dihedral angle between the C−H/(D) bond and the p-orbital on the anomeric centre.

γ-Secondary Deuterium KIE (γ-SDKIE)

The measured γ-SDKIEs are 1.018 ± 0.014 and 1.004 ± 0.007 for *Rhizopus sp*. and *A. niger* enzymes, respectively. Those effects are considered to originate from hyperconjugation and represent changes in the geometry of the O5–C5–C6 bond angle and the C5–H5 bond distances as the substrate approaches the transition state conformation.[12,29]

4.6. Conclusions

Our measured KIEs are in good agreement with ones previously reported by Tanaka et al. and are suggesting dissociative S_N1-like TSs for GH15 catalyzed hydrolyses of α-GlcF. Additionally, we have determined ring ^{18}O-KIEs of 0.9896 ± 0.0003 and 0.986 ± 0.003 for by GH15 glycoamylases from *Rhizopus sp*. and *A. niger*, respectively. These are also indicative of a late TS with significant C−F bond cleavage. Measured *V/K* KIE data is also consistent with the pH dependence pattern observed for the *V/K* KIEs for the *R. niveus* and *A. niger* reported by Tanaka et al., *V/K* KIE values decreasing with increasing pH, maximum *V/K* KIEs observed at the enzymatic pH optimum.

We will use our complete set of KIEs, including 5-^{18}O ring oxygen, as constraints to identify the various bond orders and charge delocalization at the enzymatic transition state for the *A. niger* α-glucoamylase by modern computational chemistry methods (QM/MM and DFT).

4.7. References

1. Vern L. Schramm. Enzymatic Transition-State Analysis and Transition-State Analogs. *Methods Enzymol.* **308,** 301–355 (1999).

2. Schramm, V. L. Enzymatic Transition States, Transition-State Analogs, Dynamics, Thermodynamics, and Lifetimes. *Annu. Rev. Biochem.* **80,** 703–732 (2011).

3. Kohen, A. & Limbach, H.-H. *Isotope effects in chemistry and biology*. (Taylor & Francis, 2006).

4. Williams, S. J. & Withers, S. G. Glycosyl fluorides in enzymatic reactions. *Carbohydr. Res.* **327,** 27–46 (2000).

5. Chan, J., Tang, A. & Bennet, A. J. A Stepwise Solvent-Promoted SNi Reaction of α-D-Glucopyranosyl Fluoride: Mechanistic Implications for Retaining Glycosyltransferases. *J. Am. Chem. Soc.* **134,** 1212–1220 (2012).

6. Chan, J., Sannikova, N., Tang, A. & Bennet, A. J. Transition-State Structure for the Quintessential S_N2 Reaction of a Carbohydrate: Reaction of α-Glucopyranosyl Fluoride with Azide Ion in Water. *J. Am. Chem. Soc.* **136,** 12225–12228 (2014).

7. Chan, J., Tang, A. & Bennet, A. J. Transition-state structure for the hydronium-ion-promoted hydrolysis of α- d -glucopyranosyl fluoride. *Can. J. Chem.* **93,** 463–467 (2015).

8. Banait, N. S. & Jencks, W. P. Reactions of Anionic Nucleophiles with α-D-Glucopyranosyl Fluoride in Aqueous Solution through a Concerted, ANDN(SN2) Mechanism. *J. Am. Chem. Soc.* **113,** 7951–7958 (1991).

9. Sinnott, M. L. & Jencks, W. P. Solvolysis of D-Glucopyranosyl Derivatives in Mixtures of Ethanol and 2,2,2-Trifluoroethanoll. *J. Am. Chem. Soc.* **102,** 2026–2032 (1980).

10. Banait, N. S. & Jencks, W. P. General-acid and general-base catalysis of the cleavage of .alpha.-D-glucopyranosyl fluoride. *J. Am. Chem. Soc.* **113,** 7958–7963 (1991).

11. Zhang, Y., Bommuswamy, J. & Sinnott, M. L. Kinetic Isotope Effect Study of Transition States for the Hydrolyses of a- and b-Glucopyranosyl Fluorides. *J. Am. Chem. Soc.* **116,** 7557–7563 (1994).

12. Tanaka, Y., Tao, W., Blanchard, J. S. & Hehre, E. J. Transition State Structures for the Hydrolysis of a-D-Glucopyranosyl Fluoride by Retaining and Inverting Reactions of Glycosylases. *J. Biol. Chem.* **269,** 32306–32312 (1994).

13. Chan, J., Lewis, A. R., Gilbert, M., Karwaski, M. & Bennet, A. J. A direct NMR method for the measurement of competitive kinetic isotope effects. *Nat. Chem. Biol.* **6,** 405–407 (2010).

14. Chakladar, S., Cheng, L., Choi, M., Liu, J. & Bennet, A. J. Mechanistic evaluation of MelA a-galactosidase from Citrobacter freundii: A family 4 glycosyl hydrolase in which oxidation is rate-limiting. *Biochemistry* **50,** 4298–4308 (2011).

15. Bennet, A. J. & Sinnott, M. L. Complete Kinetic Isotope Effect Description of Transition-States for Acid-Catalyzed Hydrolyzes of Methyl alpha-Glucopyranosides and beta-

Glucopyranosides. *J. Am. Chem. Soc.* **108,** 7287–7294 (1986).

16. Steinmann, A., Thimm, J., Matwiejuk, M. & Thiem, J. Formation of Homooligosaccharides Using Base-Promoted Glycosylation of Unprotected Glycosyl Fluorides. 3606–3612 (2010). doi:10.1021/ma100191d

17. Claridge, T. D. W. *High-resolution NMR techniques in organic chemistry*. (Elsevier, 2009).

18. Guido F. Pauli & Birgit U. Jaki, Lankin, D. C. Quantitative 1H NMR: Development and Potential of a Method for Natural Products Analysis. *J. Nat. Prod.* **68,** 133–149 (2005).

19. Melander, L. C. S. & Saunders, W. H. *Reaction rates of isotopic molecules*. (Wiley, 1980).

20. Swain, G. C., Stivers, E. C., Reuwer Jr., J. F. & Schaad, L. J. Use of Hydrogen Isotope Effects to Identify the Attacking Nucleophile in the Enolization of Ketones Catalyzed by Acetic Acid. *J. Am. Chem. Soc.* **80,** 5885–5893 (1958).

21. Indurugalla, D. & Bennet, A. J. A kinetic isotope effect study on the hydrolysis reactions of methyl xylopyranosides and methyl 5-thioxylopyranosides: Oxygen versus sulfur stabilization of carbenium ions. *J. Am. Chem. Soc.* **123,** 10889–10898 (2001).

22. Huang, X., Tanaka, K. S. E. & Bennet, A. J. Glucosidase-catalyzed hydrolysis of α-D-glucopyranosyl pyridinium salts: Kinetic evidence for nucleophilic involvement at the glucosidation transition state. *J. Am. Chem. Soc.* **119,** 11147–11154 (1997).

23. Lee, J. K., Bain, A. D. & Berti, P. J. Probing the Transition States of Four Glucoside Hydrolyses with13C Kinetic Isotope Effects Measured at Natural Abundance by NMR Spectroscopy. *J. Am. Chem. Soc.* **126,** 3769–3776 (2004).

24. Horenstein, N. A. Mechanisms for nucleophilic aliphatic substitution at glycosides. *Adv. Phys. Org. Chem.* **41,** 275–314 (2006).

25. Bennet, A. J., Sinnott, M. L. & Wijesundera, W. S. S. ^{18}O and secondary ^{2}H kinetic isotope effects confirm the existence of two pathways for acid-catalysed hydrolyses of α-arabinofuranosides. *J. Chem. Soc., Perkin Trans. 2* **0,** 1233–1236 (1985).

26. Shiner, V. J., Rapp, M. W., Halevi, E. A. & Wolfsberg, M. Solvolytic .alpha.-deuterium effects for different leaving groups. *J. Am. Chem. Soc.* **90,** 7171–7172 (1968).

27. Schleyer, P. v. R., Harris, J. M. & Hall, R. E. Magnitude of secondary .alpha.-deuterium isotope effects for limiting solvolyses. *J. Am. Chem. Soc.* **93,** 2551–2553 (1971).

28. Shiner, V. J. & Dowd, W. Dependence of solvolytic .alpha.-deuterium rate effects on the nature of the leaving group. *J. Am. Chem. Soc.* **93,** 1029–1030 (1971).

29. Horenstein, B. A. & Schramm, V. L. Electronic Nature of the Transition State for Nucleoside Hydrolase. A Blueprint for Inhibitor Design*. *Biochemistry* **32,** 7089–7097 (1993).

4.8. Supporting Information

Table S4.1. Individual measurements of *V/K* KIEs on the hydrolysis of α-D-glucopyranosyl fluorides by glucoamylases at pH 6.05 and 25 °C, the corresponding means and standard deviations for isotopologues **1b** – **1e**.

Enzyme	Compound	Site of substitution	KIE (k_{1a}/k_x)	Mean and SD
Rhizopus sp.	1b	5-^{18}O ring oxygen	0.9894 0.9895 0.9899	0.9896 ± 0.0003
	1c	1-^{13}C anomeric	1.016 1.012 1.012	1.013 ± 0.002
	1d	1-^{2}H alpha deuterium	1.173 1.141 1.134	1.149 ± 0.021
	1e	2-^{2}H beta deuterium	1.056 1.039 1.065	1.053 ± 0.013
A. niger	1b	5-^{18}O ring oxygen	0.989 0.983 0.986	0.986 ± 0.003
	1c	1-^{13}C anomeric	1.010 1.010 1.016	1.012 ± 0.003
	1d	1-^{2}H alpha deuterium	1.117 1.126 1.167	1.136 ± 0.027
	1e	2-^{2}H beta deuterium	1.040 1.042 1.035	1.039 ± 0.004

Table S4.2. Individual measurements of relative *V/K* KIE values on the hydrolysis of α-D-glucopyranosyl fluorides by glucoamylases at pH 6.05 and 25 °C, the calculated KIEs, and the corresponding means and standard deviations for isotopologue **1f**.

Enzyme	Compound	Site of substitution	^{Rel}KIE (k_{1f}/k_{1b})	^{calc}KIE(k_{1a}/k_{1f})	Mean and SD
Rhizopus sp.	1f	5-^{2}H gamma deuterium	0.9643 0.9661 0.9685	1.018 1.004 1.031	1.018 ± 0.014
A. niger	1f	5-^{2}H gamma deuterium	0.9646 0.9706 0.9644	1.003 1.011 0.998	1.004 ± 0.007

Figure S4.1. ^{1}H NMR spectrum for α-D-glucopyranosyl fluoride (600 MHz, D_2O)

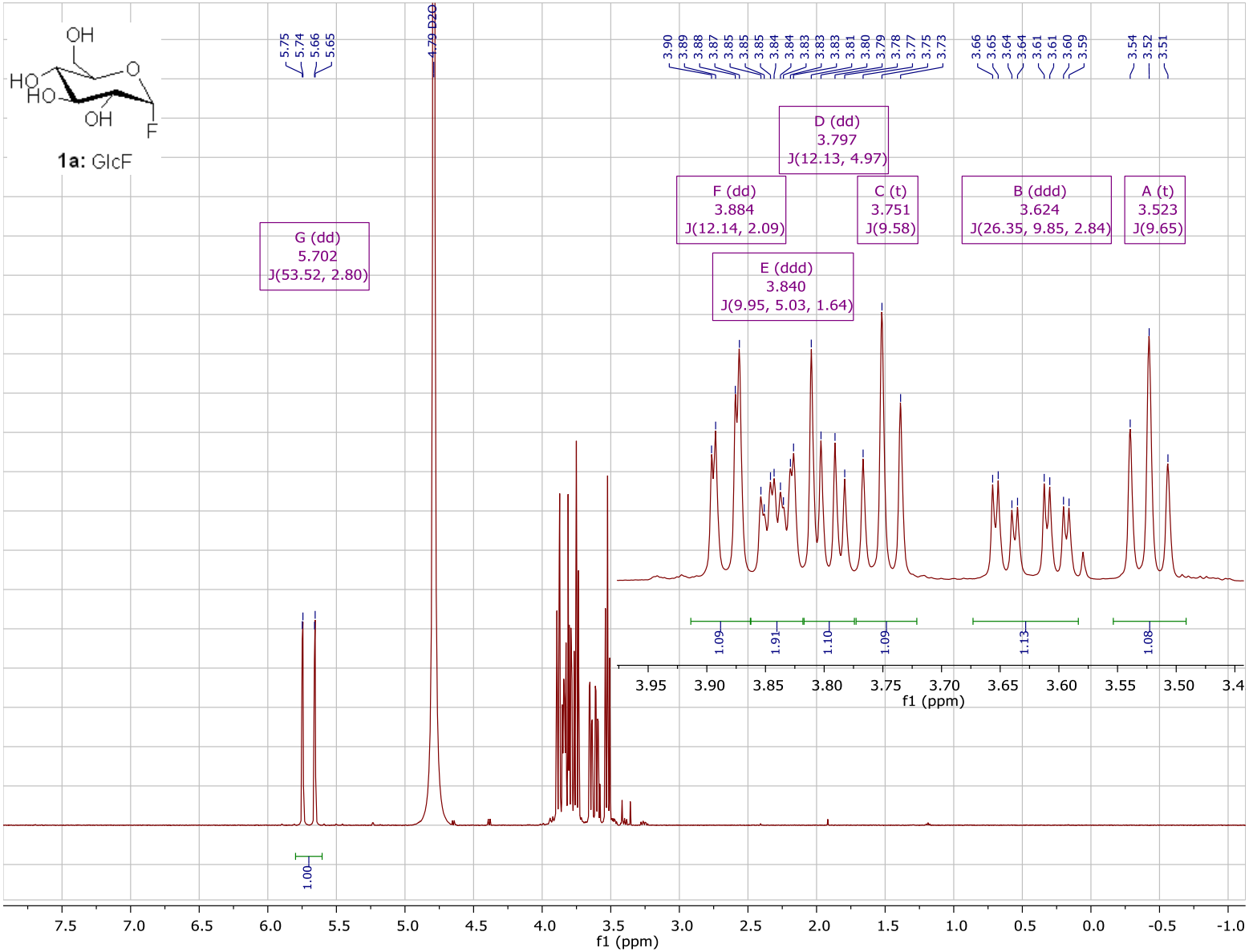

Figure S4.2. ^{13}C NMR spectrum for α-D-glucopyranosyl fluoride (151 MHz, D_2O)

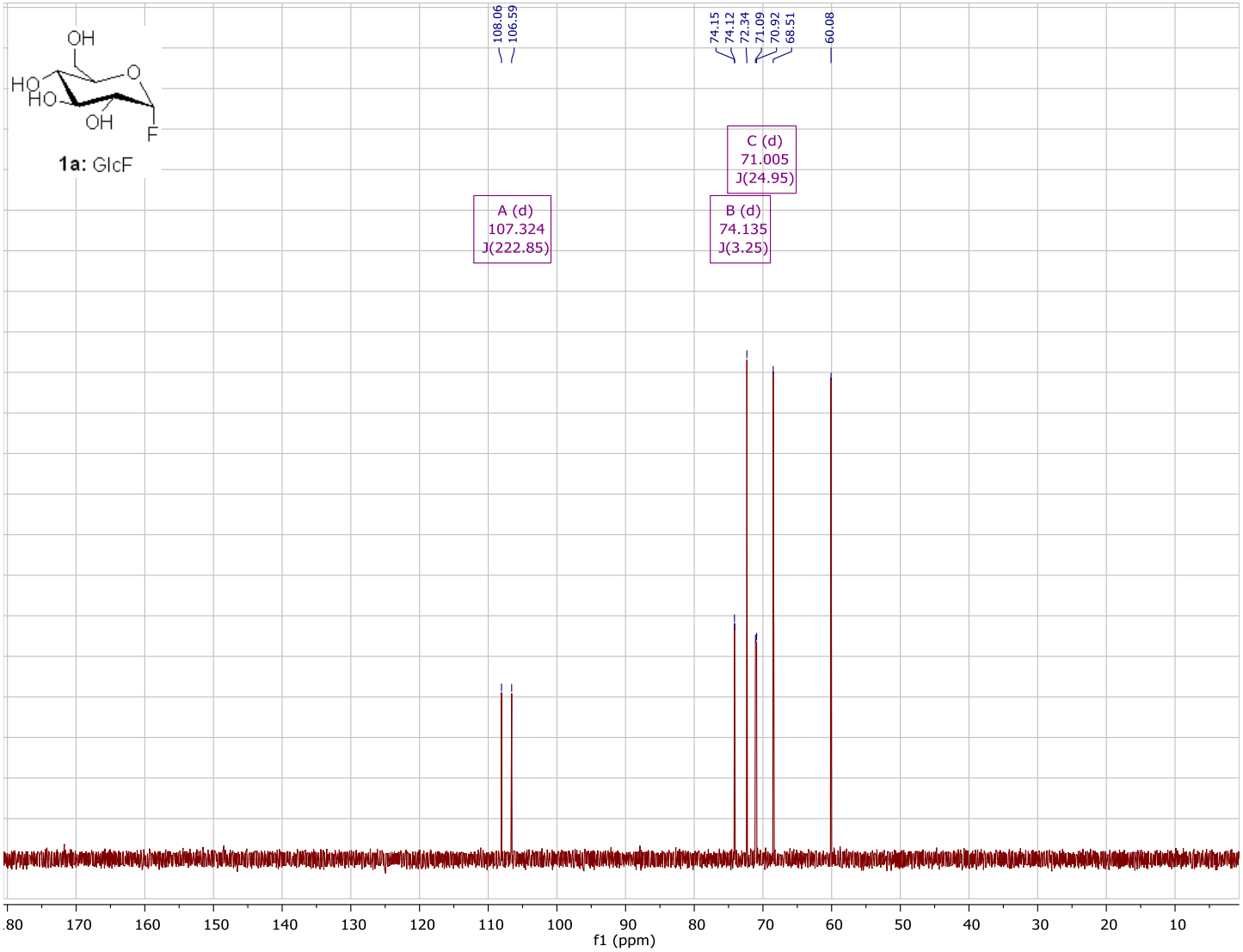

Figure S4.3. ^{1}H NMR spectrum for α-D-(1-^{2}H)glucopyranosyl fluoride (600 MHz, D_2O)

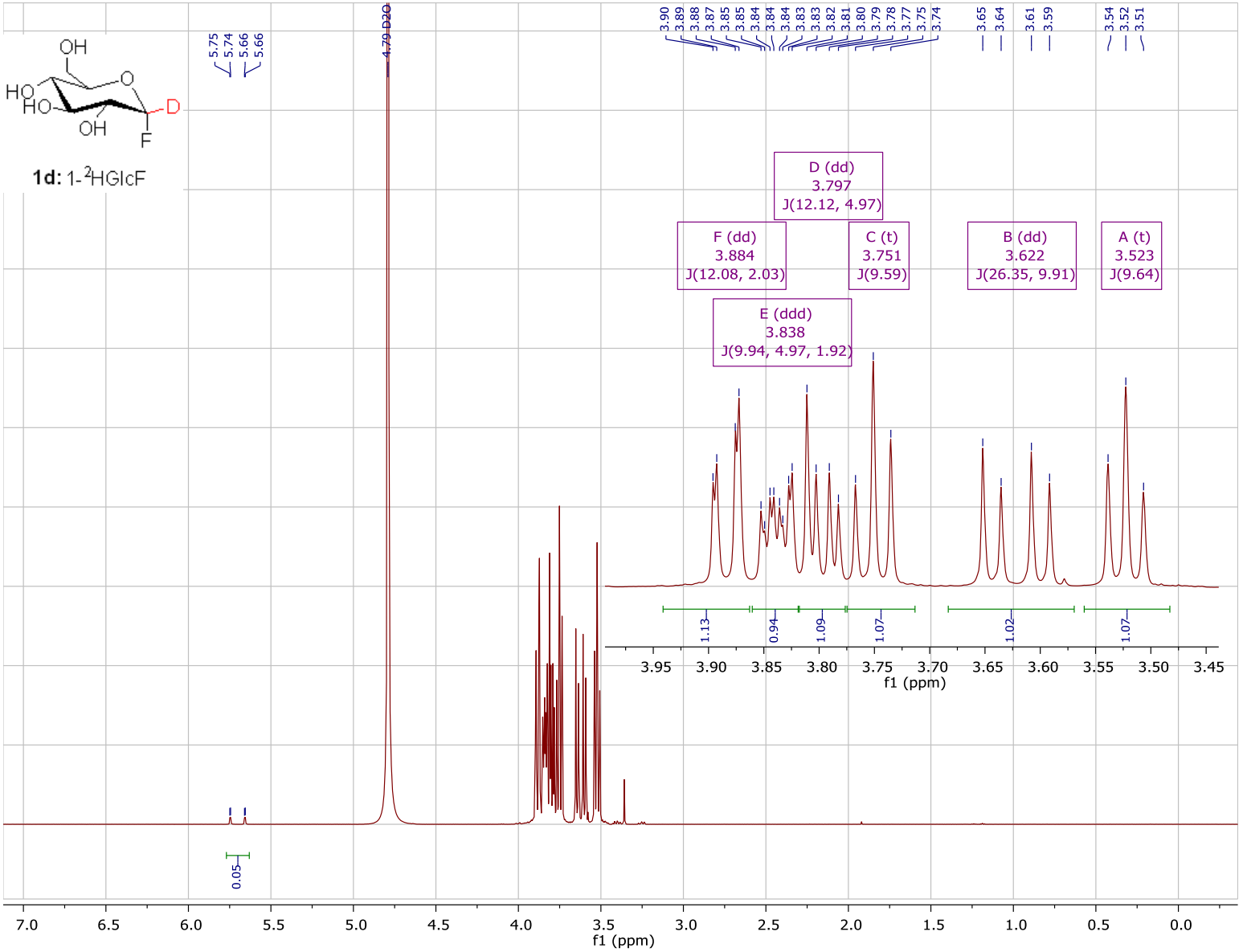

Figure S4.4. ^{13}C NMR spectrum for α-D-(1-^{2}H)glucopyranosyl fluoride (151 MHz, D_2O)

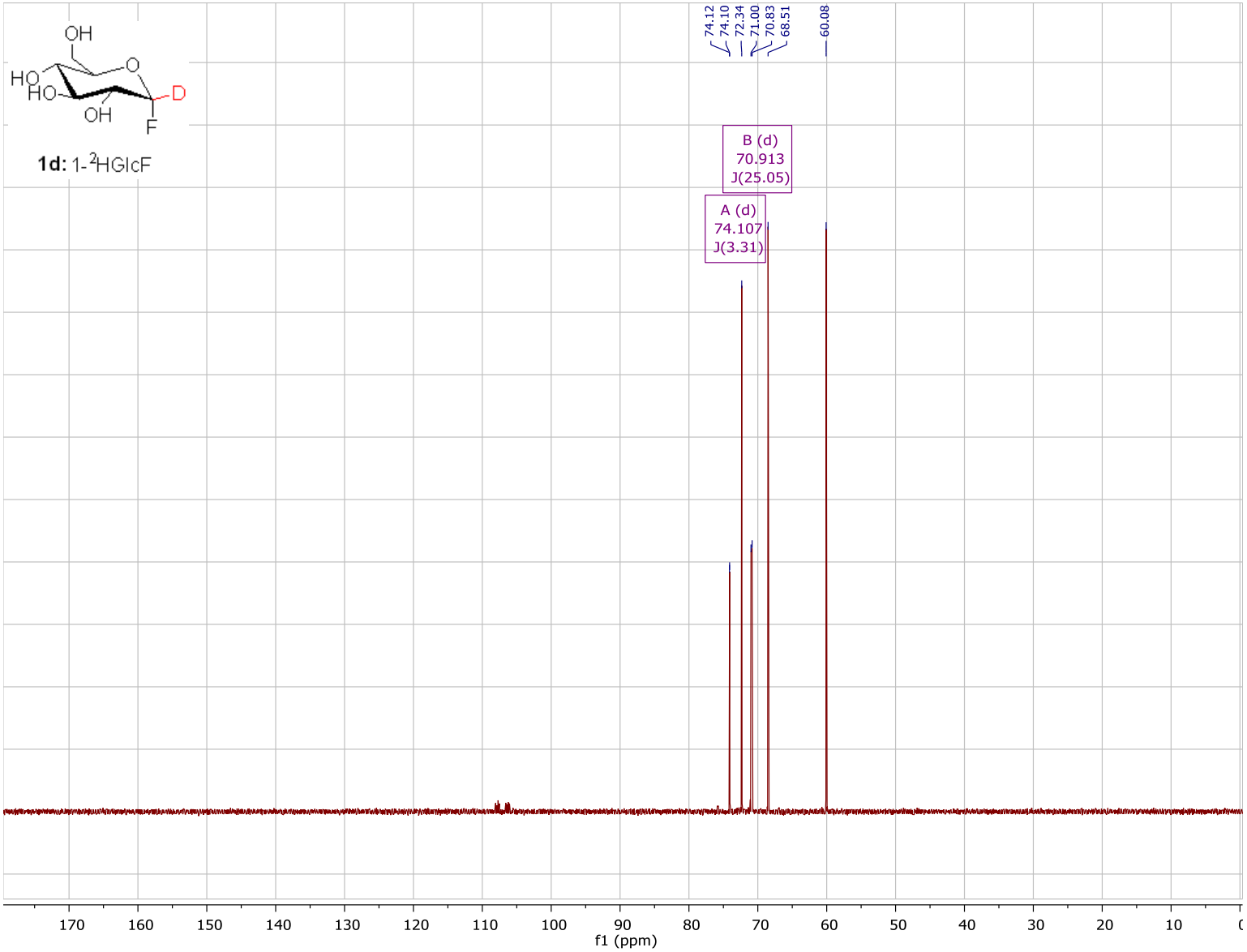

Figure S4.5. ^{1}H NMR spectrum for α-D-(2-^{2}H)glucopyranosyl fluoride (600 MHz, D_2O)

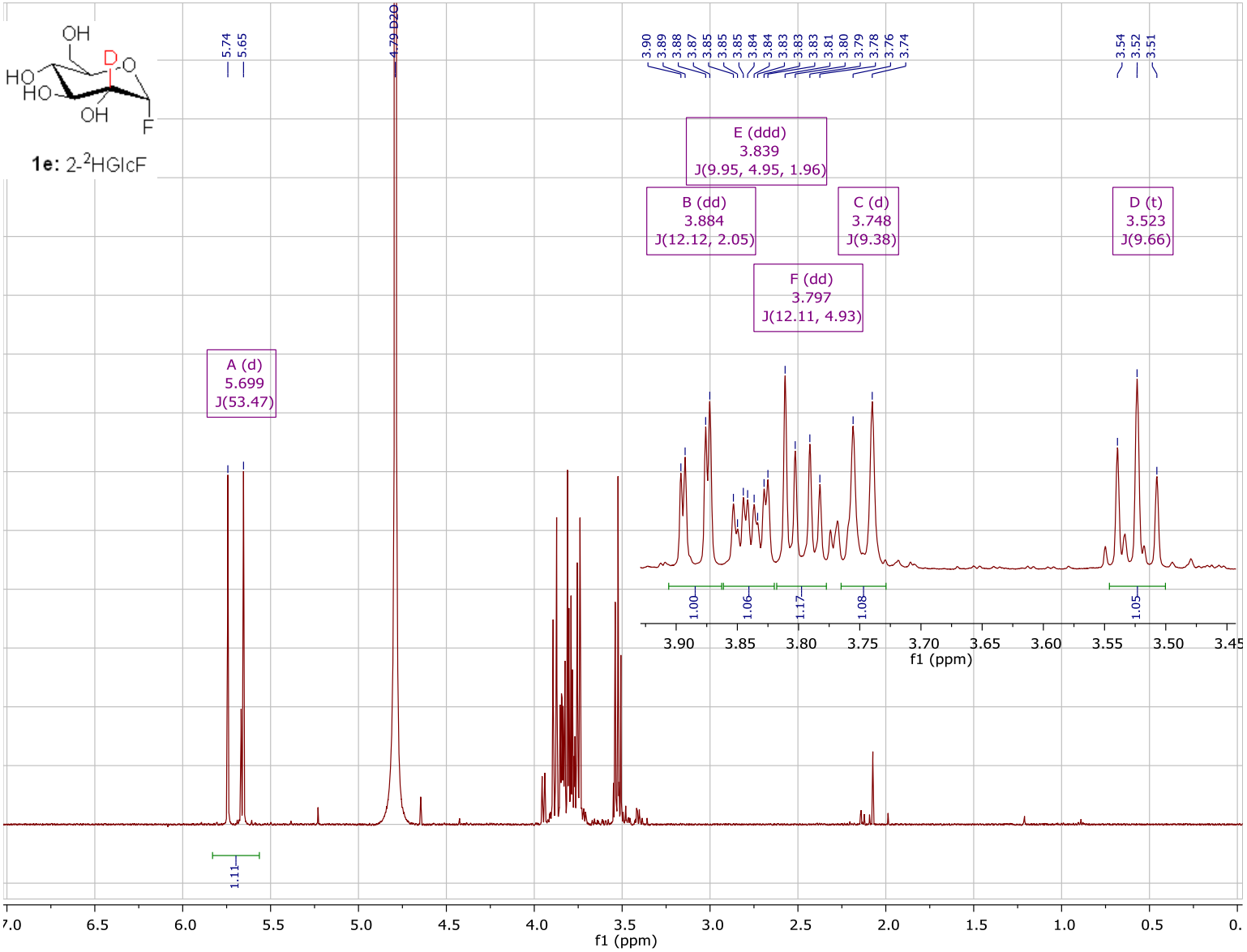

Figure S4.6. ^{13}C NMR spectrum for α-D-(2-^{2}H)glucopyranosyl fluoride (151 MHz, D_2O)

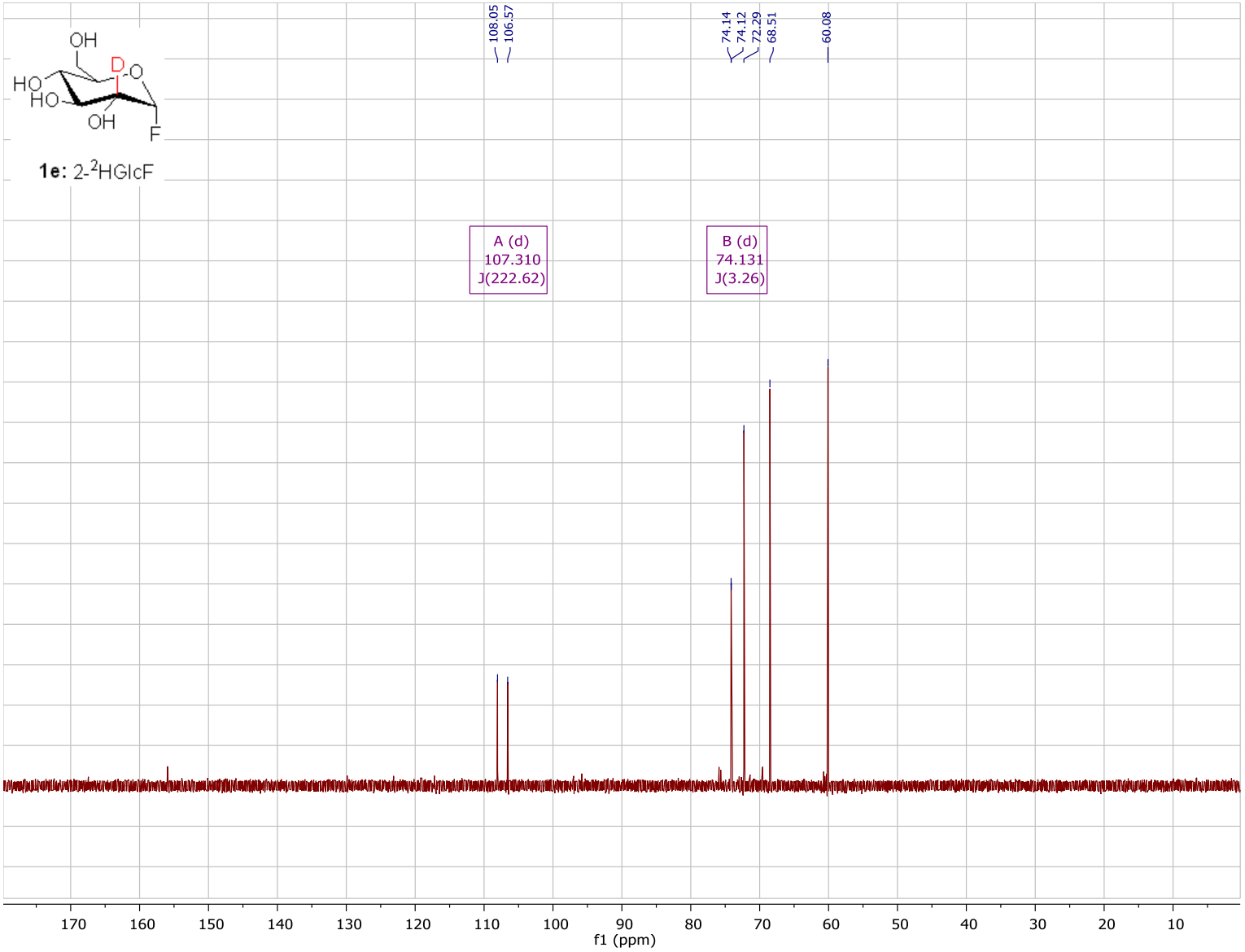

Figure S4.7. ^{1}H NMR spectrum for α-D-(5-^{2}H)glucopyranosyl fluoride (600 MHz, D_2O)

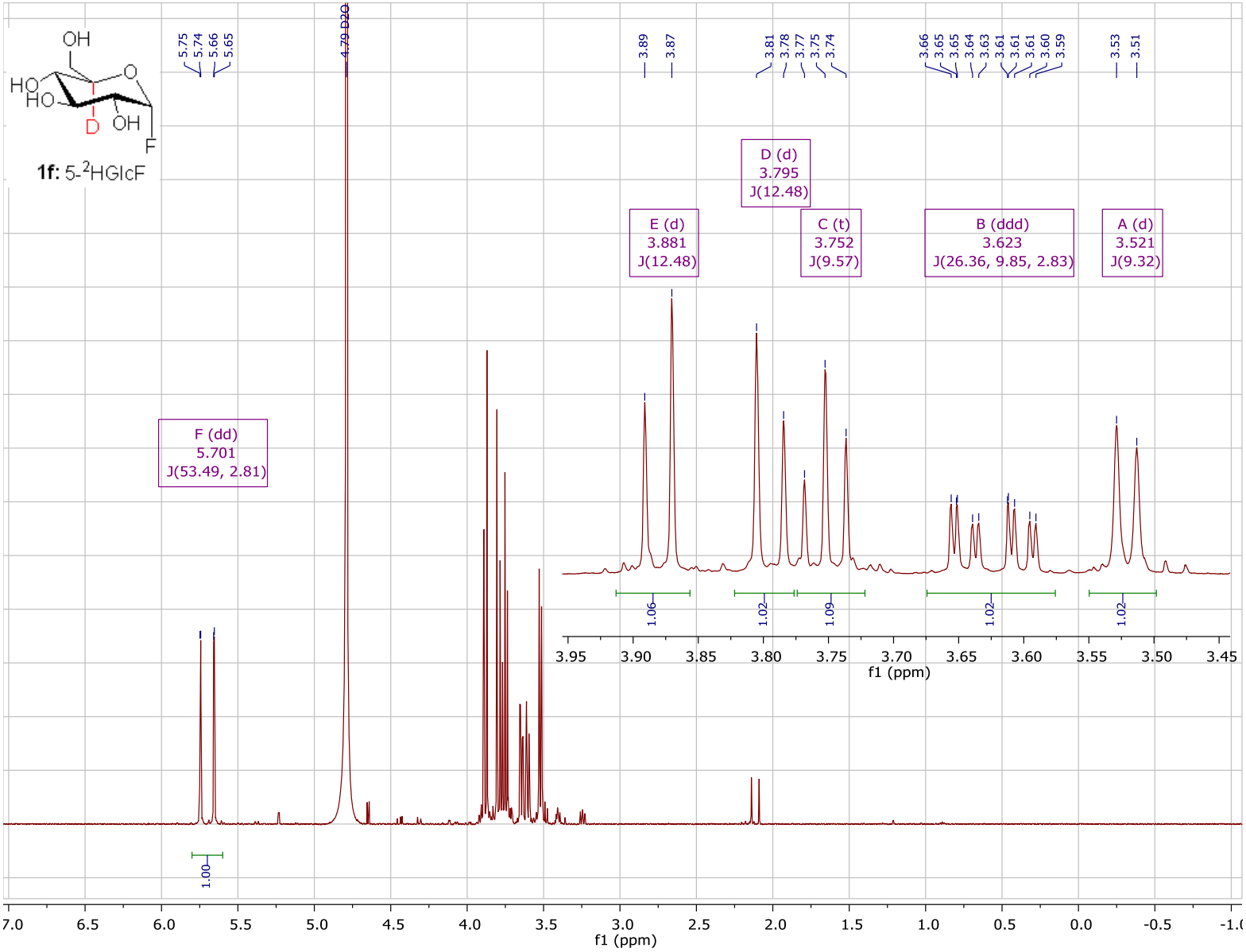

Figure S4.8. ^{13}C NMR spectrum for α-D-(5-^{2}H)glucopyranosyl fluoride (151 MHz, D_2O)

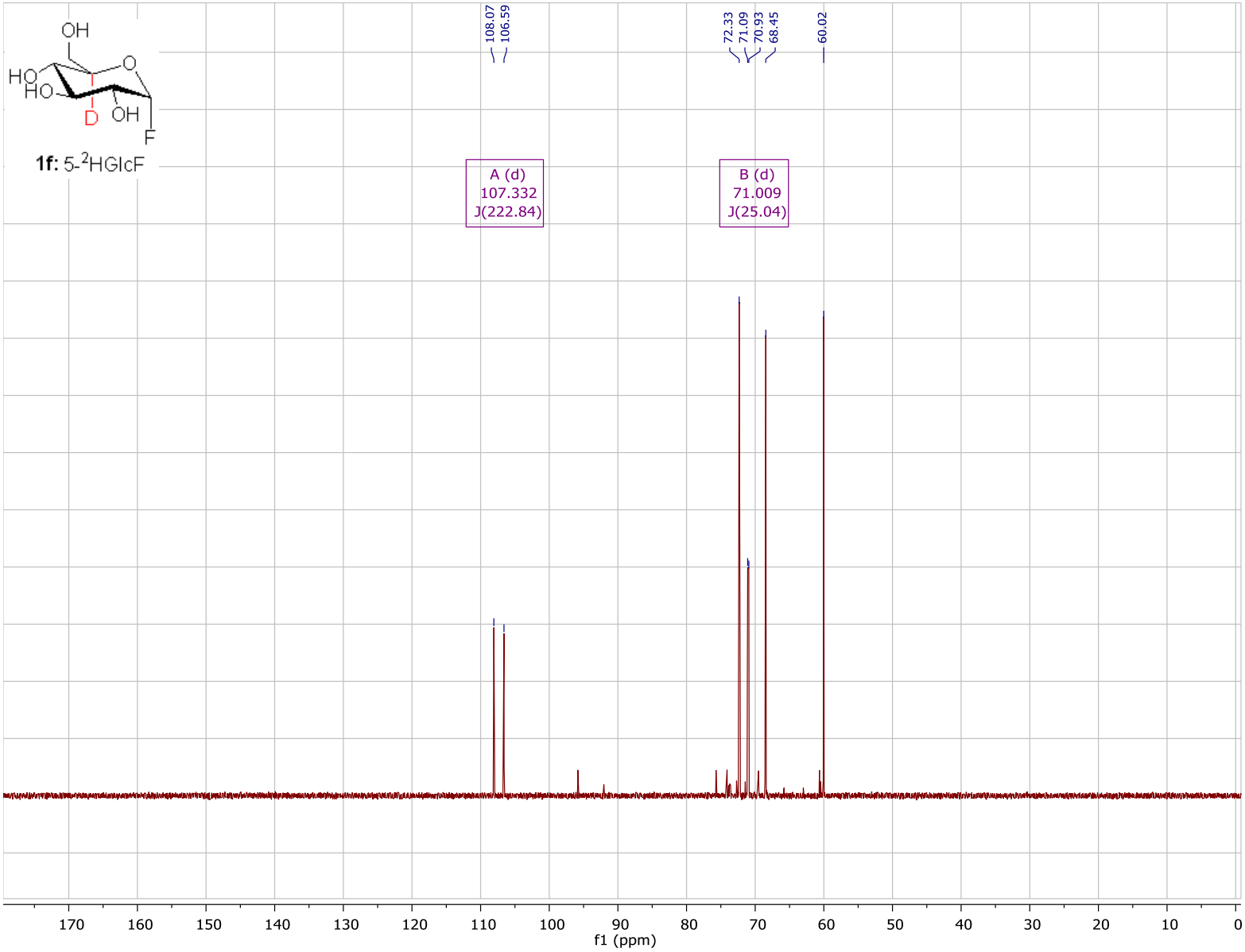

Figure S4.9. ^{1}H NMR spectrum for α-D-(5-^{18}O)glucopyranosyl fluoride (600 MHz, D_2O)

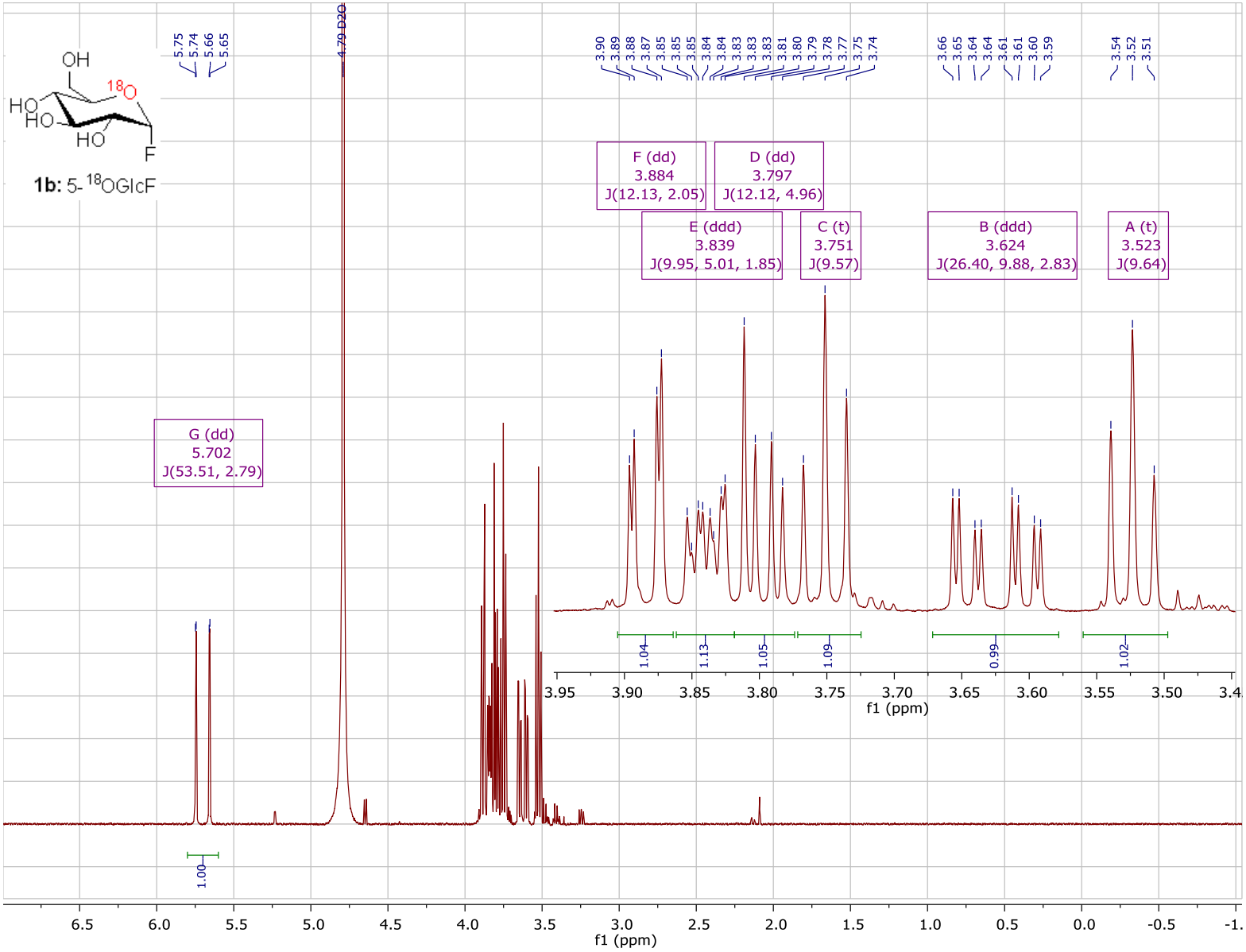

Figure S4.10. ^{13}C NMR spectrum for α-D-(5-^{18}O)glucopyranosyl fluoride (151 MHz, D_2O)

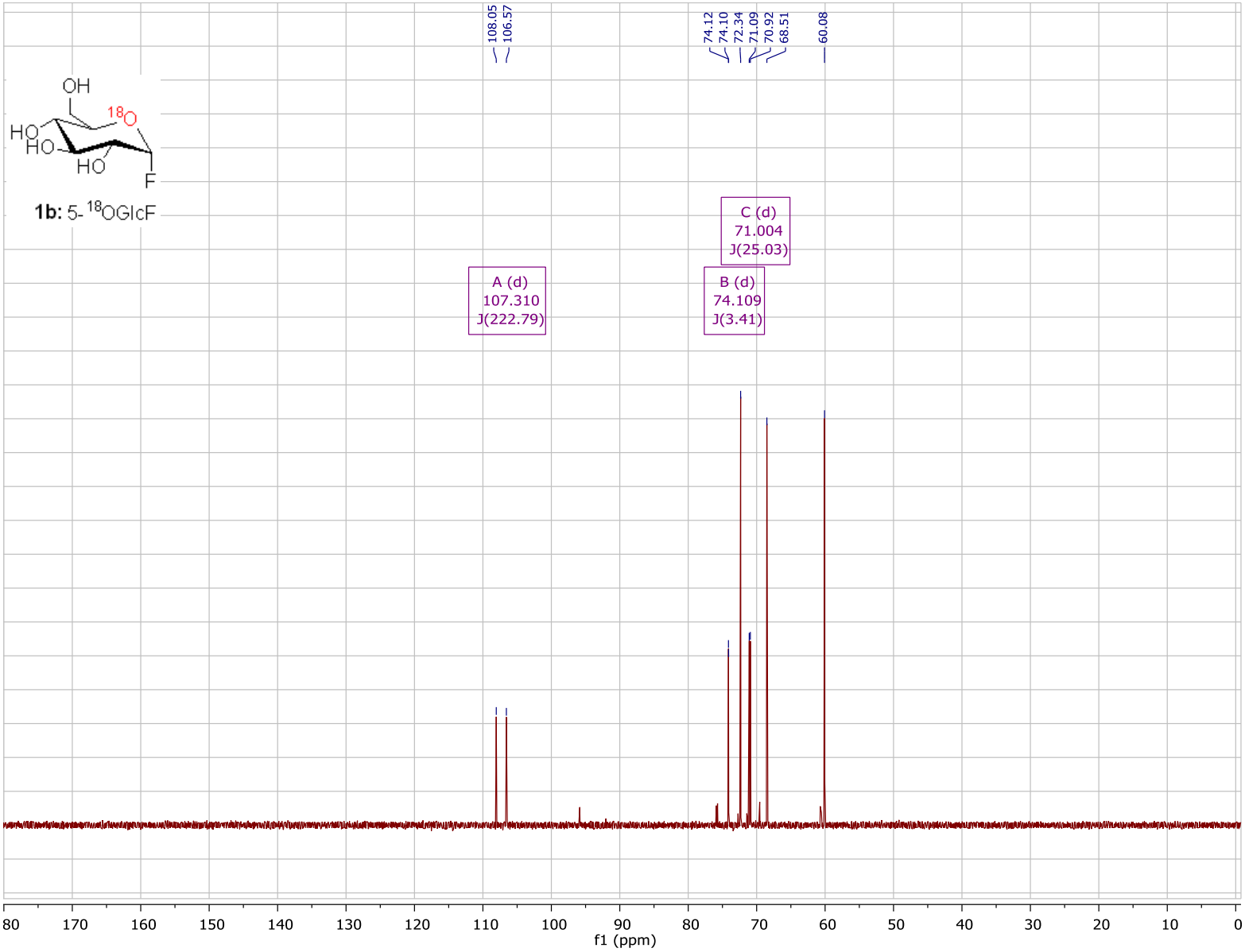

Figure S4.11. ^{1}H NMR spectrum for α-D-(1-^{13}C)glucopyranosyl fluoride (600 MHz, D_2O)

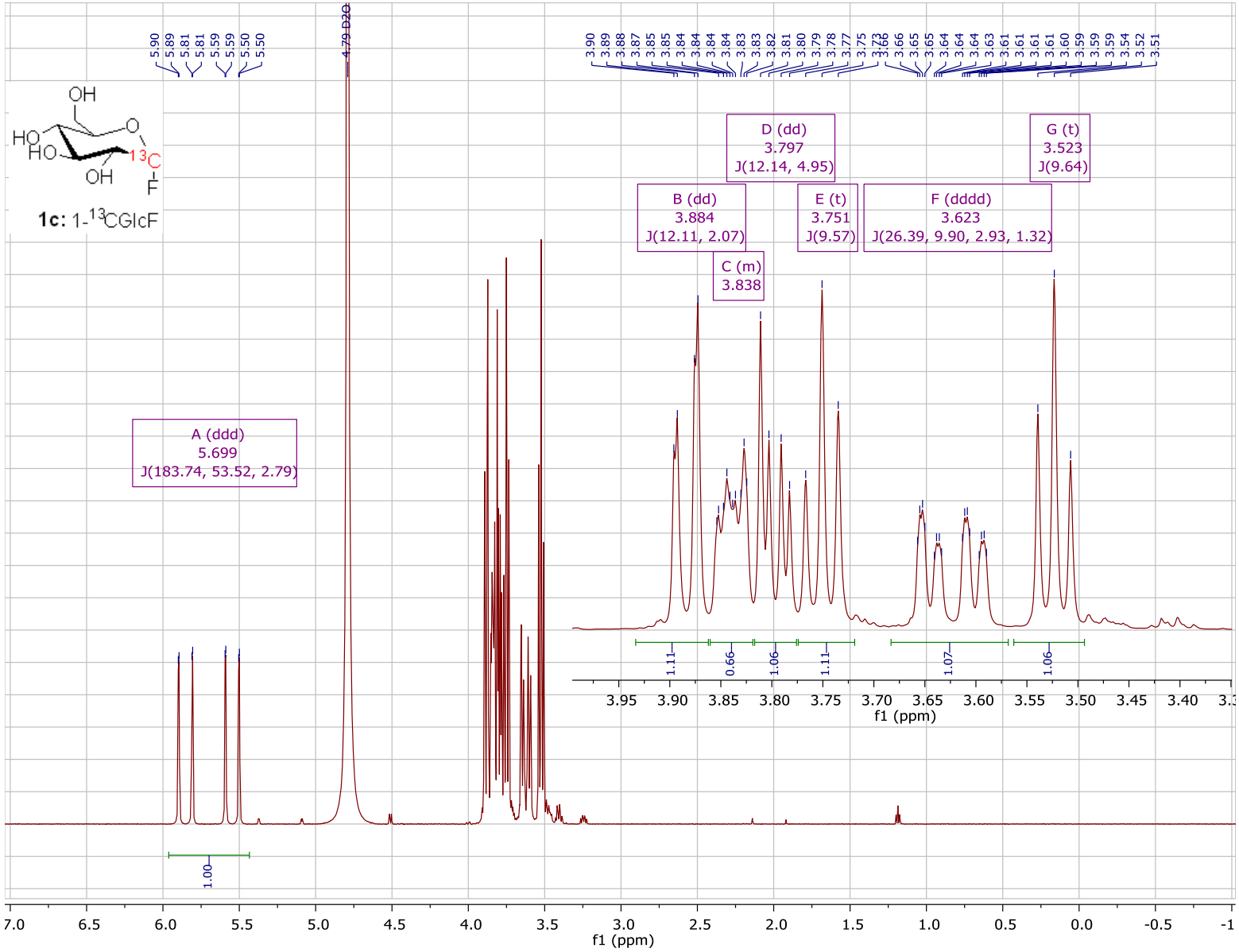

Figure S4.12. ^{13}C NMR spectrum for α-D-(1-^{13}C)glucopyranosyl fluoride (151 MHz, D_2O)

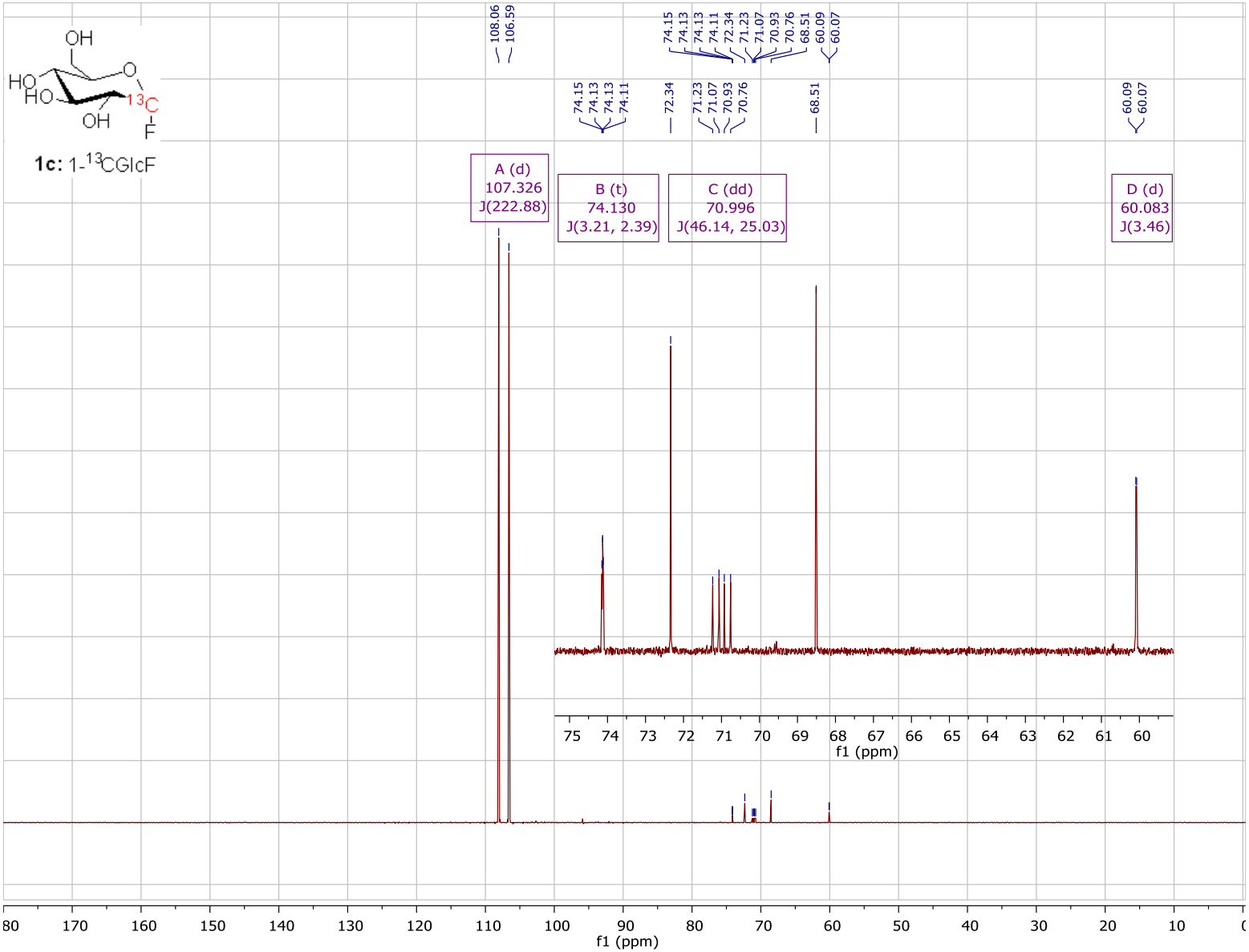

Chapter 5.

A Kinetic Isotope Effect Study on the Hydrolysis of α-D-Glucopyranosyl Fluoride by an Inverting exo-1,3-β-D-Glucanase: Transition State Evaluation for the Hehre Resynthesis-Hydrolysis Mechanism

5.1. Abstract

The inverting exo-1,3-β-glucanase from *Trichoderma virens*, which is a glycoside hydrolase family 55 enzyme (GH55), hydrolyzes α-D-glucopyranosyl fluoride (α-GlcF) via the Hehre resynthesis–hydrolysis mechanism. *T. virens* GH55 shows a non-hyperbolic dependence of reaction rate on α-GlcF concentration. Addition of acceptor sugars, such as methyl α-D-glucopyranoside and phenyl 1-thio-β-D-glucopyranoside, result in increased rates for the production of fluoride ion from α-GlcF. Such kinetic data are indicative of the Hehre resynthesis-hydrolysis mechanism for catalysis of the 'wrong' anomeric glycosyl fluoride. The transition state for the Hehre resynthesis-hydrolysis mechanism for the GH55 catalyzed hydrolysis of α-GlcF has been studied by the use of multiple kinetic isotope effect (KIE) measurements. The experimental KIEs, using phenyl 1-thio-β-D-glucopyranoside as the carbohydrate acceptor, are 1-^{2}H (1.133 ± 0.009), 2-^{2}H (1.053 ± 0.001), 5-^{2}H (1.020 ± 0.004), anomeric 1-^{13}C (1.009 ± 0.002), and ring 5-^{18}O (0.980 ± 0.012). The transition state for the Hehre resynthesis-hydrolysis reaction is late with respect to both C–F bond cleavage and proton transfer.

5.2. Introduction

Glycoside hydrolases (GH) are classified as either retaining or inverting enzymes based upon the stereochemical outcome of the hydrolysis reaction at the anomeric centre.[1,2] The inverting enzymes operate by one of the two classical mechanisms outlined by Koshland, while most retaining enzyme use the second.[1] Inverting GHs operate via single displacement mechanism involving general-acid catalyzed aglycone departure and nucleophilic attack by a water molecule that is general-base catalyzed (Fig. 5.1.A). In case of most retaining glycoside hydrolases reaction occurs via a two-step double displacement

mechanism. In the first step, glycosylation, a nucleophilic active site residue (usually a glutamate or aspartate) attacks the anomeric centre and displaces the aglycone leading to formation of the glycosyl-enzyme intermediate. The second step, deglycosylation, involves hydrolysis of the glycosyl-enzyme intermediate by a water molecule (Fig. 5.1.B).

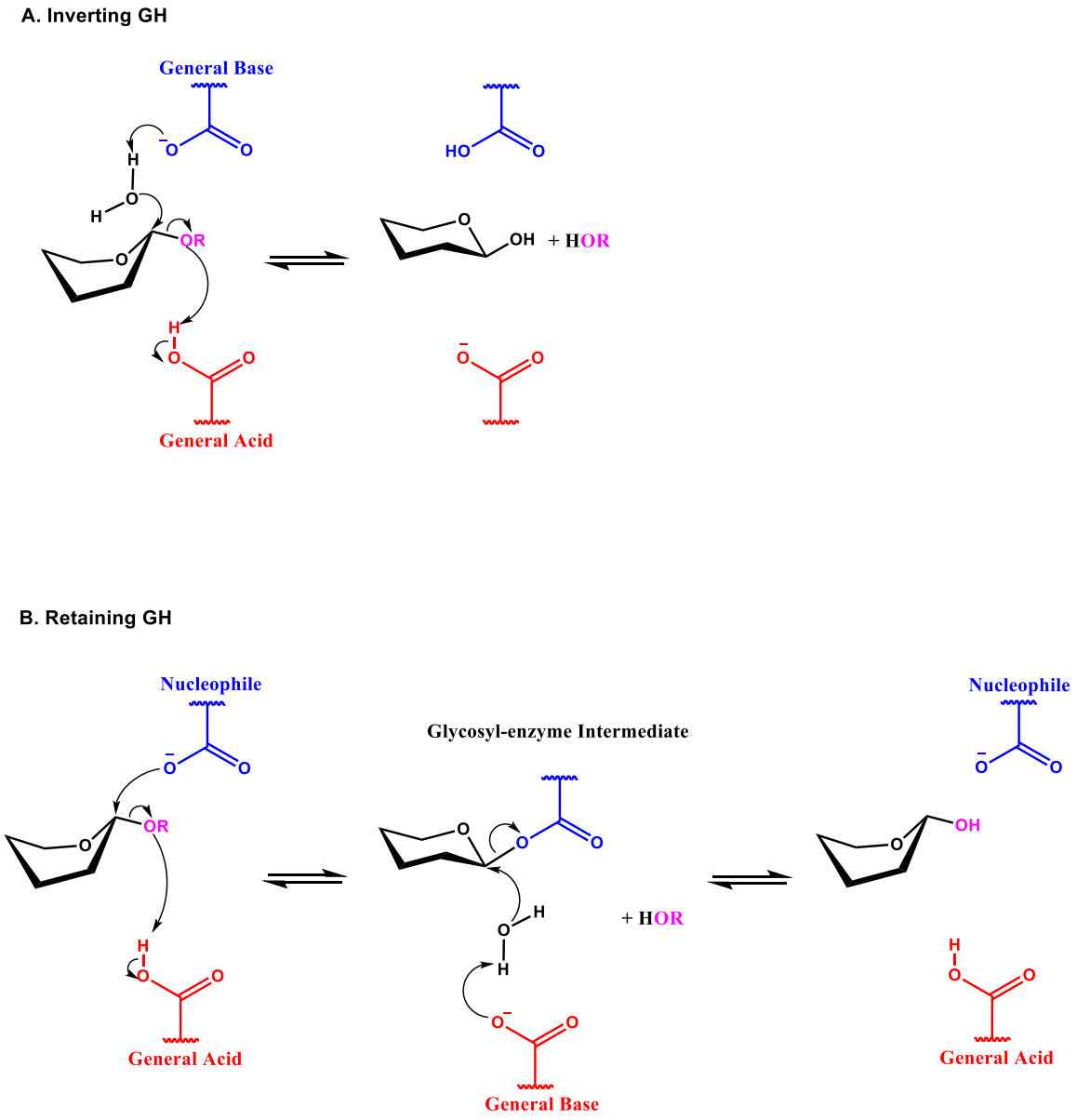

Figure 5.1. Mechanisms of classical glycoside hydrolases.

It has been shown in some cases that inverting glycoside hydrolases can hydrolyze the glycosyl fluoride of the 'wrong' anomeric configuration. This was first demonstrated by Hehre and co-workers in 1979 for β-amylase, an inverting α-glucan hydrolase.[3] This

enzyme was shown to hydrolyze β-maltosyl fluoride to β-maltose and fluoride ion. Since then hydrolysis of the 'wrong' glycosyl fluorides has been demonstrated for a number of inverting glycoside hydrolases and one retaining glycoside hydrolase.[3–7] For the inverting enzymes, the hydrolysis reaction proceeds via the so-called 'Hehre resynthesis–hydrolysis mechanism'. Specifically, hydrolysis occurs via an initial transglycosylation reaction that forms a coupled product with inversion of the anomeric configuration (Fig. 5.2). The resulting transglycosylated product has the correct anomeric stereochemistry for the enzyme and is then hydrolyzed with inversion to give a retained product, relative to configuration of the initial glycosyl fluoride. This mechanism is supported by the observation that the steady state rate of hydrolysis shows a dependence on the square of the substrate concentration and that the rate increases upon addition of alternative acceptor molecules. Also, in some cases the transglycosylation product has been isolated.[8,9]

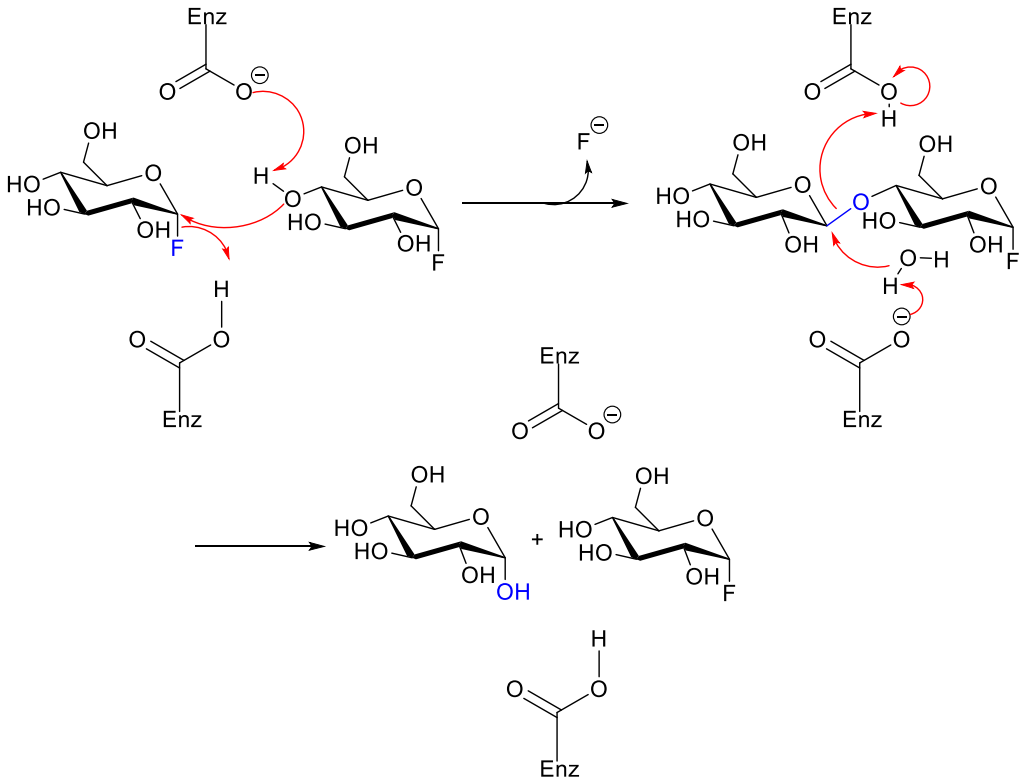

Figure 5.2. Generally accepted mechanism for the Hehre resynthesis-hydrolysis of the glucosyl fluoride of the 'wrong' anomeric configuration.

Synthesis of oligosaccharides is of great interest due to the multitude of biological functions associated with complex sugars, which include inhibition of tumor angiogenesis,[10] cell growth and differentiation control,[11,12] anti-oxidant properties,[13] and

stimulation of plant immune responses towards fungal pathogens.[14,15] In order to study these biological roles of oligosaccharides researchers have developed numerous routes to make these complex natural products. In this regard, chemoenzymatic approaches can be advantageous for the production of complex oligosaccharides as they allow researchers to simplify conventional, labour intensive, chemical synthetic procedures that invariably involve multiple protection, coupling, and deprotection steps. Moreover, chemoenzymatic protocols can deliver substantial quantities of the glycoside of interest in a timely manner. A successful strategy in glycotechnology involves the use of mutant GHs that are called glycosynthases as they catalyze the synthesis of glycosidic bonds. Glycosynthases are mutant glycoside hydrolases in which the nucleophilic amino acid (Glu/Asp) has been replaced by a small non-nucleophilic residue, typically an alanine,[16] a glycine[17] or a serine.[18] These enzymes catalyze transglycosylation of activated glycosyl fluoride donors without the normally associated hydrolysis of the coupled product (Fig. 5.3). This proposed pathway bears remarkable similarities to the Hehre resynthesis-hydrolysis mechanism.

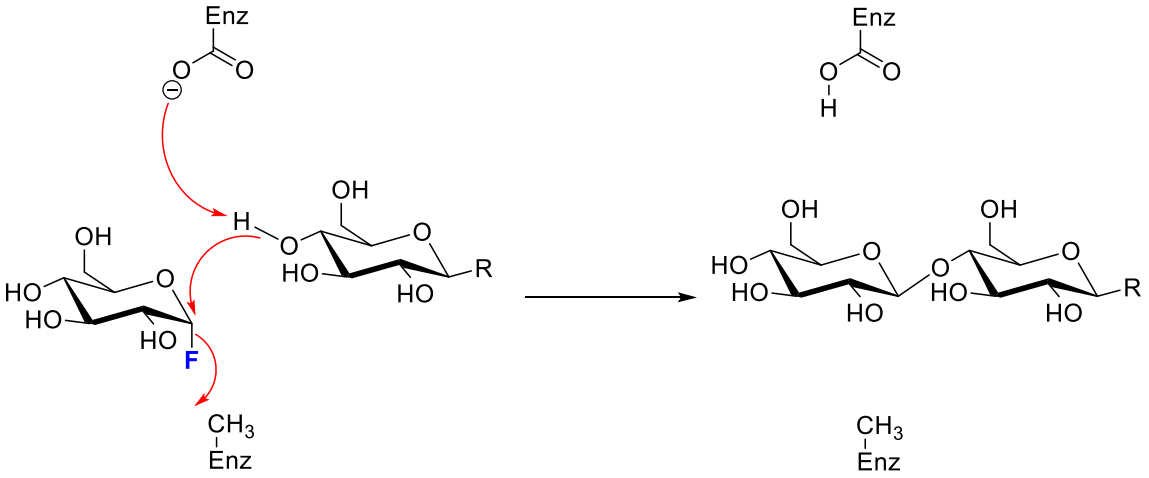

Figure 5.3. Mechanism of glycosylation with a glycosynthase.

The first glycosynthase was reported by Withers and co-workers in 1998.[16] Specifically, they converted a retaining β-glucosidase from *Agrobacterium* sp. into a glycosynthase by replacing the catalytic nucleophile Glu358 with an Ala. Since that time, various retaining GHs have been converted into glycosynthases by substituting the corresponding nucleophilic residues.[19] These enzymes mimic the Hehre resynthesis–hydrolysis mechanism (Fig. 5.2), which leads to accumulation of the oligosaccharide

product, often in high yields, because they lack the crucial catalytic residue necessary for the catalzyed hydrolysis of oligosaccharides. Of note, inverting glycoside hydrolases that perform the Hehre resynthesis–hydrolysis mechanism have been successfully converted into glycosynthases employing a different strategy. Specifically, glycosynthase activity is achieved by mutating a polar residue, which forms a hydrogen bond with the nucleophilic water and the catalytic base, in an inverting GH.[20–23] Glycosynthases are particularly useful for transglycosylation reactions with acceptor sugars, which can function as inhibitors or substrates of the wild-type enzymes.[16] Thus, studying the Hehre resynthesis–hydrolysis mechanism in more detail could lead to the design of new and improved glycosynthases.

Here we report that the GH55 inverting exo-1,3-β-glucanase from *Trichoderma virens* hydrolyzes α-D-glucopyranosyl fluoride (α-GlcF) via the Hehre resynthesis–hydrolysis mechanism and we present the first detailed kinetic isotope effect study for this mechanism.

5.3. Experimental Procedures

5.3.1. Materials

D-(1-^{13}C)Glucose was purchased from Omicron Biochemicals, Inc. D-(1-^{2}H)Glucose, D-(2-^{2}H)glucose, D-(5-^{2}H)glucose, D-(5-^{18}O)glucose and phenyl 1-thio-β-D-glucopyranoside were prepared according to known protocols.[24–26] α-D-Glucopyranosyl fluoride and its singly labelled isotopologues were prepared from the correspondingly labelled 1,2,3,4,6-penta-*O*-acetyl-D-glucopyranose in two steps according to previously reported procedure.[27] Exo-1,3-β-D-glucanase from *Trichoderma virens* was purchased from Megazyme.

Characterization details for α-D-glucopyranosyl fluoride, α-D-(1-^{2}H)-, α-D-(2-^{2}H)-, α-D-(5-^{2}H)-, α-D-(5-^{18}O)- and α-D-(1-^{13}C)glucopyranosyl fluorides can be found in Chapter 4.

Phenyl 1-thio-β-D-glucopyranoside:[26] ^{1}H NMR (600 MHz, DMSO-d_6) δ 7.49 – 7.42 (m, 2H, Ar-H), 7.30 (t, *J* = 7.7 Hz, 2H, Ar-H), 7.25 – 7.19 (m, 1H, Ar-H), 5.27 (d, *J* = 6.2 Hz, 1H, OH-2), 5.08 (d, *J* = 4.9 Hz, 1H, OH-4), 4.97 (d, *J* = 5.3 Hz, 1H, OH-3), 4.60 (d, *J* = 9.8 Hz, 1H, H-1), 4.55 (t, *J* = 5.7 Hz, 1H, OH-6), 3.69 (ddd, *J* = 11.8, 5.4, 2.1 Hz, 1H, H-6), 3.44 (dt, *J* = 12.0, 6.1 Hz, 1H, H-6'), 3.26 – 3.19 (m, 2H, H-4, H-5), 3.09 (td, *J* = 9.7,

8.9, 5.4 Hz, 1H, H-3), 3.05 (ddd, *J* = 9.8, 8.6, 6.1 Hz, 1H, H-2); ^{13}C NMR (151 MHz, DMSO) δ 135.05 (Ar), 129.53 (Ar), 128.81 (Ar), 126.27 (Ar), 87.05 (C-1), 80.97 (C-5), 78.19 (C-5), 72.39 (C-2), 69.77(C-3), 61.00 (C-6).

5.3.2. KIE Measurements

Competitive *V/K* KIEs were measured using ^{19}F NMR spectroscopy on a Bruker AVANCE III QCI cryoprobe 600 MHz spectrometer.[28] Fluorine-19 T_1 values were measured for 3,5-difluorophenyl β-D-galactopyranoside (internal standard),[29] unlabelled α-D-glucopyranosyl fluoride, α-D-(1-^{13}C)glucopyranosyl fluoride and α-D-(1-^{2}H)glucopyranosyl fluoride at a pH of 6.05 (T = 40 °C) using standard inversion recovery pulse sequence and determined to be 0.898 s, 0.936 s, 0.874 s and 1.156 s, respectively. In a typical experiment, a mixture of two or three labelled α-GlcF isotopologues (approx. 1.0 mg of each), acceptor phenyl 1-thio-β-D-glucopyranoside (approx. 10 mg) and internal standard 3,5-difluorophenyl β-D-galactopyranoside (0.5 mg) was dissolved in 450 µL buffer (100 mM sodium succinate, pH 6.05, 1% w/v BSA, 50 mM NaCl, 10% v/v D_2O) and transferred into a standard 5 mm glass NMR tube. Reactions were initiated by the addition of enzyme (100 µL; 2 mg mL^{-1}). The magnetic field was shimmed to obtain symmetrical (as close to a Lorentzian shape as possible) peaks. A ^{1}H NMR and ^{19}F NMR spectra were then acquired before sequentially acquiring more than fifty quantitative proton-decoupled ^{19}F NMR spectra using an inverse-gated pulse sequence.[30,31] FIDs were acquired for 32 scans (acquisition time per scan of 0.6 s) with a relaxation delay of 12 s (6.7 min per spectrum).

The resultant quantitative ^{19}F spectra were deconvolved by performing the following operations: i) Fourier transformation of the FIDs was performed with two-fold zero-filling and application of an exponential line broadening between 4.0–5.0 Hz; ii) spectra were manually phased and baseline corrected using MestReNova version 10.0.2; iii) spectra were fit using standard MestReNova line fitting algorithm for a generalized Lorentzian line shape; iv) to optimize the calculated fit peak positions, peak widths at half-height, peak heights and optimal combination of Lorentzian and Gaussian (L/G) shapes for each individual peak were allowed to vary; and v) the peak areas were normalized relative to that of the internal standard. Then, for each spectrum the fraction of reaction (F_1) for the lighter isotopologue and the associated R values were calculated from the

respective integrals. These data were then fit using GraphPad Prism 5.04 and a non-linear least squares regression to equation (5.1).[32]

$$R = R_0(1 - F_1)^{(1/KIE-1)} \qquad (5.1)$$

5.3.3. Enzyme Kinetics in the Absence of Inert Acceptor

The hydrolysis of unlabelled α-D-glucopyranosyl fluoride in absence of additional acceptor was measured with 1.9 μM enzyme using the same conditions as reported above for the KIE measurements, except that only 15 spectra were acquired. FID data were processed in a similar manner. Integral intensities were converted to the corresponding substrate concentrations and then plot versus time. Fitting this kinetic data by a standard linear regression in GraphPad Prism 5.04 yielded the initial rates of GH55-catalyzed hydrolysis of α-GlcF.

5.3.4. Protein Homology Modeling for *T. virens* exo-1,3-β-D-glucanase

The sequence of exo-1,3-β-D-glucanase precursor from *T. virens* (GenBank: AAL84695.1) was used for fold recognition and homology modeling. The sequence analysis and fold recognition were carried out using Phyre2.[33] The structure of Lam55A exo-1,3-β-D-glucanase from *Phanerochaete chrysosporium* (PDB code: 3EQN)[34] was used as a template (31% sequence identity). The *T. virens* exo-1,3-β-D-glucanase model analysis was carried out using UCSF Chimera version 1.13. Superposition of the model and template structures showed the identity of the active sites and substrate-binding sites.

5.4. Results and Discussion

We first tested whether the GH55 inverting β-glucosidase from *T. virens* was capable of hydrolyzing α-GlcF without any added acceptor sugars. These reactions were performed in an NMR tube using 1 mg (~9.2 mM final concentration) of unlabelled α-GlcF and 3.8 μM enzyme and the initial rate of hydrolysis was monitored by ^{19}F NMR spectroscopy. The spectrum acquired after 45 min showed the resonance for fluoride ion in aqueous media (–120 ppm). Next, we monitored the rate of fluoride ion production as a function of the addition of sugar-based acceptors to optimize the transglycosylation rate in order to determine the best conditions for the measurement of KIEs. We observed

increased rates for the production of fluoride ion from α-GlcF in presence of methyl α-D-glucopyranoside and phenyl 1-thio-β-D-glucopyranoside, the latter being the best acceptor of these two acceptors.

5.4.1. Suggested Kinetic Pathway for the Transformation of α-D-Glucopyranosyl Fluoride by the GH55 exo-1,3-β-D-glucanase from *T. virens*

The Hehre resynthesis-hydrolysis mechanism can be described by the random sequential kinetic model shown on Scheme 5.1, where E denotes enzyme, S – substrate (α-GlcF); subscript numbers refer to the binding sites of the sugar residues; α is the proportionality constant governing the ratio of binding constants. Sugar binding subsites are labelled according to accepted nomenclature for GHs: –n represents the non-reducing end, +n the reducing end, and cleavage occurs between the –1 and +1 subsites.[35]

Scheme 5.1. Kinetic scheme for the transformation of of α-D-glucopyranosyl fluoride by the GH55 exo-1,3-β-D-glucanase from *T. virens*.

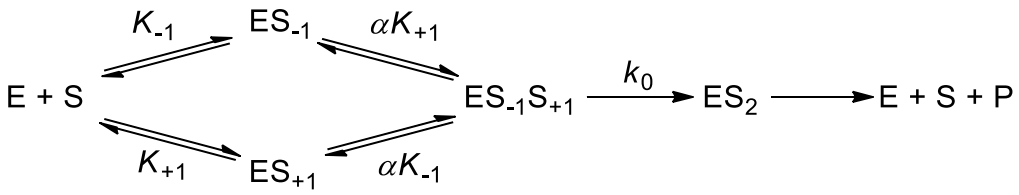

Considering the nature of the transglycosylation step and the reverse-protonated form of the enzyme needed to effect it we can assume that transglycosylation is the slow step and all subsequent steps and binding steps are fast. Activation by addition of the acceptor sugars at high substrate concentration (approx. 9.2 mM in the test hydrolysis experiments, see above) suggests that methyl α-D-glucopyranoside and phenyl 1-thio-β-D-glucopyranoside have higher affinity for +1 binding site than α-GlcF. Mixed complex of enzyme with α-GlcF and acceptor sugar has higher reactivity than the complex of the enzyme with two α-GlcF molecules.

The rate law for the resulting rapid-equilibrium random sequential mechanism then can be described by equation 5.2 (full derivation can be found in Supporting information).

$$V = \frac{k_0[E]_0[S]^2}{\alpha K_{-1}K_{+1} + \alpha(K_{-1} + K_{+1})[S] + [S]^2}\,. \qquad (5.2)$$

Equation 5.2 can be rewritten in the form of equation 5.3 and allows the determination of three independent parameters, *a*, *b*, and *c*.

$$v = \frac{a[S]^2}{b + c[S] + [S]^2} \tag{5.3}$$

We attempted to fit kinetic data to the equation 5.4 allowing all three parameters to vary, which gave a negative value for *c.* This is not possible as *c* represents the sum of binding constants. A fit of the data to the equation 5.4 with the constraint $c \geq 0$ gave a value for c = 0, within experimental error. Becker et al. have shown similar kinetics for the Hehre resynthesis-hydrolysis of α-cellobiosyl fluoride by Cel6A enzymes.[36] We then followed their approach and fit the rate/concentration data to the two-parameter model of equation 5.4 (fit shown in Supporting material Fig. S5.1), which is a special case of the Hill equation[37] with the cooperativity coefficient of 2, and fits the experimental data reasonably well.

$$v = \frac{k_{cat}[E]_0[S]^2}{K_{m2} + [S]^2} \tag{5.4}$$

This indicates infinite cooperativity for *T. virens* GH55 – α-GlcF system. Affinity of the complex of the enzyme with one α-GlcF bound for the second α-GlcF is much greater than the affinity of the free enzyme for the first α-GlcF molecule.

However, the kinetic data for the *T. virens* GH55 is fit better when the cooperativity coefficient in the Hill equation is allowed to vary. Figure 5.4 shows the initial rate of fluoride ion release from α-GlcF by the GH55 exo-1,3-β-D-glucanase from *T. virens* as a function of substrate concentration. The kinetics are sigmoidal, not hyperbolic; the rate versus substrate concentration data was fit to the Hill equation (5.5)[37] for cooperative binding of substrate. GH55 enzymes have multiple sugar-binding subsites: SacteLam55A laminarinase substrate-binding cleft consists of six sugar-binding subsites,[38] CtLam55 laminarinase has more opened substrate-binding cleft with the key interactions at -1, +1 and +2 sites providing the proper positioning of the substrate.[34] The resultant Hill cooefficient of 2.4 ± 0.2 is consistent with the Hehre mechanism that includes some kinetically active species with more than two GlcF bound into the active site, which has five aglycone carbohydrate binding sites for the natural substrate laminarin.[38]

$$v = \frac{V_{max}[S]^h}{K' + [S]^h}\text{, where} \qquad (5.5)$$

K' is apparent dissociation constant and h is Hill coefficient that describes cooperativity.

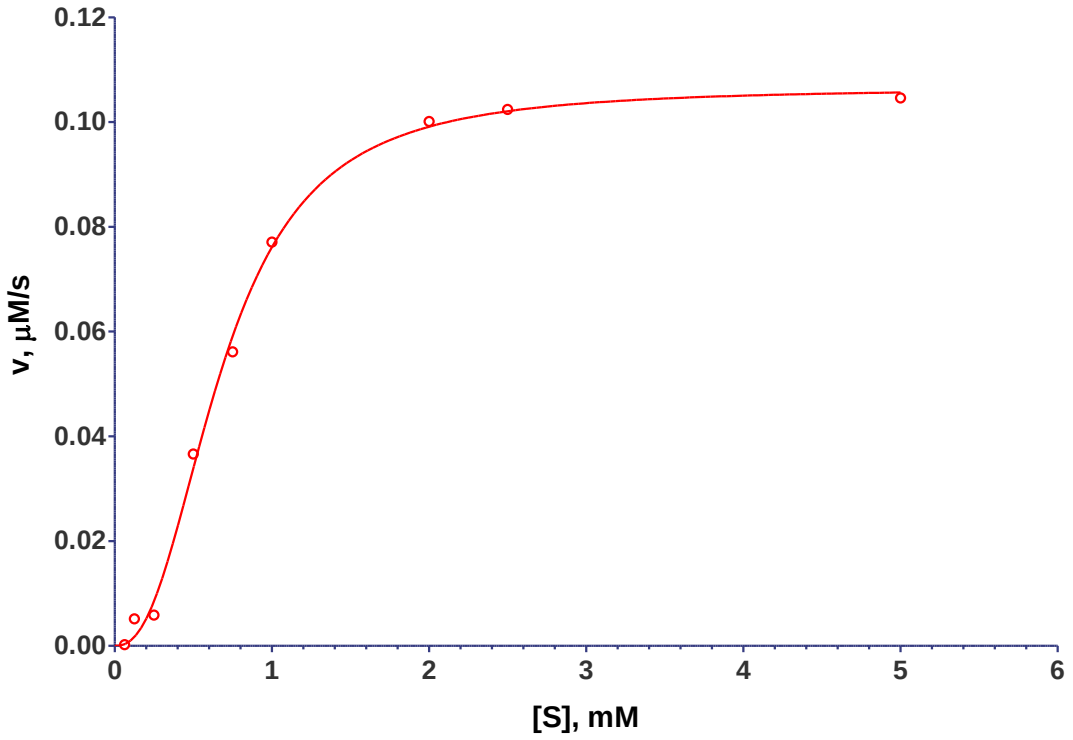

Figure 5.4. Fluoride ion release rate from α-GlcF by *T. virens* GH55 exo-1,3-β-D-glucanase.

Reactions were carried out in 100 mM sodium succinate buffer, pH 6.05 at 40 °C with 1.9 µM enzyme.

Kinetic parameters for the hydrolysis of α-GlcF by the *T. virens* enzyme obtained from fitting the data with both equations 5.2 and 5.5 are given in Table 5.1.

Table 5.1. Hydrolysis of α-D-glycopyranosyl fluoride by *T. virens* GH55 in 100 mM sodium succinate, pH 6.02 at 40 °C.

Equation	k_{cat}, s^{-1}	K_m^{app}, mM^h
Hill (h = 2.4 ± 0.2)	0.056 ± 0.001	0.40 ± 0.05
Two-parameter model	0.058 ± 0.001	0.50 ± 0.05

In order to measure a series of competitive KIEs using the direct NMR spectroscopic method[28] with a ^{19}F probe nucleus we were required to synthesize six GlcF isotopologues (Fig. 5.5, **1a–f**) with substitution at C1, H1, H2, H5 and O5.

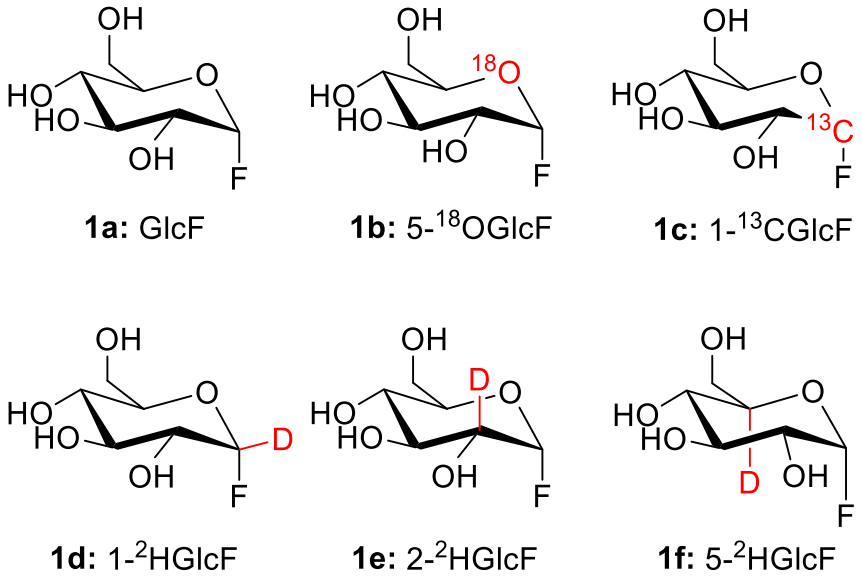

1a: GlcF **1b:** 5-^{18}OGlcF **1c:** 1-^{13}CGlcF

1d: 1-^{2}HGlcF **1e:** 2-^{2}HGlcF **1f:** 5-^{2}HGlcF

Figure 5.5. α-D-Glucopyranosyl fluoride isotopologues.

The ^{19}F leaving group was used as the probe nucleus to report on changes in the isotopologue ratios for the remaining starting material. Individual ^{19}F probe nucleus signals were integrated, and the relative ratio (R) for each isotopologue was calculated. The fraction of reaction (F_1) was determined by comparing the integration for the light isotopologue (**1a**) with the signal of the inert internal standard (3,5-difluorophenyl β-D-galactopyranoside). A representative overlay of NMR spectra for determination of α- and β-secondary deuterium KIEs at F_1 = 0 and at F_1 = 0.57 is shown in Figure 5.6, and typical examples of the nonlinear least-squares fit of the fraction of reaction versus R to equation 1 for the experimental KIE data are illustrated in Figure 5.7. Table 5.2 lists the calculated KIE mean values and the associated standard deviation values based on three replicate experiments.

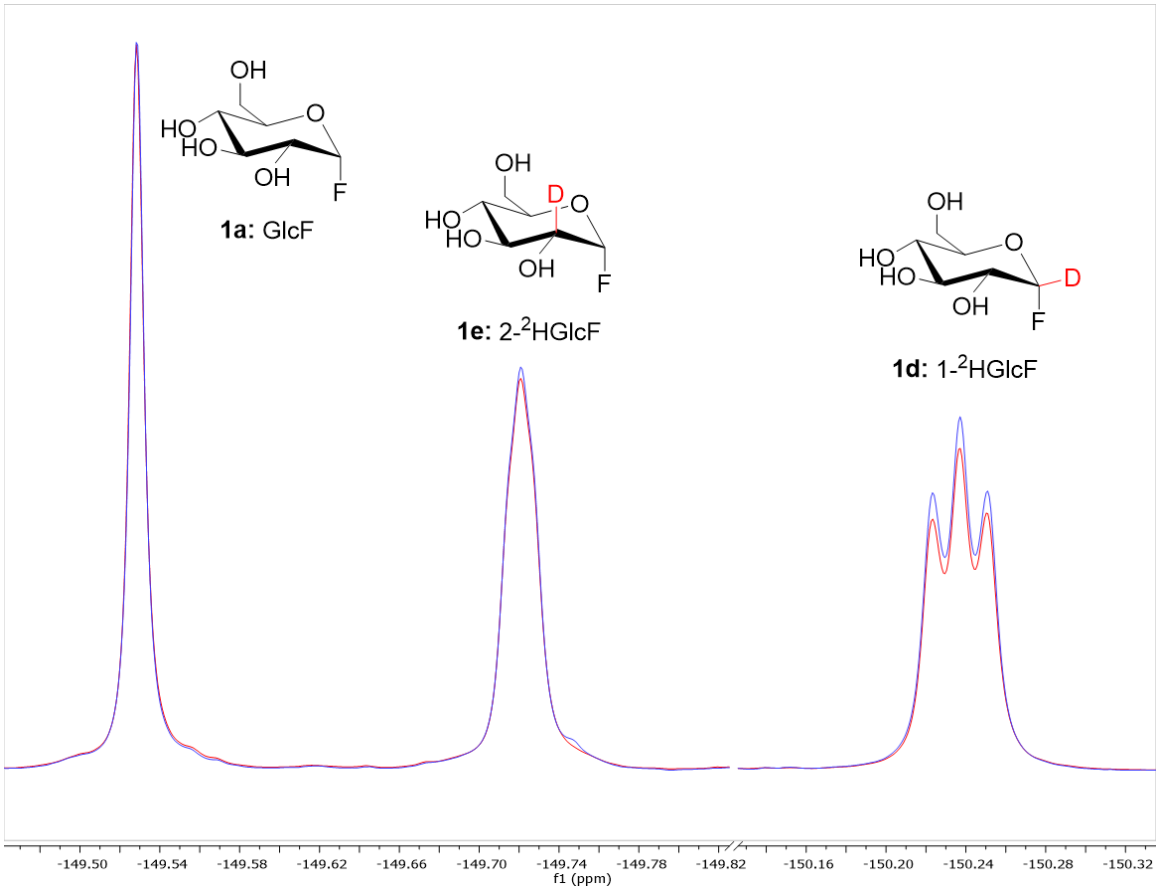

Figure 5.6. Overlaid proton-decoupled ^{19}F NMR spectra containing a mixture of 1a, 1d and 1e in the presence of GH55 enzyme.

Spectra shown for fractions of reaction F_1 = 0.00 (red) and 0.57 (blue) and have normalized peak intensities for the unlabeled isotopologue **1a**. Note the relative increase in peak heights for the **1d** and **1e** isotopologues during reaction.

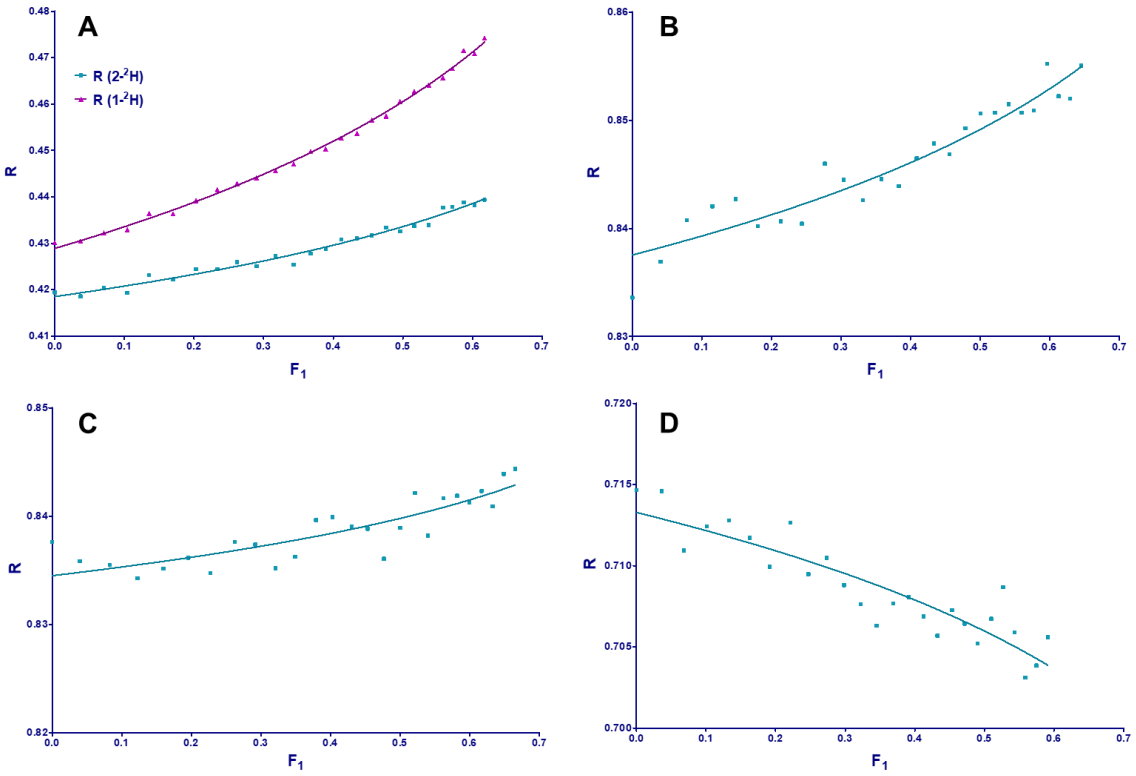

Figure 5.7. Plots of the change in integrated peak intensity ratios (R) versus fraction of reaction for the light isotopologue (F_1) for the measurement of competitive KIE values.

(A) data from an experimental measurement of $k(1\text{-}^{1}H)/k(1\text{-}^{2}H)$ (R 1-^{2}H) and $k(2\text{-}^{1}H)/k(2\text{-}^{2}H)$ (R 2-^{2}H); **(B)** data from an experimental measurement of $k(1\text{-}^{1}H)/k(5\text{-}^{2}H)$; **(C)** data from an experimental measurement of $k(1\text{-}^{12}C)/k(1\text{-}^{13}C)$; **(D)** data from an experimental measurement of $k(5\text{-}^{16}O)/k(5\text{-}^{18}O)$.

Table 5.2. Experimental *V/K* KIEs on the GH55-catalyzed hydrolysis of α-D-glucopyranosyl fluorides at pH 6.05 and 40 °C[a]

Compound	Site of substitution	KIE
1b	5-^{18}O ring oxygen	0.980 ± 0.012
1c	1-^{13}C anomeric	1.009 ± 0.002
1d	1-^{2}H alpha deuterium	1.133 ± 0.009
1e	2-^{2}H beta deuterium	1.053 ± 0.001
1f	5-^{2}H gamma deuterium	1.020 ± 0.004

[a]Values are the mean and standard deviation for three experimental determinations.

KIEs for enzymatic reactions can be measured on the turnover number or maximal rate (*V*) and on the enzymatic efficiency (*V/K*). Competitive KIE experiments on enzyme-

catalyzed reactions only allow determination of isotope effects on *V/K*, irrespective of the substrate concentration.[32] Considering the proposed kinetic scheme 5.1 for the hydrolysis of α-GlcF by *T. virens* GH55 with the initial transglycosylation being rate-limiting, our set of *V/K* KIE values report on the transglycosylation transition state in the Hehre mechanism.

5.4.2. ^{13}C KIE

The experimental anomeric ^{13}C KIE value for the hydrolysis of α-GlcF by GH55 is 1.009 ± 002. This value is consistent with a dissociative S_N1-like reaction in which the transition state is pyranosylium ion-like. Anomeric carbon KIEs (k_{12}/k_{13}) for the nucleophilic substitution reactions of glycopyranosides in solution are typically in the range of 1.005 to 1.030, with the reactions that are known to occur via dissociative S_N1-type transition states exhibiting anomeric ^{13}C-KIE values that are closer to unity;[25,39–41] for instance, the reported ^{13}C-KIEs for the uncatalyzed hydrolysis of α-D-glucopyranosyl 4-bromoisoquinolinium bromide and the acid-catalyzed reactions of methyl α-D-xylopyranosides and methyl α-D-glucopyranoside are 1.005 ± 0.002,[42] 1.006 ± 0.001,[40] and 1.007 ± 0.001,[25] respectively. For the enzyme-catalyzed hydrolysis of glycosides typical anomeric carbon ^{13}C-KIEs are in the range of 1.018–1.032 for concerted S_N2[42–45] mechanisms and 1.002−1.018 for stepwise S_N1 reactions.[43] It is therefore likely that these reactions have similar TS structures and that the GH55 promoted hydrolysis of α-GlcF has a late TS with significant C−F bond cleavage.

5.4.3. ^{18}O KIE

For non-enzymatic reactions in water where cleavage of one of the two C−O acetal bonds is rate-limiting, the leaving group ^{18}O-KIE is normal ($k_{16}/k_{18} > 1$) while the ^{18}O-KIE associated with formation of the pyranosylium ion intermediate is inverse ($k_{16}/k_{18} < 1$).[25,40,46] Using α-GlcF as a substrate does not allow measurement of a leaving group KIE by NMR spectroscopy, while ring ^{18}O-KIE for the hydrolysis of α-GlcF by GH55 is inverse being 0.980 ± 0.012. Ring ^{18}O KIEs reported for hexafluoropropan-2-ol (HFIP) solvolysis of α-GlcF the and acid-catalyzed hydrolysis of methyl α-D-glucopyranoside are less inverse being 0.997 ± 0.006[39] and 0.996 ± 0.001[25], respectively. Such effects are indicative of a poor $n_p \rightarrow \pi$ orbital overlap at the S_N1-like TS, which likely results from imperfect synchronization of the leaving group departure and the necessary ring conformational changes that are conducive to positive charge delocalization. However, ring ^{18}O KIEs for

the neutral and GH15-catalyzed hydrolysis of α-GlcF, have similar magnitudes of 0.984[47] and 0.986 (see Chapter 4 of this thesis), respectively. Comparable strongly inverse ring ^{18}O KIEs are reported for the acid-catalyzed hydrolysis of the conformationally more flexible methyl α-D-xylopyranosides (0.983)[40] and for *Vibrio cholerae* sialidase-catalyzed hydrolysis of natural substrate analogues (0.975).[28] Both values are consistent with an increased bond order between the anomeric carbon and ring oxygen at the respective TSs, which results in more extensive positive charge delocalization at the glycosylation TS. That is, the bond order between O5 and C1 is likely close to two at the transition state for the GH55-catalyzed transglycosylation reaction involving α-GlcF as the donor.

5.4.4. Secondary Deuterium KIEs

α-Secondary Deuterium KIE (α-SDKIE)

The measured α-SDKIE for the hydrolysis of α-GlcF by GH55 is 1.133 ± 0.009. The measured α-SDKIE for the solvolysis of α-GlcF in HFIP is 1.185 ± 0.006,[39] the corresponding α-SDKIE for its spontaneous hydrolysis is 1.142 ± 0.007,[47] and for its reaction with the azide α-SDKIE is 1.192 ± 0.006.[48] Solvolysis of α-GlcF in HFIP is an S_Ni ($D_N^{\ddagger}$*A_{Nss}) reaction with a late transition state,[39] spontaneous hydrolysis and reaction with the azide occur via an exploded S_N2 (A_ND_N) TS.[47,49] The maximal α-SDKIE values depend on the identity of the leaving group[50–52] and are primarily associated with weakening of an out-of-plane bending vibration as the steric crowding at the reaction becomes weaker on approach to an oxacarbenium ion-like transition state. The measured α-SDKIE for the hydrolysis of α-GlcF by GH55 appears to be lower than one for the solvolysis of α-GlcF in HFIP although the mechanisms are likely similar for these two reactions. Considering that we measured a notable inverse ring ^{18}O KIE, we suggest that the O5−C1 bond has significant double bond character and this leads to tighter stretching vibration of C1−H1 bond. Such bond strengthening can account for a lower observed α-SDKIE. In fact, a similar pattern is evident in reported values for the neutral hydrolysis of α-GlcF.

β-Secondary Deuterium KIE (β-SDKIE)

The β-SDKIE for the hydrolysis of α-GlcF by GH55 is 1.053 ± 0.001. β-SDKIEs values mainly originate from the hyperconjugative weakening of the C2−H/(D) bond as charge develops at the anomeric centre. The reported β-SDKIEs for the HFIP solvolysis, the water-promoted hydrolysis, and the S_N2 azide reaction of α-GlcF are 1.080 ± 0.010,[39]

1.067 ± 0.008,[47] and 1.046 ± 0.007,[48] respectively. The magnitude of β-SDKIEs can provide insights into TS conformations:[25,47] a maximal β-SDKIE is predicted when the C–H/(D) bond and the developing p-orbital are aligned in the TS, while a β-SDKIE value of close to unity suggests an orthogonal alignment of these two orbitals.

γ-Secondary Deuterium KIE (γ-SDKIE)

The measured γ-SDKIE is 1.020 ± 0.004 for GH55 enzyme. Traditionally, this type of KIE was analyzed as originating from an inductive effect, however, Perrin has argued that negative hyperconjugation is the cause of these remote effects.[53,54] Remote SDKIEs are commonly observed in enzymatic reactions and likely result from enzymes using binding interactions remote from the reaction site to properly position substrate and promote catalysis. Normal γ-SDKIE in this case is likely to represent changes of the O5–C5–C6 bond angle and the C5–H5 bond length as the substrate approaches the transition state conformation.[55,56] This suggests remote SDKIEs have hyperconjugative nature rather than inductive as the latter would not account for this KIE to be conformationally sensitive.

5.4.5. Homology Model Analysis

An analysis of the amino acid sequence of *T. virens* exo-1,3-β-D-glucanase suggests that the protein 3D structure is similar to that of other GH55 family members, PcLam55A (31% sequence identity),[34] CtLam55 (29% sequence identity),[57] and SacteLam55A (20% sequence identity)[38] with high confidence.[33] We choose to model the structure of *T. virens* exo-1,3-β-D-glucanase based on the enzyme with highest sequence identity, PcLam55A (PDB code: 3EQN), in order to probe the active site of the GH55 from *T. virens*. A general view of the overlapped structures of CtLam55 (teal), SacteLam55A (yellow) and T. virens GH55 homology model (orange) is shown in Fig. 5.8.A. The amino acid residues forming the –1 subsite are highly conserved in these fungal GH55s; the key residues from PcLam55A that form the active site and contact the bound product analogue gluconolactone (PDB: 3EQO) are all conserved and overlap with residues interacting with glucose in the SacteLam55A (PDB: 4PEX) and CtLam55 (PDB: 5M60) structures. The same residues have been located in the modelled structure of *T. virens* GH55, which suggests that the substrate binds in a similar mode.

Figure 5.8.B shows an overlay of the modelled *T. virens* GH55 active site (beige colour) and the corresponding region in the SacteLam55A structure that has a bound laminarihexaose and nucleophilic water molecule. Similar overlays for the PcLam55A and CtLam55 structures (not shown) suggest that in *T. virens* GH55 Glu-627 (corresponds to SacteLam55A Glu-502, yellow) is likely to be the catalytic acid, and that Tyr-630 (corresponds to SacteLam55A Tyr-505, cyan) orients Glu-627 and the anomeric oxygen for better catalysis. Glu-604 (corresponds to SacteLam55A Glu-480, grey) is also strictly conserved throughout GH55 family[38] and is possibly the general base. Of note, the identification of the general base catalytic residue in GH55 enzymes has been problematic,[34,38,57] however, SacteLam55A mutants lacking Glu-480 residue (E480A and E480Q) are completely inactive, which indicates that this residue is catalytically important. However, the carboxylate group is too distant to interact with the nucleophilic water directly, but it likely assists in the precise positioning of substrate (laminarihexaose in Fig. 5.8.B, pink) by formation of hydrogen bonds with O2 and O3, so that it participates in a proton relay network that includes Gln-174, Ser-198 and Thr-149 shown in orange in Fig. 5.8.B (residues that correspond to Gln-187, Ser-216 and Glu-155 of *T. virens* GH55).

Another distinct feature of GH55 enzymes is called the “aromatic block” that caps one end of the binding cleft. In SacteLam55A this “aromatic block” is formed by Phe-153, Trp-444 and Trp-446 (Fig. 5.8.C, yellow); similar residues are observed in the corresponding positions in the aligned structures of PcLam55A (not shown), CtLam55 (teal) and the homology model of *T. virens* GH55 (orange). These residues force these GH55 family member enzymes to be exo-acting: endo-glucanases like GH16,[58] GH17[59] and GH64[60] have binding clefts that are open on both ends, thus, allowing cleavage of glycosidic bonds in the middle of the oligosaccharide chain. Modelling also suggests that *T. virens* GH55 has extended curved substrate-binding cleft similar to SacteLam55A and PcLam55A. This cleft with several sugar-binding subsites can accommodate second α-GlcF molecule or another carbohydrate acceptor thus promoting Hehre resynthesis-hydrolysis of α-GlcF.

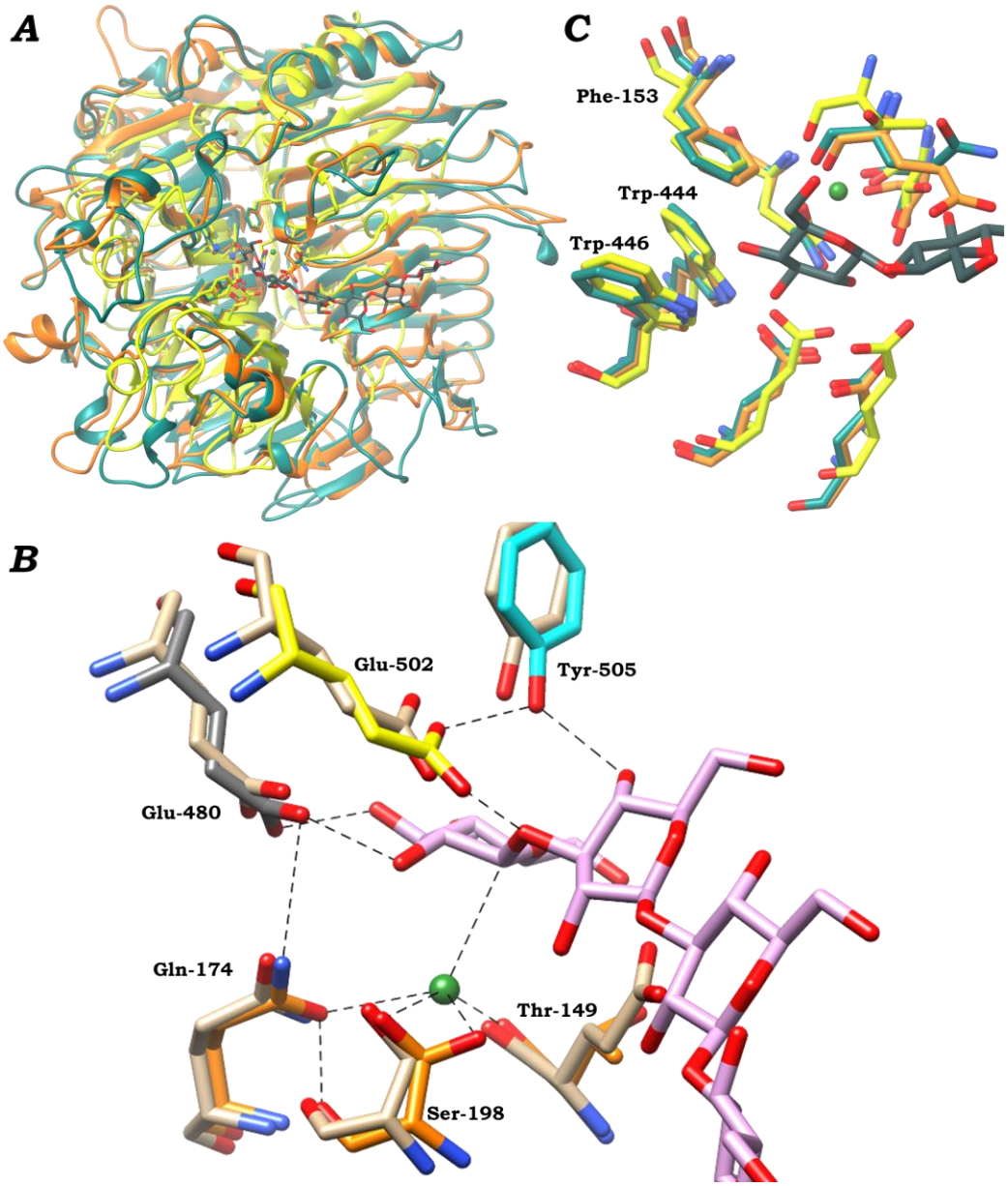

Figure 5.8. Overlay of the structures of SacteLam55A[38], CtLam55 and the homology model for *T. virens* exo-1,3-beta-D-glucanase.

A. Overlay of the crystal structure of SacteLam55A (yellow), CtLam55 (teal) and homology model of *T. virens* exo-1,3-beta-D-glucanase.

B. Overlay of the active site structure of SacteLam55A[38] and the modeled active site for *T. virens* exo-1,3-beta-D-glucanase. Key interactions are shown for the SacteLam55A: catalytic acid Glu-502 (yellow) protonates ring oxygen, Tyr-505 (cyan) stabilizes this interaction. Glu-480 (grey) positions the substrate and assists Gln-174, Ser-198 and Thr-149 (orange) to activate a water (green sphere) for nucleophilic attack on anomeric carbon. Comparable active site residues for *T. virens* GH55 are shown in beige.

C. "Aromatic block" in SacteLam55A (yellow), CtLam55 (teal) and homology model of *T. virens* exo-1,3-beta-d-glucanase (orange).

5.5. Conclusions

GH55 hydrolyzes α-GlcF via a Hehre resynthesis-hydrolysis mechanism. The reaction kinetics require a minimum of two GlcFs to be bound into the active site, to presumably form β-D-glucopyranosyl-(1→3)-α-D-glucopyranosyl fluoride as an intermediate that undergoes rapid GH55-catalyzed hydrolysis. Addition of either methyl α-D-glucopyranoside or phenyl 1-thio-β-D-glucopyranoside as acceptors accelerates the production of fluoride ion product.

KIEs are measured for the GH55-catalysed hydrolysis of α-GlcF, suggesting S_N1-like mechanism. Based on the obtained KIE values transition state has a pyranosylium ion-like character with substantial charge delocalization on the ring oxygen and is late with significant C−F bond cleavage.

5.6. References

1. Koshland, D. E. Stereochemistry and the Mechanism of Enzymatic Reactions. *Biol. Rev.* **28,** 416–436 (1953).

2. Sinnott, M. L. Catalytic mechanism of enzymic glycosyl transfer. *Chem. Rev.* **90,** 1171–1202 (1990).

3. Hehre, E. J., Brewer, C. F. & Genghof, D. S. Scope and Mechanism of Carbohydrase Action: Hydrolytic and Nonhydrolytic Actions of b-Amylase on a- and b-Maltosyl Fluoride. *J. Biol. Chem.* **254,** 5942–5950 (1979).

4. Matsui, H., Tanaka, Y., Brewer, C. F., Blanchard, J. S. & Hehre, E. J. Hydrolysis of α- and β-d-glucosyl fluoride by individual glucosidases: new evidence for separately controlled “plastic” and “conserved” phases in glycosylase catalysis. *Carbohydr. Res.* **250,** 45–56 (1993).

5. Hehre, E. J., Sawai, T., Brewer, C. F., Nakano, M. & Kanda, T. Trehalase: Stereocomplementary Hydrolytic and Glucosyl Transfer Reactions with a- and b-D-Glucosyl Fluoride. *Biochemistry* **21,** 3090–3097 (1982).

6. Hehre, E. J., Matsui, H. & Brewer, C. F. Hydrolysis of β-d-glucopyranosyl fluoride to α-d-glucose catalyzed by Aspergillus niger α-d-glucosidase. *Carbohydr. Res.* **198,** 123–132 (1990).

7. Becker, D., Johnson, K. S., Koivula, A., Schülein, M. & Sinnott, M. L. Hydrolyses of alpha- and beta-cellobiosyl fluorides by Cel6A (cellobiohydrolase II) of Trichoderma reesei and Humicola insolens. *Biochem. J.* (2000). doi:10.1042/0264-6021:3450315

8. Kasumi, T. *et al.* Catalytic Versatility of Bacillus pumilus ß-Xylosidase: Glycosyl Transfer and Hydrolysis Promoted with a-and ß-D-Xylosyl Fluoride1" *Biochemistry* **26,** 3010–3016 (1987).

9. Kitahata, S., Brewer, C. F., Genghof, D. S., Sawai, T. & Hehre, E. J. Scope and Mechanism of Carbohydrase Action: Stereocomplementary Hydrolytic and Glucosyl-Transferring Actions of Glucoamylase and Glucodextranase with a- and b-D-Glucosyl Fluoride. *J. Biol. Chem.* **256,** 6017–6026 (1981).

10. Wang, Z. *et al.* N-Acetylchitooligosaccharide is a potent angiogenic inhibitor both in vivo and in vitro. *Biochem. Biophys. Res. Commun.* (2007). doi:10.1016/j.bbrc.2007.03.094

11. Snaar-Jagalska, B. E., Krens, S. F. G., Robina, I., Wang, L. X. & Spaink, H. P. Specific activation of ERK pathways by chitin oligosaccharides in embryonic zebrafish cell lines. *Glycobiology* (2003). doi:10.1093/glycob/cwg103

12. Semino, C. E. & Allende, M. L. Chitin oligosaccharides as candidate patterning agents in zebrafish embryogenesis. *Int. J. Dev. Biol.* (2000).

13. Ngo, D. N., Kim, M. M. & Kim, S. K. Chitin oligosaccharides inhibit oxidative stress

in live cells. *Carbohydr. Polym.* (2008). doi:10.1016/j.carbpol.2008.02.005

14. Kaku, H. *et al.* Plant cells recognize chitin fragments for defense signaling through a plasma membrane receptor. *Proc. Natl. Acad. Sci. U. S. A.* (2006). doi:10.1073/pnas.0508882103

15. Miya, A. *et al.* CERK1, a LysM receptor kinase, is essential for chitin elicitor signaling in Arabidopsis. *Proc. Natl. Acad. Sci.* (2007). doi:10.1073/pnas.0705147104

16. Mackenzie, L. F., Wang, Q., Antony, R., Warren, J. & Withers, S. G. Glycosynthases: Mutant Glycosidases for Oligosaccharide Synthesis. *J. Am. Chem. Soc.* **120,** 5583–5584 (1998).

17. Moracci, M., Trincone, A., Perugino, G., Ciaramella, M. & Rossi, M. Restoration of the Activity of Active-Site Mutants of the Hyperthermophilic β-Glycosidase from Sulfolobus solfataricus: Dependence of the Mechanism on the Action of External Nucleophiles†. *Biochemistry* **37,** 17262–17270 (1998).

18. Mayer, C., Zechel, D. L., Reid, S. P., Warren, R. A. J. & Withers, S. G. The E358S mutant of Agrobacterium sp. β-glucosidase is a greatly improved glycosynthase. *FEBS Lett.* **466,** 40–44 (2000).

19. Shaikh, F. A. & Withers, S. G. Teaching old enzymes new tricks: engineering and evolution of glycosidases and glycosyl transferases for improved glycoside synthesis. *Biochem. Cell Biol.* **86,** 169–177 (2008).

20. Honda, Y. & Kitaoka, M. The First Glycosynthase Derived from an Inverting Glycoside Hydrolase. *J. Biol. Chem.* **281,** 1426–1431 (2006).

21. Kitaoka, M. *et al.* Conversion of inverting glycoside hydrolases into catalysts for synthesizing glycosides employing a glycosynthase strategy. *Trends Glycosci. Glycotechnol.* **21,** 23–39 (2009).

22. Ohnuma, T. *et al.* A glycosynthase derived from an inverting GH19 chitinase from the moss Bryum coronatum. *Biochem. J* **444,** 437–443 (2012).

23. Ohnuma, T., Dozen, S., Honda, Y., Kitaoka, M. & Fukamizo, T. A glycosynthase derived from an inverting chitinase with an extended binding cleft. *J. Biochem.* **160,** 93–100 (2016).

24. Chakladar, S., Cheng, L., Choi, M., Liu, J. & Bennet, A. J. Mechanistic evaluation of MelA a-galactosidase from Citrobacter freundii: A family 4 glycosyl hydrolase in which oxidation is rate-limiting. *Biochemistry* **50,** 4298–4308 (2011).

25. Bennet, A. J. & Sinnott, M. L. Complete Kinetic Isotope Effect Description of Transition-States for Acid-Catalyzed Hydrolyzes of Methyl alpha-Glucopyranosides and beta-Glucopyranosides. *J. Am. Chem. Soc.* **108,** 7287–7294 (1986).

26. Boulineau, F. P. & Wei, A. Mirror-Image Carbohydrates: Synthesis of the

Unnatural Enantiomer of a Blood Group Trisaccharide. *J. Org. Chem.* **69,** 3391–3399 (2004).

27. Steinmann, A., Thimm, J., Matwiejuk, M. & Thiem, J. Formation of Homooligosaccharides Using Base-Promoted Glycosylation of Unprotected Glycosyl Fluorides. 3606–3612 (2010). doi:10.1021/ma100191d

28. Chan, J., Lewis, A. R., Gilbert, M., Karwaski, M. & Bennet, A. J. A direct NMR method for the measurement of competitive kinetic isotope effects. *Nat. Chem. Biol.* **6,** 405–407 (2010).

29. Sannikova, N. *et al.* Both Chemical and Non-Chemical Steps Limit the Catalytic Efficiency of Family 4 Glycoside Hydrolases. *Biochemistry* **57,** 3378–3386 (2018).

30. Claridge, T. D. W. *High-resolution NMR techniques in organic chemistry*. (Elsevier, 2009).

31. Guido F. Pauli & Birgit U. Jaki, Lankin, D. C. Quantitative 1H NMR: Development and Potential of a Method for Natural Products Analysis. *J. Nat. Prod.* **68,** 133–149 (2005).

32. Melander, L. C. S. & Saunders, W. H. *Reaction rates of isotopic molecules*. (Wiley, 1980).

33. Kelley, L. A., Mezulis, S., Yates, C. M., Wass, M. N. & Sternberg, M. J. E. The Phyre2 web portal for protein modeling, prediction and analysis. *Nat. Protoc.* **10,** 845–858 (2015).

34. Ishida, T. *et al.* Crystal Structure of Glycoside Hydrolase Family 55 β-1,3-Glucanase from the Basidiomycete Phanerochaete chrysosporium. *J. Biol. Chem.* **284,** 10100–10109 (2009).

35. Davies, G. J., Wilson, K. S. & Henrissat, B. Nomenclature for sugar-binding subsites in glycosyl hydrolases. *Biochem. J.* **321,** 557–559 (1997).

36. Becker, D., Johnson, K. S. H., Koivula, A., Schu $ Lein, M. & Sinnott, M. L. Hydrolyses of α-and β-cellobiosyl fluorides by Cel6A (cellobiohydrolase II) of Trichoderma reesei and Humicola insolens. *Biochem. J* **345,** 315–319 (2000).

37. Copeland, R. A. *Enzymes: A Practical Introduction to Structure, Mechanism, and Data Analysis*. (John Wiley & Sons, Inc., 2000). doi:10.1002/0471220639

38. Bianchetti, C. M. *et al.* Active site and laminarin binding in glycoside hydrolase family 55. *J. Biol. Chem.* **290,** 11819–32 (2015).

39. Chan, J., Tang, A. & Bennet, A. J. A Stepwise Solvent-Promoted SNi Reaction of α-D-Glucopyranosyl Fluoride: Mechanistic Implications for Retaining Glycosyltransferases. *J. Am. Chem. Soc.* **134,** 1212–1220 (2012).

40. Indurugalla, D. & Bennet, A. J. A kinetic isotope effect study on the hydrolysis reactions of methyl xylopyranosides and methyl 5-thioxylopyranosides: Oxygen

versus sulfur stabilization of carbenium ions. *J. Am. Chem. Soc.* **123,** 10889–10898 (2001).

41. Chan, J., Tang, A. & Bennet, A. J. Transition-state structure for the hydronium-ion-promoted hydrolysis of α- d -glucopyranosyl fluoride. *Can. J. Chem.* **93,** 463–467 (2015).

42. Huang, X., Tanaka, K. S. E. & Bennet, A. J. Glucosidase-catalyzed hydrolysis of α-D-glucopyranosyl pyridinium salts: Kinetic evidence for nucleophilic involvement at the glucosidation transition state. *J. Am. Chem. Soc.* **119,** 11147–11154 (1997).

43. Lee, J. K., Bain, A. D. & Berti, P. J. Probing the Transition States of Four Glucoside Hydrolyses with13C Kinetic Isotope Effects Measured at Natural Abundance by NMR Spectroscopy. *J. Am. Chem. Soc.* **126,** 3769–3776 (2004).

44. Singh, V., Lee, J. E., Núñez, S., Howell, P. L. & Schramm, V. L. Transition state structure of 5′-methylthioadenosine/S- adenosylhomocysteine nucleosidase from Escherichia coli and its similarity to transition state analogues. *Biochemistry* **44,** 11647–11659 (2005).

45. Berti, P. J., Blanke, S. R. & Schramm, V. L. Transition state structure for the hydrolysis of NAD+ catalyzed by diphtheria toxin. *J. Am. Chem. Soc.* **119,** 12079–12088 (1997).

46. Bennet, A. J., Sinnott, M. L. & Wijesundera, W. S. S. ^{18} O and secondary ^{2} H kinetic isotope effects confirm the existence of two pathways for acid-catalysed hydrolyses of α-arabinofuranosides. *J. Chem. Soc., Perkin Trans. 2* **0,** 1233–1236 (1985).

47. Zhang, Y., Bommuswamy, J. & Sinnott, M. L. Kinetic Isotope Effect Study of Transition States for the Hydrolyses of a- and b-Glucopyranosyl Fluorides. *J. Am. Chem. Soc.* **116,** 7557–7563 (1994).

48. Chan, J., Sannikova, N., Tang, A. & Bennet, A. J. Transition-State Structure for the Quintessential S_N2 Reaction of a Carbohydrate: Reaction of α-Glucopyranosyl Fluoride with Azide Ion in Water. *J. Am. Chem. Soc.* **136,** 12225–12228 (2014).

49. Banait, N. S. & Jencks, W. P. Reactions of anionic nucleophiles with .alpha.-D-glucopyranosyl fluoride in aqueous solution through a concerted, ANDN (SN2) mechanism. *J. Am. Chem. Soc.* **113,** 7951–7958 (1991).

50. Shiner, V. J., Rapp, M. W., Halevi, E. A. & Wolfsberg, M. Solvolytic .alpha.-deuterium effects for different leaving groups. *J. Am. Chem. Soc.* **90,** 7171–7172 (1968).

51. Schleyer, P. v. R., Harris, J. M. & Hall, R. E. Magnitude of secondary .alpha.-deuterium isotope effects for limiting solvolyses. *J. Am. Chem. Soc.* **93,** 2551–2553 (1971).

52. Shiner, V. J. & Dowd, W. Dependence of solvolytic .alpha.-deuterium rate effects

on the nature of the leaving group. *J. Am. Chem. Soc.* **93,** 1029–1030 (1971).

53. Perrin, C. L. & Flach, A. No Contribution of an Inductive Effect to Secondary Deuterium Isotope Effects on Acidity. *Angew. Chemie Int. Ed.* **50,** 7674–7676 (2011).

54. Perrin, C. L., Ohta, B. K., Kuperman, J., Liberman, J. & Té Erdé, M. Stereochemistry of-Deuterium Isotope Effects on Amine Basicity. (2005). doi:10.1021/ja0511927

55. Tanaka, Y., Tao, W., Blanchard, J. S. & Hehre, E. J. Transition State Structures for the Hydrolysis of a-D-Glucopyranosyl Fluoride by Retaining and Inverting Reactions of Glycosylases. *J. Biol. Chem.* **269,** 32306–32312 (1994).

56. Horenstein, B. A. & Schramm, V. L. Electronic Nature of the Transition State for Nucleoside Hydrolase. A Blueprint for Inhibitor Design*. *Biochemistry* **32,** 7089–7097 (1993).

57. Anastassios C. Papageorgioua, ∗, Jinyin Chenb & Duochuan Li. Crystal structure and biological implications of a glycoside hydrolase family 55 β-1,3-glucanase from Chaetomium thermophilum. *BBA - Proteins Proteomics* **8,** 1030–1038 (2017).

58. Labourel, A. *et al.* The β-glucanase ZgLamA from Zobellia galactanivorans evolved a bent active site adapted for efficient degradation of algal laminarin. *J. Biol. Chem.* **289,** 2027–42 (2014).

59. Wojtkowiak, A., Witek, K., Hennig, J. & Jaskolski, M. Structures of an active-site mutant of a plant 1,3-β-glucanase in complex with oligosaccharide products of hydrolysis. *Acta Crystallogr. Sect. D Biol. Crystallogr.* **69,** 52–62 (2013).

60. Wu, H.-M. *et al.* Structure, mechanistic action, and essential residues of a GH-64 enzyme, laminaripentaose-producing beta-1,3-glucanase. *J. Biol. Chem.* **284,** 26708–15 (2009).

5.7. Supporting Information

Figure S5.1. Fluoride ion release rate from α-GlcF by *T. virens* GH55 exo-1,3-β-D-glucanase. Data fit with the equation 5.5. Reactions were carried out in 100 mM sodium succinate buffer, pH 6.05 at 40 °C with 1.9 μM enzyme.

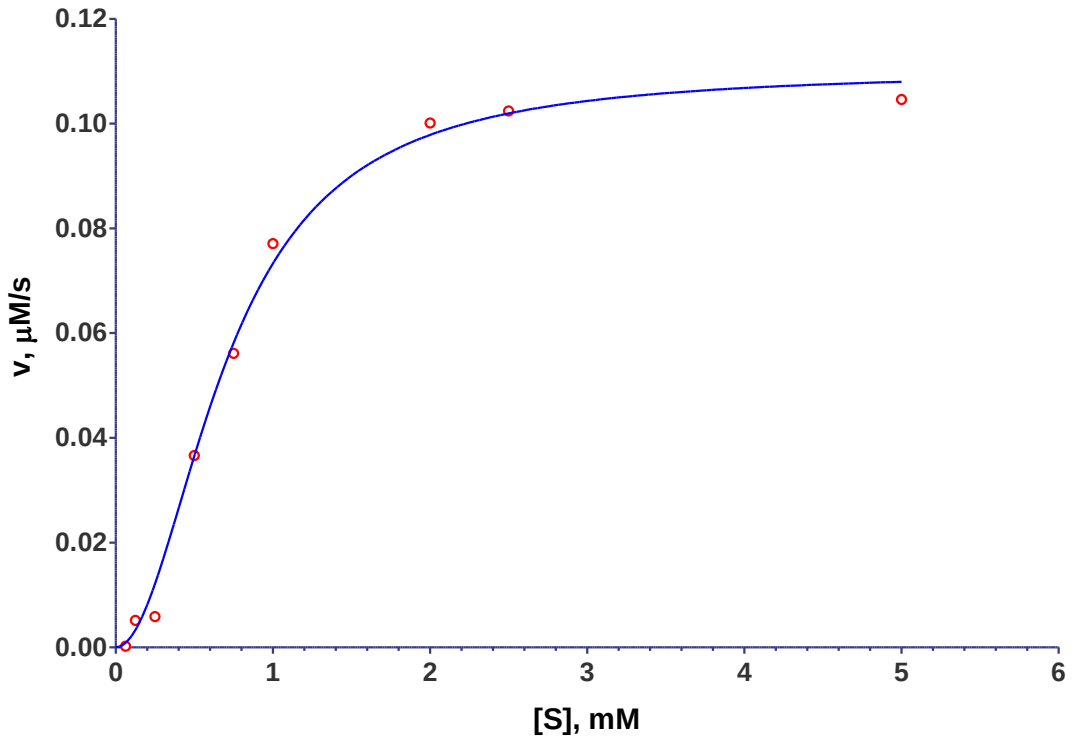

Derivation of the equation 5.3.

Experimental conditions: $[E]_0 \ll [S]$

Conservation equations: $[E]_0 = [E] + [ES_{-1}] + [ES_{+1}] + [ES_{-1}S_{+1}]$

$$[S]_0 = [S] + [ES_{-1}] + [ES_{+1}] + [ES_{-1}S_{+1}] = [S]$$

Definition of binding constants: $K_{-1} = \frac{[E][S]}{[ES_{-1}]}; \frac{K_{-1}}{[S]} = \frac{[E]}{[ES_{-1}]}$

$$K_{+1} = \frac{[E][S]}{[ES_{+1}]}; \frac{K_{+1}}{[S]} = \frac{[E]}{[ES_{+1}]}$$

$$\boldsymbol{\alpha K_{-1}} = \frac{[\boldsymbol{ES_{+1}}][\boldsymbol{S}]}{[\boldsymbol{ES_{-1}S_{+1}}]};\ \frac{\boldsymbol{\alpha K_{-1}}}{[\boldsymbol{S}]} = \frac{[\boldsymbol{ES_{+1}}]}{[\boldsymbol{ES_{-1}S_{+1}}]}$$

$$\boldsymbol{\alpha K_{+1}} = \frac{[\boldsymbol{ES_{-1}}][\boldsymbol{S}]}{[\boldsymbol{ES_{-1}S_{+1}}]};\ \frac{\boldsymbol{\alpha K_{+1}}}{[\boldsymbol{S}]} = \frac{[\boldsymbol{ES_{-1}}]}{[\boldsymbol{ES_{-1}S_{+1}}]}$$

Statement of rate dependence: $\boldsymbol{v_0 = k_0[ES_{-1}S_{+1}]}$

Derivation of rate equation:

$$\frac{\boldsymbol{v_0}}{[\boldsymbol{E}]_{\boldsymbol{0}}} = \frac{\boldsymbol{k_0[ES_{-1}S_{+1}]}}{[\boldsymbol{E}] + [\boldsymbol{ES_{-1}}] + [\boldsymbol{ES_{+1}}] + [\boldsymbol{ES_{-1}S_{+1}}]}$$

$$\frac{\boldsymbol{v_0}}{[\boldsymbol{E}]_{\boldsymbol{0}}} = \frac{\boldsymbol{k_0}}{\frac{[\boldsymbol{E}]}{[\boldsymbol{ES_{-1}S_{+1}}]} + \frac{[\boldsymbol{ES_{-1}}]}{[\boldsymbol{ES_{-1}S_{+1}}]} + \frac{[\boldsymbol{ES_{+1}}]}{[\boldsymbol{ES_{-1}S_{+1}}]} + \boldsymbol{1}}$$

$$\frac{\boldsymbol{v_0}}{[\boldsymbol{E}]_{\boldsymbol{0}}} = \frac{\boldsymbol{k_0}}{\frac{[\boldsymbol{E}][\boldsymbol{ES_{-1}}]}{[\boldsymbol{ES_{-1}S_{+1}}][\boldsymbol{ES_{-1}}]} + \frac{\boldsymbol{\alpha K_{+1}}}{[\boldsymbol{S}]} + \frac{\boldsymbol{\alpha K_{-1}}}{[\boldsymbol{S}]} + \boldsymbol{1}}$$

$$\frac{\boldsymbol{v_0}}{[\boldsymbol{E}]_{\boldsymbol{0}}} = \frac{\boldsymbol{k_0}}{\frac{\boldsymbol{\alpha K_{-1}K_{+1}}}{[\boldsymbol{S}]^{\boldsymbol{2}}} + \frac{\boldsymbol{\alpha K_{+1}}}{[\boldsymbol{S}]} + \frac{\boldsymbol{\alpha K_{-1}}}{[\boldsymbol{S}]} + \boldsymbol{1}}$$

$$\frac{\boldsymbol{v_0}}{[\boldsymbol{E}]_{\boldsymbol{0}}} = \frac{\boldsymbol{k_0}[\boldsymbol{S}]^{\boldsymbol{2}}}{\boldsymbol{\alpha K_{-1}K_{+1}} + \boldsymbol{\alpha}[\boldsymbol{S}](\boldsymbol{K_{-1}} + \boldsymbol{K_{+1}}) + [\boldsymbol{S}]^{\boldsymbol{2}}}$$

$$\boldsymbol{v_0} = \frac{k_0[E]_0[S]^2}{\alpha K_{-1}K_{+1} + \alpha(K_{-1} + K_{+1})[S] + [S]^2}$$

Table S1. Individual measurements of *V/K* KIEs on the hydrolysis of α-D-glucopyranosyl fluorides by *T. virens* GH55 exo-1,3-β-D-glucanase at pH 6.05 and 40 °C, the corresponding means and standard deviations for isotopologues **1b** – **1f**.

Compound	**Site of substitution**	**KIE (k_{1a}/k_x)**	**Mean and SD**
1b	5-^{18}O ring oxygen	0.9639 0.9917 0.9854	0.980 ± 0.012
1c	1-^{13}C anomeric	1.006 1.012 1.009	1.009 ± 0.002
1d	1-^{2}H alpha deuterium	1.121 1.134 1.144	1.133 ± 0.009
1e	2-^{2}H beta deuterium	1.054 1.051 1.053	1.053 ± 0.001
1f	5-^{2}H gamma deuterium	1.024 1.020 1.015	1.020 ± 0.004

Chapter 6.

Future Work

The mechanistic studies presented in this thesis have provided better understanding about three glycoside hydrolases' mode of action: NAD^+-dependent, classical single step inverting and the Hehre resynthesis-hydrolysis mechanisms. The newly gleaned information concerning the enzymatic transition state(s) for these mechanisms is important given that GHs are widely distributed in nature and because of their important roles in pathological processes. As a result, the conclusions outlined in this thesis should stimulate the design of new GHs inhibitors.

6.1. Both Chemical and Non-Chemical Steps Limit the Catalytic Efficiency of Family 4 Glycoside Hydrolases

A remote labelling protocol was developed to augment the “Bennet” NMR method for the determination of competitive KIEs, and this can be applied to different enzymatic systems to probe transition state structures. This new method has the advantage of circumventing the use of multiply labelled, expensive, isotopic starting materials and as a result reduces the synthetic complexity needed to make the necessary substrates. Using this approach KIEs on natural substrates can also be measured.

Based on our studies of GH4 catalysis the conformationally constrained cyclopropyl and allyl sugar analogues (Fig. 6.1) developed in our group can be investigated as potential inhibitors of these bacterial glycoside hydrolases.

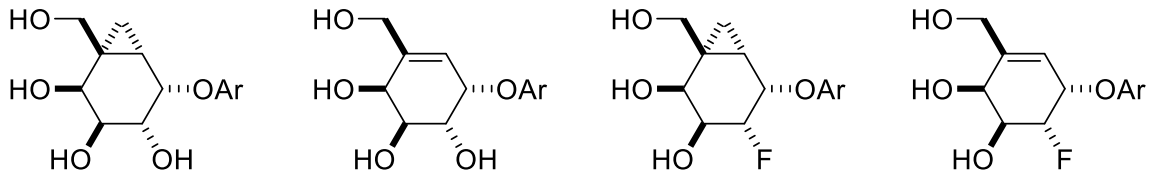

Figure 6.1. Conformationally constrained GH inhibitors.

6.2. Kinetic Isotope Effects and Transition State Structure for the Hydrolysis of α-D-Glucopyranosyl Fluoride by Inverting Glucoamylases

The next logical step for this project is to model the transition states using modern computational chemistry methods (QM/MM and DFT). That is, our complete set of measured KIEs, including the 5-^{18}O ring oxygen effect, can be used as constraints in the modelling so as to identify critical TS parameters, such as bond orders, ring conformation, and degree of proton transfer(s) for the *A. niger* α-glucoamylase. These results will enable us to develop strategies for probing enzymatic transition states for more complex cases, such as mechanism-based inactivation of GHs.

6.3. A Kinetic Isotope Effect Study on the Hydrolysis of α-D-Glucopyranosyl Fluoride by an Inverting exo-1,3-β-D-Glucanase: Transition State Evaluation for the Hehre Resynthesis-Hydrolysis Mechanism

The measured KIEs provide important insights into the Hehre resynthesis-hydrolysis mechanism. To our knowledge, this is the first KIE study on this mechanism that is a common feature for a number of glycoside hydrolases. Our findings should encourage the design of glycosynthases from other GHs.

The nature of this mechanism potentially allows measuring of KIE on nucleophile if a 3-^{18}O labelled acceptor sugar is used. This would be extremely difficult for the classical mechanism of inverting GH-promoted hydrolysis as the specific labelling of an oxygen atom, as well as the adjacent reporter atom in a disaccharide would be extremely expensive and time consuming.